# NOAA Atlas NESDIS 5

## WORLD OCEAN ATLAS 1994
## VOLUME 5: INTERANNUAL VARIABILITY OF UPPER OCEAN THERMAL STRUCTURE

Washington, D.C.
December 1994

**U.S. DEPARTMENT OF COMMERCE**
**National Oceanic and Atmospheric Administration**
National Environmental Satellite, Data, and Information Service

# NOAA Atlas NESDIS 5

## WORLD OCEAN ATLAS 1994
## VOLUME 5: INTERANNUAL VARIABILITY OF UPPER OCEAN THERMAL STRUCTURE

Sydney Levitus
Timothy P. Boyer
National Oceanographic Data Center
Ocean Climate Laboratory

and

John Antonov
State Hydrological Institute
St. Petersburg, Russia

Washington, D.C.
December 1994

**U.S. DEPARTMENT OF COMMERCE**
**Ronald H. Brown, Secretary**

**National Oceanic and Atmospheric Administration**
D. James Baker, Under Secretary

National Environmental Satellite, Data, and Information Service
Robert S. Winokur, Assistant Administrator

## National Oceanographic Data Center
## USER SERVICES

Additional copies of this publication, as well as information about NODC data holdings, products, and services, are available on request directly from the NODC. NODC information and data are also available over the Internet through the NODC Home Page on the World Wide Web and the NODC Gopher server.

National Oceanographic Data Center
User Services Branch
NOAA/NESDIS E/OC21
Washington, DC 20235

Telephone: (202) 606-4549

Fax: (202) 606-4586

E-mail: services@nodc.noaa.gov

NODC Home Page: http://www.nodc.noaa.gov/

NODC Gopher server: gopher.nodc.noaa.gov

# Contents

# List of Figures

**APPENDIX A**

**APPENDIX B**

**APPENDIX C**

**APPENDIX D**



**APPENDIX E**

**APPENDIX F**



**APPENDIX G**

**APPENDIX H**

**APPENDIX I**

# Preface

This atlas extends an earlier work entitled *Climatological Atlas of the World Ocean* (Levitus, 1982). This earlier work has proven to be of utility to the international oceanographic, climate research, and operational communities. In particular, the objectively analyzed fields of temperature and salinity have been used in a variety of ways. These include use as boundary and/or initial conditions in numerical ocean circulation models, for verification of numerical simulations of the ocean, as a form of "sea truth" for satellite measurements such as altimetric observations of sea surface height, and for planning oceanographic expeditions. We have expanded the earlier work to now include maps of annual temperature anomaly fields for the upper ocean for the period 1960 through 1990 as described in this atlas. The analyses and signals represented by such maps can be expected to play a role in describing, and hence understanding air-sea interaction on gyre and basin space scales. We have also expanded this earlier work to include chemical parameters such as phosphate, nitrate, and silicate because: 1) our belief that a comprehensive set of objectively analyzed parameter fields describing the state of the ocean, based on all existing oceanographic data, should be available as a matter of course to the international research community and 2) the immediate, compelling need for such analyses in order to study the role of biogeochemical cycles in determining how the earth's climate system works. For example, it is well known that the amount of carbon dioxide in the earth's atmosphere is expected to double during the next century. Regardless of one's scientific and/or political view of a possible "enhanced greenhouse warming" due to the increase of carbon dioxide, it is a necessity that the international scientific community have access to the most complete historical oceanographic data bases to study this problem, as well as other scientific and environmental problems.

The production of global analyses of oceanographic data is a major undertaking. Such work benefits from the input of many individuals and organizations. We have tried to structure the data sets and analyses that constitute this atlas in such a way as to encourage feedback from experts around the world who have knowledge that can improve future atlases. The production of works like this atlas series is becoming easier because of advances in computer hardware and software. These include: 1) the development of relatively inexpensive but powerful workstations that can be dedicated to data processing and analysis and 2) the development of high resolution printers and interactive graphics software that minimize the need for expensive, time consuming manual drafting and photographic processing. Because of the substantial increase in the historical oceanographic data bases expected over the next several years, the Ocean Climate Laboratory plans to update and expand this atlas series on a relatively frequent basis that will be determined by the accession of significant amounts of new data. We plan to publish volumes that focus on derived quantities, higher resolution analyses, and additional parameters such as chlorophyll, primary production, and plankton taxa and biomass.

The objective analyses in this atlas, and data on which they are based, are being made available internationally without restriction on various magnetic media as well as CD-ROMs. This is to insure the widest possible distribution.

In each acknowledgement section of this atlas series we have expressed our view that such a series is only possible through international cooperation of scientists, data managers, and scientific administrators throughout the international community. I would also like to thank my co-authors, colleagues, and staff from the Ocean Climate Laboratory of NODC for their dedication to the project leading to publication of this atlas series. Their integrity and thoroughness have made possible this multi-volume atlas series. Oceanography is a field of increasing specialization, and it is my belief that the development of national and international oceanographic data archives is best performed by scientists who are actively working with the historical data. Margarita Conkright and Timothy Boyer receive my particular thanks.

Sydney Levitus
Director, Ocean Climate Laboratory
National Oceanographic Data Center
Washington, D.C.
December 1994

# Acknowledgements

The establishment of a research group at the National Oceanographic Data Center to focus on the preparation of research quality oceanographic data sets and their objective analyses sets has been made possible by a grant from the NOAA Climate and Global Change Program. Substantial amounts of historical oceanographic data used in this study were located and digitized (Data Archaeology and Rescue projects) with funding from the NOAA Climate and Global Change Program, the NOAA Environmental Services Data and Information Management Program, the National Science Foundation, and the Office of Naval Research. John Antonov was supported as a Research Associate sponsored by the National Research Council and the NOAA Climate and Global Change Program.

The work described in this atlas was made possible by scientists, technicians, ships' crew, data managers, and science administrators from the international scientific community. This atlas represents the results of several different research/data management projects of the NODC Ocean Climate Laboratory at the National Oceanographic Data Center (NODC), Washington, D.C. The products in this atlas are all based on the master oceanographic data archives maintained by NODC/WDC-A as well as data acquired as a result of the NODC Data Archaeology and Rescue (NODAR) project and the IODE/IOC Global Oceanographic Data Archaeology and Rescue (GODAR) project. These archives and data sets exist because scientists of the international scientific community have submitted their data to national and regional data centers. In turn these centers have submitted data to the World Data Center system established under the International Council of Scientific Unions and the Intergovernmental Oceanographic Commission. This atlas and similar works would not exist without these international efforts. In particular we would like to thank data managers at these centers and the administrators and staff of these international organizations. The archiving of oceanographic data at international data centers means that the substantial expenditures in human and capital resources devoted to oceanographic measurement programs will be fully exploited, both for present and future scientific studies.

Although many data managers from the international community have been instrumental in the building of global oceanographic data bases we would like to thank in particular Harry Dooley of the International Council for Exploration of the Sea, Osamu Yamada, Director of the Japanese Oceanographic Data Center, Yuri Sychev of the Russian National Oceanographic Data Center, Hou Wen-Feng of the Chinese National Oceanographic Data Center, Shin Tani formerly of the Japanese Oceanographic Data Center, and Ronald Wilson of the Marine Environmental Data Service, Canada.

Jeff Burney provided excellent system administration and programming support. Daphne Johnson provided invaluable assistance in unpacking numerous data sets used in this project and preparing figures. Robert Gelfeld was instrumental in the acquisition of numerous data sets as part of the NODAR and GODAR Projects. Margarita Conkright provided assistance in the preparation of figures and of this atlas in general. Our colleagues at NODC/WDC-A provided support for various data management projects related to this atlas. Jennifer Campbell helped in preparing the manuscript for publication. The support of Gregory Withee and Bruce Douglas, former and present directors of NODC is appreciated. Management support by Dave Goodrich and Bill Murray of the NOAA Office of Global Programs is appreciated.

We would like to thank Grigory Isayev and Ron-Hua Zhang for their review of this work. We also would like to thank Clara Deser and her colleagues for their excellent work in reviewing this work. Their careful efforts led to a reanalysis of an earlier version of this work, which resulted in new procedures being implemented to compute the yearly temperature anomaly fields.

The data sets and products represented by this atlas are distributed internationally without restriction in accordance with U.S. Climate and Global Change as well as ICSU/IOC data management policies in support of Global Change Research.

# WORLD OCEAN ATLAS 1994, VOLUME 5: INTERANNUAL VARIABILITY OF UPPER OCEAN THERMAL STRUCTURE

*Sydney Levitus, and Timothy Boyer*
National Oceanographic Data Center
Washington, D.C.

*John Antonov*
State Hydrological Institute
St. Petersburg, Russia

## ABSTRACT

This atlas contains maps of yearly *in situ* upper ocean temperature anomaly fields at selected standard levels of the world ocean, computed on a one-degree latitude-longitude grid, for the 1960-1990 period. The fields used to generate these maps were computed by objective analysis of historical data. Data distribution maps are presented for individual years at selected standard levels. In addition, figures showing the results of multivariate analyses of these fields, linear temperature trends occurring in the upper ocean, and difference fields between selected years are presented

### 1. INTRODUCTION

This atlas represents an analysis of all historical temperature data available from the National Oceanographic Data Center (NODC), Washington, D.C., plus data gathered as a result of two data management projects: the NODC Oceanographic Data Archaeology and Rescue (NODAR) project and the Intergovernmental Oceanographic Commission (IOC) Global Oceanographic Data Archaeology and Rescue (GODAR) project. Data used here have been analyzed in a consistent, objective manner on a one-degree latitude-longitude grid at standard oceanographic analysis levels between the surface and a maximum depth of 400m. The objective analysis scheme is similar to that presented by Levitus and Boyer (1994).

Objective analyses shown in this atlas are limited by the nature of the data base (non-synoptic, scattered in space) and characteristics of the objective analysis techniques, and the grid used. These limitations and characteristics will be described and discussed. Our purpose is to produce gridded annual temperature anomaly fields within the limitations of the available data.

Fields of annual *in situ* temperature anomaly are presented for the period 1960-1990 at the sea surface, 125 m, and 250 m depth. For brevity of text we shall refer to *in situ* temperature simply as temperature. The present analyses are primarily intended for use in the study of the role of the world ocean as part of the earth's climate system. Levitus *et al.* (1994a) have used these fields to describe the spatial distribution of a quasi-decadal scale oscillation that occurs in the upper part of the North Atlantic Ocean that appears to be directly linked to an oscillation of the sea surface pressure fields over the North Atlantic known as the East Atlantic Oscillation (Cayan, 1992). This feature was demonstrated (Levitus *et al.*, 1995) to exist to depths of approximately 400 m at the location of Ocean Weather Station "C" in the North Atlantic (52.75°N, 35.5°W)

## 2. DATA AND DATA DISTRIBUTION

Data sources and quality control procedures are described below and by Levitus and Boyer (1994). Because quality control procedures are so important, a technical report has been prepared fully describing these procedures (Boyer and Levitus, 1994).

### 2.1 Data sources

The Station Data and S/CTD used in this project were obtained from the National Oceanographic Data Center (NODC), Washington, D.C. and represent all the data available in the Oceanographic Station Data (SD) file and S/CTD file as of the first quarter of 1993 (NODC, 1993), plus data gathered as a result of the NODAR and GODAR projects (Levitus *et al.*, 1994b) that have not yet been archived in the NODC digital archives. In addition, the collection of international oceanographic profiles that comprise the Hydrographic Atlas of the Southern Ocean developed by Olbers *et al.* (1992) at the Alfred Wegener Institute for Polar and Marine Research were included. S/CTD that are received at coarse, vertical resolution are often placed in the Station Data file. We have transferred these data to the S/CTD file. Expendible bathythermograph (XBT) data and Mechanical Bathythermograph (MBT) data as of the third quarter of 1993 were used in our study. XBT and MBT data sent to NODC at non-standard levels are placed in the SBT (Special Bathythermograph Temperature) file. We have put these data into the XBT and MBT files as appropriate. The MBT instrument is no longer in frequent use in many countries, having been superseded by the XBT. The work by Couper and LaFond (1970) describes the MBT instrument and some of its history.

Appendix A shows yearly geographic distribution of all historical temperature observations (SD, CTD, XBT, MBT merged together) at the sea surface, 125 m, and 250 m depth for the 1960-1990 period. There are specific reason for displaying the data distributions at these standard levels. Instrument depth limitations determine the amount of data available for the study of upper ocean thermal variability (and thus the length of the time series we can develop). For example the early versions of the MBT had a maximum penetration depth of 140 m. Later versions of this instrument had a maximum penetration depth of 295 m. One of the purposes of our work is to develop the most complete historical oceanographic data bases possible. The upper 125 m of the ocean represents the region which will have the most data for the post-1940 period. This is obvious from inspection of the data distributions for individual years at 125 m and 250 m depth during the pre-1955 period.

### 2.2 Data Quality Control

#### *2.2a Subjective elimination of data*

The data were averaged by one-degree squares by individual years for input to the objective analysis program. After initial objective analyses of the upper ocean annual temperature anomaly fields were computed, unrealistic features were found. These occurred because the input set of one-degree means still contained suspicious data. Examination of these features indicated that some of them were due to particular oceanographic cruises. In such cases data from an entire cruise were eliminated from further use by setting a flag on each profile from the cruise.

#### *2.2b Representativeness of the data*

To clarify discussions of the amount of available data, quality control techniques, and representativeness of the data, the reader should examine in detail the maps showing the yearly distributions of upper ocean temperature data in Appendix A. These maps are provided to give the reader a quick, simple way of examining the historical data distributions.

#### *2.2c XBT drop rate error correction*

Recently it has been demonstrated that XBT temperature profiles made using T4, T6, and T7 probes exhibit a systematic error with depth that is associated with an inadequate drop rate equation for these instruments (Banes and Sessions, 1984; Hanawa and Yoritaka, 1987; Wright and Szabados, 1989; Singer, 1990; Hallock and Teague, 1992). The error in depth has a magnitude that equals approximately five percent of the actual depth. XBT instruments only measure temperature and time directly. The depth of an instrument is estimated from a manufacturer supplied drop rate equation plus the time elapsed after the probe enters the water. T4, T6, and T7 XBT probes in fact, fall faster than the manufacture's specification.

A task team of the International Global Ocean Services System (IGOSS) of the Intergovernmental Oceanographic Commission (IOC) on "Quality Control for Automated Systems" is addressing the problem of how the international community should treat XBT data (IOC, 1992a ; IOC, 1992b). One of their recommendations is that IGOSS continue using the existing drop-rate equations, until international agreement is reached on a solution. It has been recommended that data centers continue to receive and distribute XBT data that are uncorrected for the systematic error. Following this philosophy **we have made no correction to the depths of the observed level XBT profiles**. Thus investigators can make whatever correction they desire to the observed level profiles we are providing, since we have not corrected these profiles for this error. However, in order to merge XBT data with other types of temperature measurements, and in order to produce climatologies and other analyses, by necessity we have corrected the drop-rate error in XBT profiles, as part of the process of interpolating to standard levels. **All T4, T6, T7 XBT profiles we have used in generating products at standard levels, or made available as part of our standard level profile data sets, have been corrected for the drop-rate error.** T5 XBT profiles were not corrected because depth estimates using the manufacturer's equation for this instrument type were found to be within the limit stated by the manufacturer (Boyd and Linzell, 1992). However a small systematic bias might be occurring with these instruments also. The correction (Szabados, personal communication) we have used for the T4, T6, T7 probes has not yet been designated as the "official" correction, but based on tests by several independent investigating groups, it is clear that the correction formula we have used will be quite close to the official correction procedure that will be defined. **If in fact, users wish to use another procedure, but still use the XBT data set we have compiled, they can do so by applying their correction procedure to our observed level XBT profile data set, which has not been corrected for the drop rate error.**

The corrected depth, $Z_c$ (meters), is determined using the following formula,

$$z_c = 6.733t - 0.00254t^2$$

in which "t", the elapsed time since the instrument entered the ocean, is determined from

$$t = 1498.14 - (2244447.430 - 462.963z_0)^{1/2}$$

in which

$z_0$ = originally calculated depth.

#### *2.2d MBT calibration corrections*

Several thousand MBT profiles were corrected for systematic calibration errors. These corrections were supplied by Roger Bauer. As a point of information for users, these corrections were made several years ago to the U.S. Navy MOODS file.

## 3. DATA PROCESSING PROCEDURES

### 3.1 Vertical interpolation to standard levels

Vertical interpolation of observed level data to standard levels followed procedures in UNESCO (1991). These procedures are in part based on the work of Reiniger and Ross (1968). Details are described by Boyer and Levitus (1994).

### 3.2 Methods of analysis

#### *3.2a Overview*

It is accurate to state that little knowledge exists about the time and spatial scales of subsurface ocean temperature anomalies. In order to gain information about temporal and spatial characteristics of upper ocean temperature anomalies for the world ocean, we used the following analysis procedures. We subtracted the standard level values of each temperature profile from the corresponding climatological monthly mean temperature values for the month during which the profile was measured. In this way we generated a set of "anomaly" profiles. This procedure was used in order to remove the effect of the annual cycle of temperature from the historical data sets. Having eliminated or minimized the effect of the annual cycle on the profiles we could choose any compositing period desired. The choice depending on the amount of data available, and the time scales of the anomaly fields we wish to describe. We chose to use one-year compositing periods. One degree-square averages of anomaly values were computed for each individual one-degree square at each upper ocean standard level, and for each year from 1941 through 1990. These one-degree-square anomaly fields were objectively analyzed using the same procedures described by Levitus and Boyer (1994).

### *3.2b First guess field determination*

To provide a first guess field for the annual temperature anomaly analyses for any particular year at any standard level, we used a value of zero at each ocean gridpoint. This choice has the effect of minimizing the magnitude of the anomaly fields but we see no other choice. Future work will investigate other possible choices.

### *3.2c Quality control*

The first attempt at producing the yearly anomalies resulted in an additional quality control procedure (and the procedures described by Levitus and Boyer (1994) and Boyer and Levitus (1994) ) being applied. This step was to eliminate from use any temperature anomaly value that exceeded a magnitude of four degrees centigrade Celsius. This choice was made empirically and will also be the subject of future investigations

## 4. RESULTS

There is a substantial amount of material that could be presented in this section. We have chosen to present what we believe to be a relatively succinct portion of the most important results. Our purpose is to document some of the results we have found so as to illustrate the importance of historical data. The availability of our analyses allows individual researchers to perform additional investigations.

We have structured our results section to first describe the data distributions and temperature anomaly fields for individual years at selected depths of the upper ocean. We describe the linear trend for a large part of the world ocean because we remove this trend before performing multivariate analyses for individual basins. We examine variability in the Atlantic and then the Pacific by presenting the results of Empirical Orthogonal Function analyses at selected depths. Temperature anomaly fields for averages of selected years are presented for the Pacific and Atlantic oceans based on periods when extrema occur in their respective time series of the loading functions of the EOF analyses. A section describing variability associated with the ENSO phenomenon is presented also.

### 4.1 Yearly temperature anomaly fields 1960-1990

Appendices B, C, and D show yearly temperature anomalies for individual years during the 1960-1990 period. At gridpoints where three or fewer one degree squares contribute to the correction of the first-guess field we do not plot the analyzed fields and in fact place the letter " x" at each of these gridpoints. This provides a quick, visual means of identifying those regions where the existing data may be inadequate for the preparation of anomaly fields.

We present anomalies at the sea surface, in addition to the subsurface anomaly fields, so that comparisons can be made with similar analyses that can be performed with the much larger surface marine data sets such as the Comprehensive Ocean-Atmosphere Data Set (Woodruff *et al.*, 1987; Slutz *et al.*, 1985) recognizing that the COADS data set contains many more observations. The yearly anomaly fields at all three depths presented exhibit a rich set of gyre and basin-scale patterns of variability. For example at 125 m depth the 1966-1971 period is characterized by a positive anomaly in the central portion of the midlatitude North Pacific. Beginning around 1977 the anomaly pattern in this region reverses sign and remains negative until approximately 1988. The change around 1977 is approximately coincident with the large-scale changes in atmospheric circulation noted by several authors including Trenberth (1990), and Miller *et al.* (1994).

We note that in 1980 and 1981 at 125 m depth that the subsurface temperature field of the eastern Pacific exhibited a positive anomaly, well before the intense 1982-83 El Nino event. During 1982 the eastern tropical Pacific exhibits large-scale anomalies exceeding 0.5°C and even 1.0 °C, particularly centered along 15°N. During 1983 the warm anomaly along 15°N moves westward and by 1984 has reached 125 °E. The North Atlantic also exhibits large-scale variability at 125 m depth with magnitudes typically on the order of 0.5-1.0°C. For example the 1989-1990 period is characterized by a relatively cold subarctic gyre and warm subtropical gyre.

### 4.2 Statistical measure of interannual variability of upper ocean temperature

We have computed the standard deviation of the yearly anomaly fields for the 1960-1990 period and present these results for the sea surface, 125 m depth, and 250 m depth in Appendix E (Figs. E1-E3) . At subsurface depths the largest standard deviations occur in the tropics of all oceans which is associated with variability of the shallow tropical thermocline.

### 4.3 Linear temperature trends in the upper layers of the North Atlantic and North Pacific

We have computed the magnitude of linear temperature trend in the world ocean for selected depths (0 m, 125 m, 250 m) for the 1960-1990 period as shown in Appendix E (Figs. E4-E6). This particular time period is determined by requirements for multivariate analyses that we performed and which we describe in following sections. We present results only for the Atlantic and Pacific Ocean because of the lack of data for the Indian Ocean. We detrended the temperature anomaly fields before performing the multivariate analysis. However a different period is better for isolating the linear variability of subsurface temperature of the North Atlantic. Hence we isolate the North Atlantic Ocean for individual analysis in later sections. The North Pacific during this period undergoes major changes but a linear trend does not describe these changes well so we present no other material regarding linear trends for the Pacific. Results of tests of statistical significance accompany the linear trend analyses at each depth as shown in Appendix E (Figs. E7-E9) . Areas with statistically significant linear trends are shaded. In addition the percent variance of the interannual variability of these annual anomaly fields accounted for by the linear trends at these selected standard levels are presented in Appendix E (Figs. E10-E12). At the 125 and 250 m depth levels the linear trends accounts for a larger percentage of the interannual variability of these anomaly fields and over a much larger area as compared to the sea surface. This may occur because of the smaller amplitude of the annual cycle of temperature at these depths as compared to the sea surface. We regard the annual cycle of temperature as relatively high frequency noise for the purpose of studying interannual to decadal scale variability.

### 4.4 Variability of the North Atlantic Ocean, 1960-1990

### 4.4a EOF analyses of temperature at selected depth levels in the North Atlantic Ocean

Results of Empirical Orthogonal Function (EOF) analyses for selected depths (0 m, 125 m, 250 m) of the North Atlantic Ocean for the 1960-1990 period are presented in Appendix F (Figs. F1-F18). The EOF analyses were performed on the linearly detrended temperature anomaly fields averaged over ten-degree squares. Most of the variance associated with the temporal variability of the North Atlantic Ocean at the subsurface depths we present here is associated with a quasi-decadal scale oscillation. Figures F1 through F6 show the loading patterns and the temporal variability of the first three EOFs for the North Atlantic at the sea surface. Figures F7 through F12 show the loading patterns and the temporal variability of the first three EOFs for the North Atlantic at 125 m depth. Figures F13 through F18 show the loading patterns and the temporal variability of the first three EOFs for the North Atlantic at the 250 m depth level. Levitus et al. (1994a) have described the quasi-decadal scale oscillation of upper ocean thermal structure of the North Atlantic and its association with the East Atlantic Oscillation sea surface pressure field. Fig. F19 shows the correspondence between the 1st EOF at 125 m depth and the linearly detrended temperature anomaly time series at Ocean Weather Station "C" (OWS "C") which is located in the southern part of the subarctic gyre of the North Atlantic Ocean at 34.5°W and 52.75°N. This oscillation feature is described by Levitus *et al.* (1994a,1995) and appears to be associated with the East Atlantic sea surface pressure oscillation (Cayan,1992). Deser and Blackmon (1993) described this oscillation in the historical sea surface temperature record. The subsurface temperature difference fields associated with this quasi-decadal scale oscillation are described in the next section. The Soviet observations used by Levitus et al. (1994a) were daily means and thus are not included in the data base used to prepare Fig. F19.

### 4.4b Upper ocean temperature difference fields of the North Atlantic Ocean

We describe difference in the subsurface temperature fields associated with extremes of the oscillation described in section 4.4a and Fig. F19. Fig. F20 is the temperature difference fields at 125 m depth for the 1972-75 mean minus the 1965-68 mean. This represents a period when relatively cold conditions occurred at OWS "C" minus the temperature field when relatively warm conditions occurred at OWS "C". Fig. F21 is the 1979-82 temperature mean field minus the 1972-75 mean field. This represents a period when relatively warm conditions occurred at OWS "C" minus the temperature field during the period when relatively cold conditions occurred at OWS "C". Figs. 22-23 show the mean difference fields for the same time periods but for 250 m depth. The difference fields show that the gyre and basin scale temperature changes are of the order of several tenths of a degree centigrade throughout the North Atlantic. This represents a substantial redistribution of heat between these periods.

### 4.4c Temperature anomaly difference versus depth cross-sections for selected regions in the North Atlantic

Figs. F24-F29 show the temperature differences versus depth for extremes of the oscillation shown in Fig. F19 for the same periods used in the previous sections. Subsurface difference fields commonly exceed 0.4°C

## 4.5 Variability of the North Atlantic Ocean, 1966-1990

Our analyses of the annual temperature anomaly fields (Levitus et al., 1994a) indicates that 1966 was a year in which a warming (cooling) trend reversed sign in the subarctic (subtropical) parts of the North Atlantic Ocean. Hence we choose to describe variability in this period.

### 4.5a Linear trend analysis of the North Atlantic Ocean upper thermal structure, 1966-90

Figs. G1-G6 show the linear temperature trend at the sea surface, 75 m, 150 m, 250 m, 300 m, and 400 m depths. Figs. G7-G12 show the significance of these trends (t-test), and Figs. G13-18 show the percent variance accounted for by the linear trend at each depth level. It is clear that in the upper 150 m of the water column the subarctic gyre of the North Atlantic exhibited a linear cooling trend during the 1966-90 period. Maximum cooling occurred just east of Newfoundland. Examination of the trends for the 250 m through 400 m layers indicate that midlatitudes also exhibited a cooling trend during this period with the signal being most pronounced at 400 m depth.

### 4.5b Linear temperature trends for selected vertical cross-sections in the North Atlantic Ocean

In order to better describe the vertical extent of linear trends of upper ocean temperature we present Figs. G19-G24. These figures are vertical cross-sections along selected longitudes .

## 4.6 Variability of the North Pacific Ocean, 1960-90

### 4.6a EOF analyses of temperature at selected depth levels of the North Pacific Ocean

Results of Empirical Orthogonal Function (EOF) analyses for selected depths of the North Pacific Ocean (20°N-65°N) for the 1960-1990 period are presented in Appendix H. The EOF analyses were performed on the linearly detrended temperature anomaly fields. Figures H1 through H18 show the loading patterns and temporal variability of the first three EOFs for the North Pacific at the sea surface, 125 m, and 250 m depth levels. Fig. H19 shows the time variability of the first EOF at 125 m depth and the second EOF at 250 m depth (multiplied by -1). It is clear from the correlation between these two time series and the loading patterns shown in Figs. H7 and H14 that these two EOFs represent the same variability pattern at these two depths.

### 4.6b Temperature anomaly fields for selected periods and standard level depths of the North Pacific

We present temperature anomaly fields at the 125 m and 250 m standard levels for three and five year averages. The averaging periods were chosen to maximize differences in the temperature anomaly structure of the North Pacific between the extremes described by the time series of the EOF loading patterns given Fig. H19 in section 4.6a. Figs. H20-H27 show the temperature anomaly fields for 1960-62, 1965-69, 1981-85, and 1988-90 for the 125 m depth levels and 250 m depth levels. Clearly documented is the observation that temperature in the North Pacific at these depths and latitude has changed with a very characteristic structure. Maximum changes are centered in the 30°N-50°N latitude belt. The sign of the anomaly field is the same for an area defining the central part of the North Pacific and of opposite sign along the periphery of this feature. Average anomaly values exceed 0.2°C over large areas and exceed 0.4°C during some periods. The existence of these anomalies at subsurface depths has been described in part by Watanabe and Mizuno (1994).

### 4.6c Temperature difference versus depth cross-sections for selected regions in the North Pacific Ocean

Figs. H28-H33 show temperature anomaly versus depth cross sections along the 164.5°E, 174.5°W, 156.5°W meridians of the North Pacific for the 1960-62 period and the 1988-90 period.

### 4.7 Comparison of El Nino and La Nina thermal structure

To further describe variability of the upper ocean thermal structure we have composited our annual anomaly fields into El Nino and La Nina averages based on the magnitude of the El Nino Southern Oscillation (ENSO) index (Quinn et al., 1992). We have averaged all fields for 1969, 1972, 1976, 1982, and 1986 which were years when the Southern Oscillation Index (SOI) was high. We also averaged all fields for the years 1964, 1970, 1973, 1975, and 1988 when the SOI was low. We recognize that variability associated with El Nino and La Nina episodes are not necessarily the same. However we believe the production of these composite fields will provide basic information regarding these episodes. Future studies will attempt to describe variability between such episodes of such phenomena as the data permit.

### 4.7a Composite thermal structure during El Nino and La Nina at upper ocean standard depth levels

Figs. I1-I3 show the composite El Nino temperature anomaly field at the sea surface, 125 m, and 250 m depth. The tropical Pacific sea surface temperature field exhibits positive anomalies east of 160°E as is well known. At 125 m depth the area exhibiting such anomalies is reduced in size. A warm anomaly appears along the west coast of North America. This warming is described in several papers in the book edited by Wooster and Fluharty (1985). At 250 m depth the size of the tropical region with a warm anomaly is reduced as well as the magnitude of the anomaly.

Figs. I4-I6 show the composite La Nina temperature anomaly field at the sea surface, 125 m, and 250 m depths. At the sea surface, cool conditions occur over a large portion of the eastern Pacific, at 125 m depth the cold anomaly is most intense along the equator and at 250 m depth the anomaly pattern is quite weak.

### 4.7b Composite temperature difference fields at standard levels for El Nino minus La Nina periods

Figs. I7-I9 show the difference fields of our composite El Nino minus La Nina thermal structure at the sea surface, 125 m depth, and 250 m depth. Figs. I7-I9 show the temperature difference fields for the El Nino composites minus the La Nina composite. These figures indicate that the differences between the thermal structure associated with the El Nino and La Nina phenomenon at 250 m depth are relatively small except in the western equatorial Pacific which is characterized by differences exceeding 0.5°C.

### 4.7c Composite temperature difference cross-sections at selected regions for composites based on ENSO and El Nino minus La Nina periods

Figs. I10-I12 show the temperature composite anomaly structure for the El Nino composite at latitudes 9.5°N, 0.5°N, and 9.5°S . Figs. I13-I15 are similar to Figs. I10-I12 but are for the La Nina composite.

Figs. I16-I18 show the temperature difference of the El Nino composite minus the La Nina composite along the same latitude belts. Along 0.5°N differences exceeding 1.0°C exist only in the upper 150 m of the water column except in the far western Pacific Ocean. Along 9.5°N and 9.5°S a similar situation occurs.

## 5. SUMMARY

We have presented yearly temperature anomaly fields at selected upper ocean standard levels for the Pacific and

Atlantic Oceans for the 1960-1990 period. The results ofEmpirical Orthogonal Function analyses have been presented as well as estimation of the linear trend of upper ocean temperature.

## 6. FUTURE WORK

Substantial amounts of upper ocean thermal data are being archived in digital form as a result of the NODAR and GODAR projects. We expect to add these new data and publish an updated version of this atlas during 1996. We also intend to: 1) perform more thorough studies of the frequency distribution of temperature anomies in the upper ocean in order to improve quality control methods used to produce the data sets used in such studies; 2) attempt to improve the analysis techniques used to produce the anomaly fields described in this atlas, particularly with respect to the determination of the first-guess field for the anomaly analyses.

# References


Banes, J., and M.H. Sessions, 1984: A field performance test of the Sippican deep aircraft-deployed expendable bathythermograph. *J. Geophys. Res.*, 89, 3615-3621.

Boyd, and Linzell, 1992: The temperature and depth accuracy of Sippican T-5 XBTs. *J. Atmosph. and Oceanic Tech.*, 10, 128-136.

Cayan, D., 1992: Latent and sensible heat flux anomalies over the Northern oceans: Driving the sea surface temperature. *J. Phys. Oceanogr.*, 22, 859-881.

Boyer, T., and S. Levitus, 1994: Quality control of historical temperature, salinity, and oxygen data. *NOAA Technical Report NESDIS* In preparation.

Couper, B.K., and E.C. LaFond, 1970: Mechanical Bathythermograph: An historical review. Advances in Instrumentation, Paper 735-70, 25(3), 1-27.

da Silva, A., C. Young, and S. Levitus, 1994a: *Atlas of Surface Marine Data 1994, Vol. 1: Algorithms and procedures. NOAA Atlas NESDIS 6.* U.S. Government Printing Office, Washington, D.C, In preparation.

da Silva, A., C. Young, and S. Levitus, 1994b: *Atlas of Surface Marine Data 1994, Vol. 2: Anomalies of Directly Observed Quantities. NOAA Atlas NESDIS 7*, U.S. Government Printing Office, Washington, D.C., 416 pp.

da Silva, A., C. Young, and S. Levitus, 1994c: *Atlas of Surface Marine Data 1994 Vol. 3: Anomalies of Fluxes of Heat and Momentum. NOAA Atlas NESDIS 8.* U.S. Government Printing Office, Washington, D.C, In preparation.

da Silva, A., C. Young, and S. Levitus, 1994d: *Atlas of Surface Marine Data 1994 Vol. 4: Anomalies of Fresh Water Fluxes. NOAA Atlas NESDIS 9.* U.S. Government Printing Office, Washington, D.C, In preparation.

da Silva, A., C. Young, and S. Levitus, 1994e: *Atlas of Surface Marine Data 1994 Vol. 5: Miscellaneous Derived Quantities. NOAA Atlas NESDIS 10.* U.S. Government Printing Office, Washington, D.C, In preparation.

Deser, C., and M.L. Blackmon, 1993: Surface climate variations over the North Atlantic during Winter: 1900-1989. *J. Climate*, 6, 1743-1753.

Hallock, Z. R., and W.J. Teague, 1992: The fall rate of the T-7 XBT. *J. Atmosph. and Oceanic Tech.*, 9, 470-483.

Hanawa, K., and H. Yoritaka, 1987: Detection of systematic errors in XBT data and their correction. *J. Oceanogr. Soc. Japan*, 43, 68-76.

IOC, 1992a: Summary report of the IGOSS task team on quality control for automated systems and addendum to the summary report. *IOC/INF-888,* 1992.

IOC, 1992b: Summary report of the IGOSS task team on quality control for automated sytems and addendum to the summary report. *IOC/INF-888-append.,* 1992.

Levitus, S., 1982: *Climatological Atlas of the World Ocean,* NOAA Professional Paper No. 13, U.S. Gov. Printing Office, 173 pp.

Levitus, S., and T.P. Boyer , 1994: *World Ocean Atlas 1994, Vol. 4: Temperature. NOAA Atlas NESDIS 4*, U.S. Gov. Printing Office, Washington, D.C., 117 pp.

Levitus, S., J. Antonov, and T.P. Boyer, 1994a: Interannual variability of temperature at a depth of 125 meters in the North Atlantic Ocean, *Science*, 266, 96-99.

Levitus, S., R. Gelfeld, T. Boyer, and D. Johnson, 1994b: *Results of the NODC Oceanographic Data Archaeology and Rescue Projects*. Key to Oceanographic Records Documentation No. 19, NODC, Washington, D.C. , 73 pp.

Levitus, S., J. Antonov, X. Zhou, H. Dooley, K. Selemenov, and V. Tereschenkov, 1995: Decadal-Scale Variability of the North Atlantic Ocean. Accepted by National Academy of Sciences Press, *Natural Climate Variability on decade-to-century time scales.*

Miller, A.J., D.R. Cayan, T.P. Barnett, N.E. Graham, J.M. Oberhuber, 1994: Interdecadal variability of the Pacific Ocean: model response to observed heat flux and wind stress anomalies. *Climate Dynamics*, 9, 287-302.

Olbers, D., V. Gouretzki, G. Seib, J. Schroeter, 1992: *The Hydrographic Atlas of the Southern Ocean*, Alfred-Wegener-Institute for Polar and Marine Research, Bremerhaven, 17 pp., 82 plates.

Quinn, W.H., 1992: A study of Southern Oscillation-related climatic activity for A.D. 622-1990 incorporating Nile River flood data, in *El Nino: Historical and Paleoclimatic Aspects of the Southern Oscillation*, Eds. H.F. Diaz and V. Markgraf, Cambridge University Press., Cambridge, 119-150.

Reiniger, R. F., and C. F. Ross, 1968: A method of interpolation with application to oceanographic data. *Deep-Sea Res.*, 9, 185-193.

Singer, J. J., 1990: On the error observed in electronically digitized T-7 XBT data. *J. Atmos. Oceanic Technol.*, 7, 603-611.

Slutz, R.J., S.J. Lubker, J.D. Hiscox, S.D. Woodruff, R.L. Jenne, D.H. Joseph, P.M. Steurer, and J.D. Elms, 1985: COADS, Comprehensive Ocean-Atmosphere Data Set, Release 1. Climate Research Program, Environmental research Laboratory, Boulder, CO, pp. 262.

Trenberth, K.E., 1990: Recent observed interdecadal changes in the Northern Hemisphere. *Bull. Amer. Soc.*, 71, 988-993.

UNESCO, 1991: *Processing of Oceanographic Station Data*. Imprimerie des Presses Unibversitaires de France, Imprimerie des Presses Universitaires de France, Vendome, 138 pp.

Watanabe, T., and Mizuno, K., 1994: Decadal scale changes in the thermal structure in the North Pacific. International WOCE Newsletter, 15, unpublished manuscript, 10-12.

Woodruff, S. D., R.J. Slutz, R.L. Jenne, and P. Steurer, 1987: A comprehensive ocean-atmosphere data set. *Bull. Amer. Meteorol. Soc.*, 68, 1239-1249.

Wooster, W.S. and D.L. Fluharty, 1985:El Nino North, Washington Sea Grant Program, College of Fisheries and Oceanography, U. Washington, pp 312.

Wright, D., and M. Szabados, 1989: Field evaluation of real-time XBT systems. *Oceans 89 Proc.*, 5, 1621-1626.

Wright, D., 1989: Field evaluation of the XBT bowing problem. *NOS OOD Data Report 91-2*, National Ocean Service, NOAA, Rockville, Maryland, U.S.A.

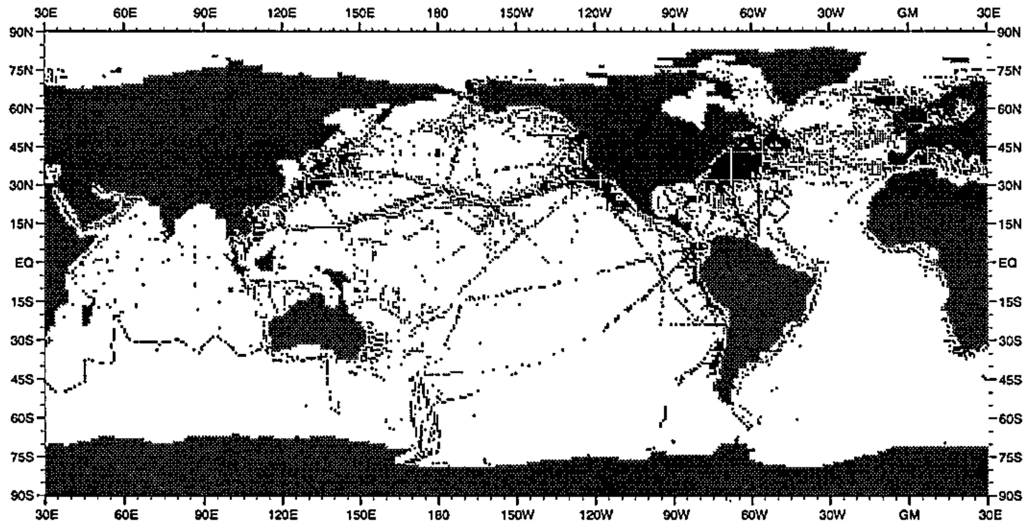


Fig. A1 Distribution of temperature observations at the surface for year 1960

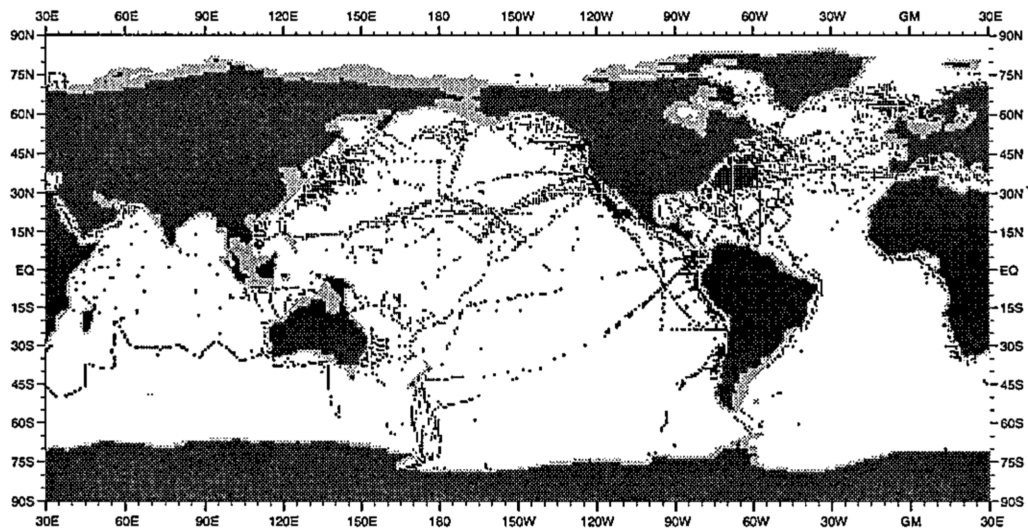


Fig. A2 Distribution of temperature observations at 125 m depth for year 1960

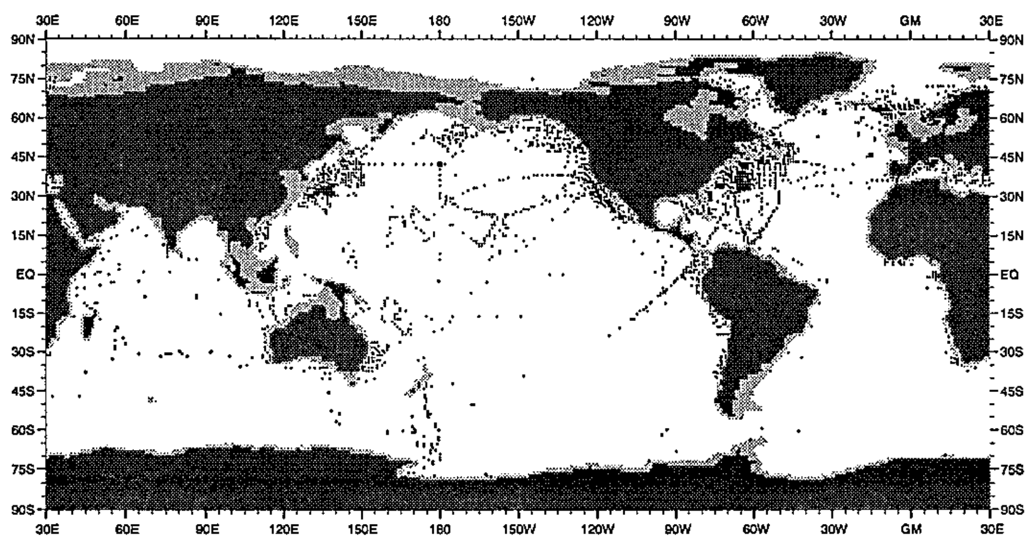


Fig. A3 Distribution of temperature observations at 250 m depth for year 1960

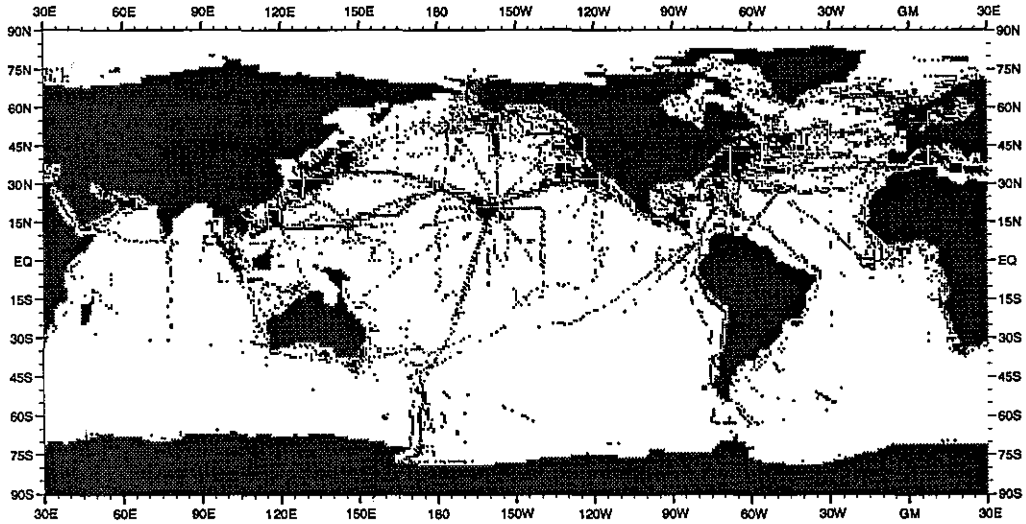


Fig. A4 Distribution of temperature observations at the surface for year 1961

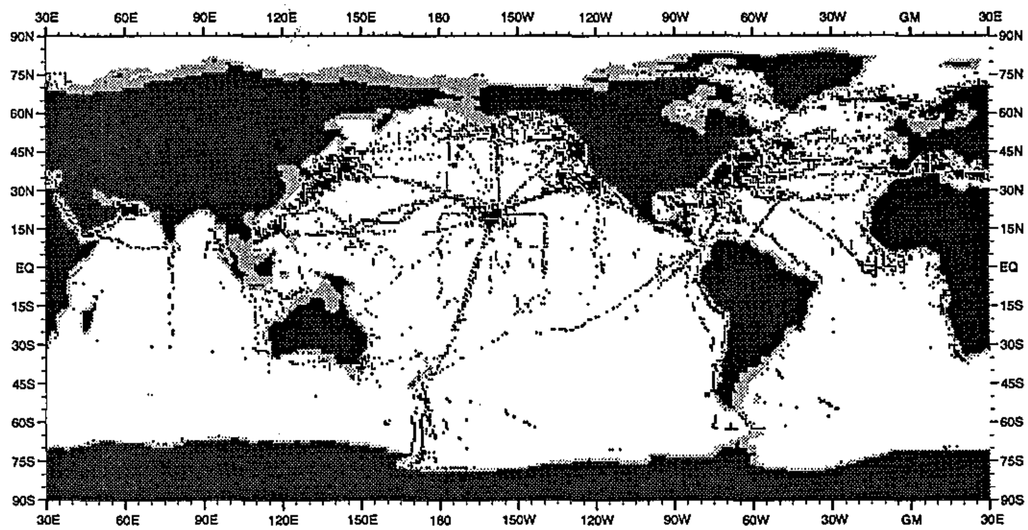


Fig. A5 Distribution of temperature observations at 125 m depth for year 1961

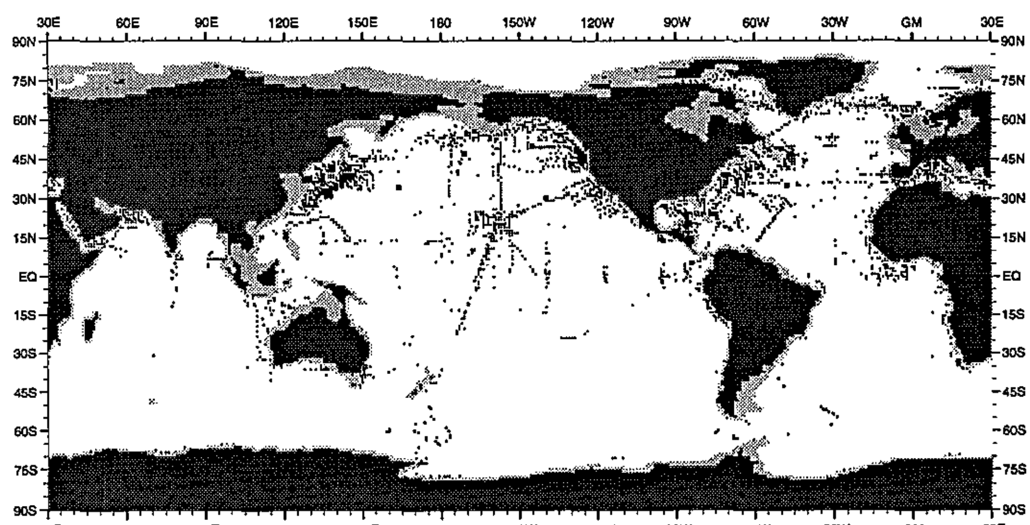


Fig. A6 Distribution of temperature observations at 250 m depth for year 1961

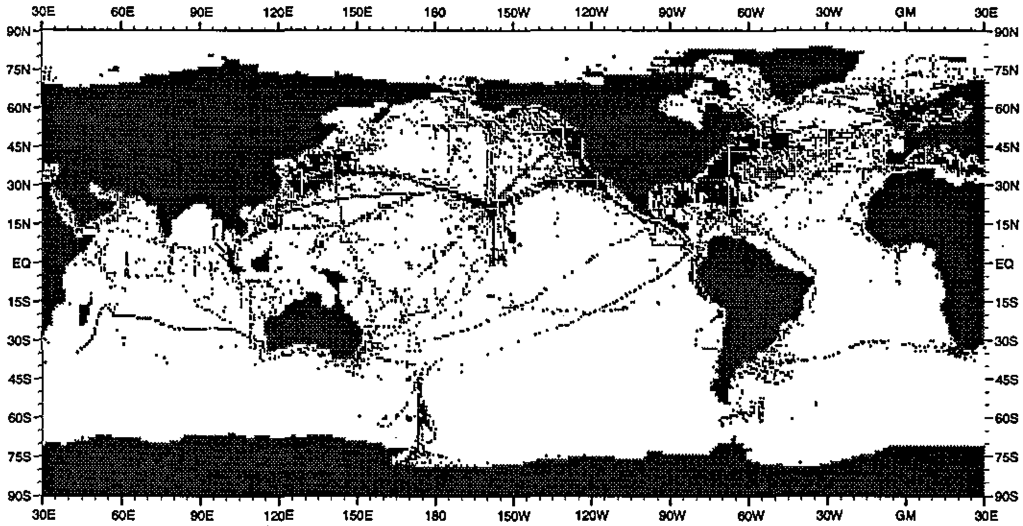


Fig. A7 Distribution of temperature observations at the surface for year 1962

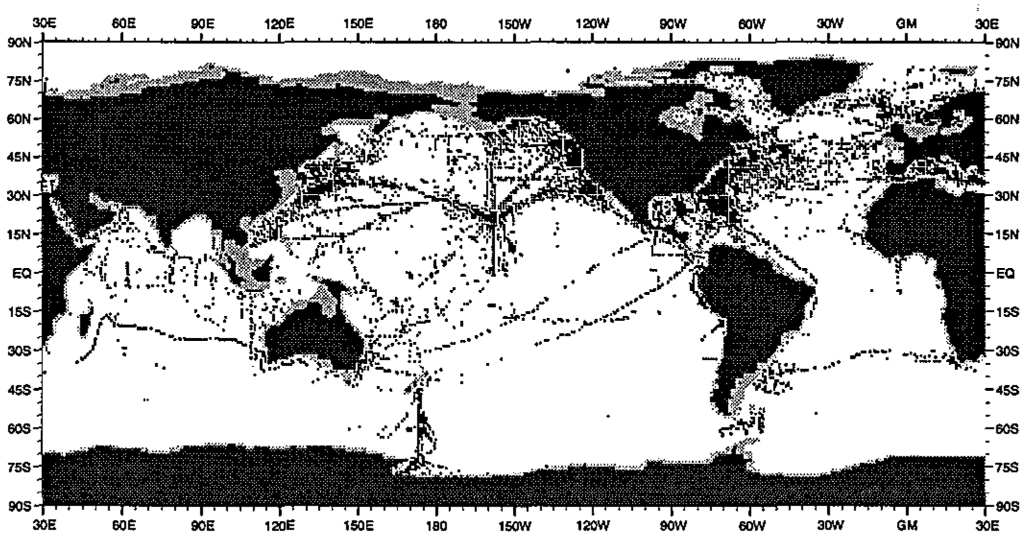


Fig. A8 Distribution of temperature observations at 125 m depth for year 1962

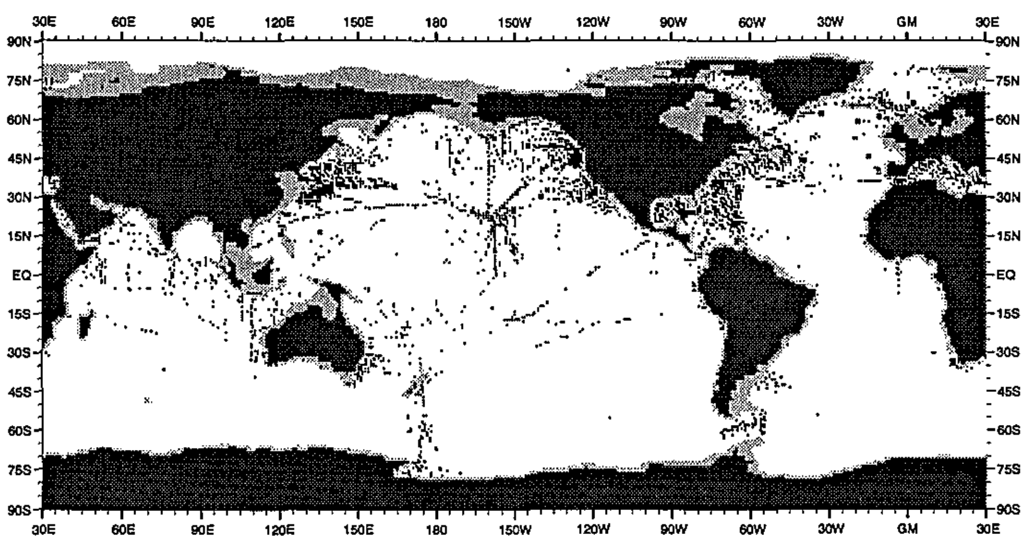


Fig. A9 Distribution of temperature observations at 250 m depth for year 1962

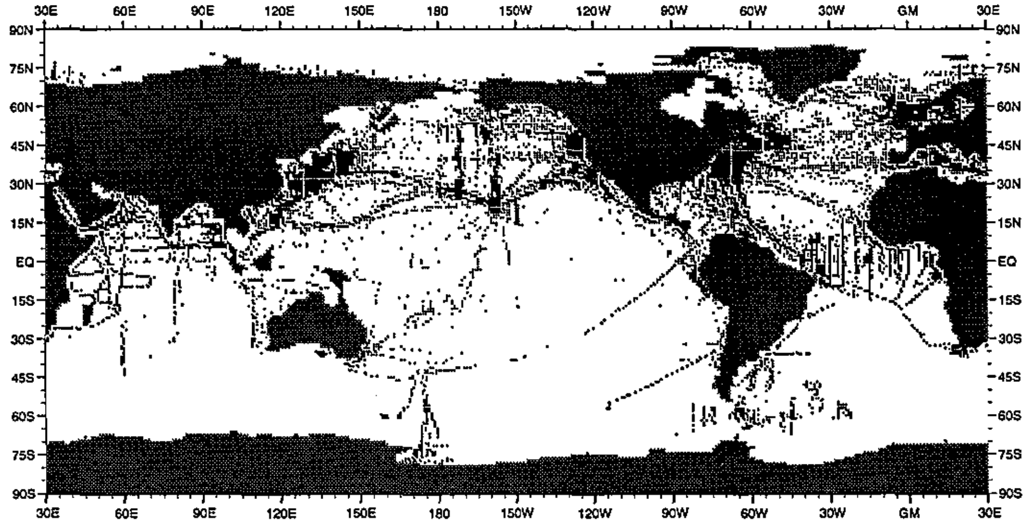


Fig. A10 Distribution of temperature observations at the surface for year 1963

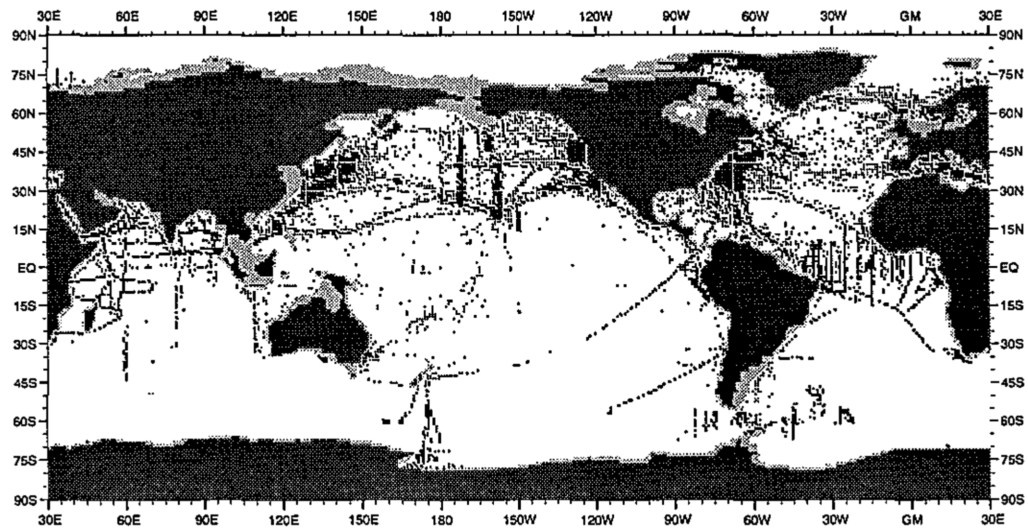


Fig. A11 Distribution of temperature observations at 125 m depth for year 1963

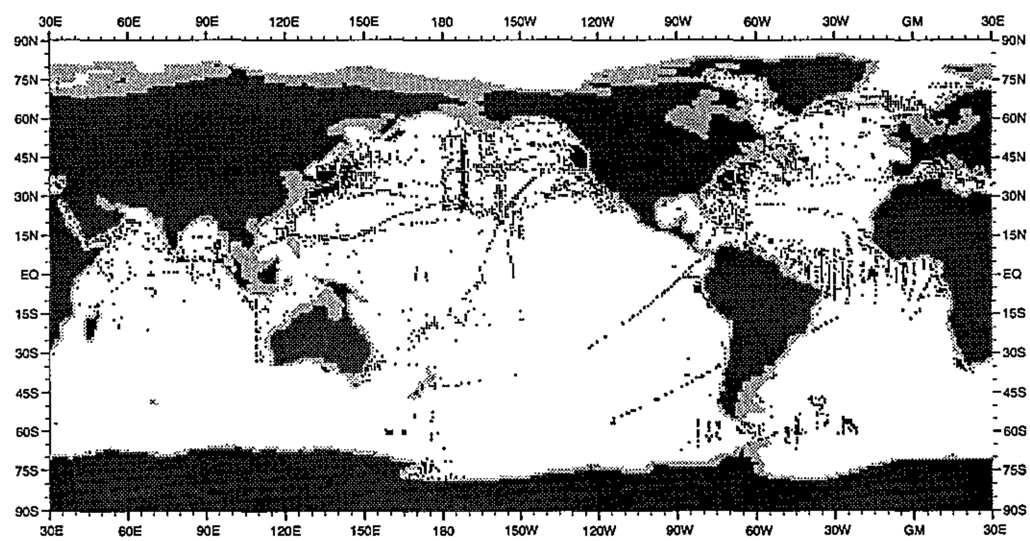


Fig. A12 Distribution of temperature observations at 250 m depth for year 1963

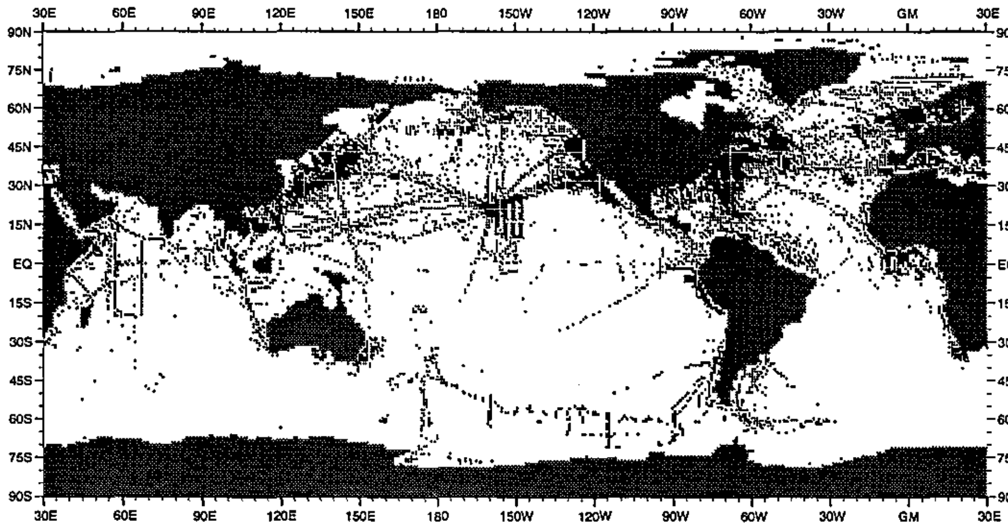


Fig. A13 Distribution of temperature observations at the surface for year 1964

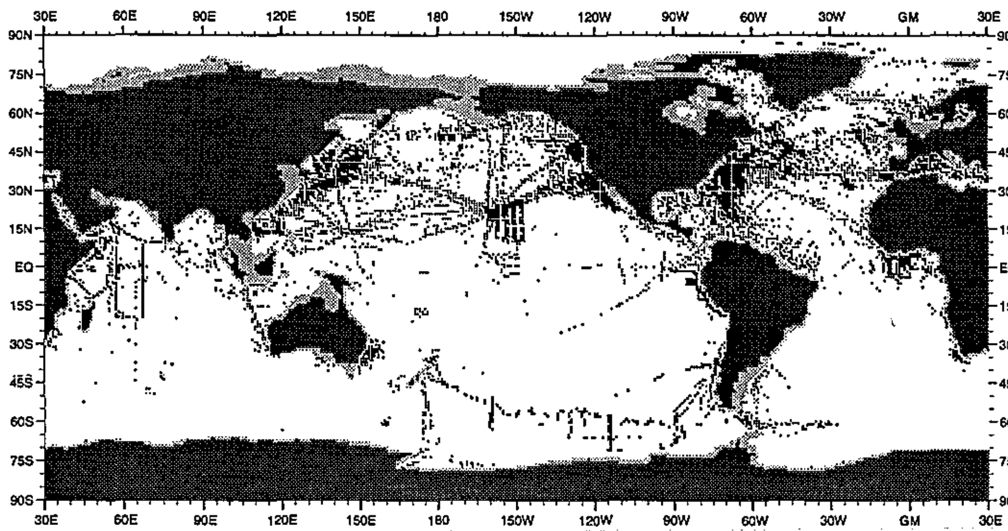


Fig. A14 Distribution of temperature observations at 125 m depth for year 1964

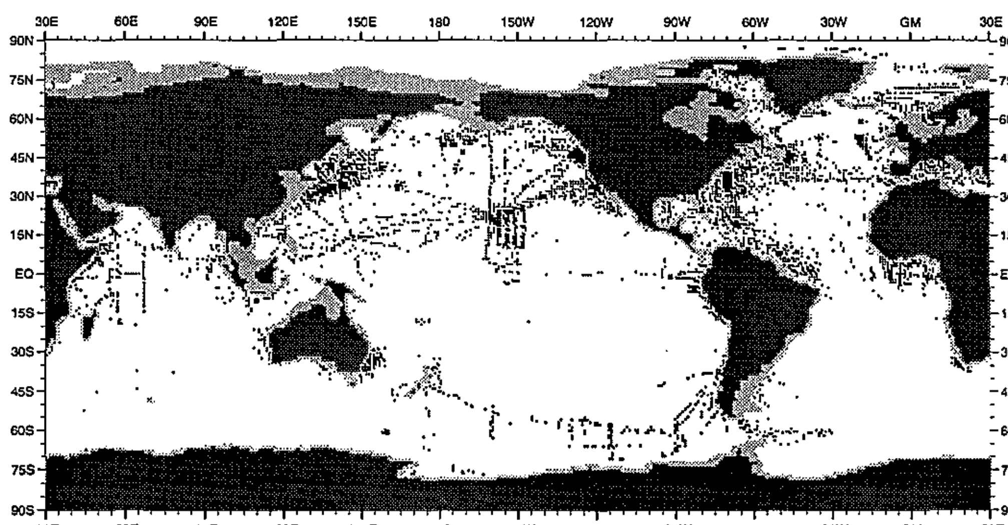


Fig. A15 Distribution of temperature observations at 250 m depth for year 1964

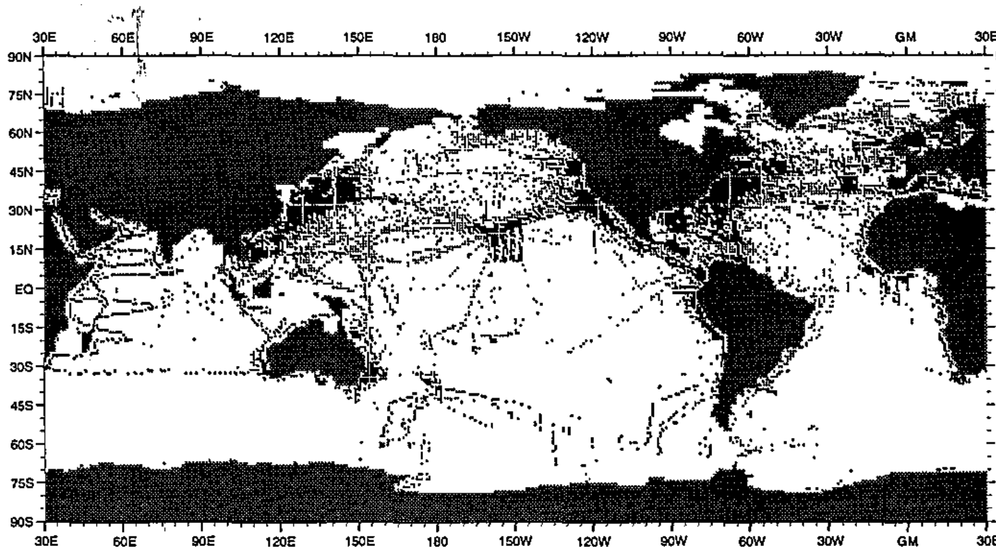


Fig. A16 Distribution of temperature observations at the surface for year 1965

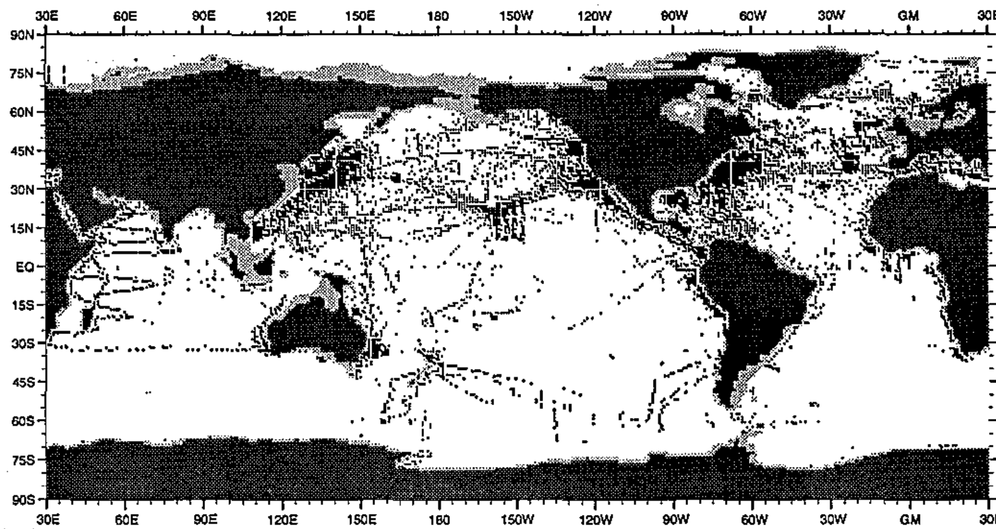


Fig. A17 Distribution of temperature observations at 125 m depth for year 1965

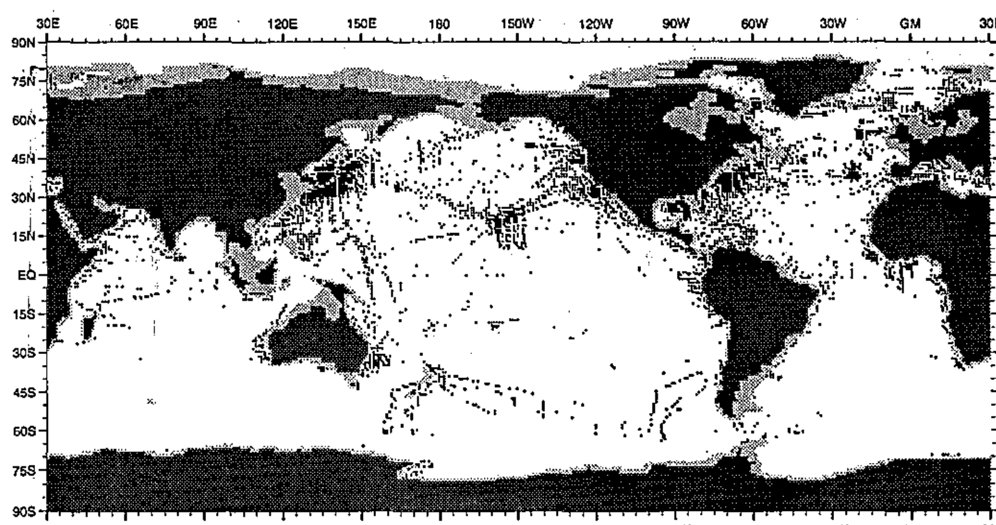


Fig. A18 Distribution of temperature observations at 250 m depth for year 1965

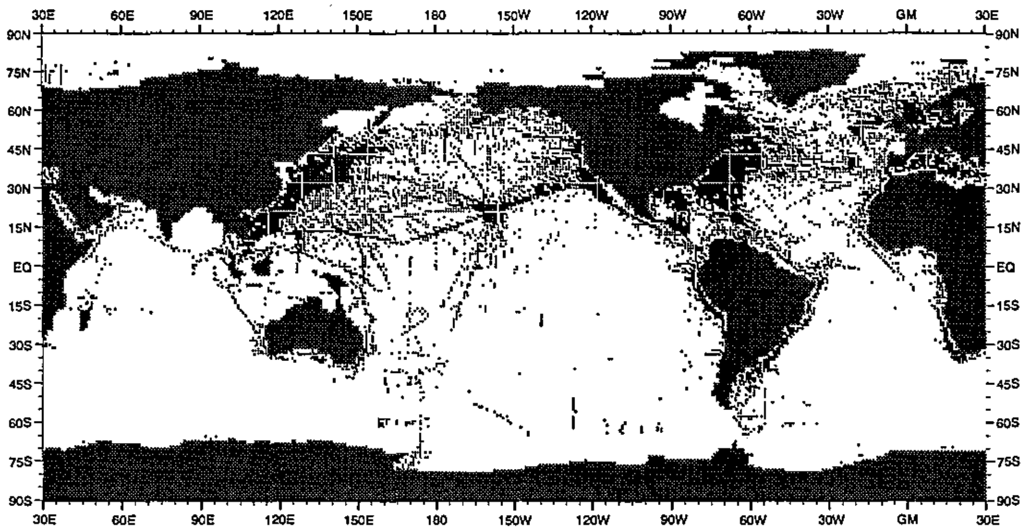


Fig. A19 Distribution of temperature observations at the surface for year 1966

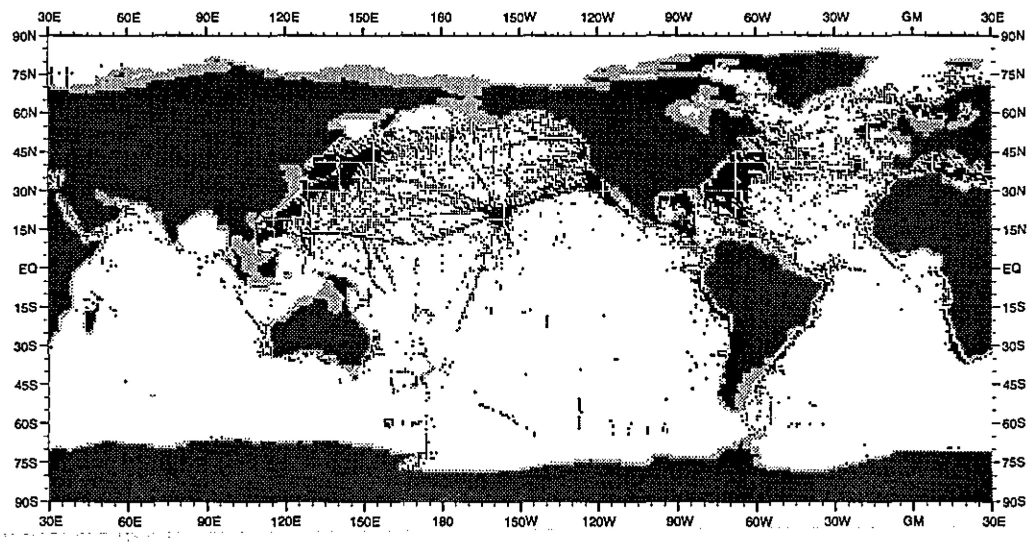


Fig. A20 Distribution of temperature observations at 125 m depth for year 1966

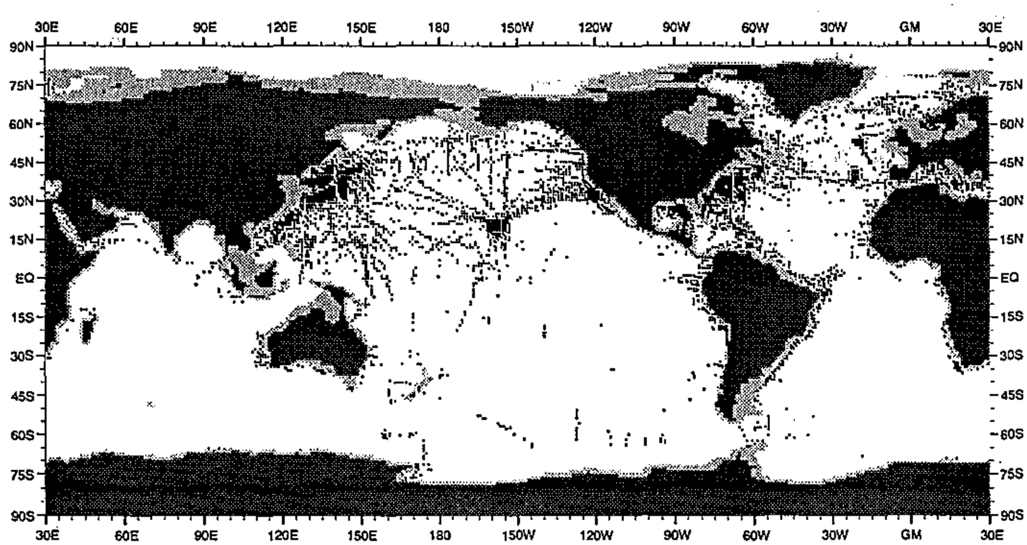


Fig. A21 Distribution of temperature observations at 250 m depth for year 1966

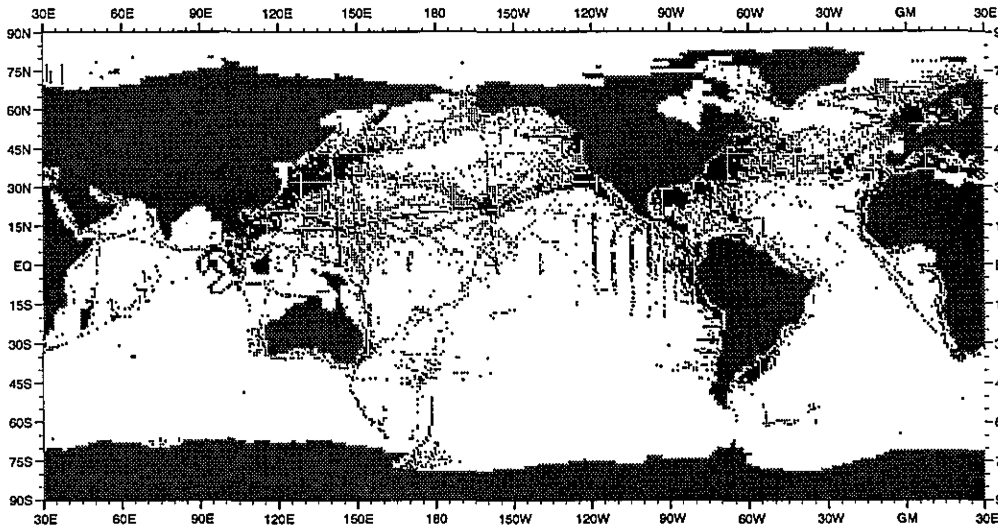


Fig. A22 Distribution of temperature observations at the surface for year 1967

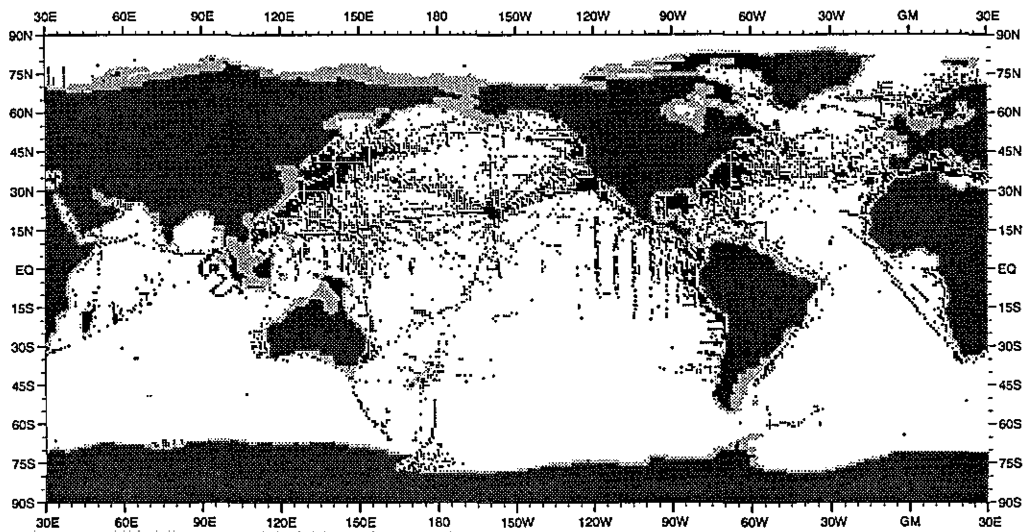


Fig. A23 Distribution of temperature observations at 125 m depth for year 1967

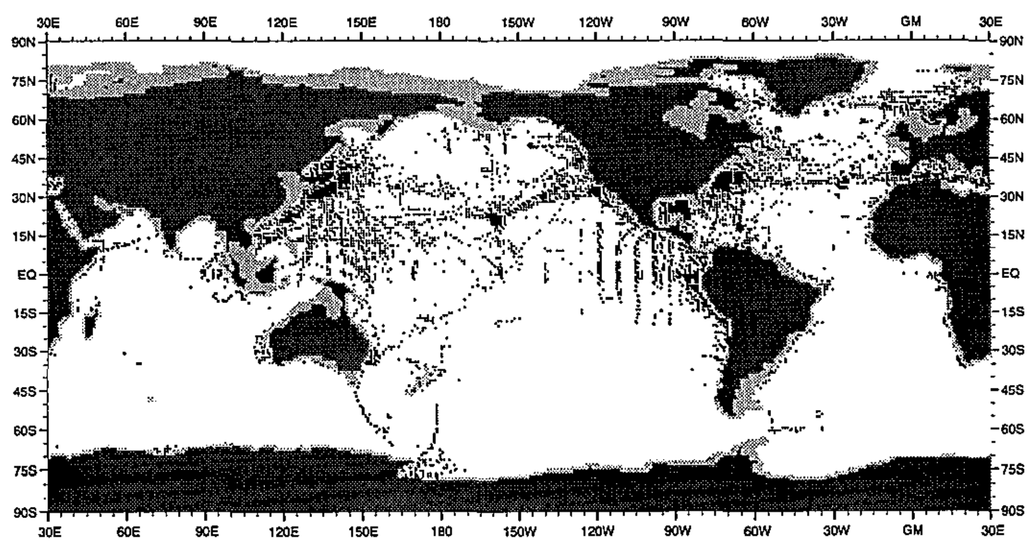


Fig. A24 Distribution of temperature observations at 250 m depth for year 1967

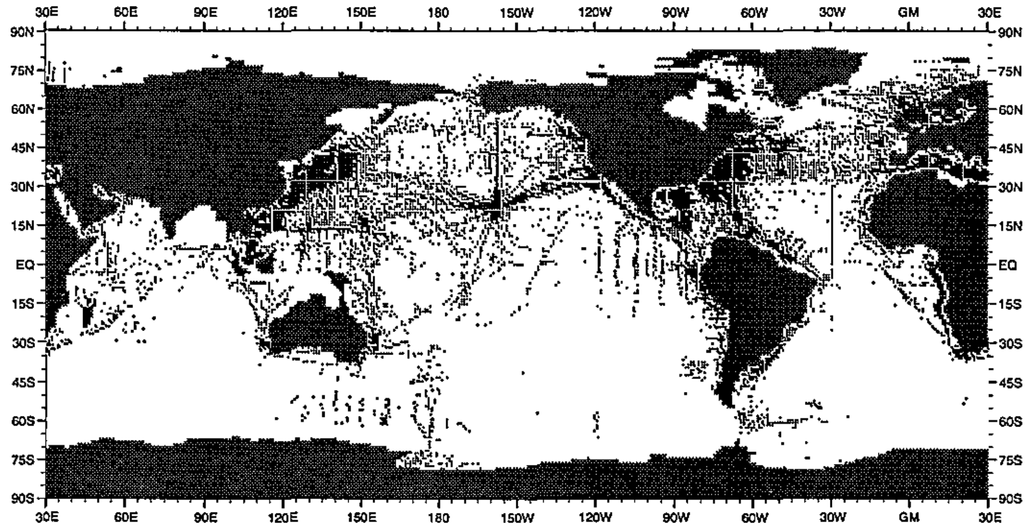


Fig. A25 Distribution of temperature observations at the surface for year 1968

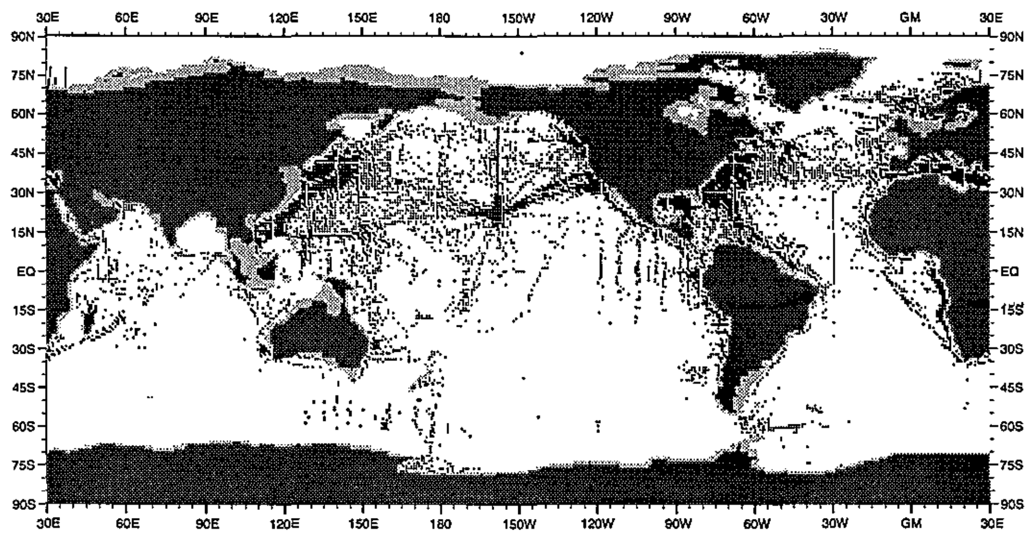


Fig. A26 Distribution of temperature observations at 125 m depth for year 1968

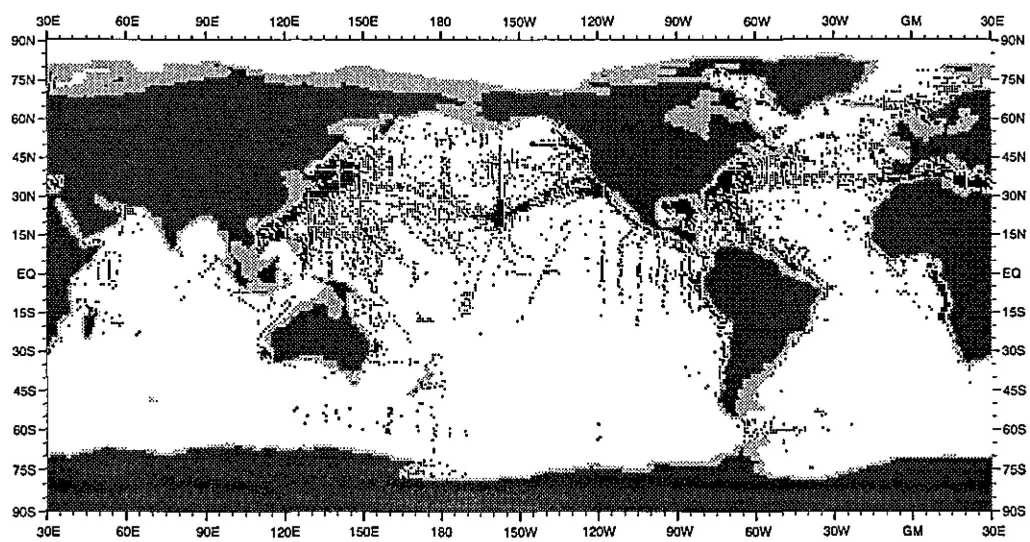


Fig. A27 Distribution of temperature observations at 250 m depth for year 1968

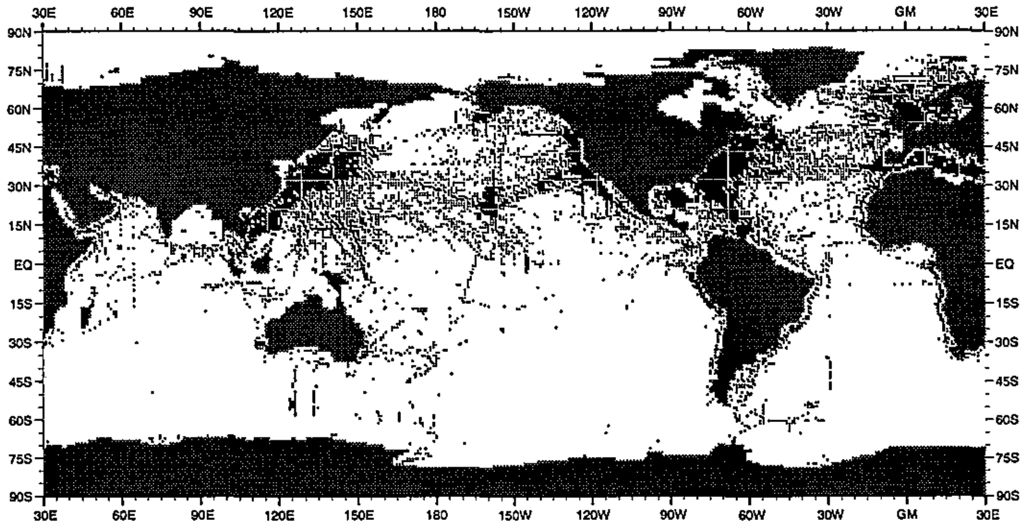


Fig. A28 Distribution of temperature observations at the surface for year 1969

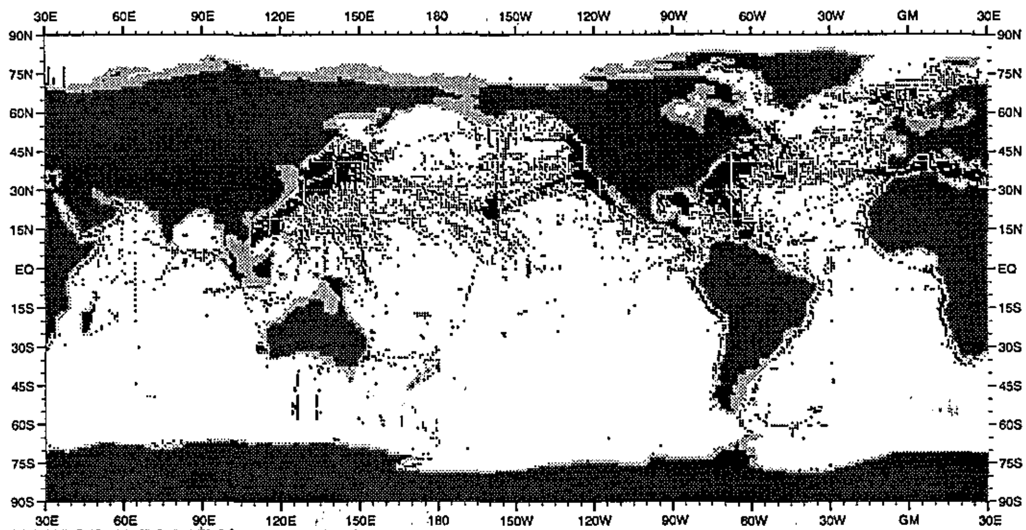


Fig. A29 Distribution of temperature observations at 125 m depth for year 1969

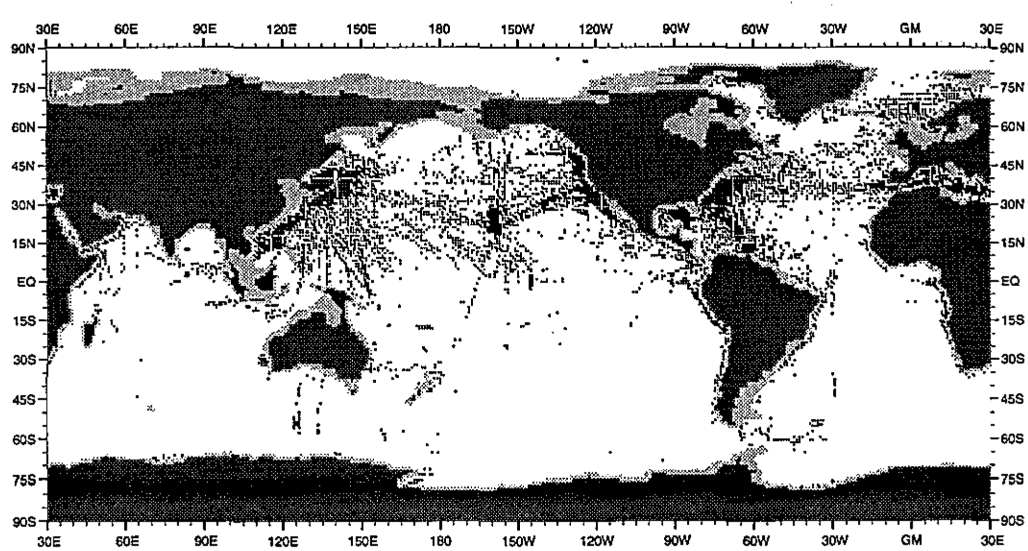


Fig. A30 Distribution of temperature observations at 250 m depth for year 1969

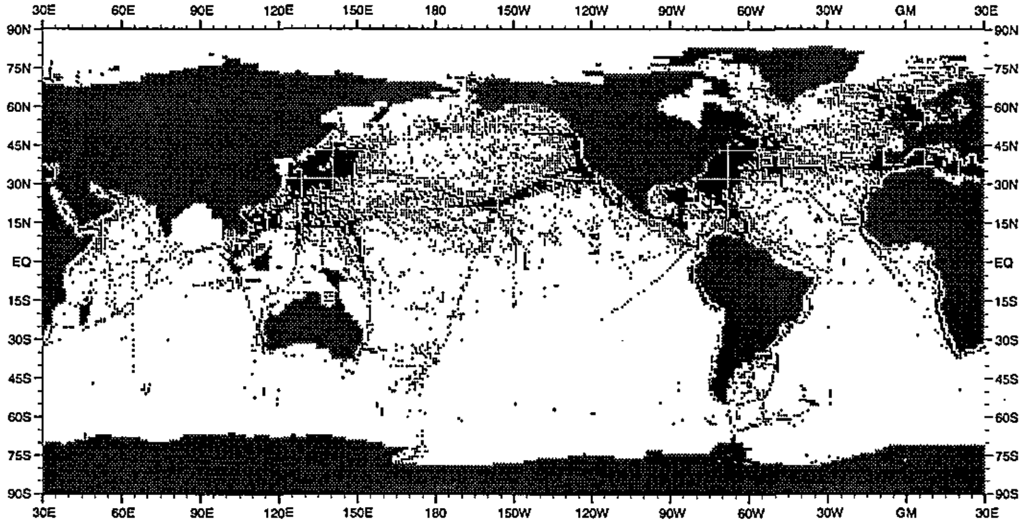


Fig. A31 Distribution of temperature observations at the surface for year 1970

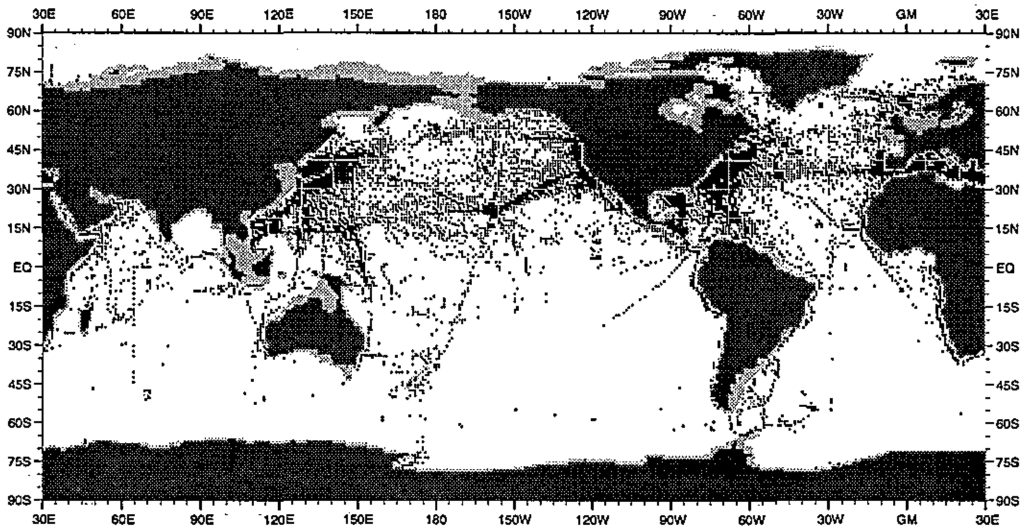


Fig. A32 Distribution of temperature observations at 125 m depth for year 1970

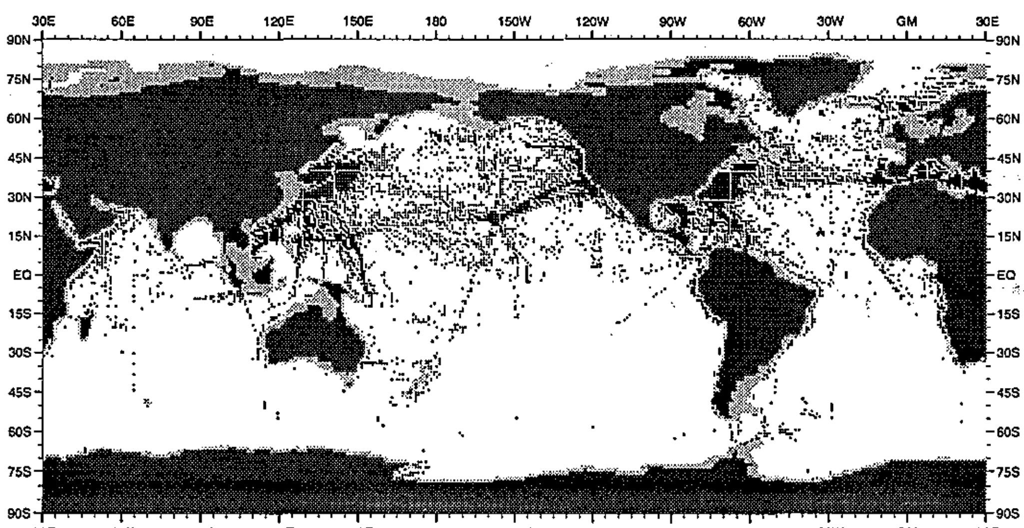


Fig. A33 Distribution of temperature observations at 250 m depth for year 1970

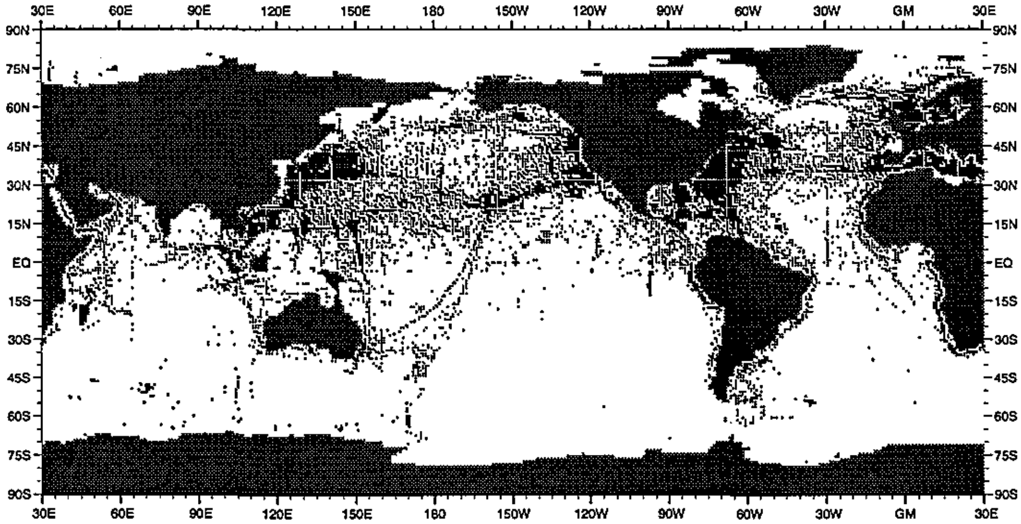


Fig. A34 Distribution of temperature observations at the surface for year 1971

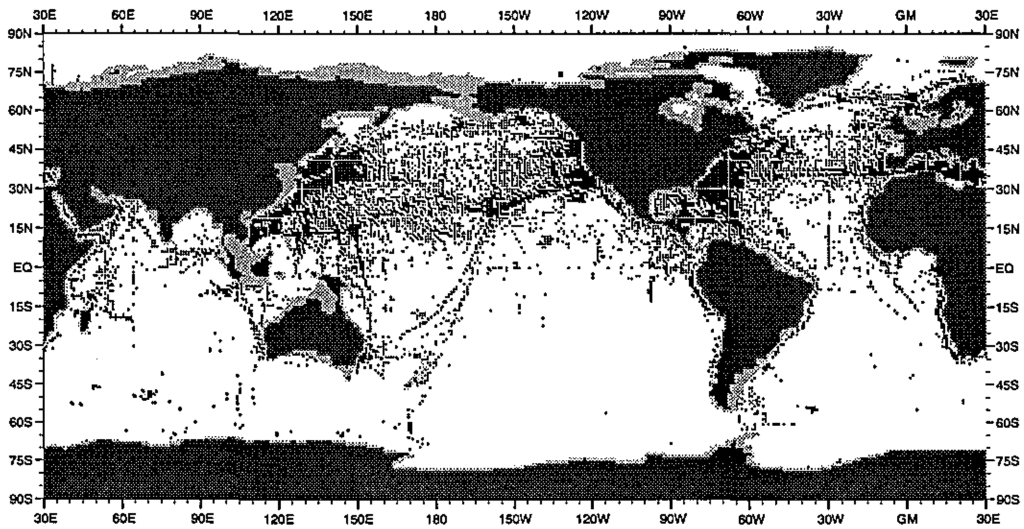


Fig. A35 Distribution of temperature observations at 125 m depth for year 1971

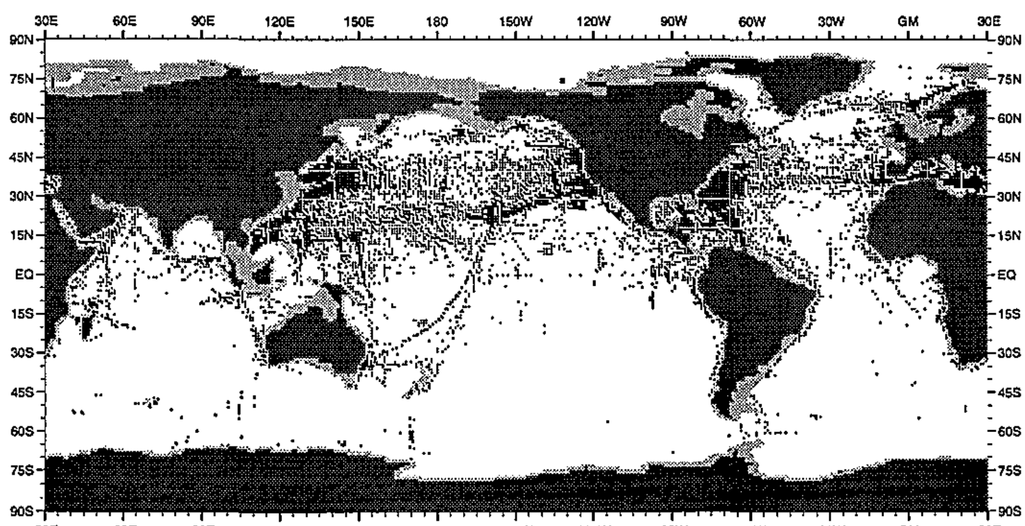


Fig. A36 Distribution of temperature observations at 250 m depth for year 1971

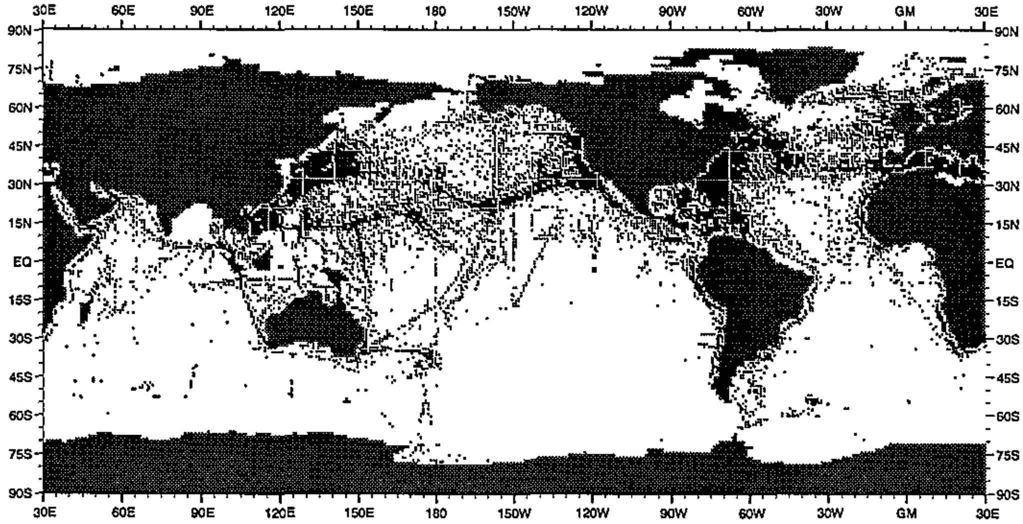


Fig. A37 Distribution of temperature observations at the surface for year 1972

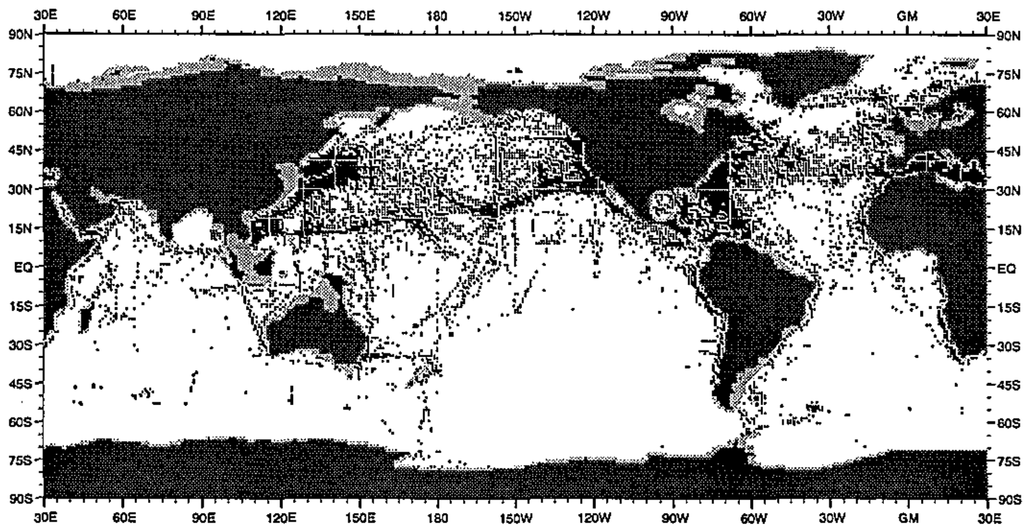


Fig. A38 Distribution of temperature observations at 125 m depth for year 1972

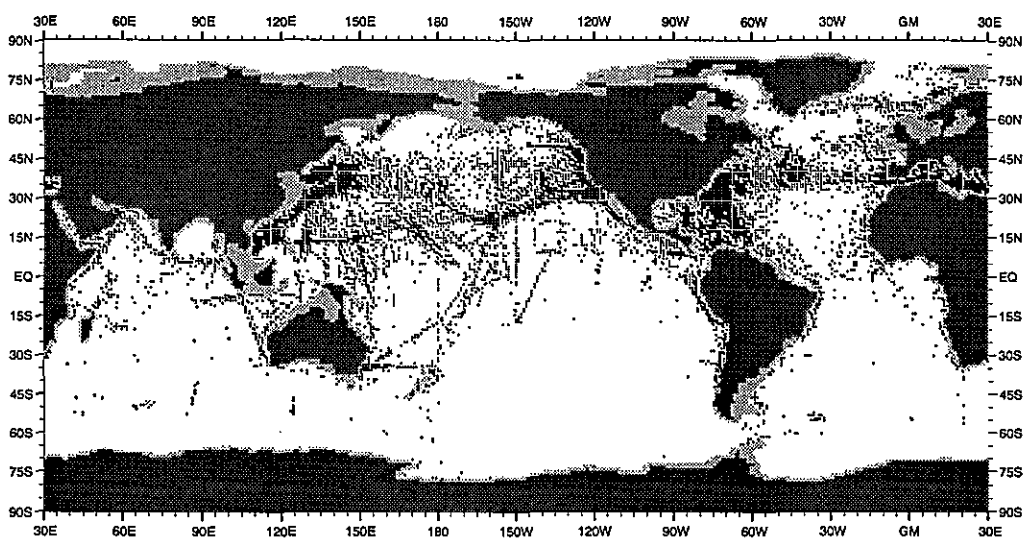


Fig. A39 Distribution of temperature observations at 250 m depth for year 1972

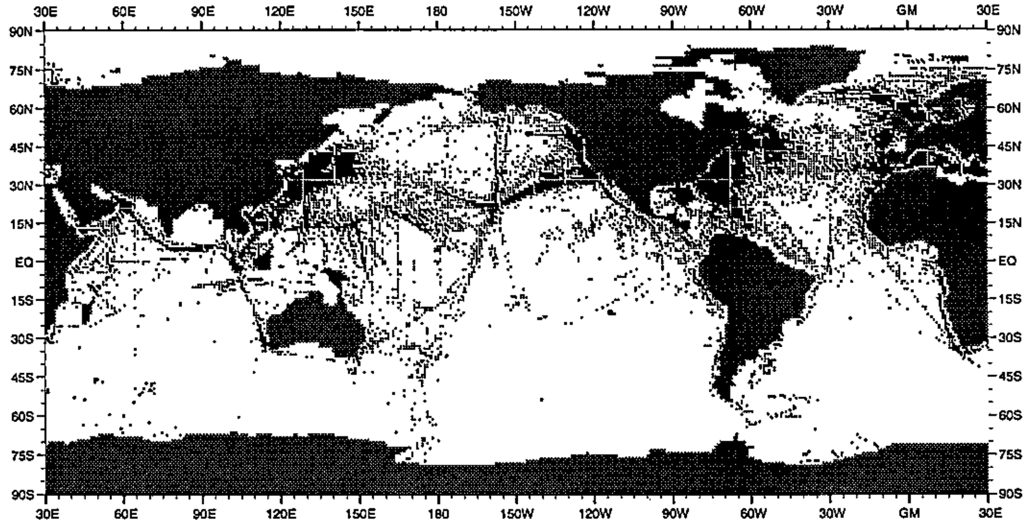


Fig. A40 Distribution of temperature observations at the surface for year 1973

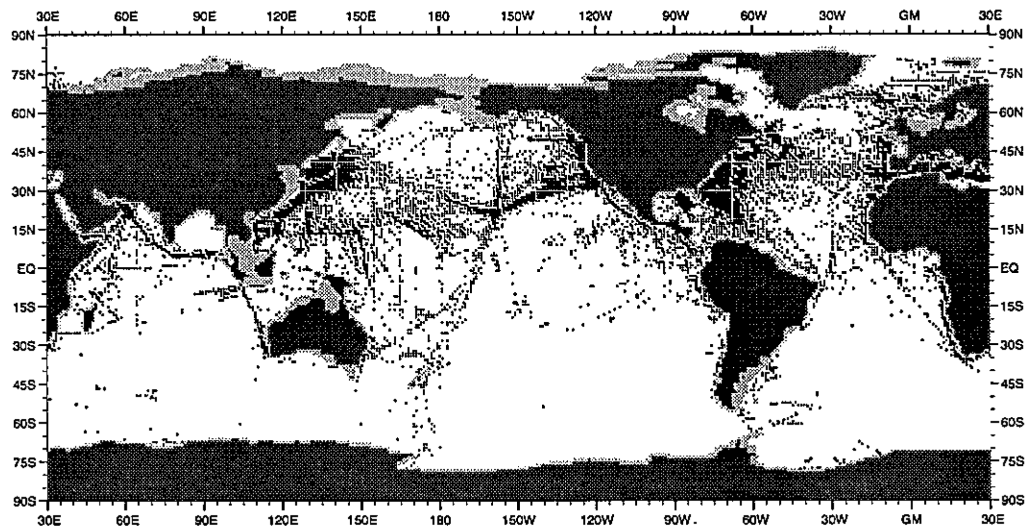


Fig. A41 Distribution of temperature observations at 125 m depth for year 1973

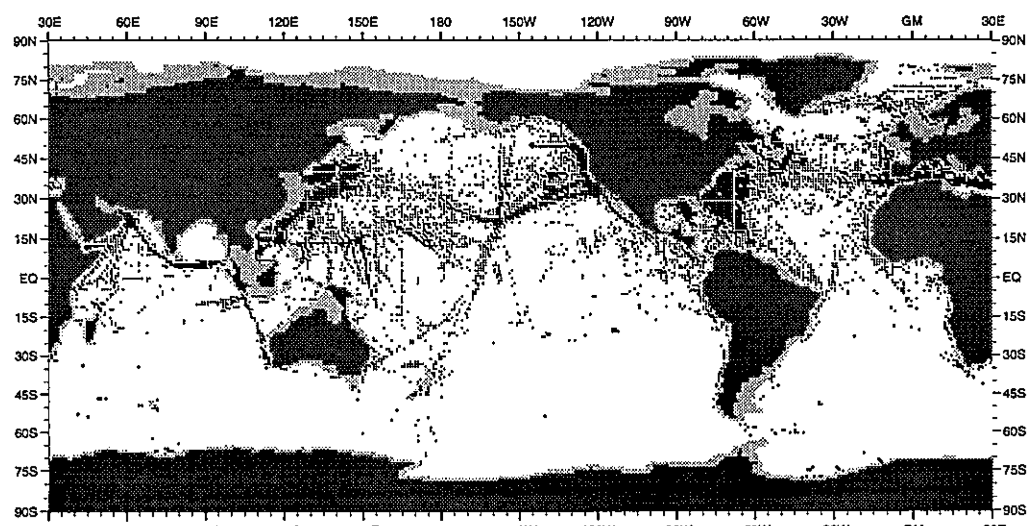


Fig. A42 Distribution of temperature observations at 250 m depth for year 1973

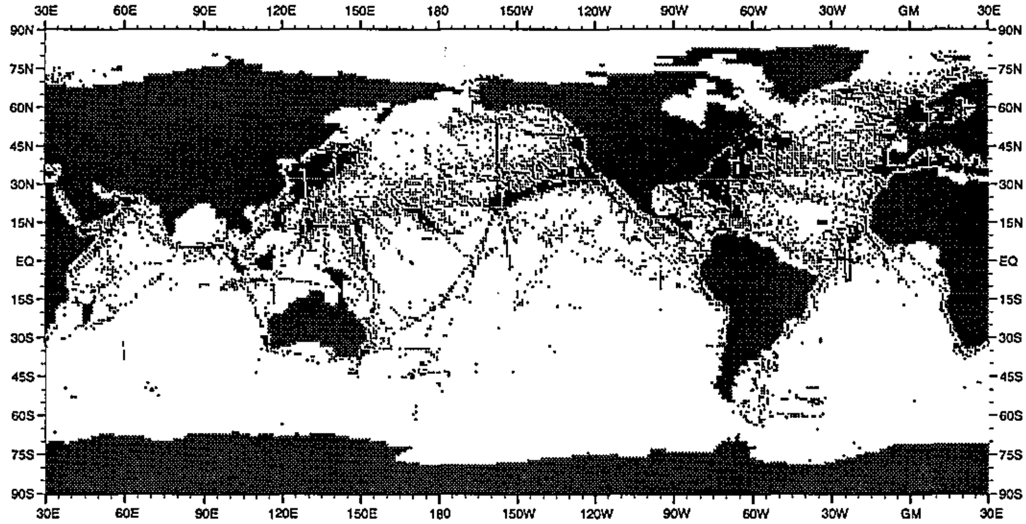


Fig. A43 Distribution of temperature observations at the surface for year 1974

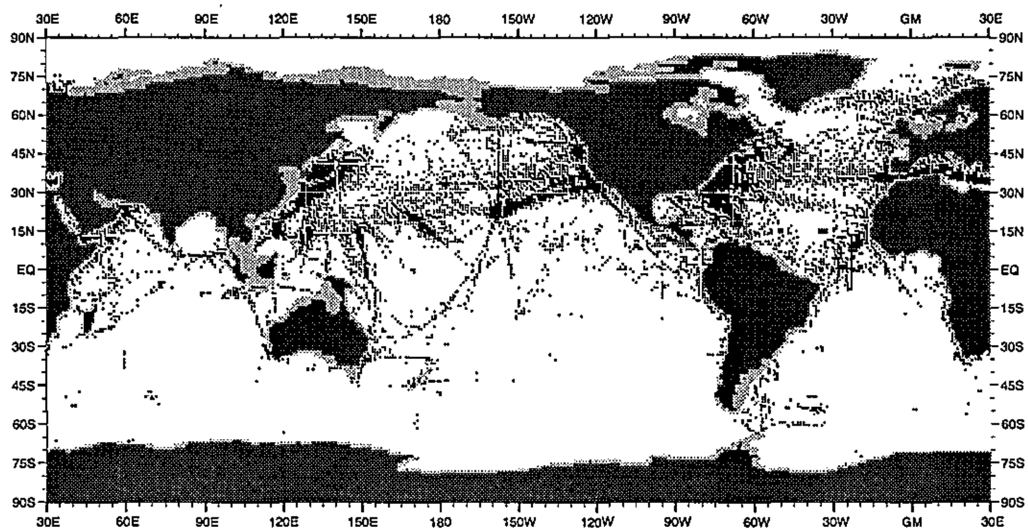


Fig. A44 Distribution of temperature observations at 125 m depth for year 1974

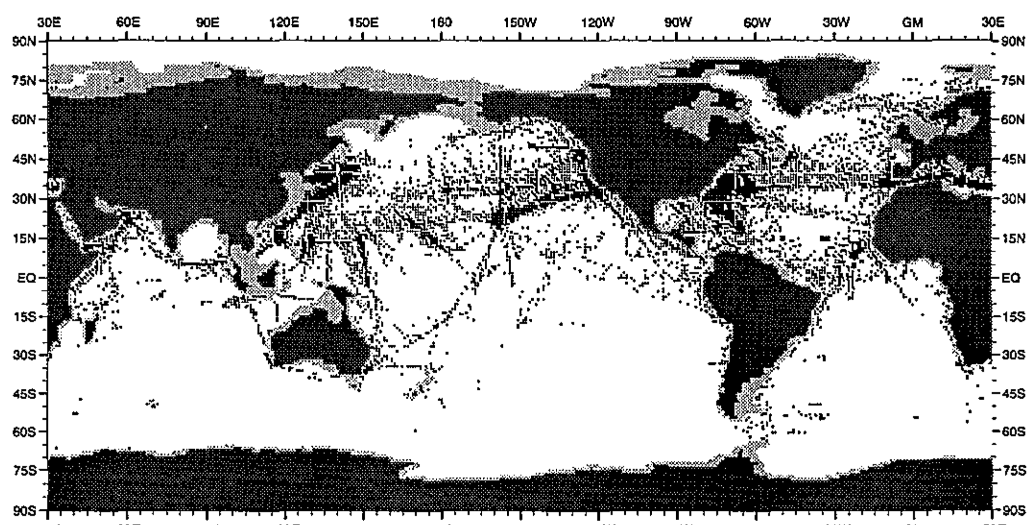


Fig. A45 Distribution of temperature observations at 250 m depth for year 1974

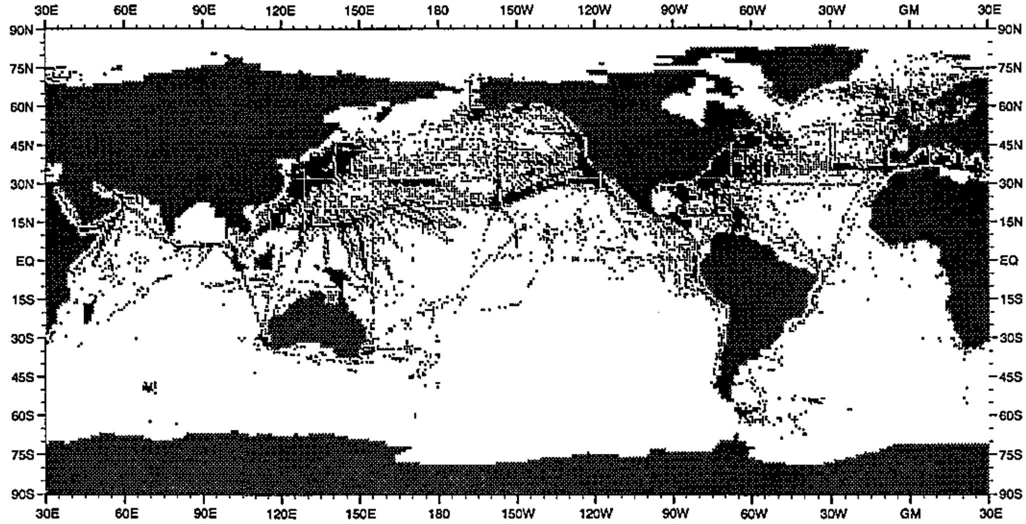


Fig. A46 Distribution of temperature observations at the surface for year 1975

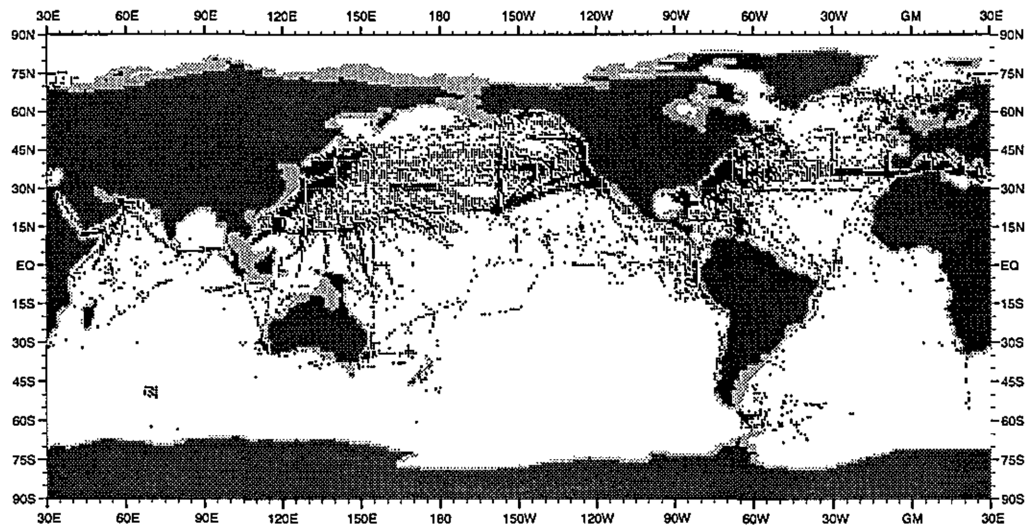


Fig. A47 Distribution of temperature observations at 125 m depth for year 1975

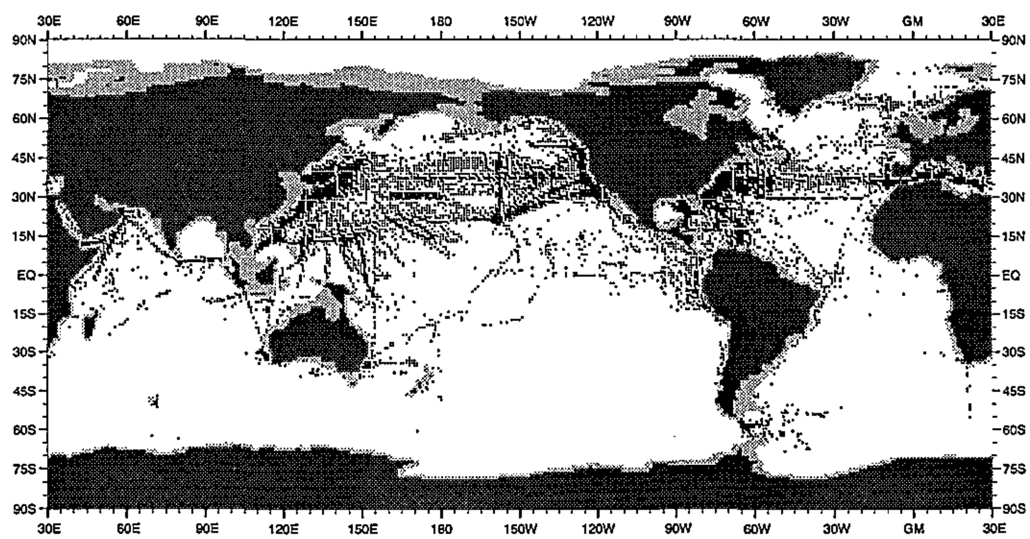


Fig. A48 Distribution of temperature observations at 250 m depth for year 1975

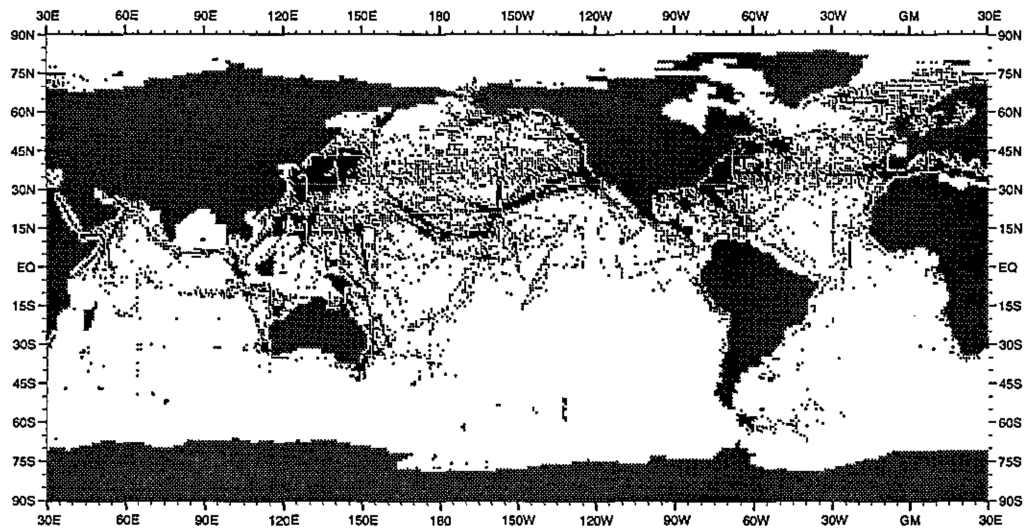


Fig. A49 Distribution of temperature observations at the surface for year 1976

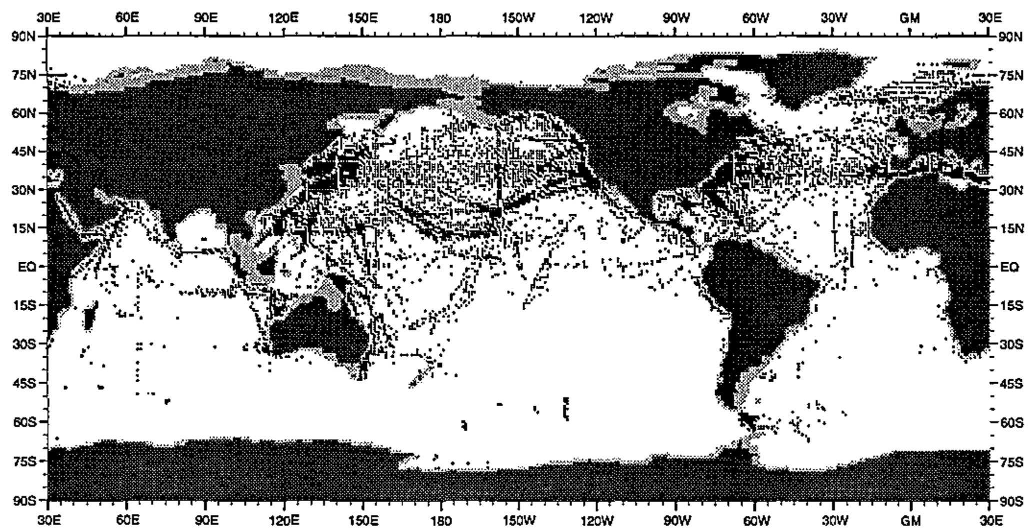


Fig. A50 Distribution of temperature observations at 125 m depth for year 1976

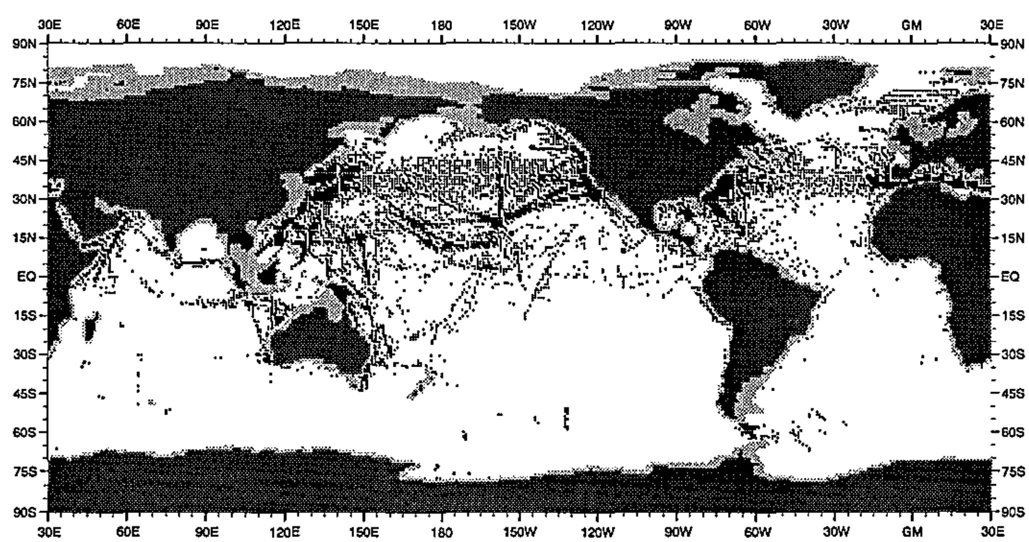


Fig. A51 Distribution of temperature observations at 250 m depth for year 1976

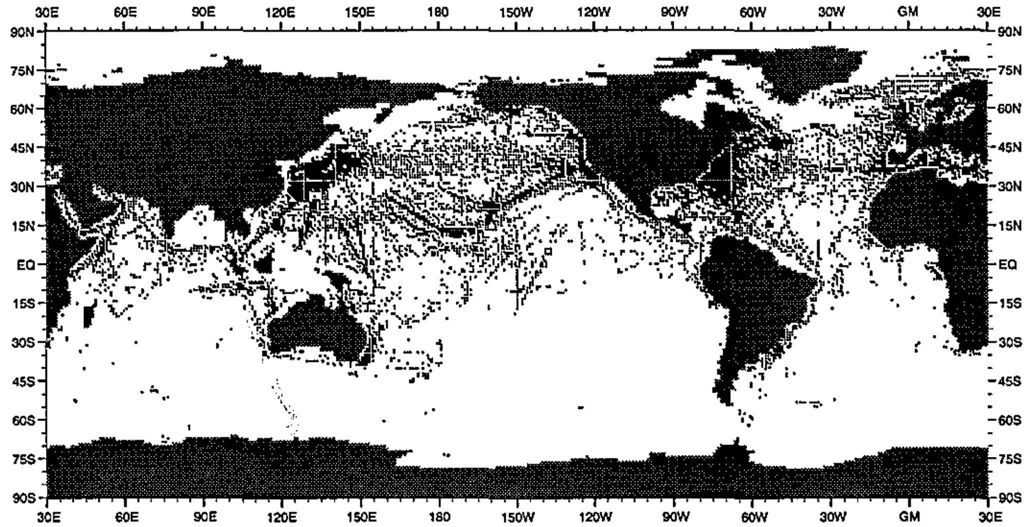


Fig. A52 Distribution of temperature observations at the surface for year 1977

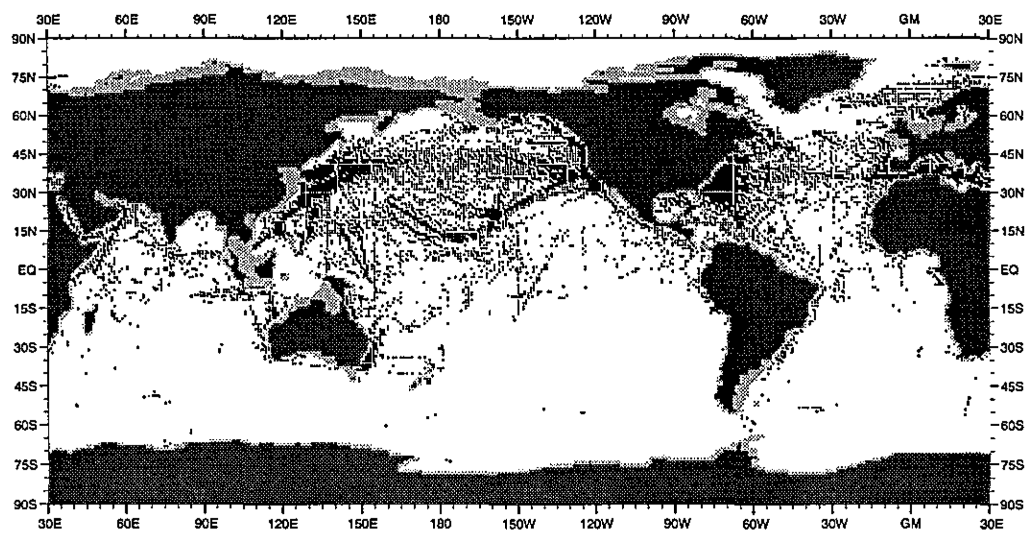


Fig. A53 Distribution of temperature observations at 125 m depth for year 1977

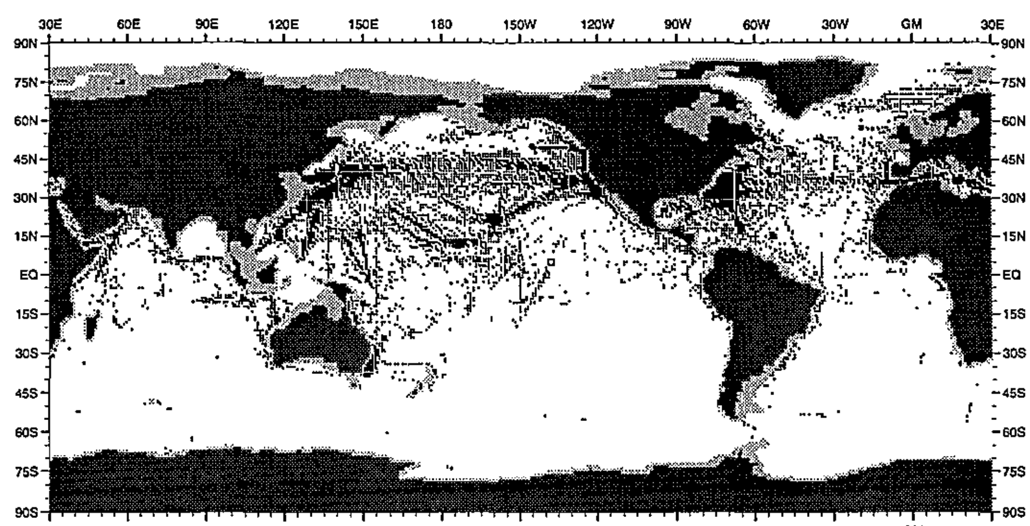


Fig. A54 Distribution of temperature observations at 250 m depth for year 1977

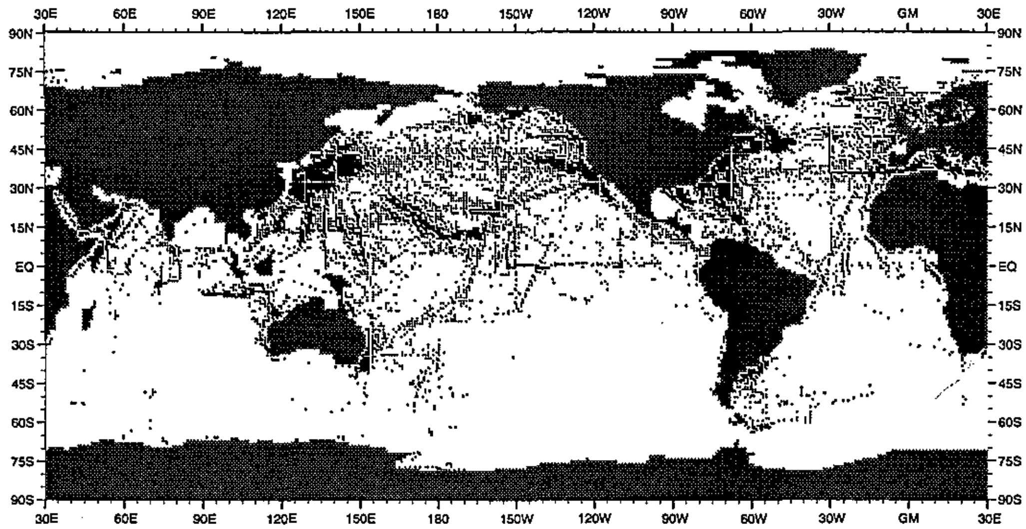


Fig. A55 Distribution of temperature observations at the surface for year 1978

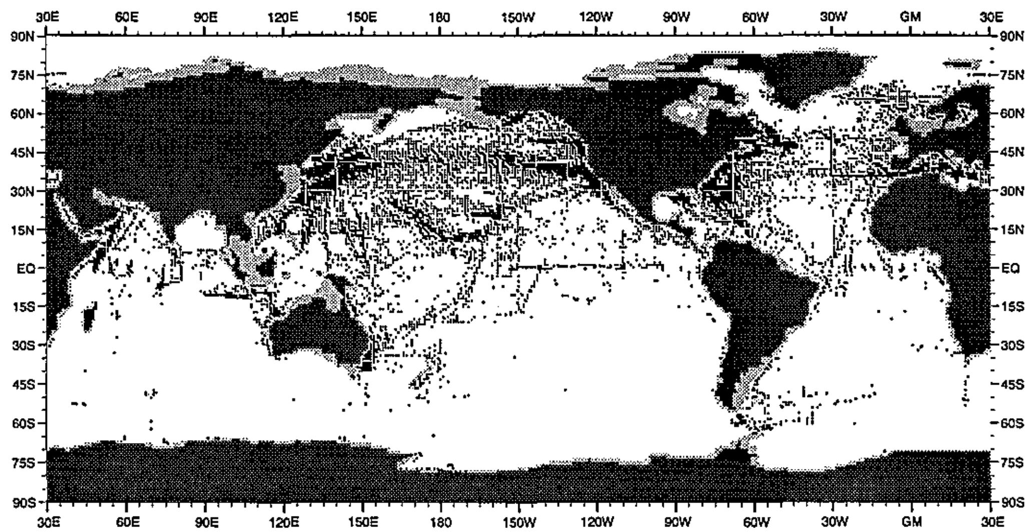


Fig. A56 Distribution of temperature observations at 125 m depth for year 1978

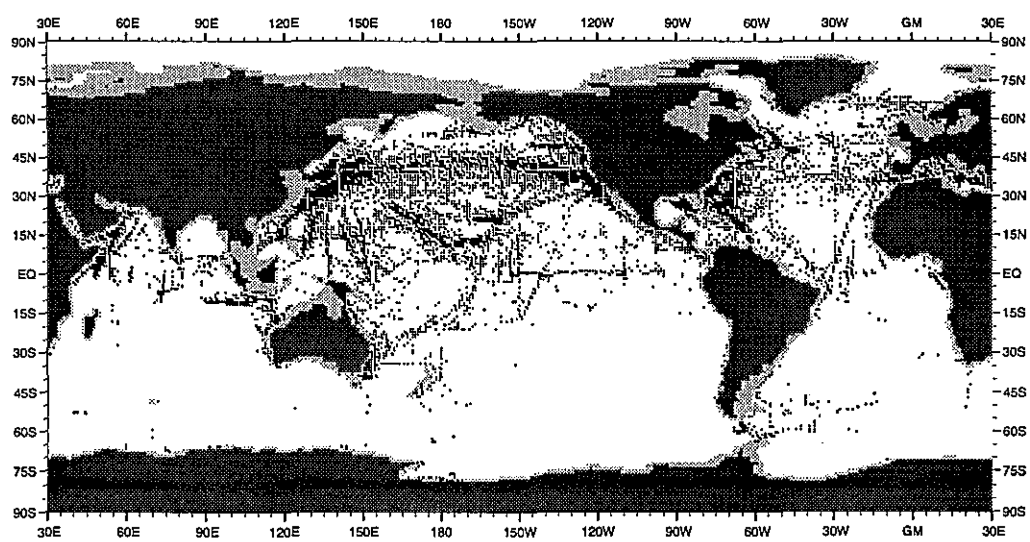


Fig. A57 Distribution of temperature observations at 250 m depth for year 1978

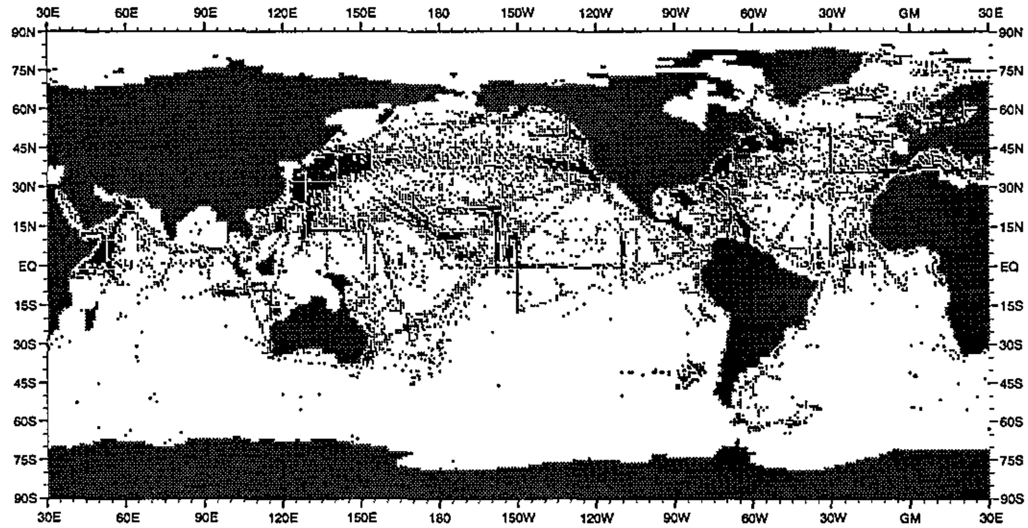


Fig. A58 Distribution of temperature observations at the surface for year 1979

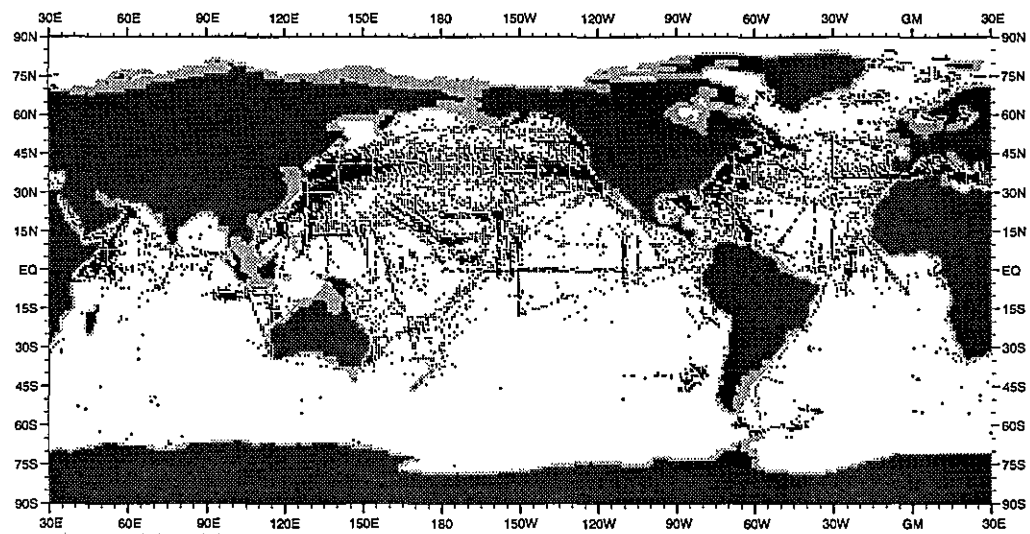


Fig. A59 Distribution of temperature observations at 125 m depth for year 1979

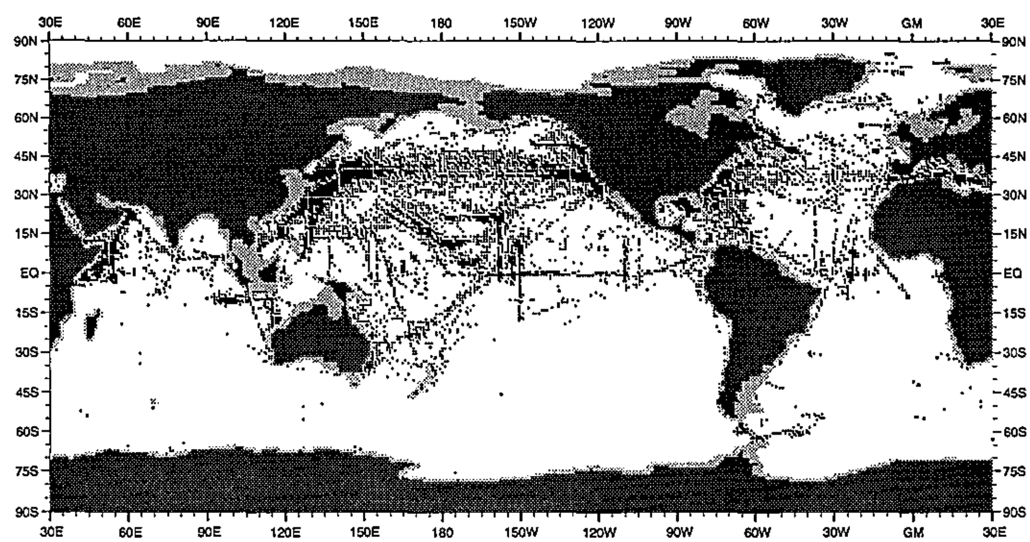


Fig. A60 Distribution of temperature observations at 250 m depth for year 1979

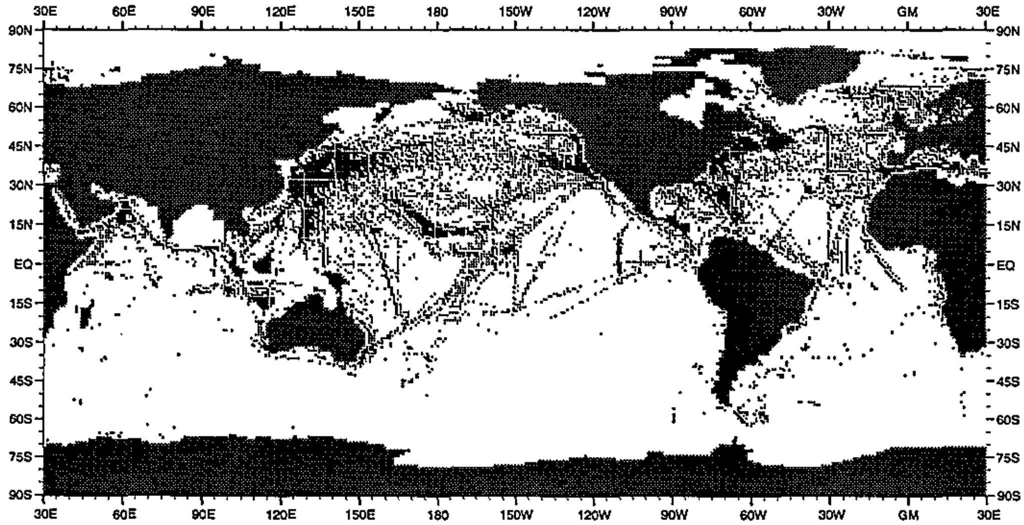


Fig. A61 Distribution of temperature observations at the surface for year 1980

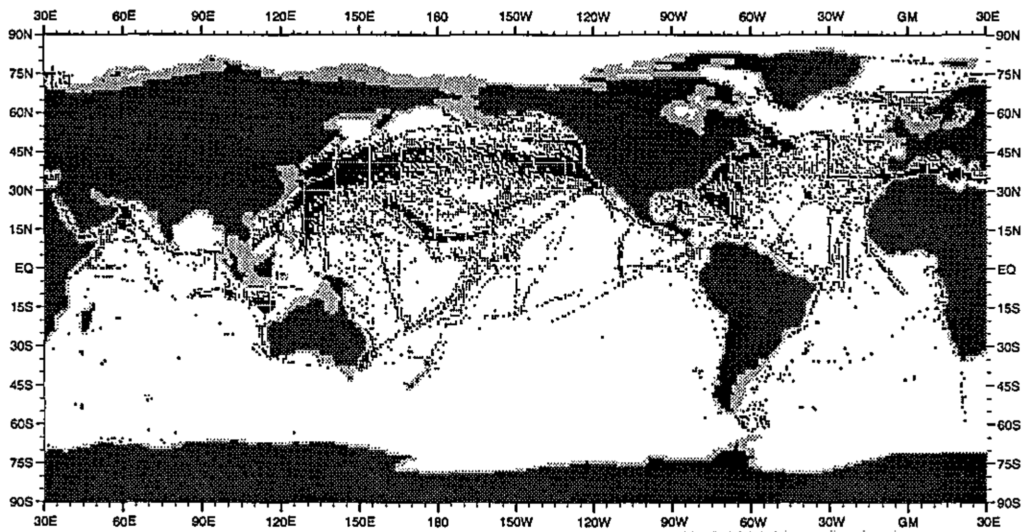


Fig. A62 Distribution of temperature observations at 125 m depth for year 1980

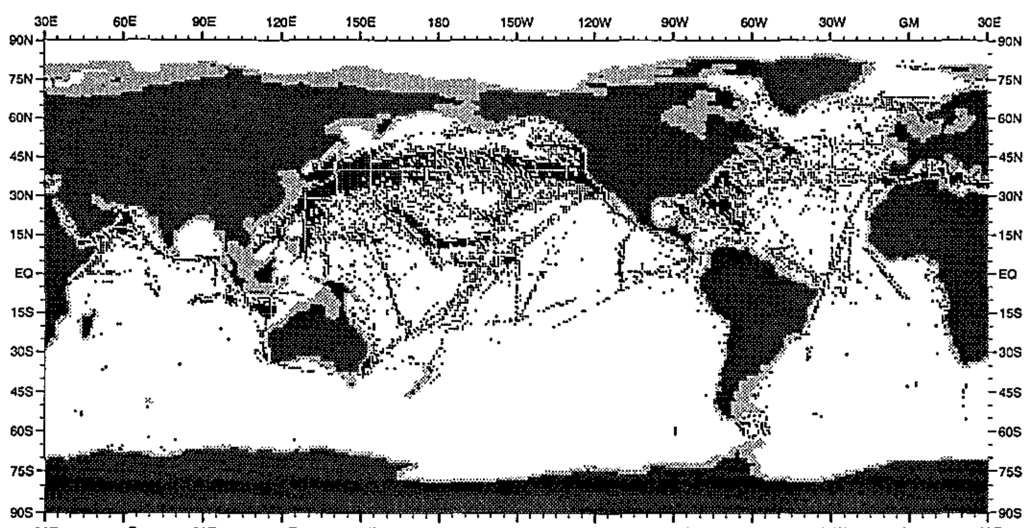


Fig. A63 Distribution of temperature observations at 250 m depth for year 1980

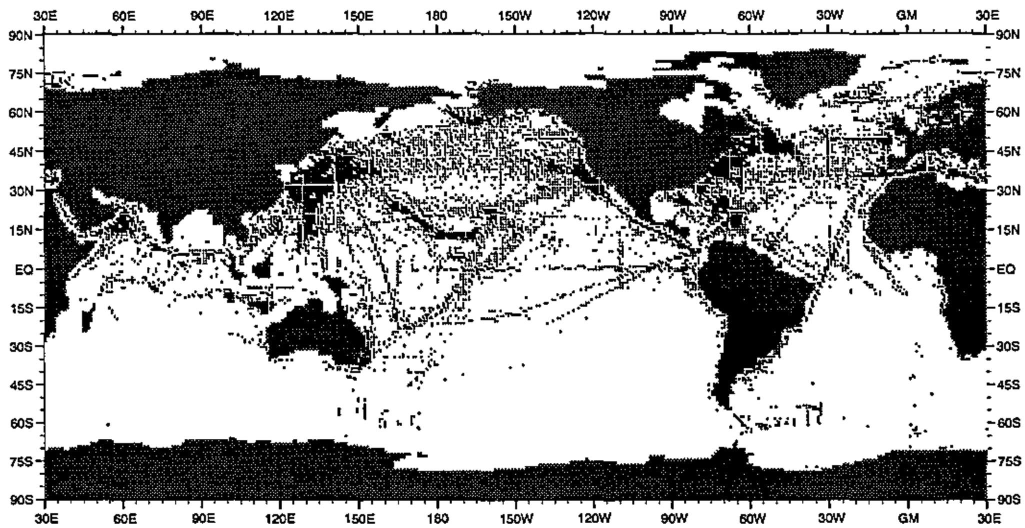


Fig. A64 Distribution of temperature observations at the surface for year 1981

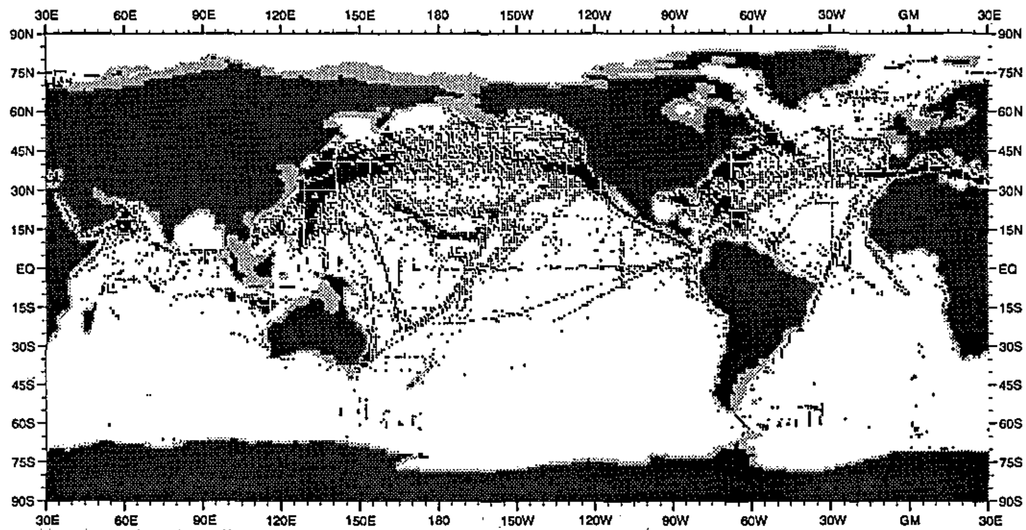


Fig. A65 Distribution of temperature observations at 125 m depth for year 1981

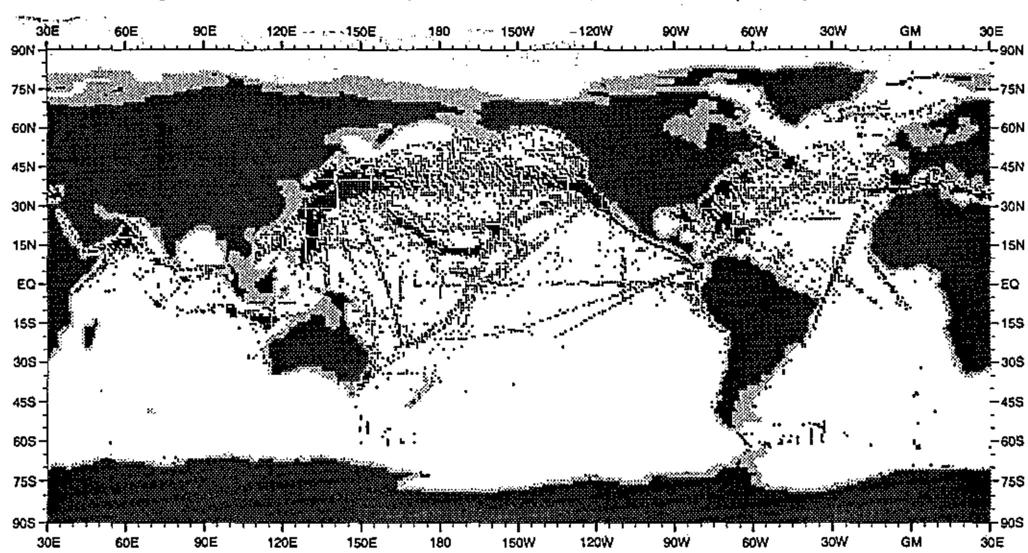


Fig. A66 Distribution of temperature observations at 250 m depth for year 1981

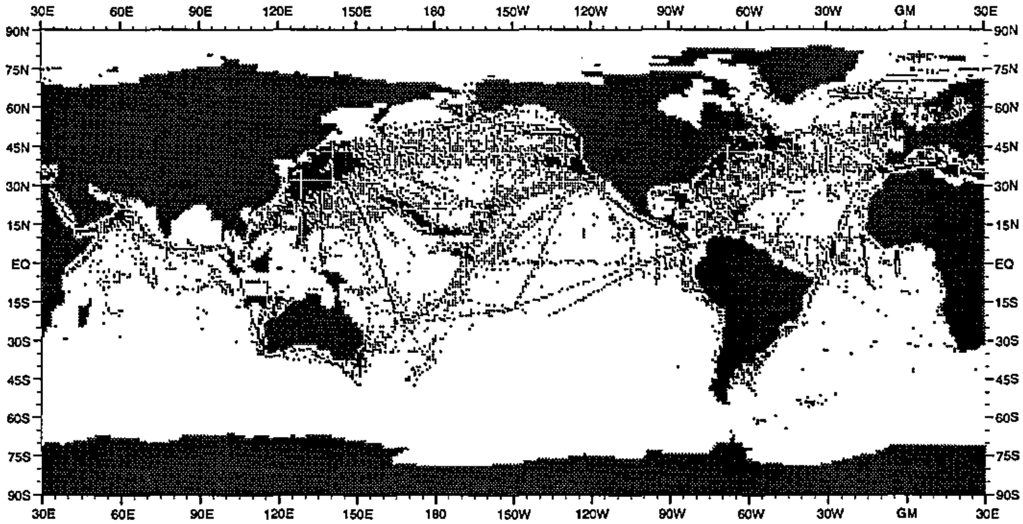


Fig. A67 Distribution of temperature observations at the surface for year 1982

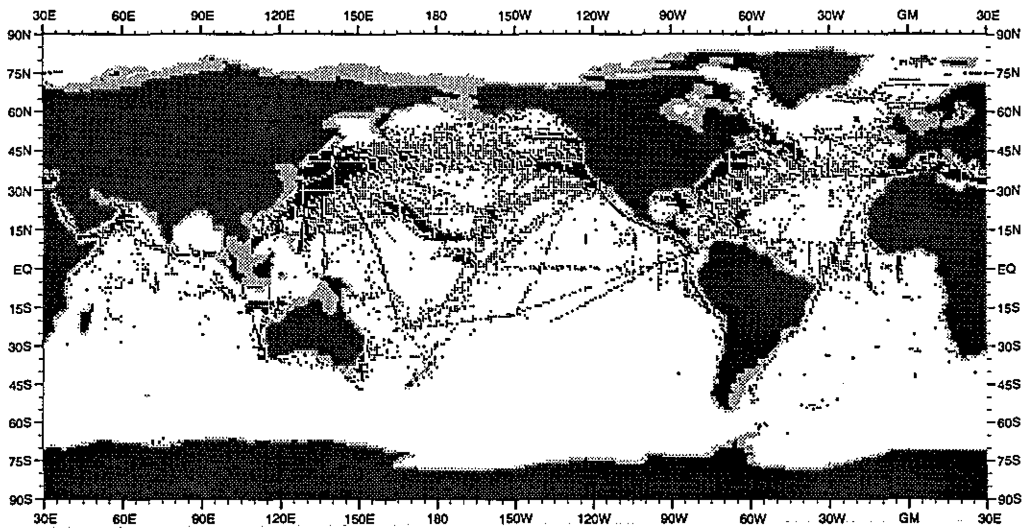


Fig. A68 Distribution of temperature observations at 125 m depth for year 1982

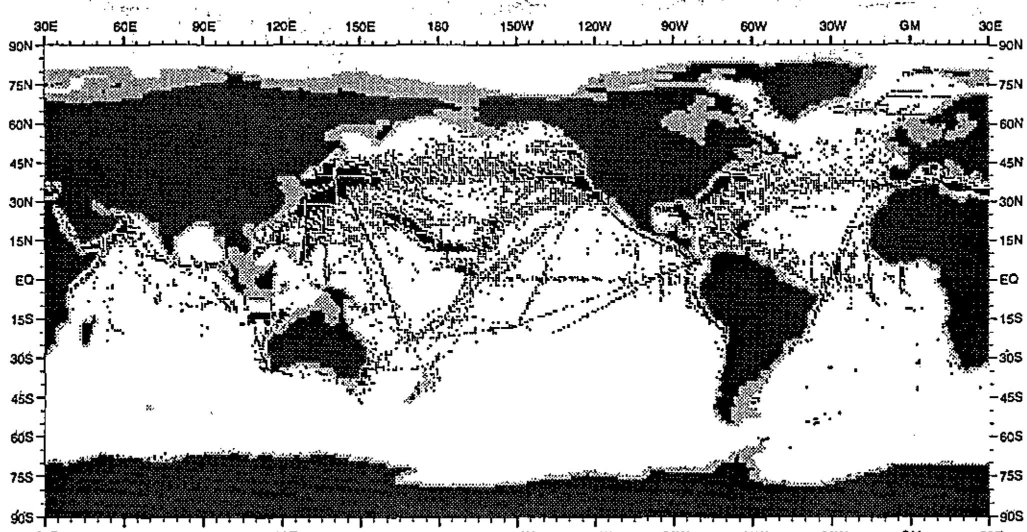


Fig. A69 Distribution of temperature observations at 250 m depth for year 1982

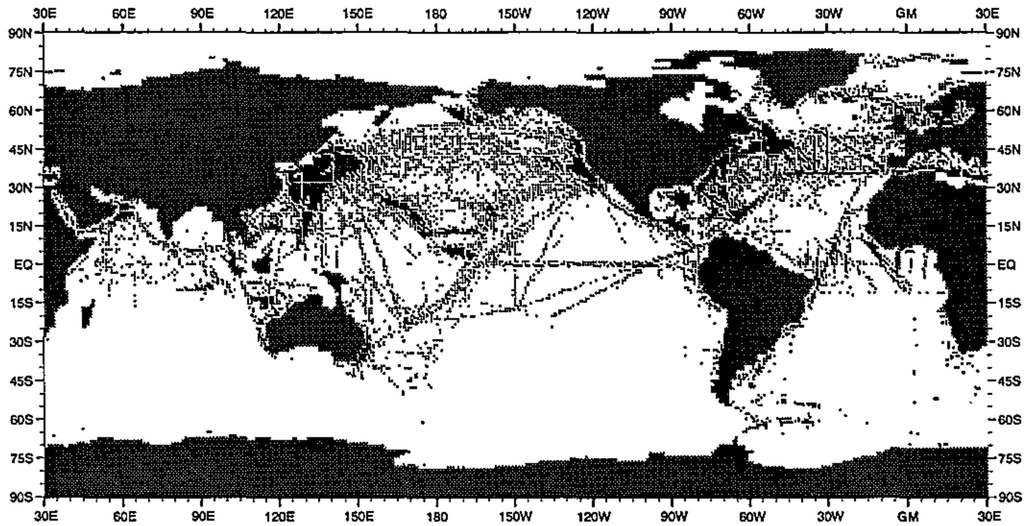


Fig. A70 Distribution of temperature observations at the surface for year 1983

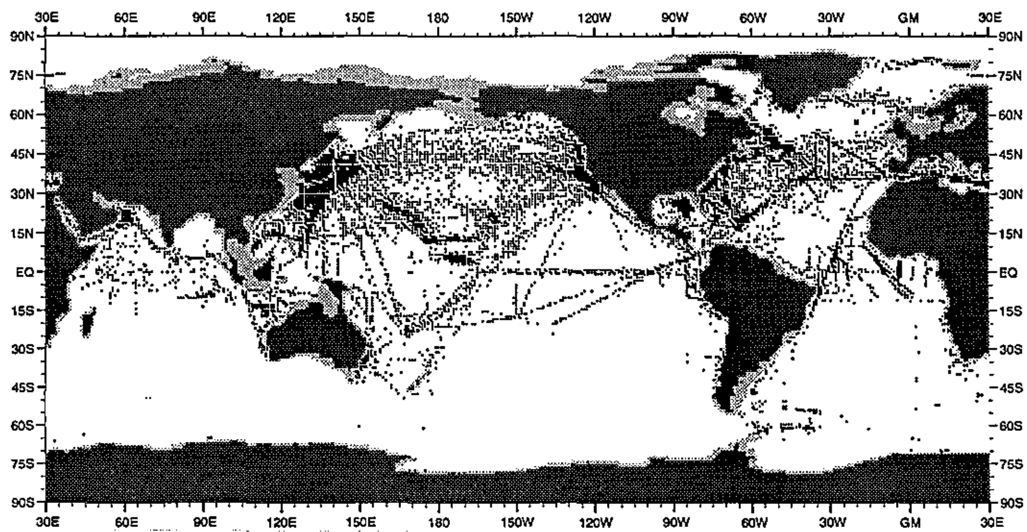


Fig. A71 Distribution of temperature observations at 125 m depth for year 1983

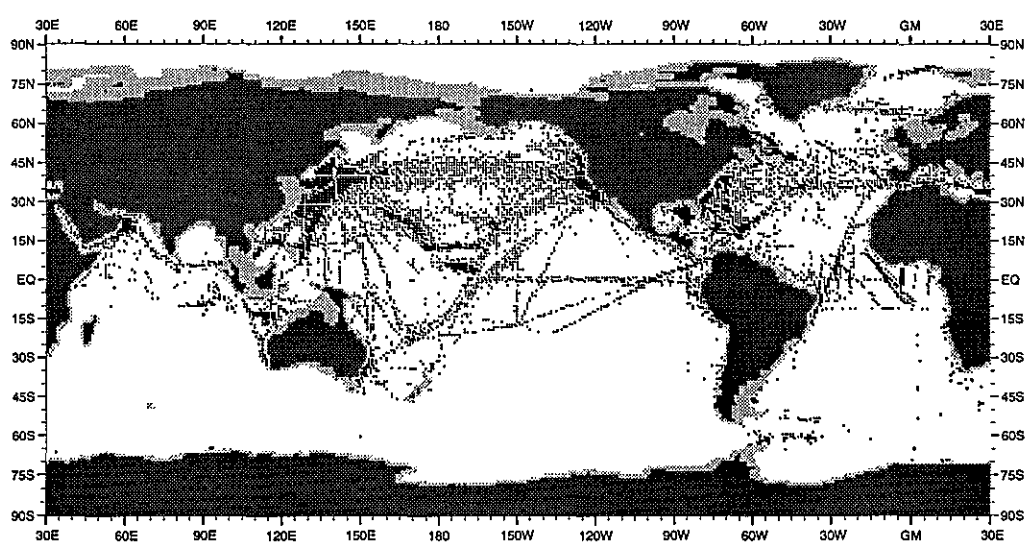


Fig. A72 Distribution of temperature observations at 250 m depth for year 1983

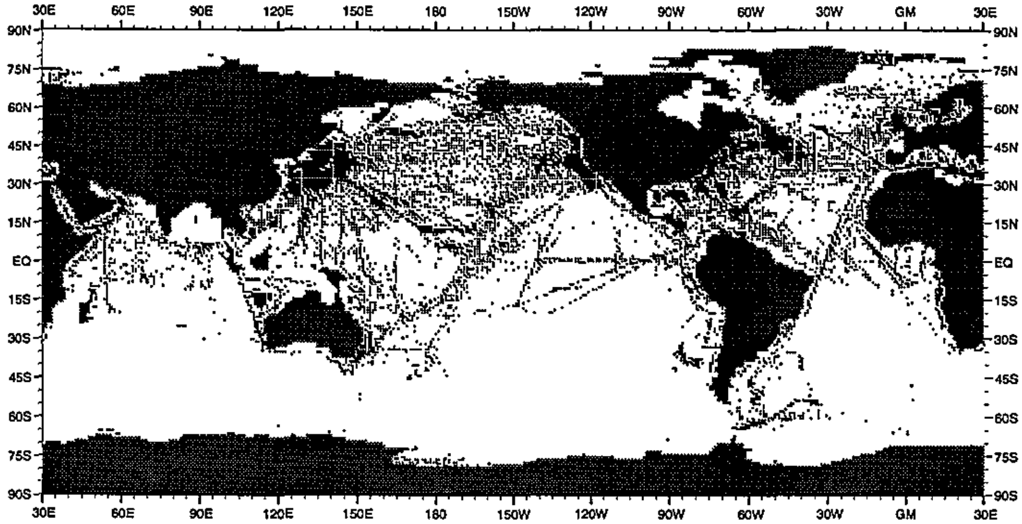


Fig. A73 Distribution of temperature observations at the surface for year 1984

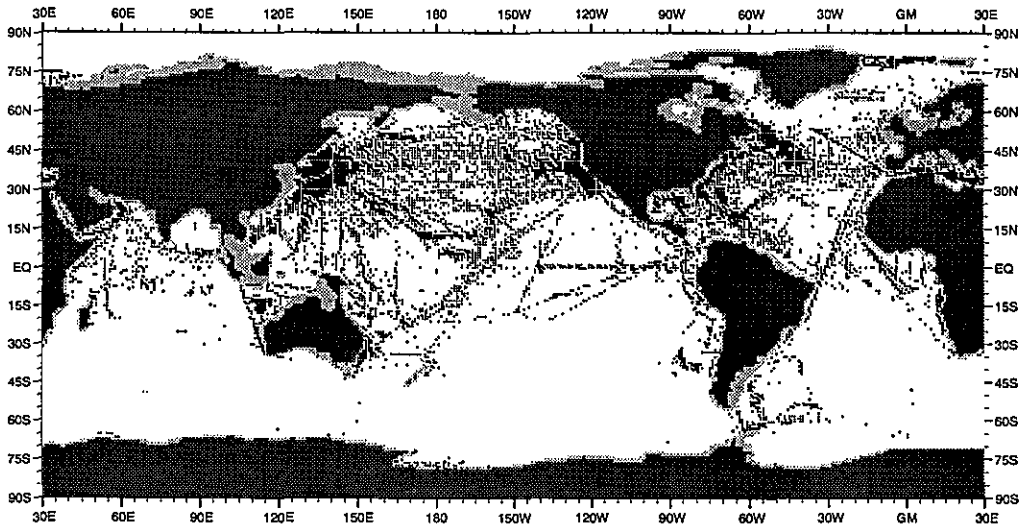


Fig. A74 Distribution of temperature observations at 125 m depth for year 1984

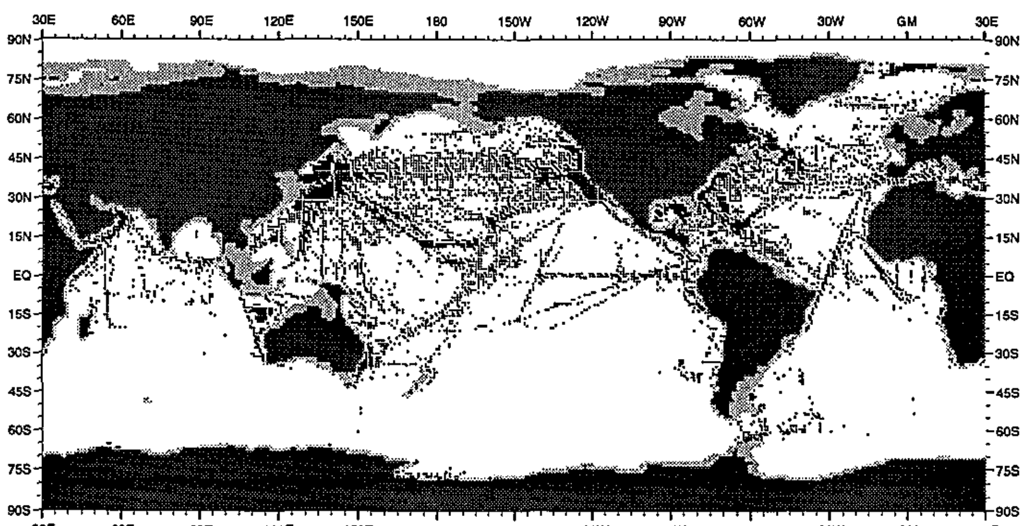


Fig. A75 Distribution of temperature observations at 250 m depth for year 1984

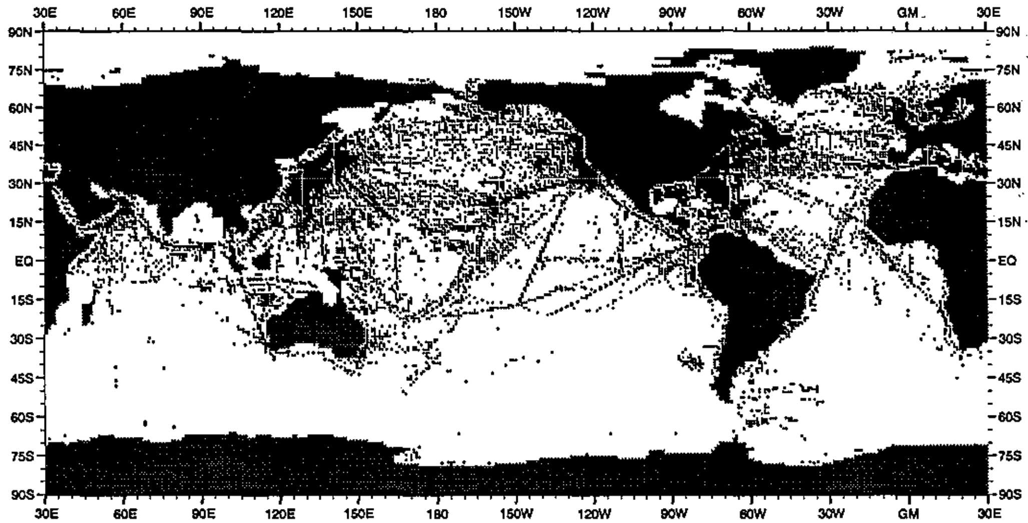


Fig. A76 Distribution of temperature observations at the surface for year 1985

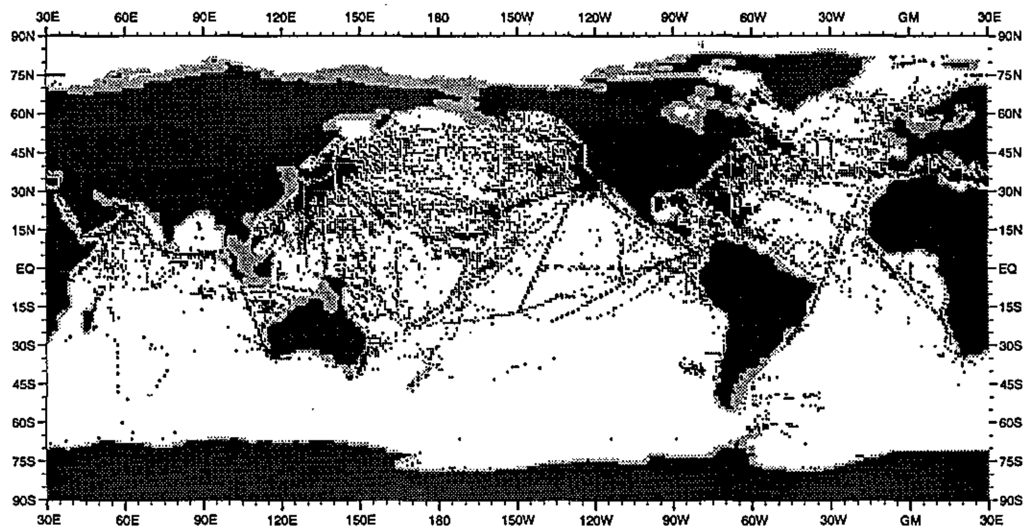


Fig. A77 Distribution of temperature observations at 125 m depth for year 1985

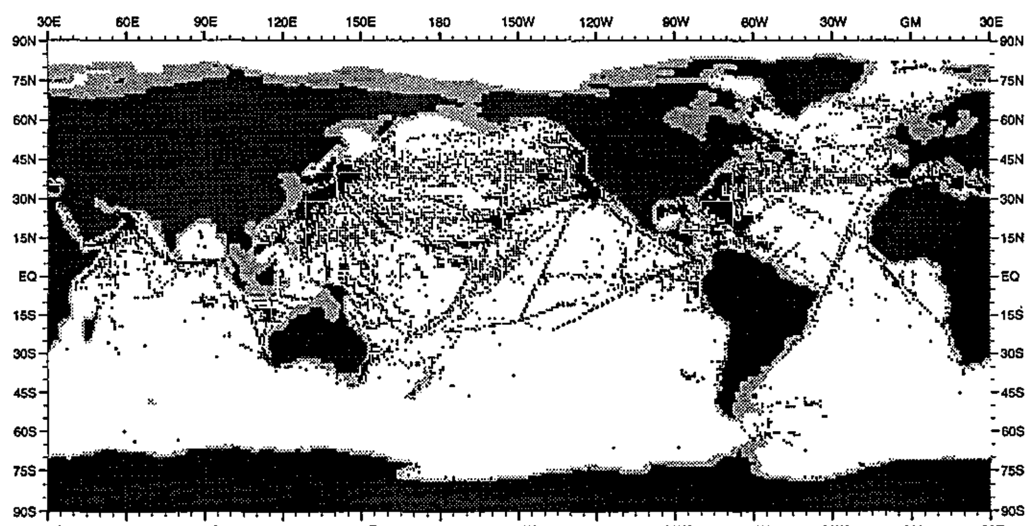


Fig. A78 Distribution of temperature observations at 250 m depth for year 1985

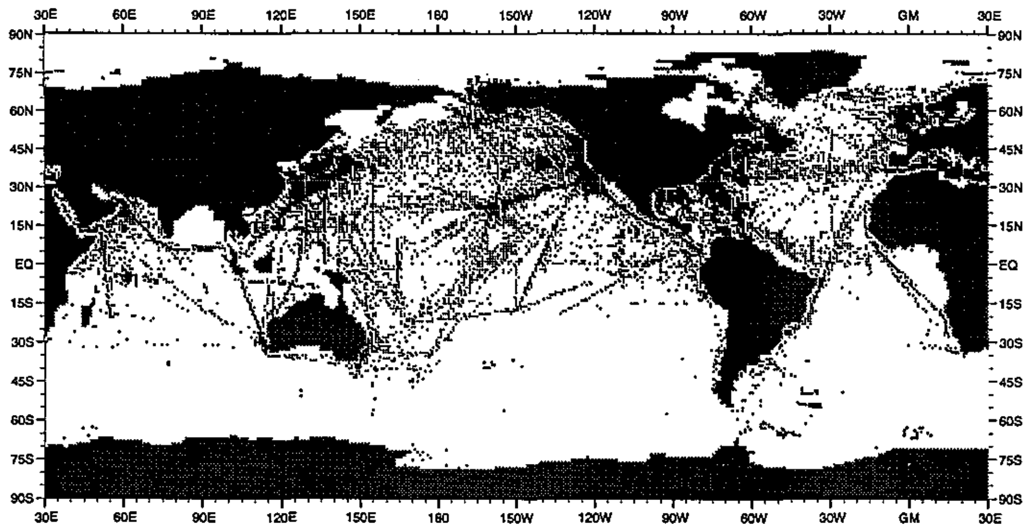


Fig. A79 Distribution of temperature observations at the surface for year 1986

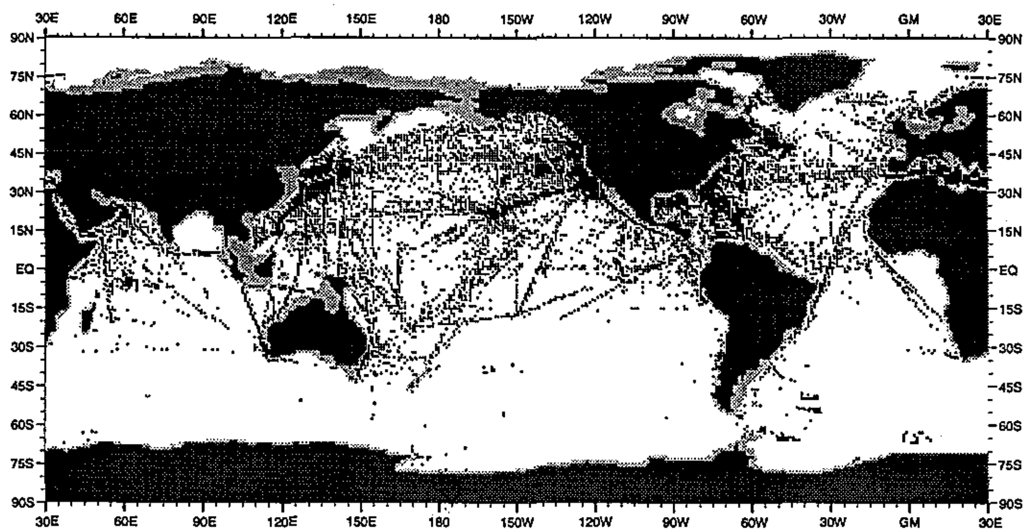


Fig. A80 Distribution of temperature observations at 125 m depth for year 1986

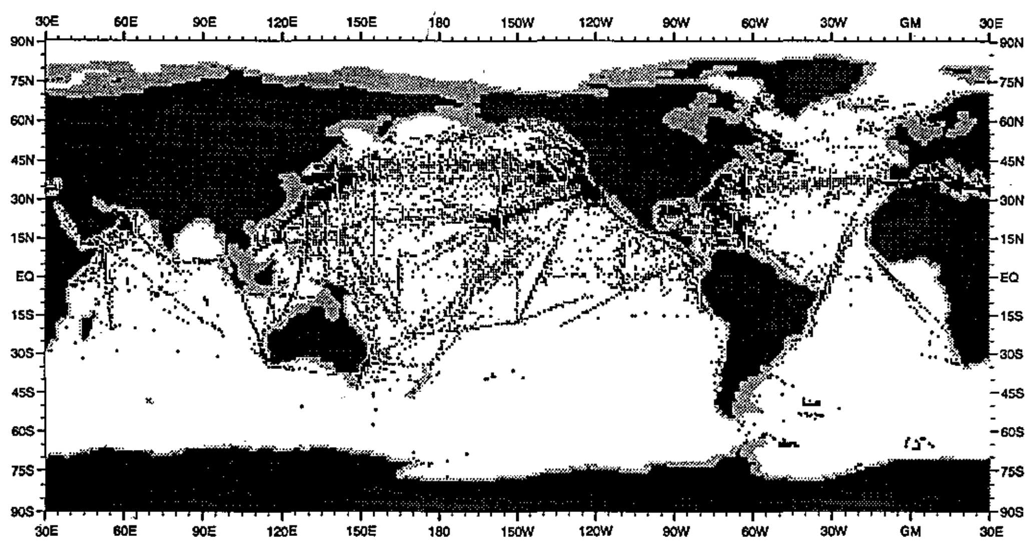


Fig. A81 Distribution of temperature observations at 250 m depth for year 1986

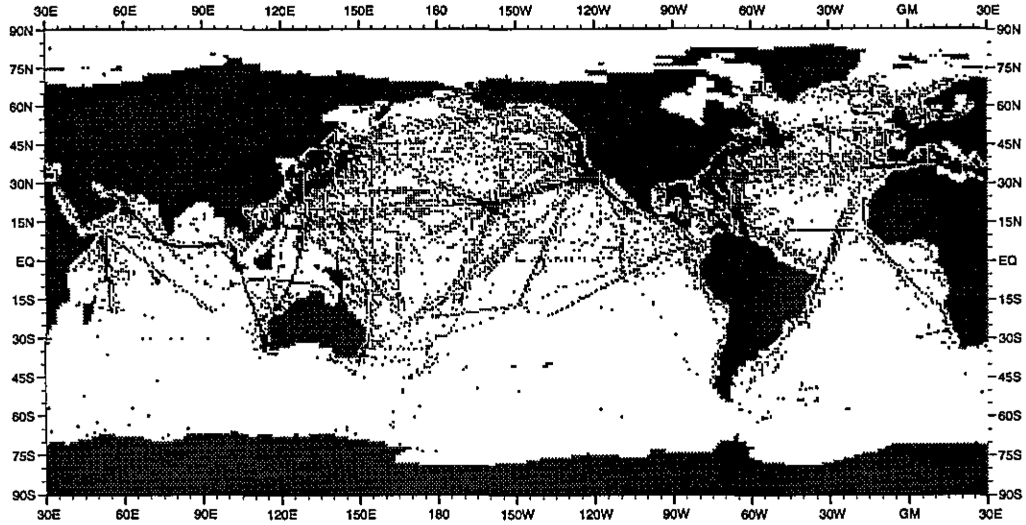


Fig. A82 Distribution of temperature observations at the surface for year 1987

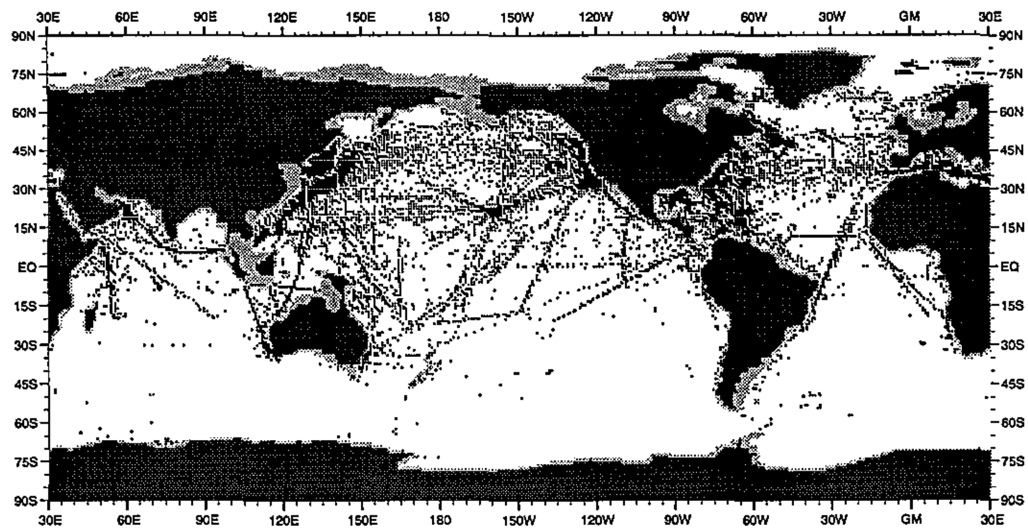


Fig. A83 Distribution of temperature observations at 125 m depth for year 1987

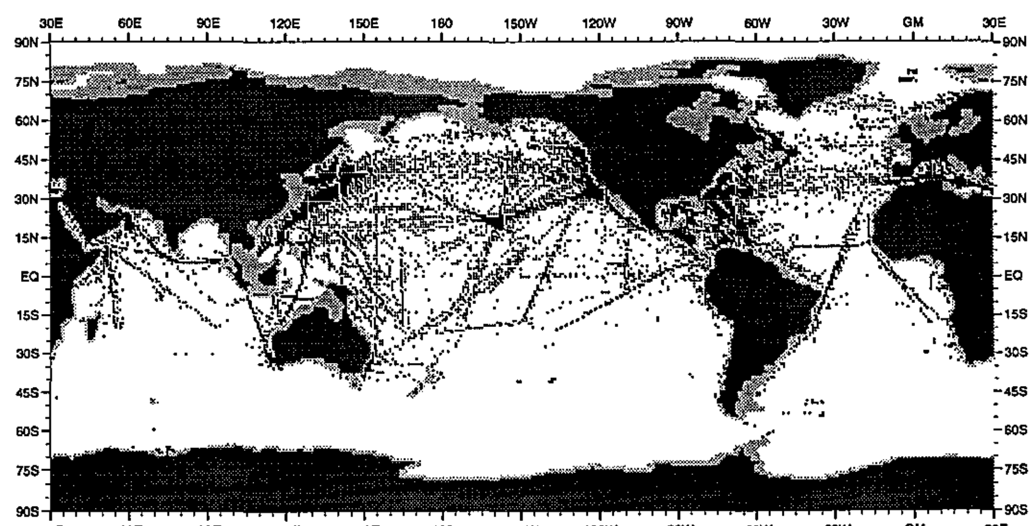


Fig. A84 Distribution of temperature observations at 250 m depth for year 1987

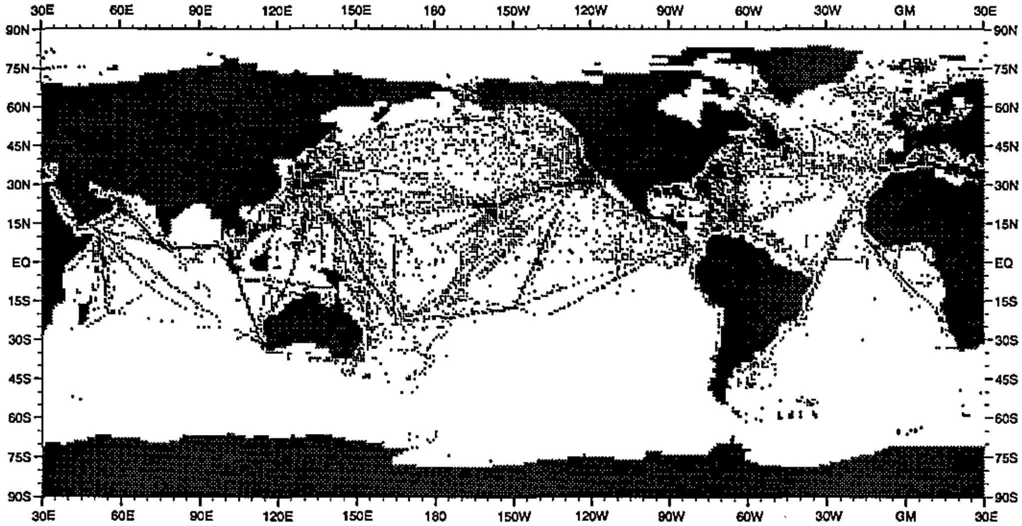


Fig. A85 Distribution of temperature observations at the surface for year 1988

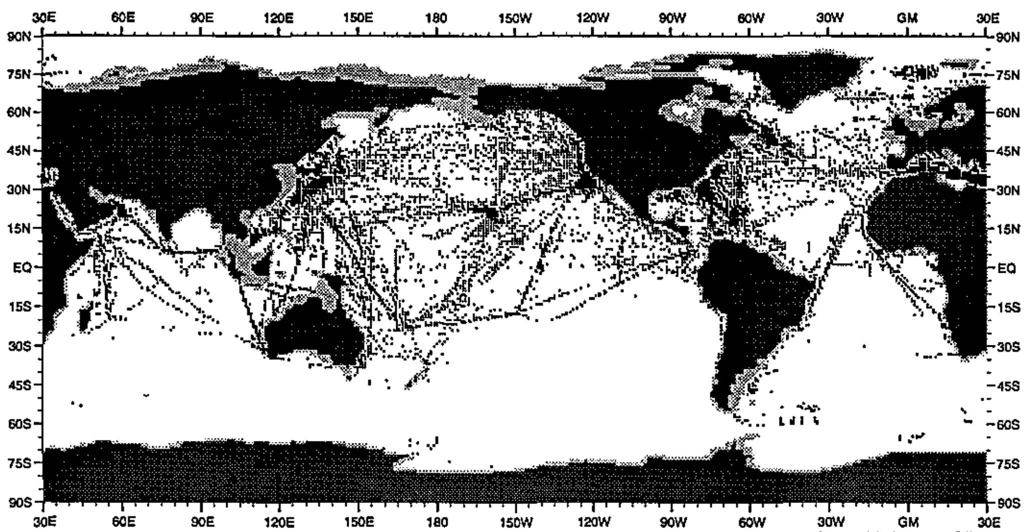


Fig. A86 Distribution of temperature observations at 125 m depth for year 1988

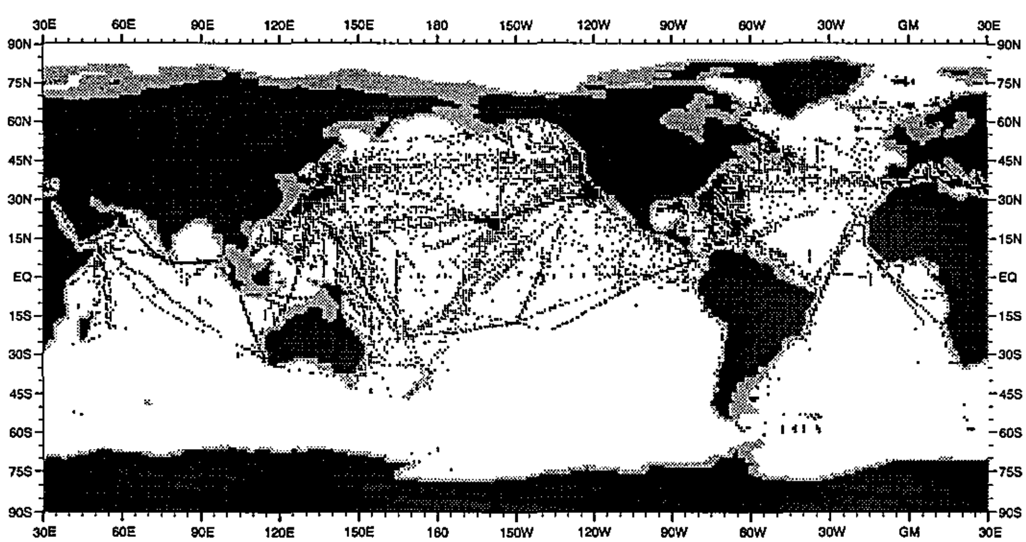


Fig. A87 Distribution of temperature observations at 250 m depth for year 1988

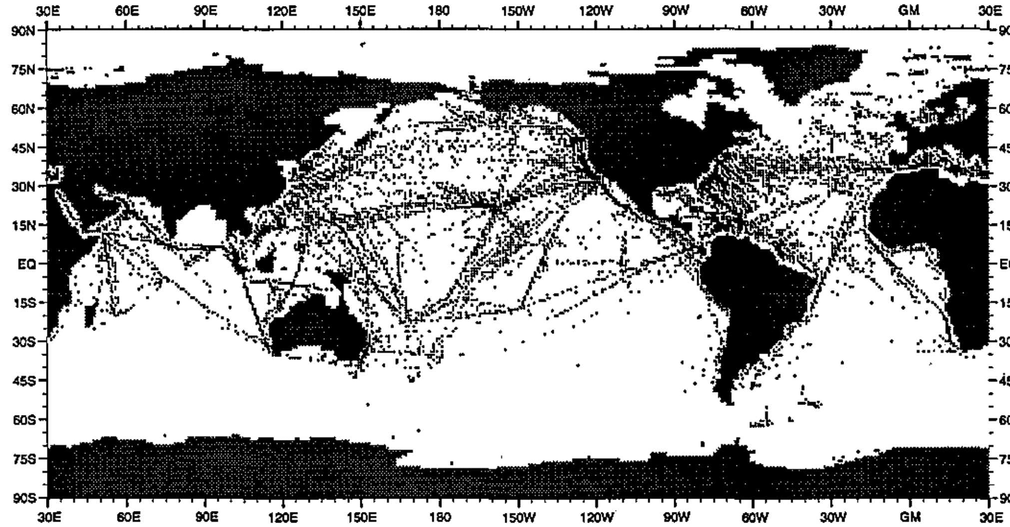


Fig. A88 Distribution of temperature observations at the surface for year 1989

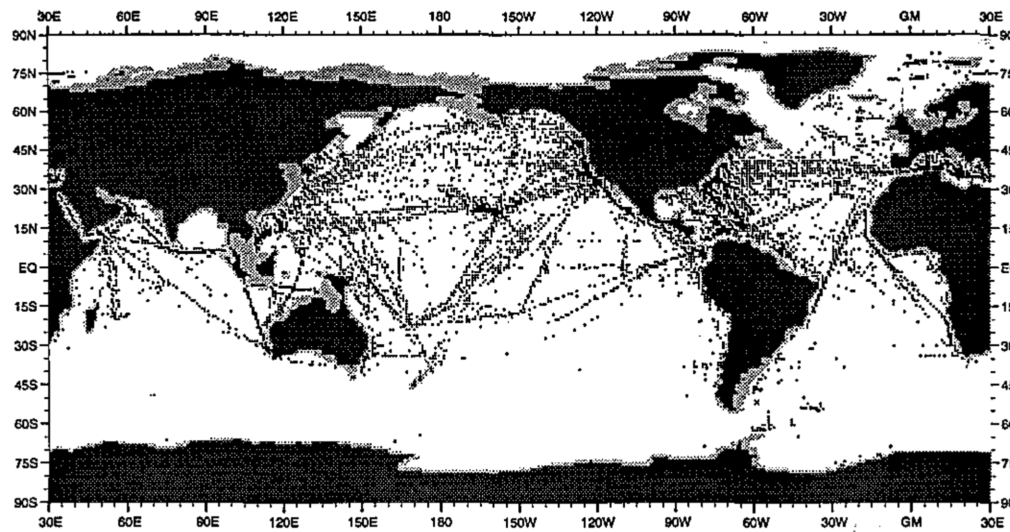


Fig. A89 Distribution of temperature observations at 125 m depth for year 1989

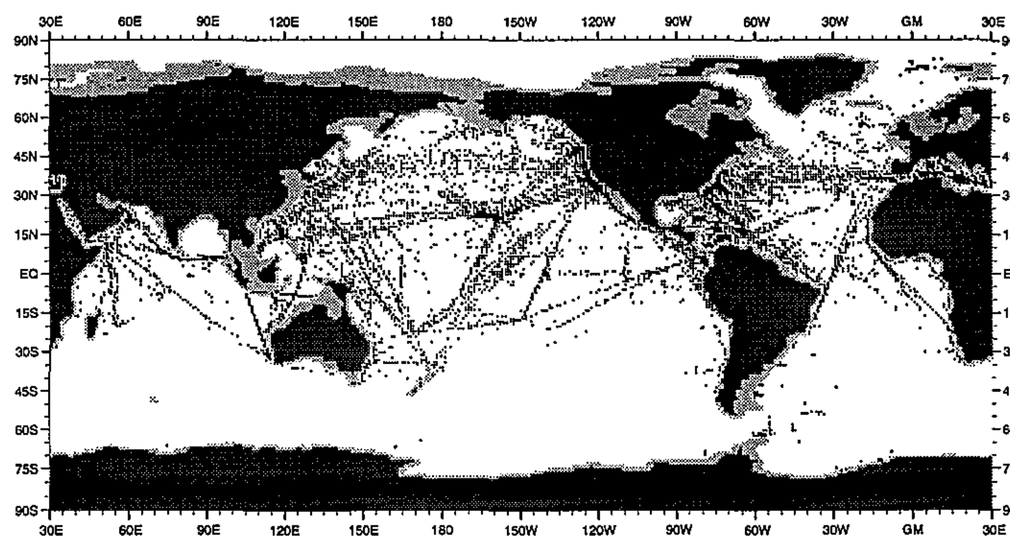


Fig. A90 Distribution of temperature observations at 250 m depth for year 1989

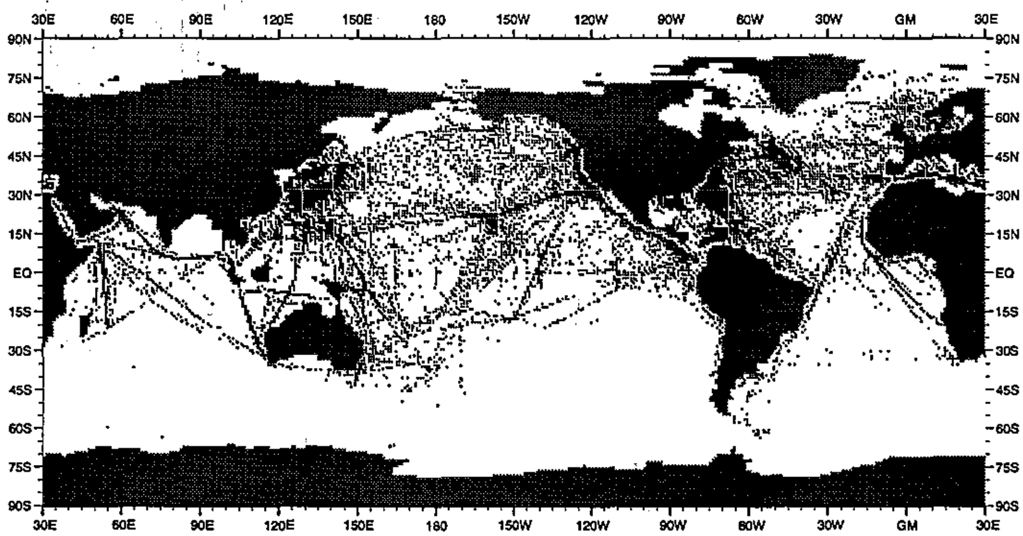


Fig. A91 Distribution of temperature observations at the surface for year 1990

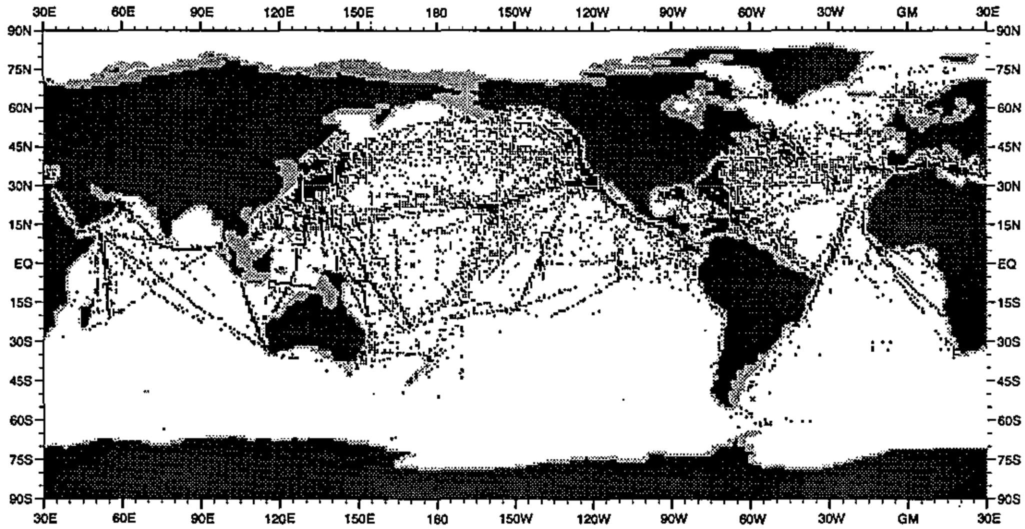


Fig. A92 Distribution of temperature observations at 125 m depth for year 1990

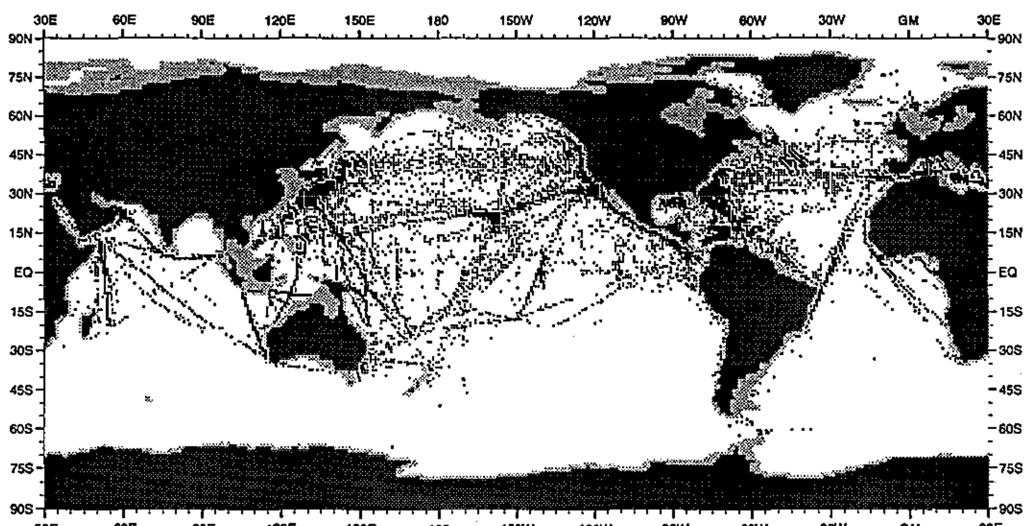


Fig. A93 Distribution of temperature observations at 250 m depth for year 1990

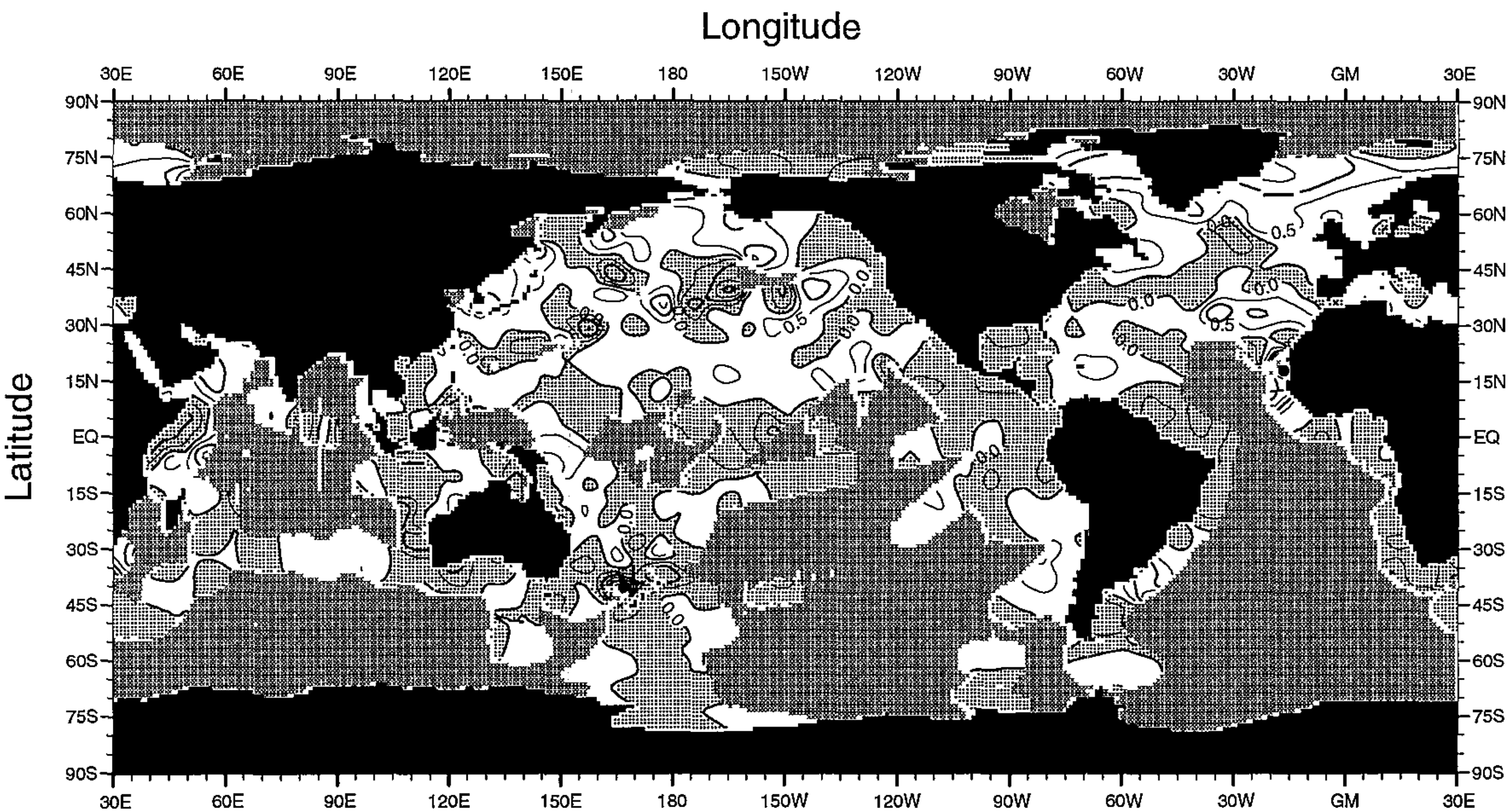


Minimum Value -3.05 Maximum Value 3.17 Contour Interval 0.50

Fig. B1 Temperature anomaly (°C) at the surface for year 1960

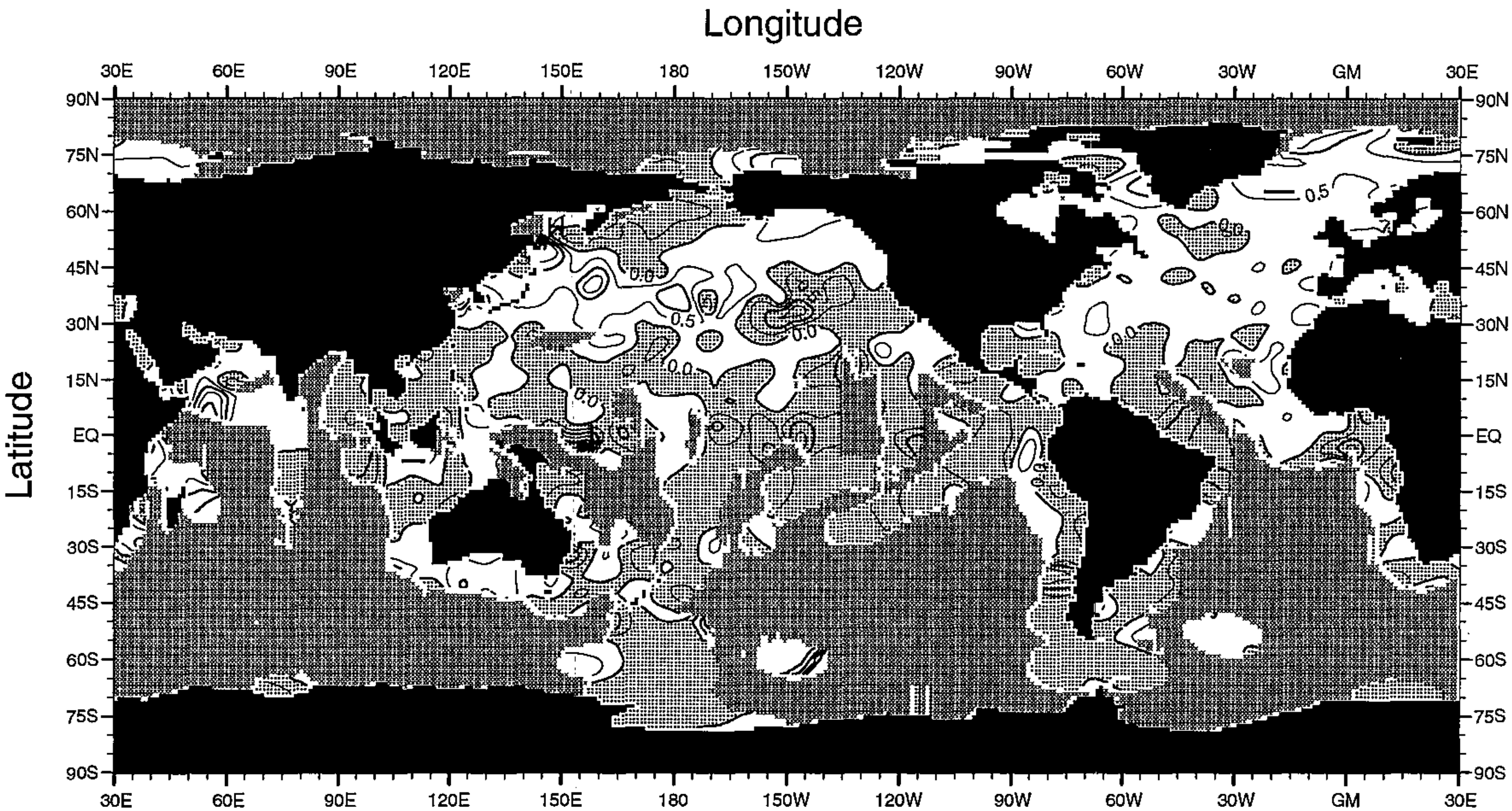


Minimum Value -2.61 Maximum Value 2.47 Contour Interval 0.50

Fig. B2 Temperature anomaly (°C) at the surface for year 1961

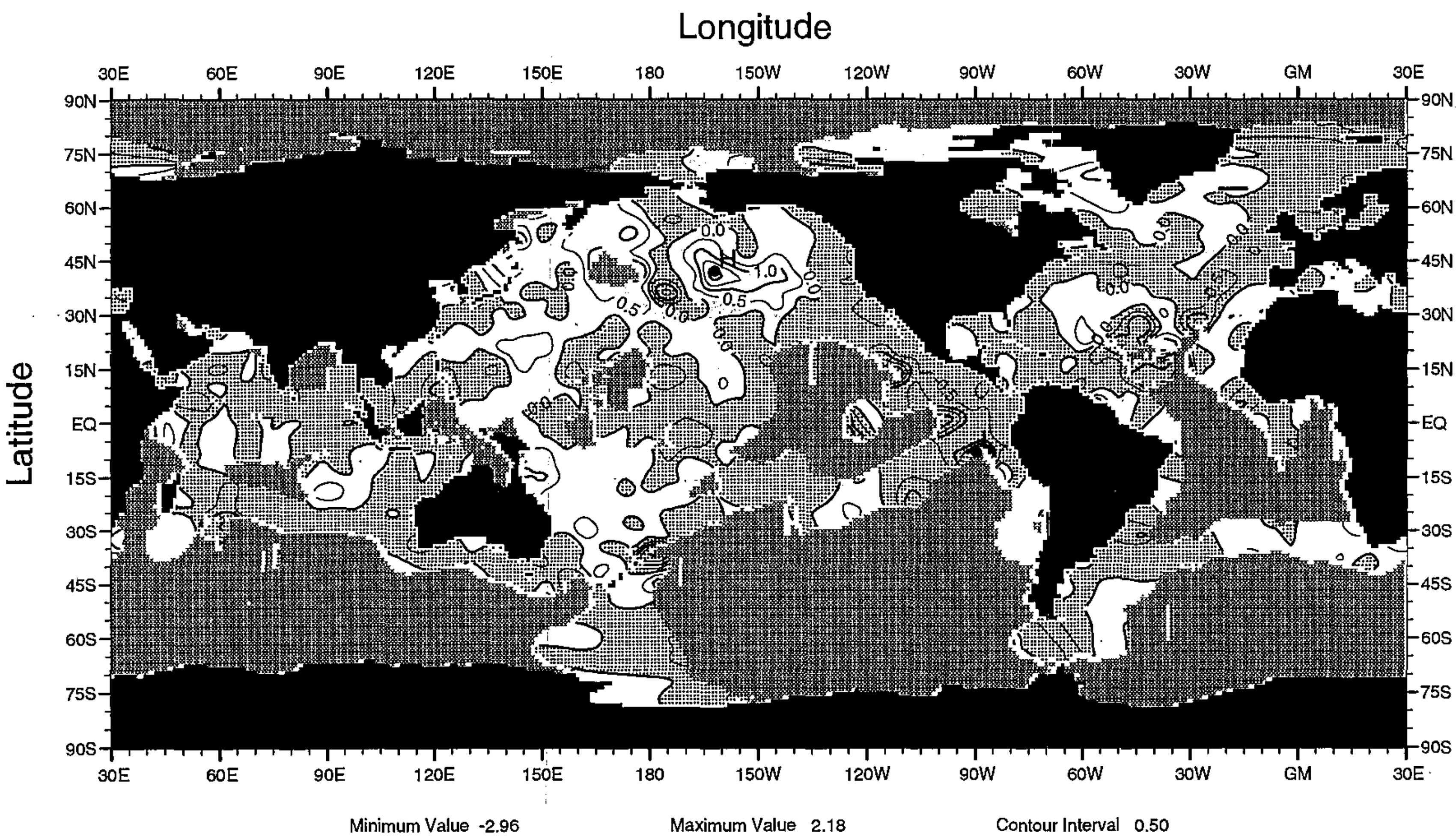


Fig. B3 Temperature anomaly (°C) at the surface for year 1962

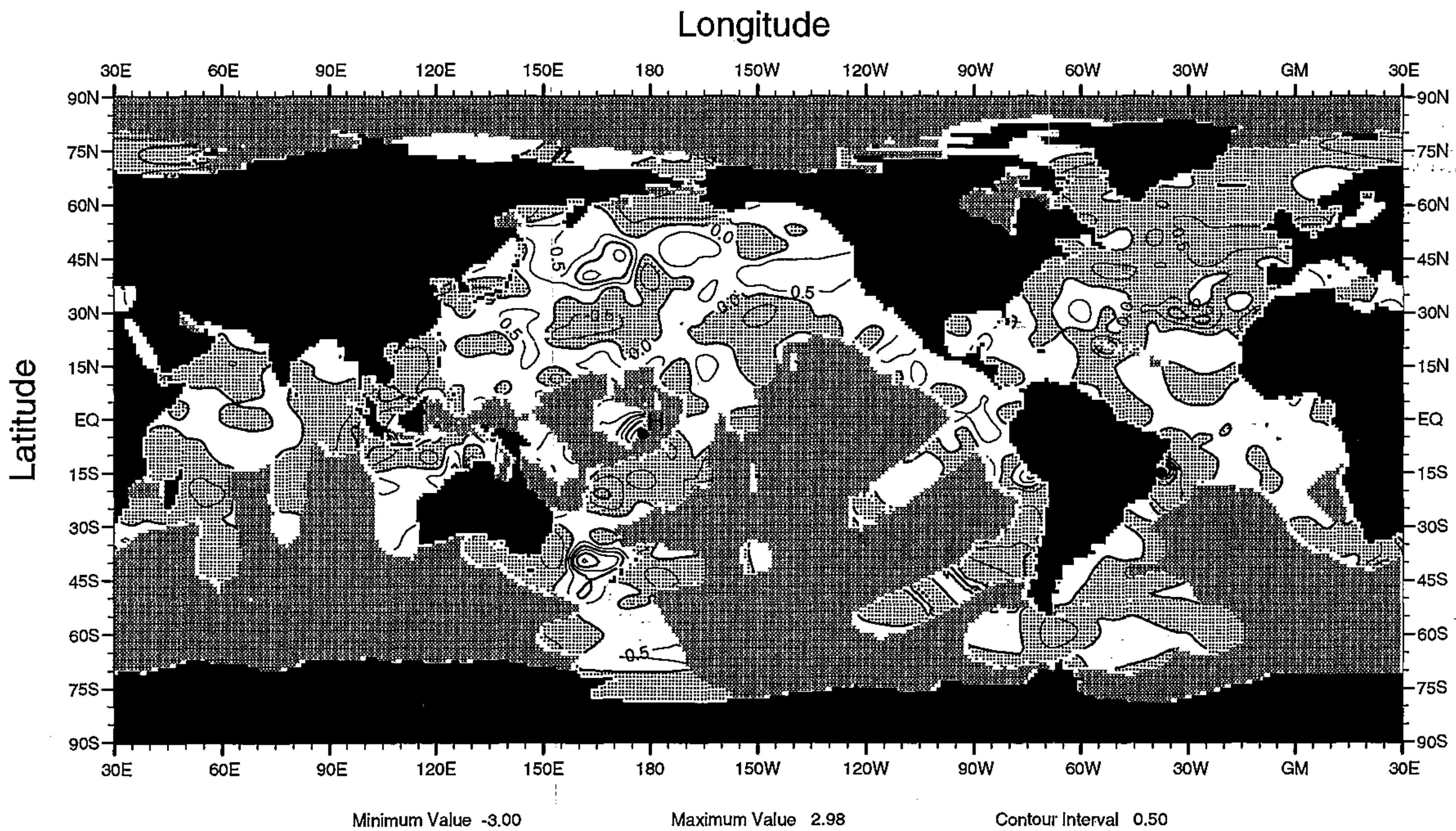


Fig. B4 Temperature anomaly (°C) at the surface for year 1963

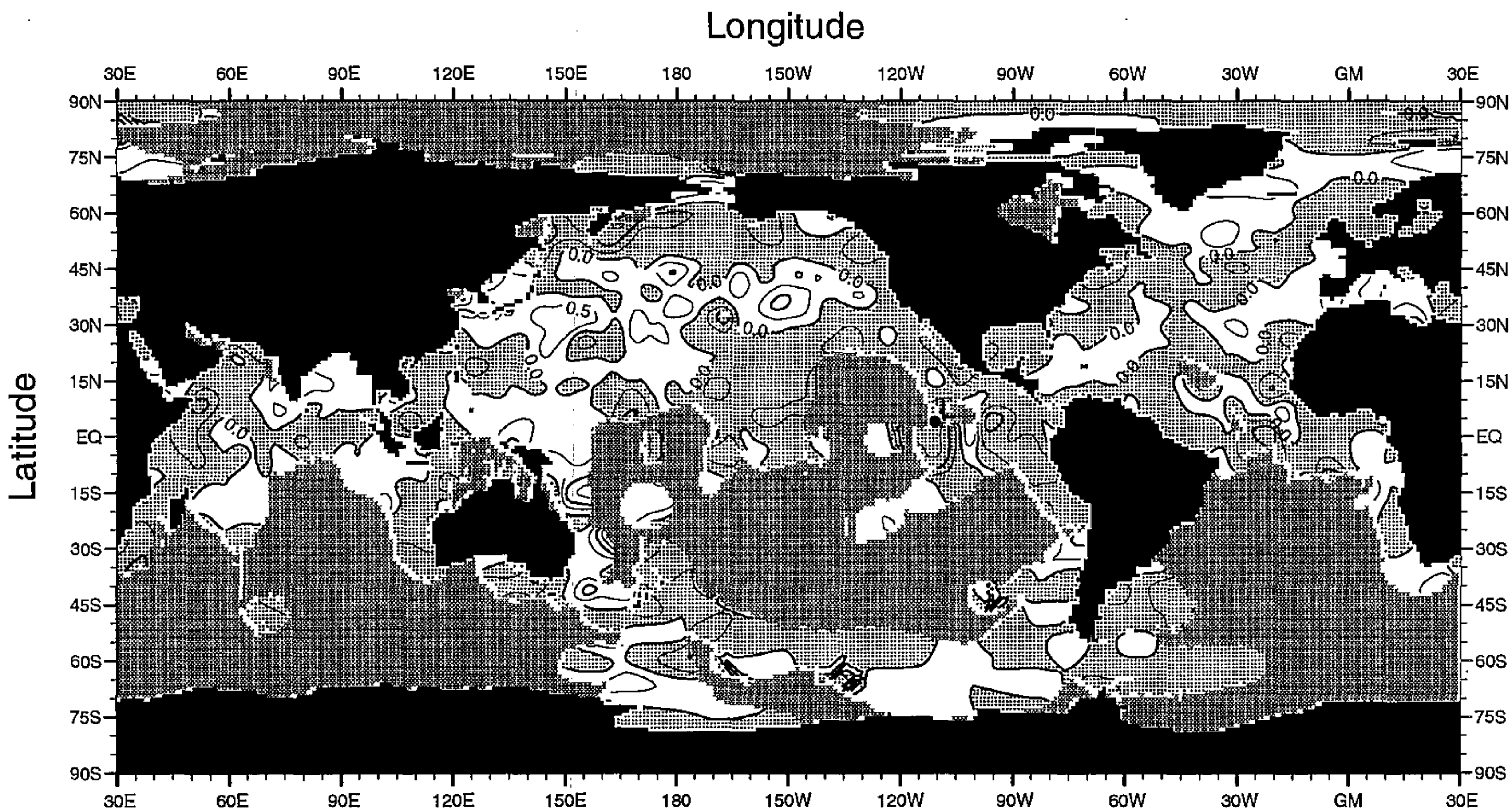


Minimum Value -1.81 Maximum Value 2.46 Contour Interval 0.50

Fig. B5 Temperature anomaly (°C) at the surface for year 1964

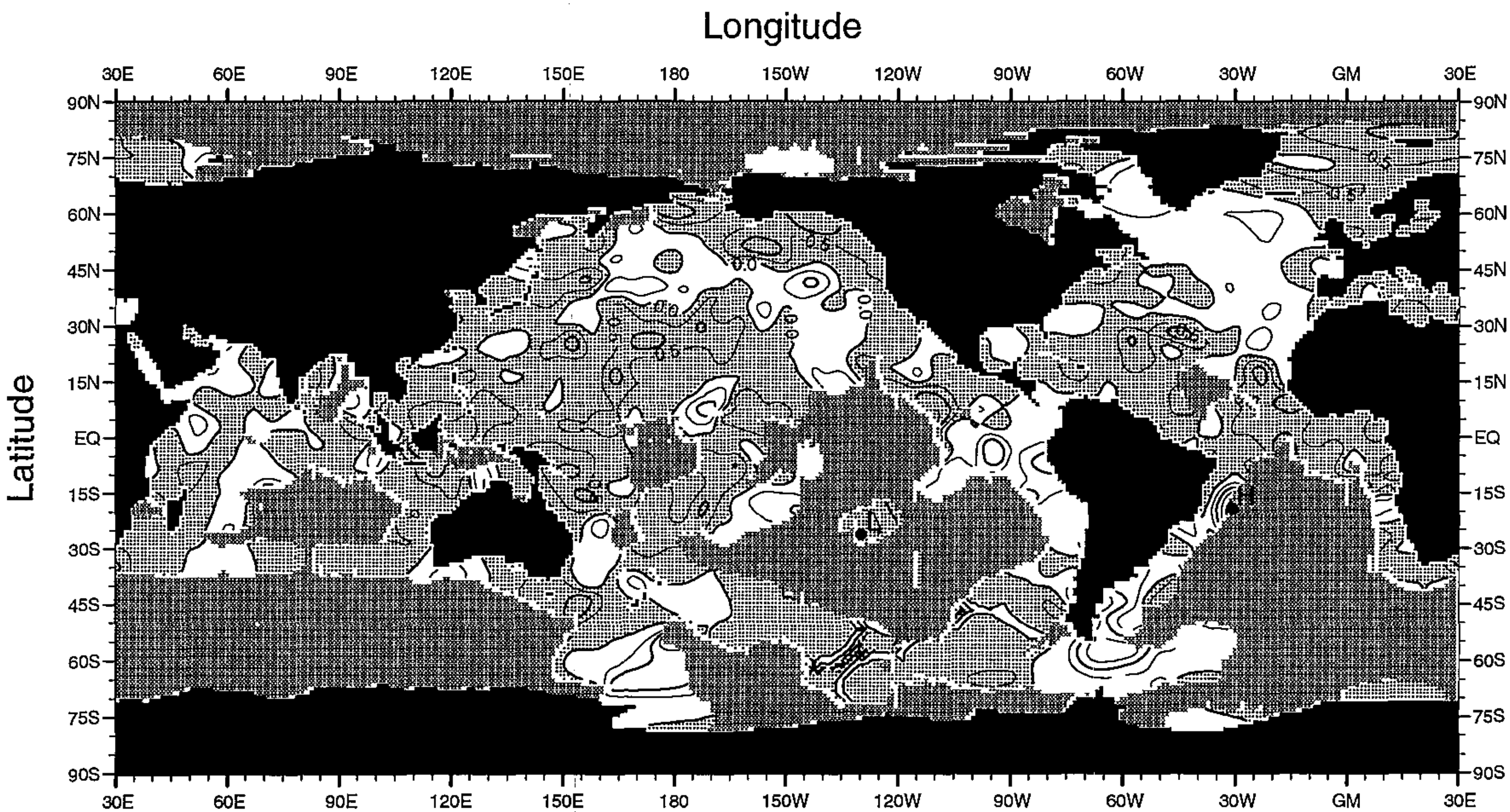


Minimum Value -1.99 Maximum Value 2.22 Contour Interval 0.50

Fig. B6 Temperature anomaly (°C) at the surface for year 1965

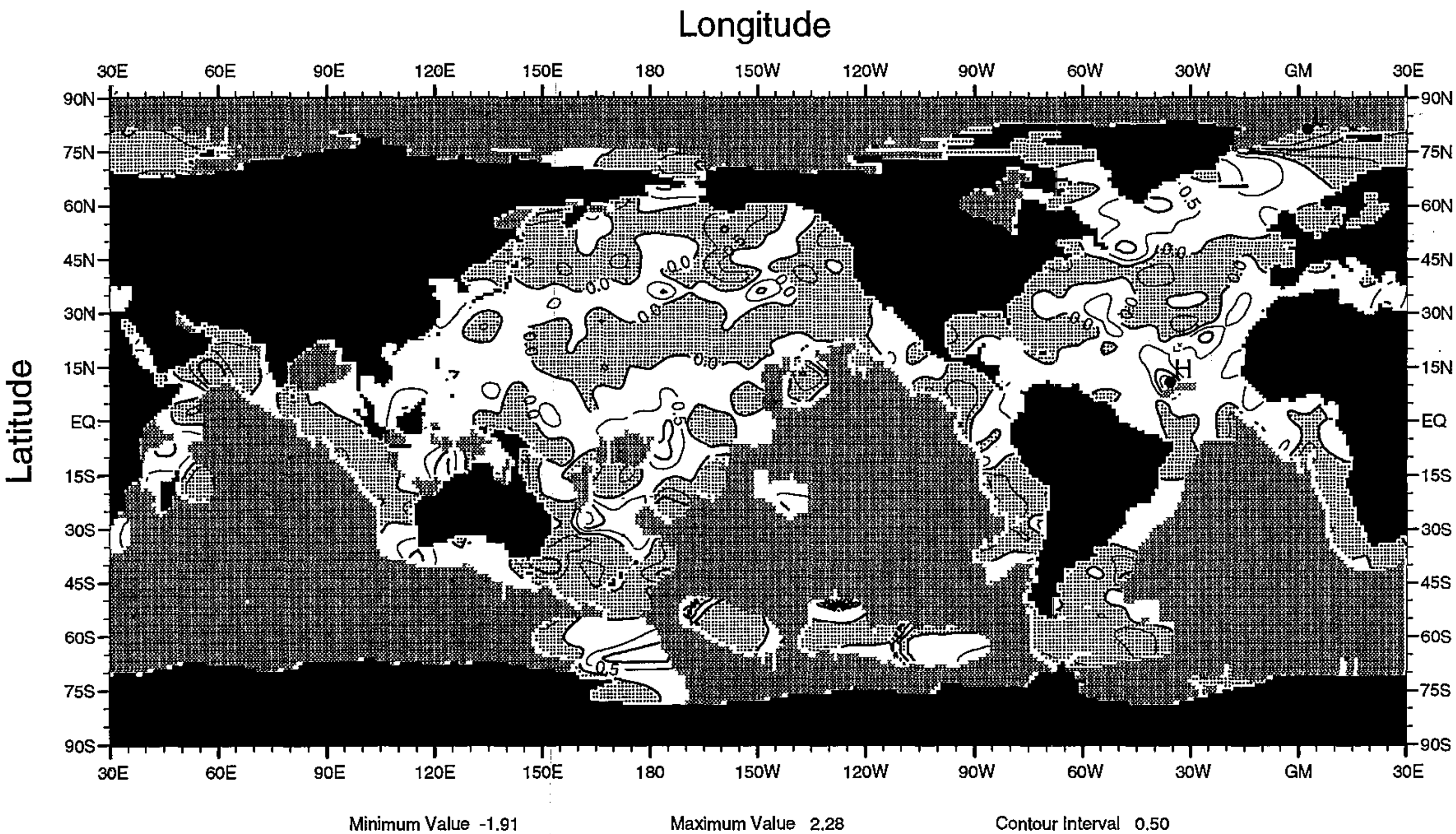


Fig. B7 Temperature anomaly (°C) at the surface for year 1966

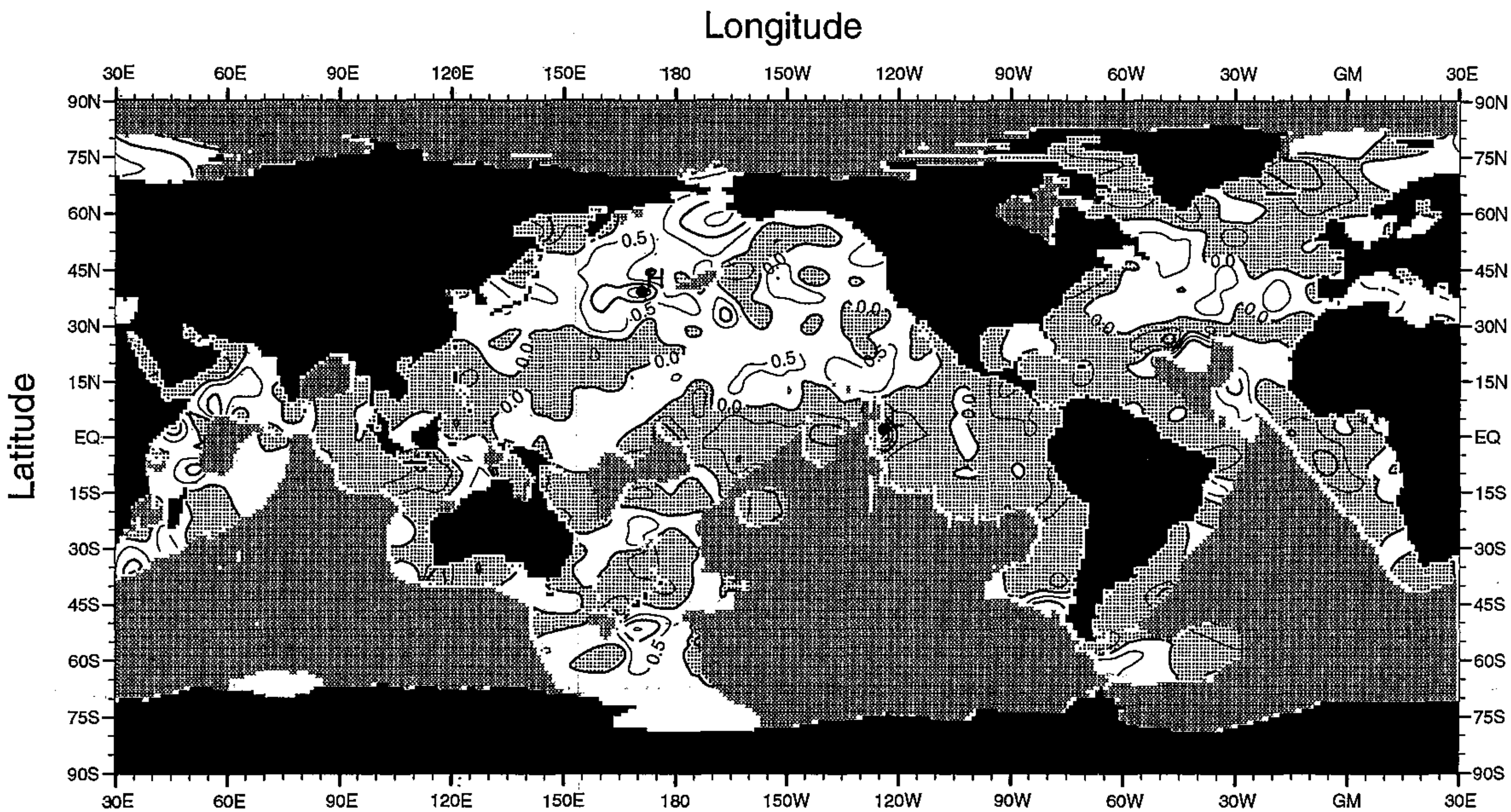


Minimum Value -2.87 Maximum Value 1.90 Contour Interval 0.50

Fig. B8 Temperature anomaly (°C) at the surface for year 1967

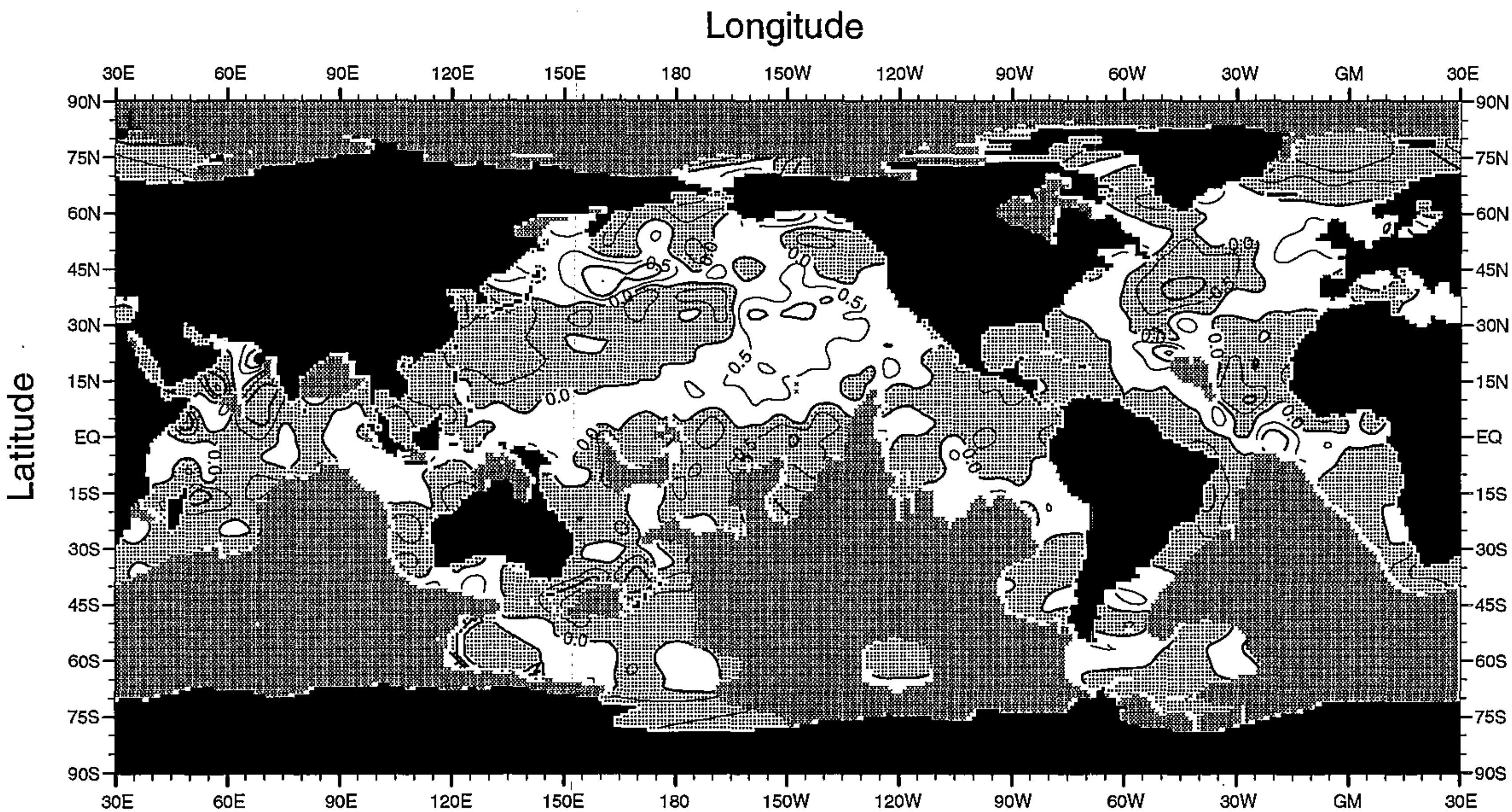


Minimum Value -2.19 Maximum Value 1.74 Contour Interval 0.50

Fig. B9 Temperature anomaly (°C) at the surface for year 1968

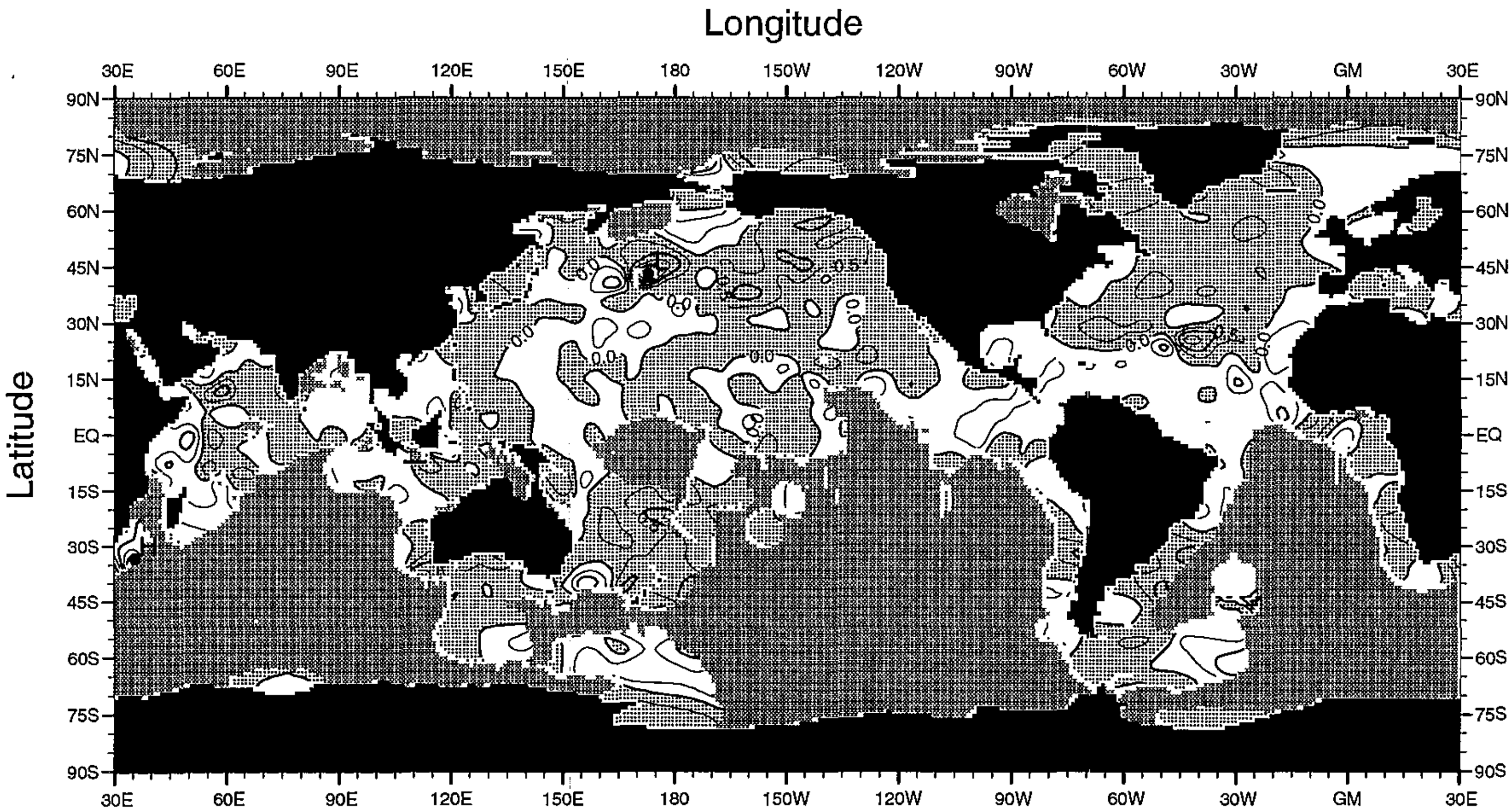


Minimum Value -2.83 Maximum Value 2.49 Contour Interval 0.50

Fig. B10 Temperature anomaly (°C) at the surface for year 1969

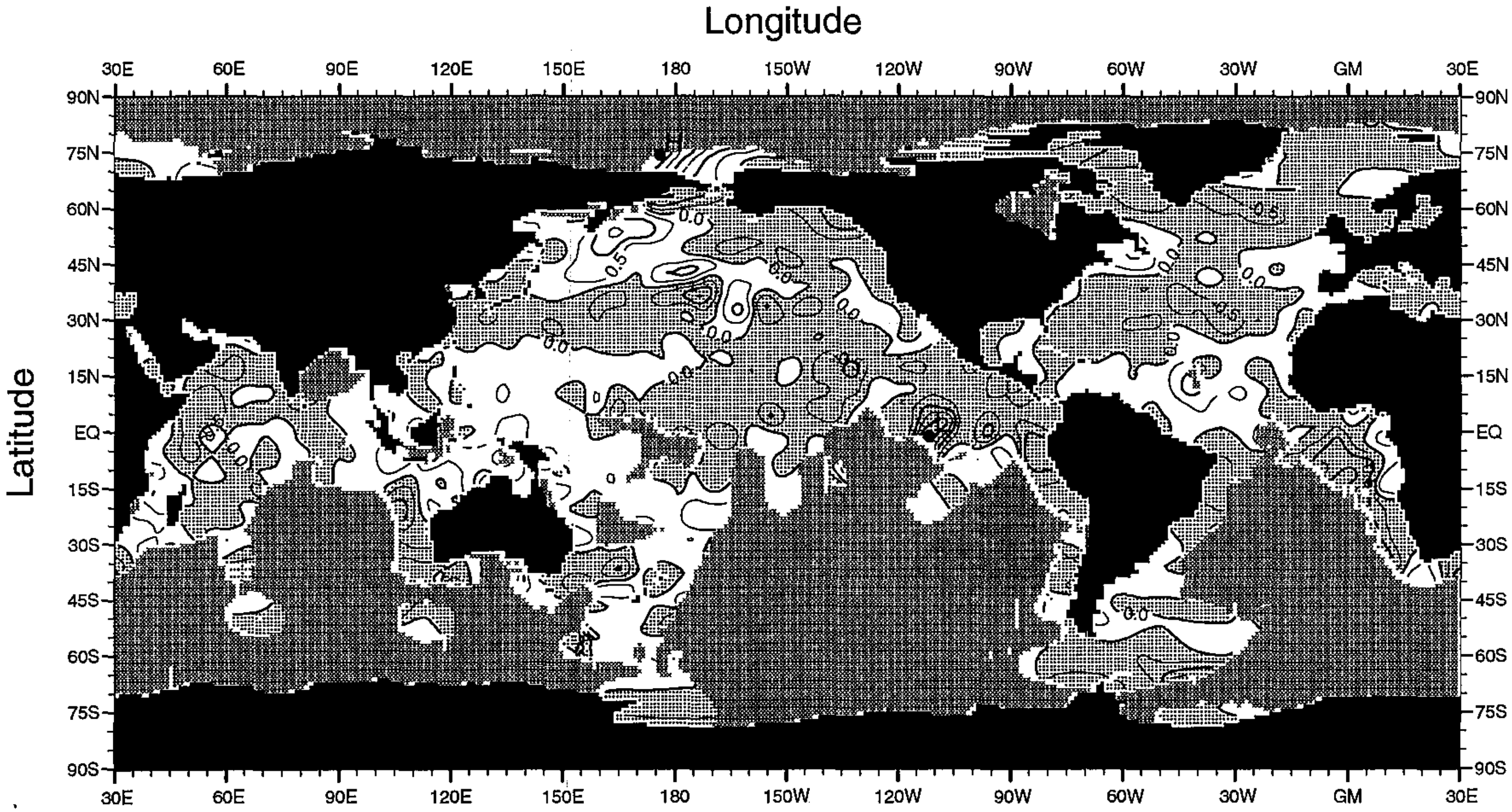


Minimum Value -2.32 Maximum Value 3.43 Contour Interval 0.50

Fig. B11 Temperature anomaly (°C) at the surface for year 1970

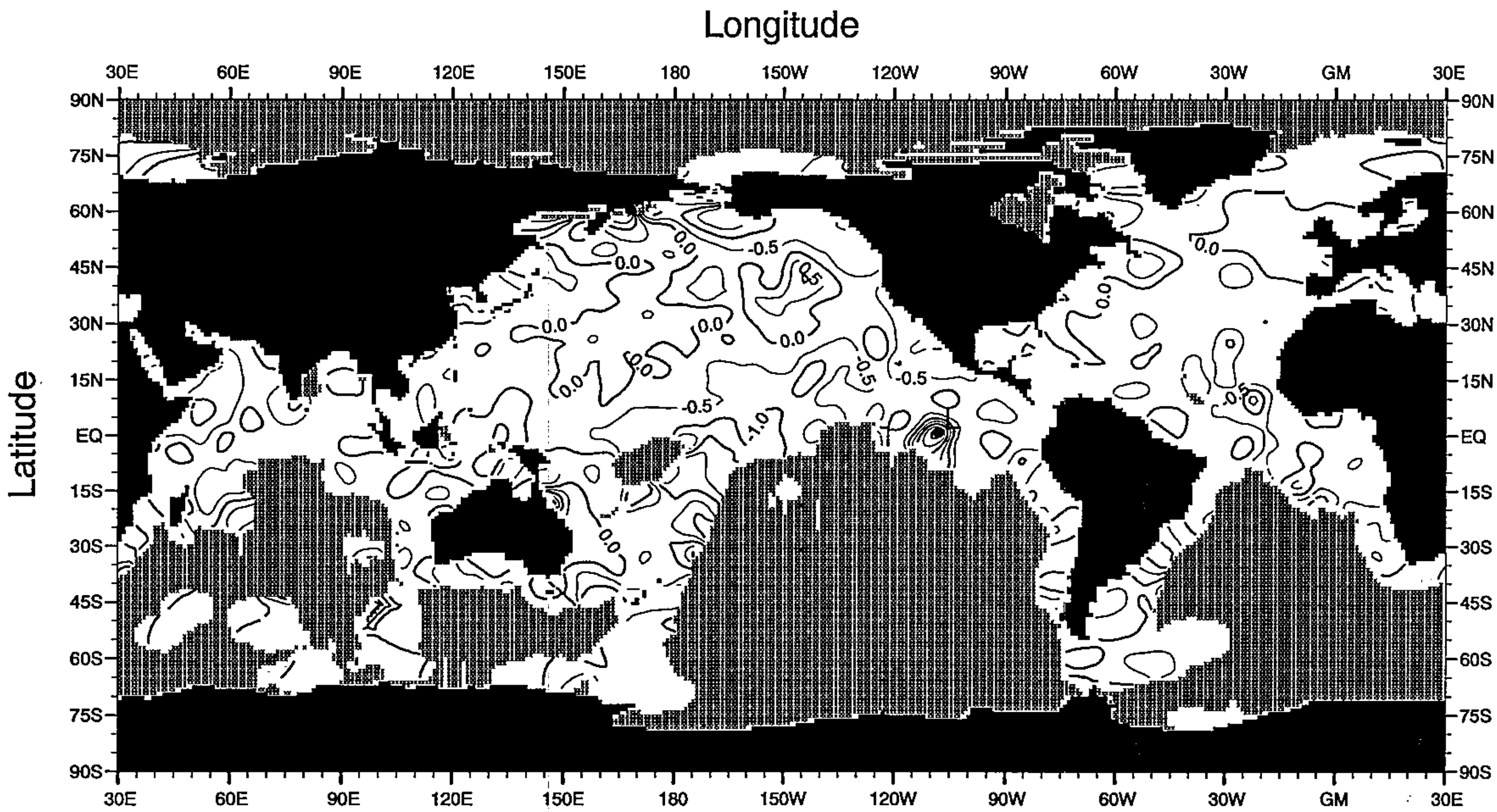


Minimum Value -3.20 Maximum Value 2.43 Contour Interval 0.50

Fig. B12 Temperature Anomaly (°C) at the surface for year 1971

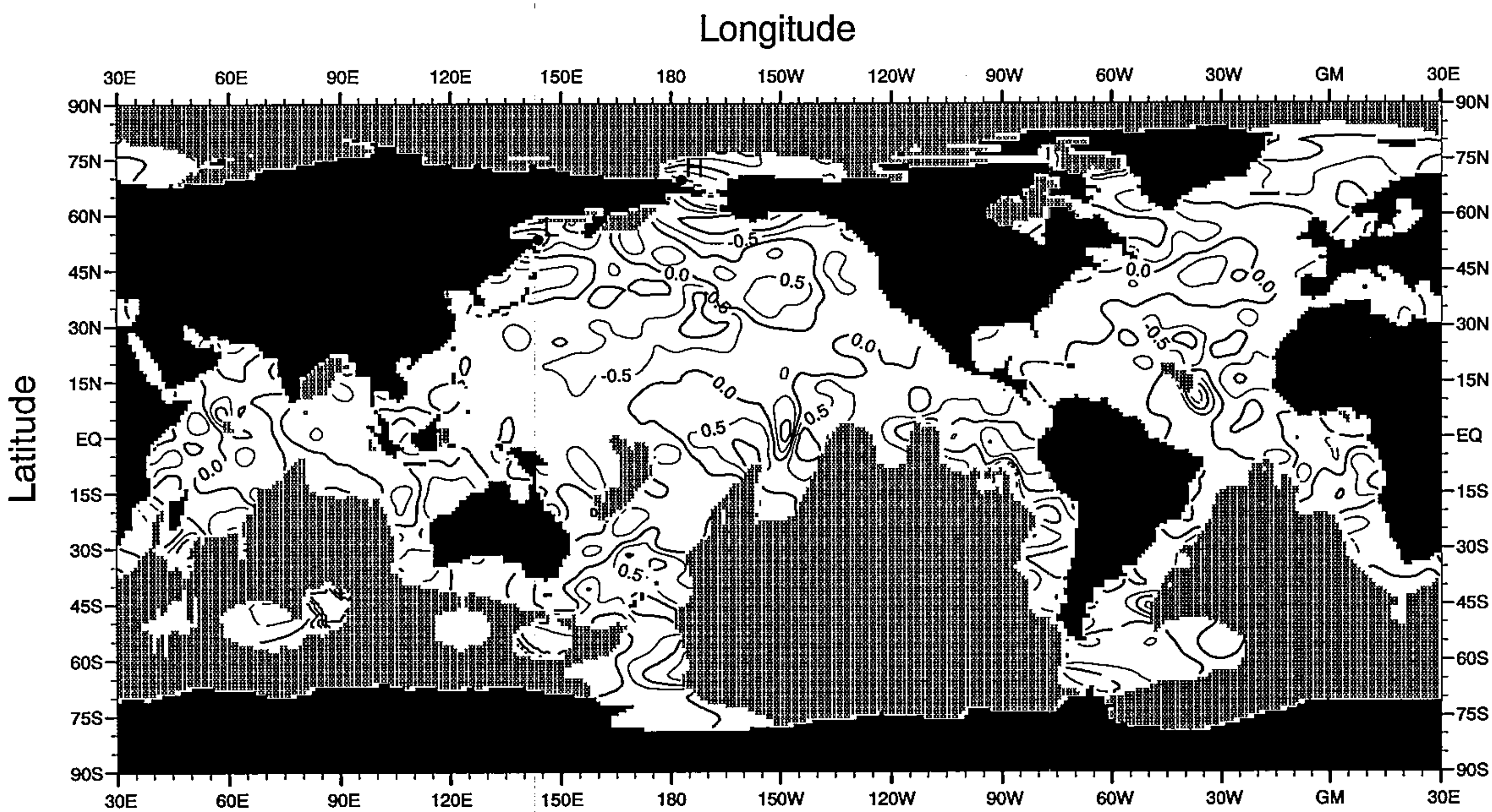


Minimum Value -1.94  Maximum Value 2.37  Contour Interval 0.50

Fig. B13 Temperature Anomaly (°C) at the surface for year 1972

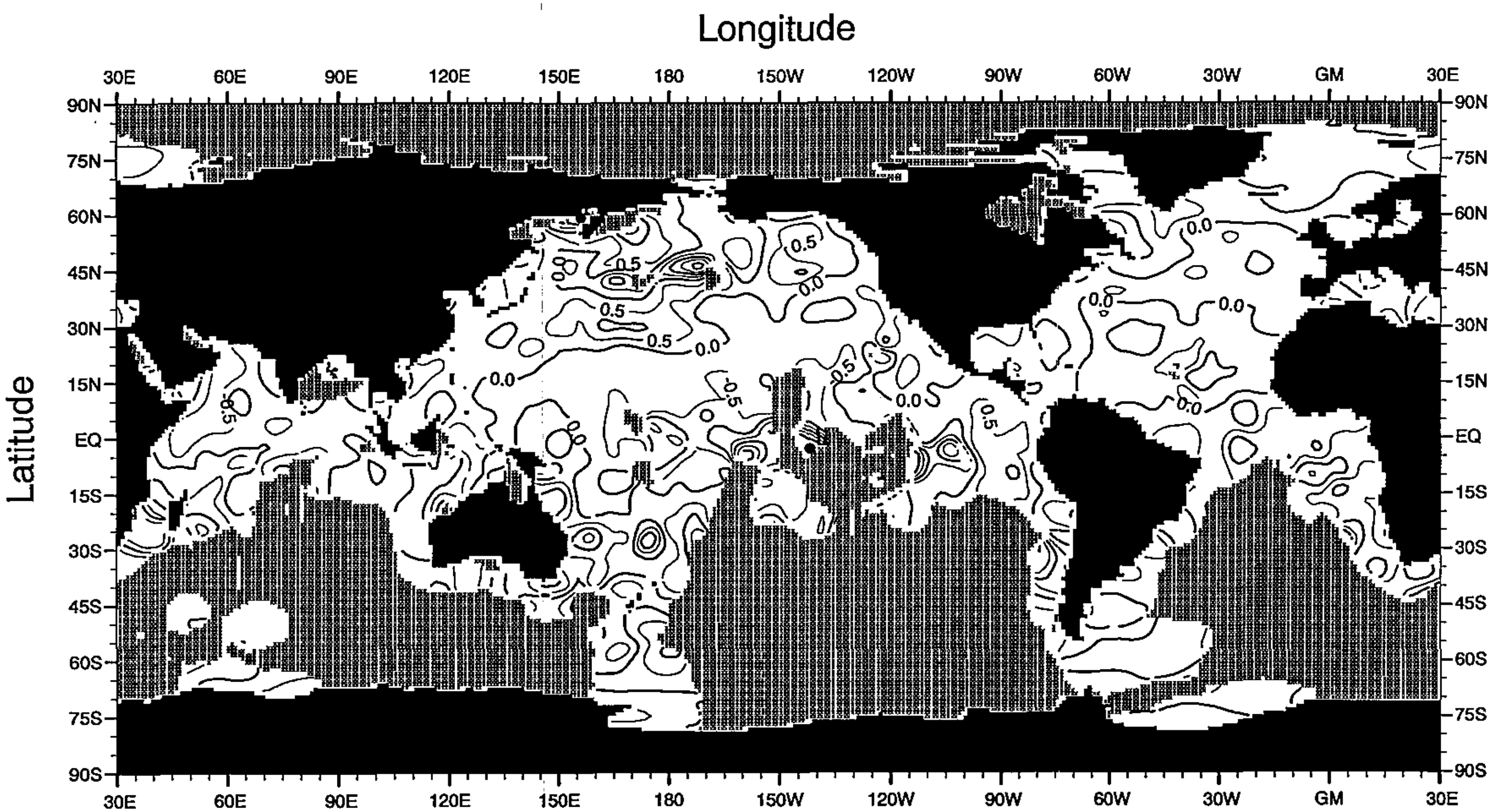


Minimum Value -3.76 Maximum Value 2.32 Contour Interval 0.50

Fig. B14 Temperature Anomaly (°C) at the surface for year 1973

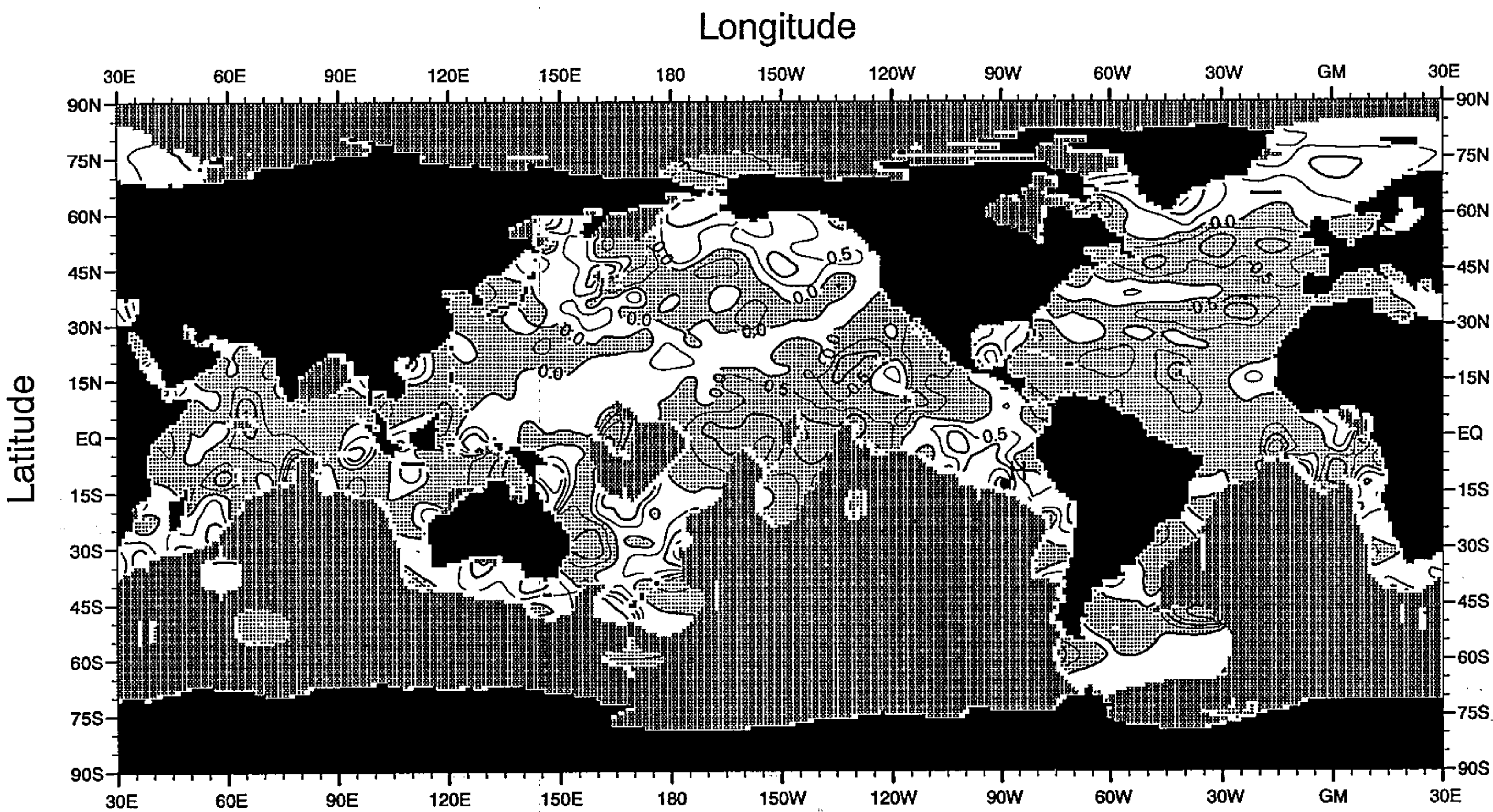


Minimum Value -3.05 Maximum Value 2.26 Contour Interval 0.50

Fig. B15 Temperature anomaly (°C) at the surface for year 1974

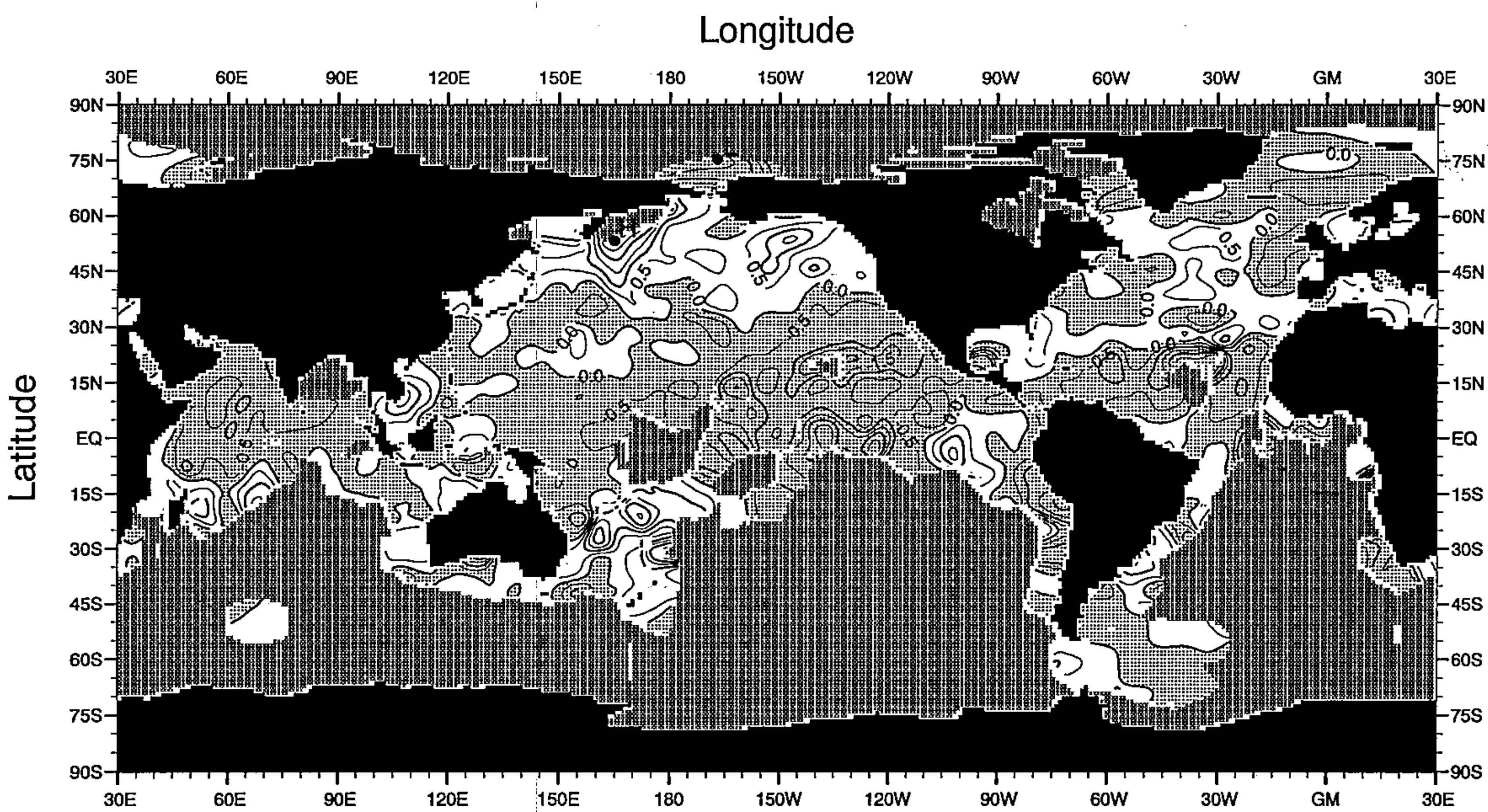


Minimum Value -2.99 Maximum Value 2.99 Contour Interval 0.50

Fig. B16 Temperature anomaly (°C) at the surface for year 1975

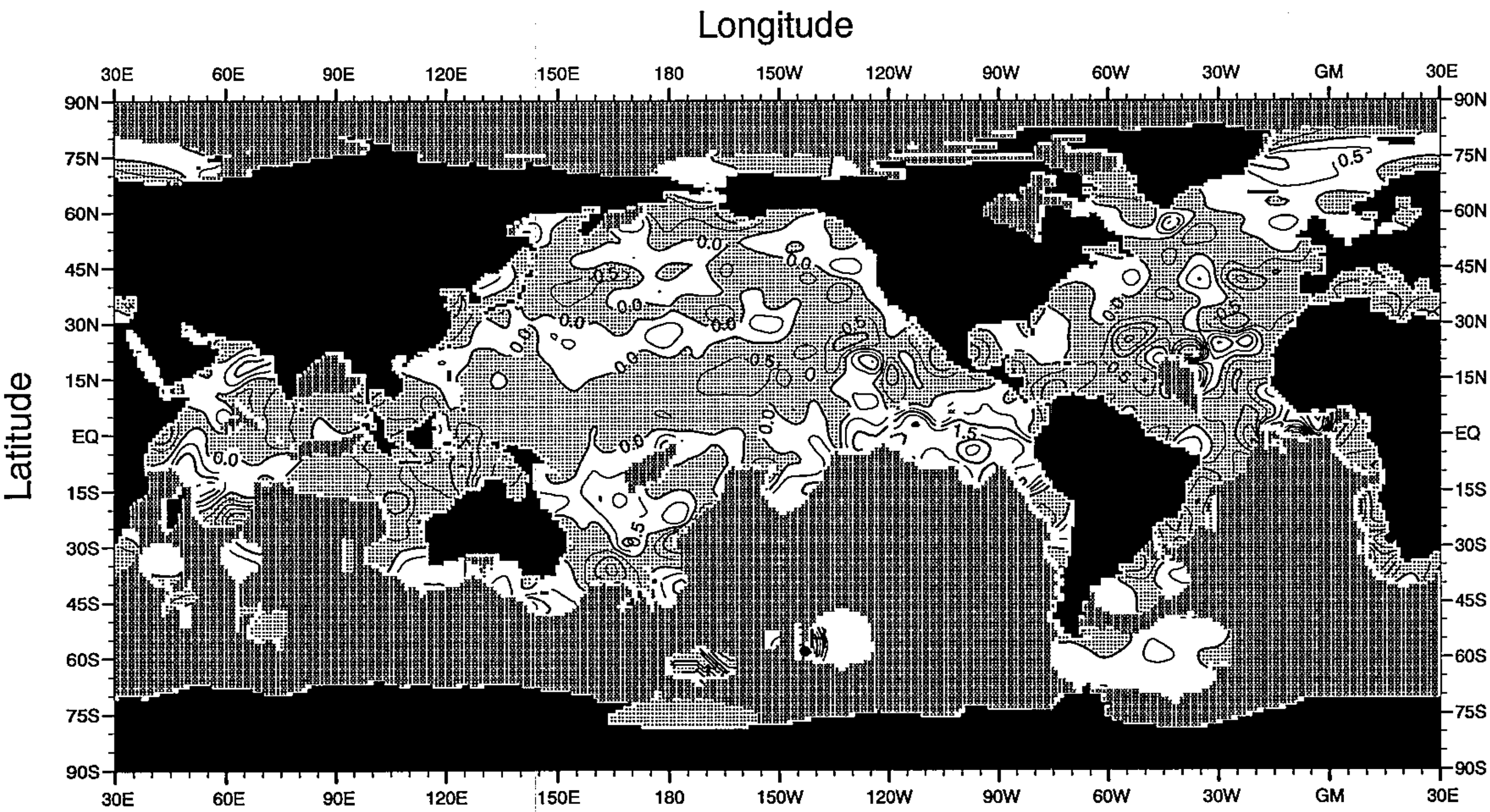


Minimum Value -3.14 Maximum Value 3.37 Contour Interval 0.50

Fig. B17 Temperature anomaly (°C) at the surface for year 1976

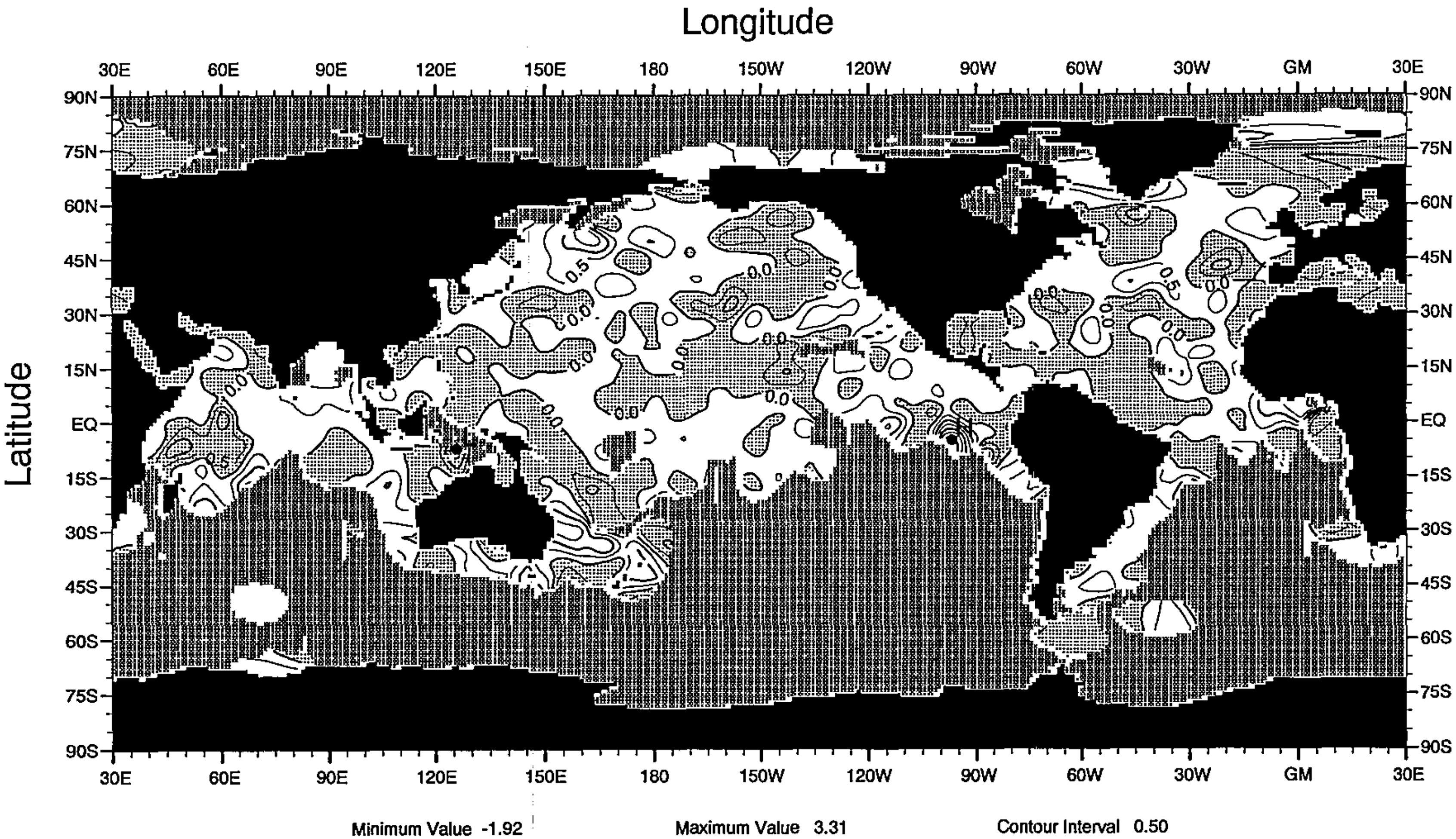


Fig. B18 Temperature anomaly (°C) at the surface for year 1977

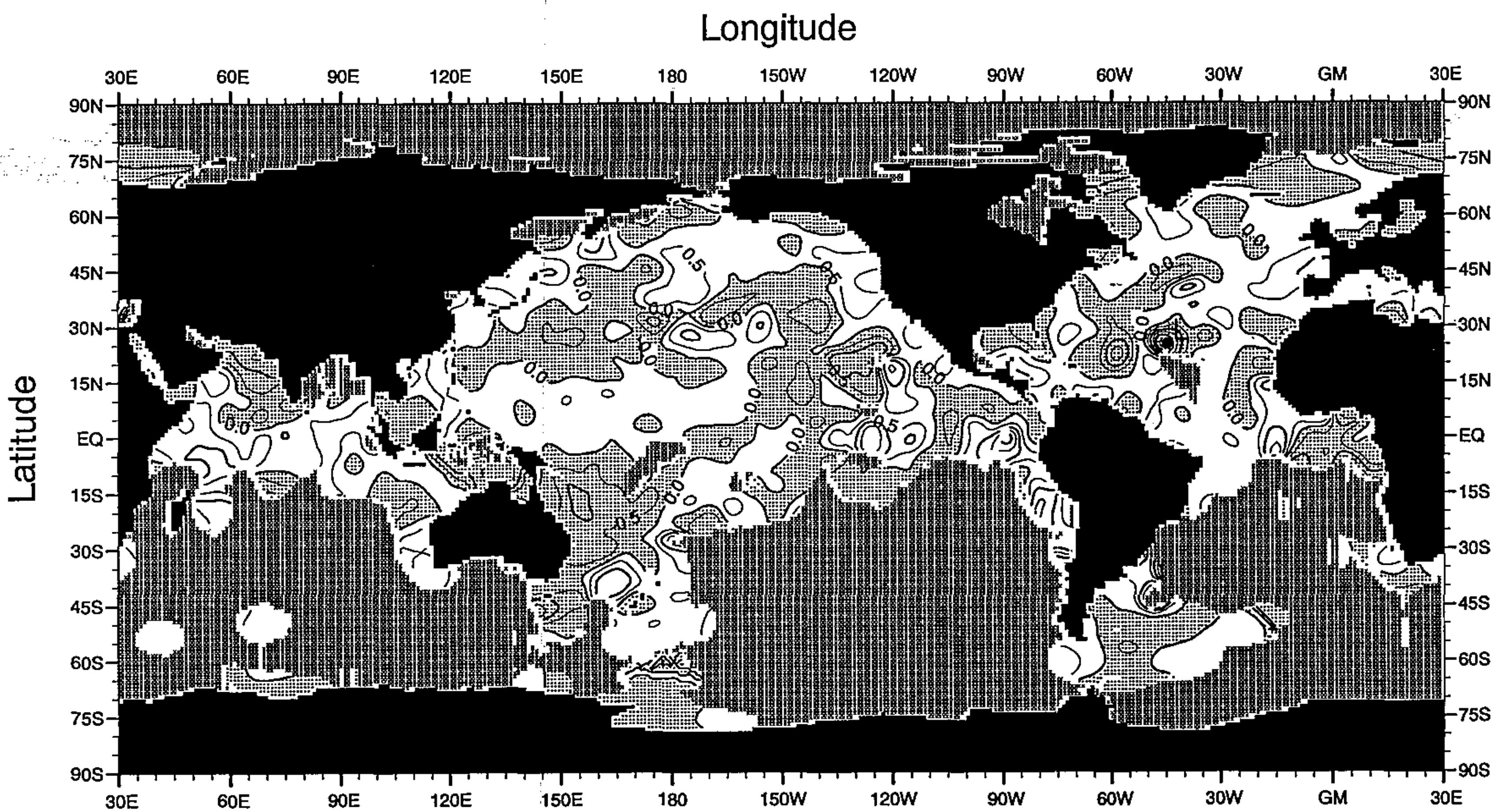


Minimum Value -2.73 Maximum Value 2.79 Contour Interval 0.50

Fig. B19 Temperature anomaly (°C) at the surface for year 1978

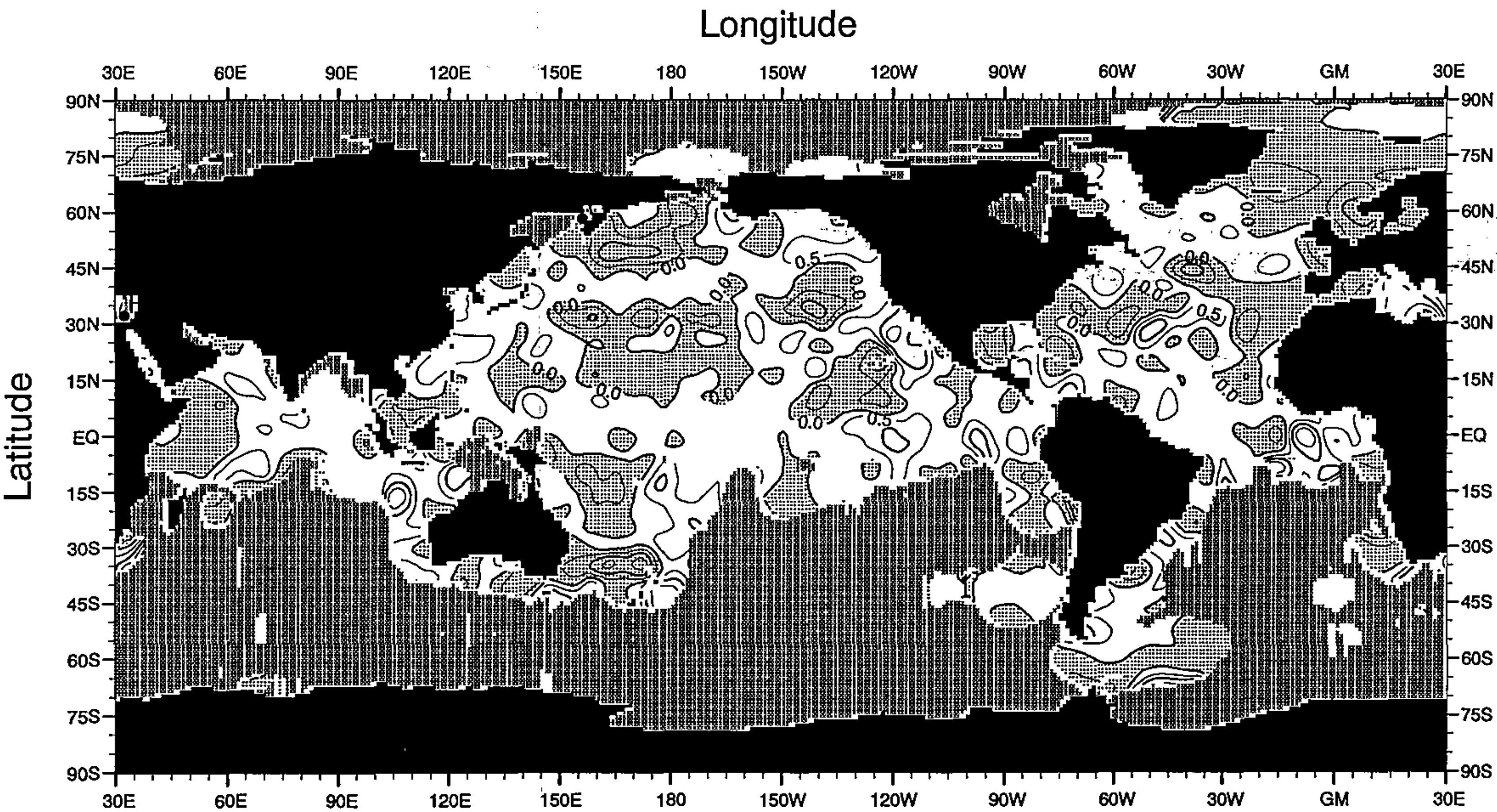


Minimum Value -1.82 Maximum Value 3.48 Contour Interval 0.50

Fig. B20 Temperature anomaly (°C) at the surface for year 1979

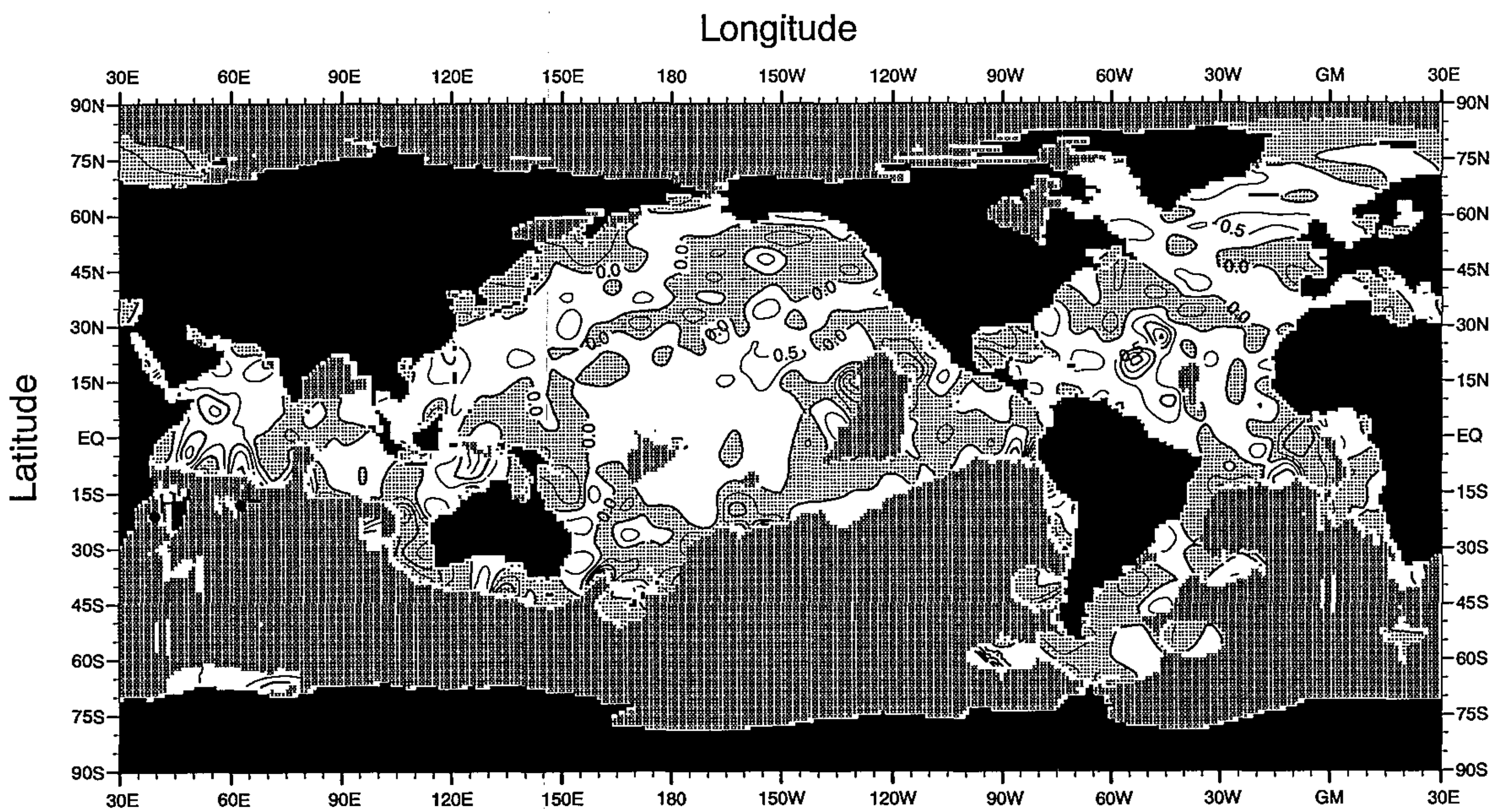


Minimum Value -3.13 Maximum Value 3.05 Contour Interval 0.50

Fig. B21 Temperature anomaly (°C) at the surface for year 1980

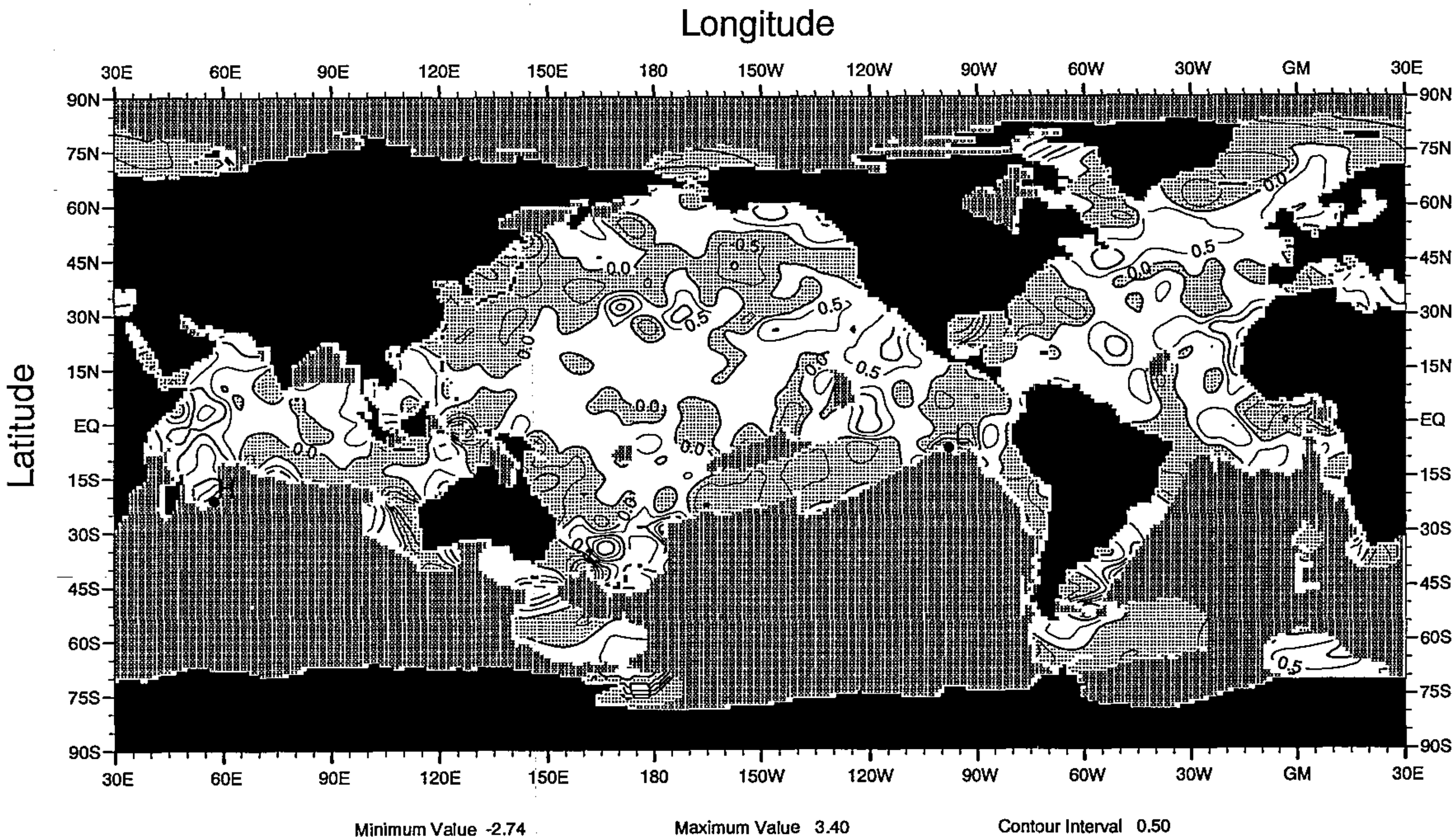


Fig. B22 Temperature anomaly (°C) at the surface for year 1981

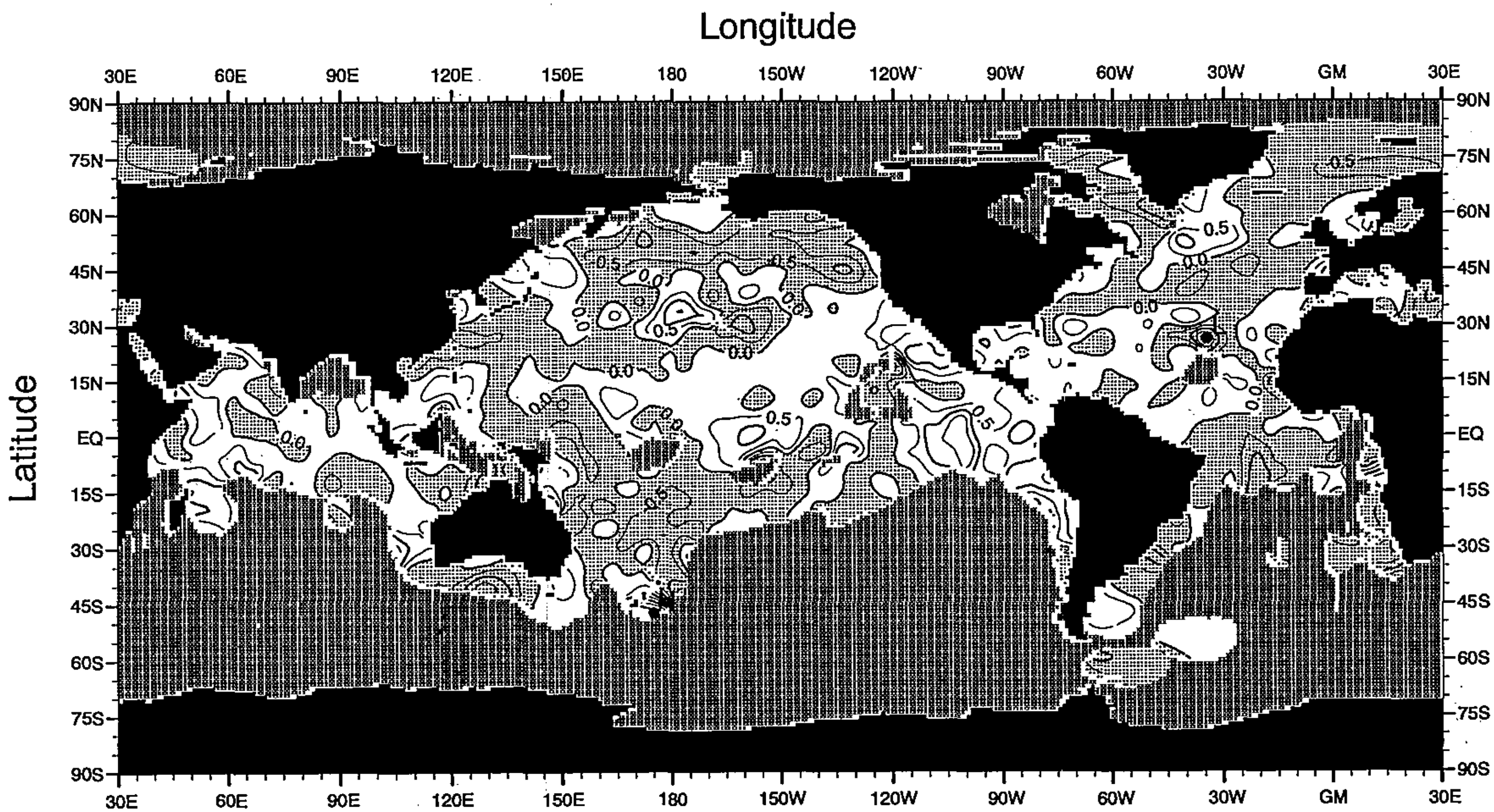


Minimum Value -2.18 Maximum Value 3.23 Contour Interval 0.50

Fig. B23 Temperature anomaly (°C) at the surface for year 1982

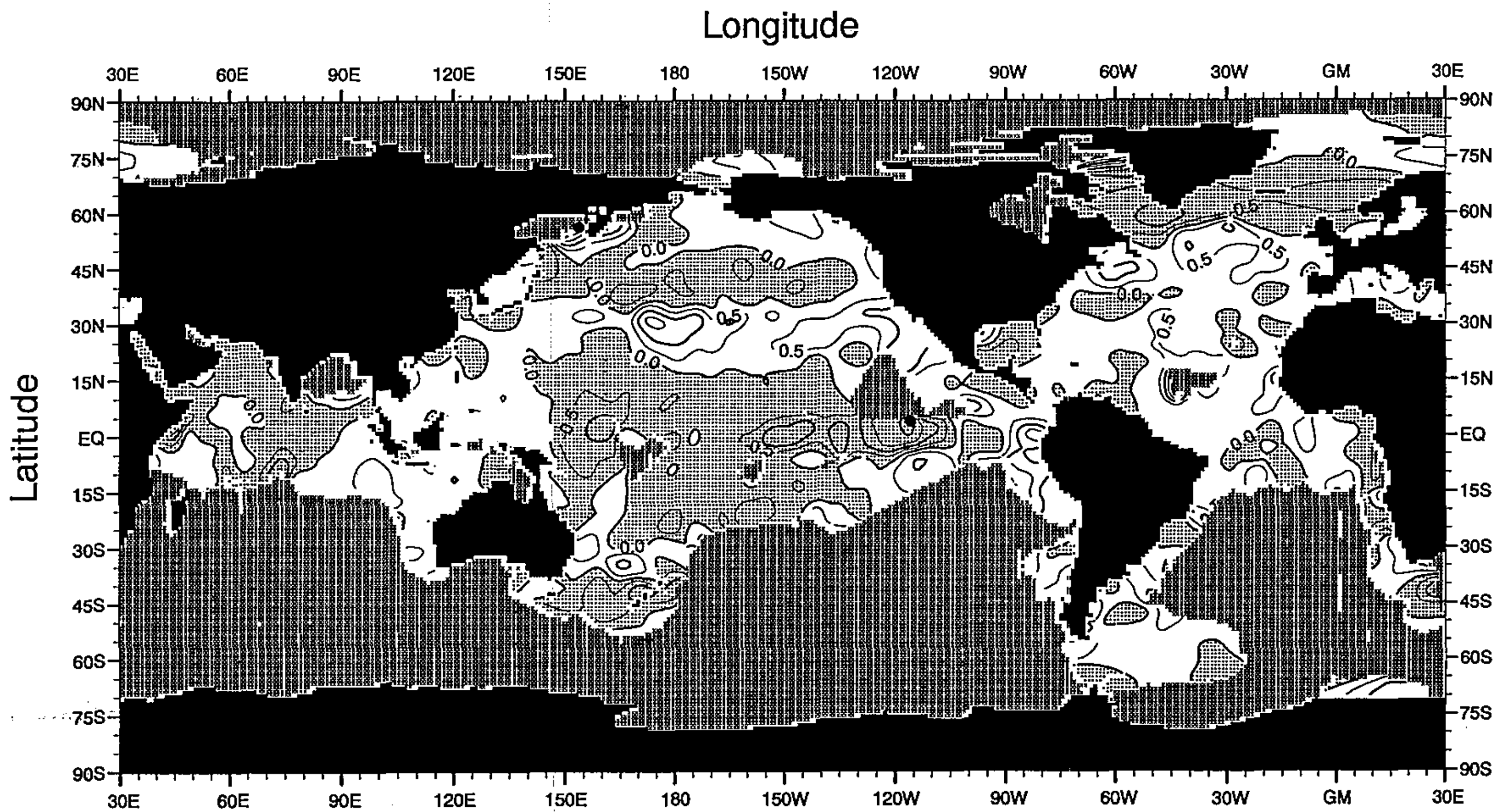


Minimum Value -2.36 Maximum Value 2.35 Contour Interval 0.50

Fig. B24 Temperature anomaly (°C) at the surface for year 1983

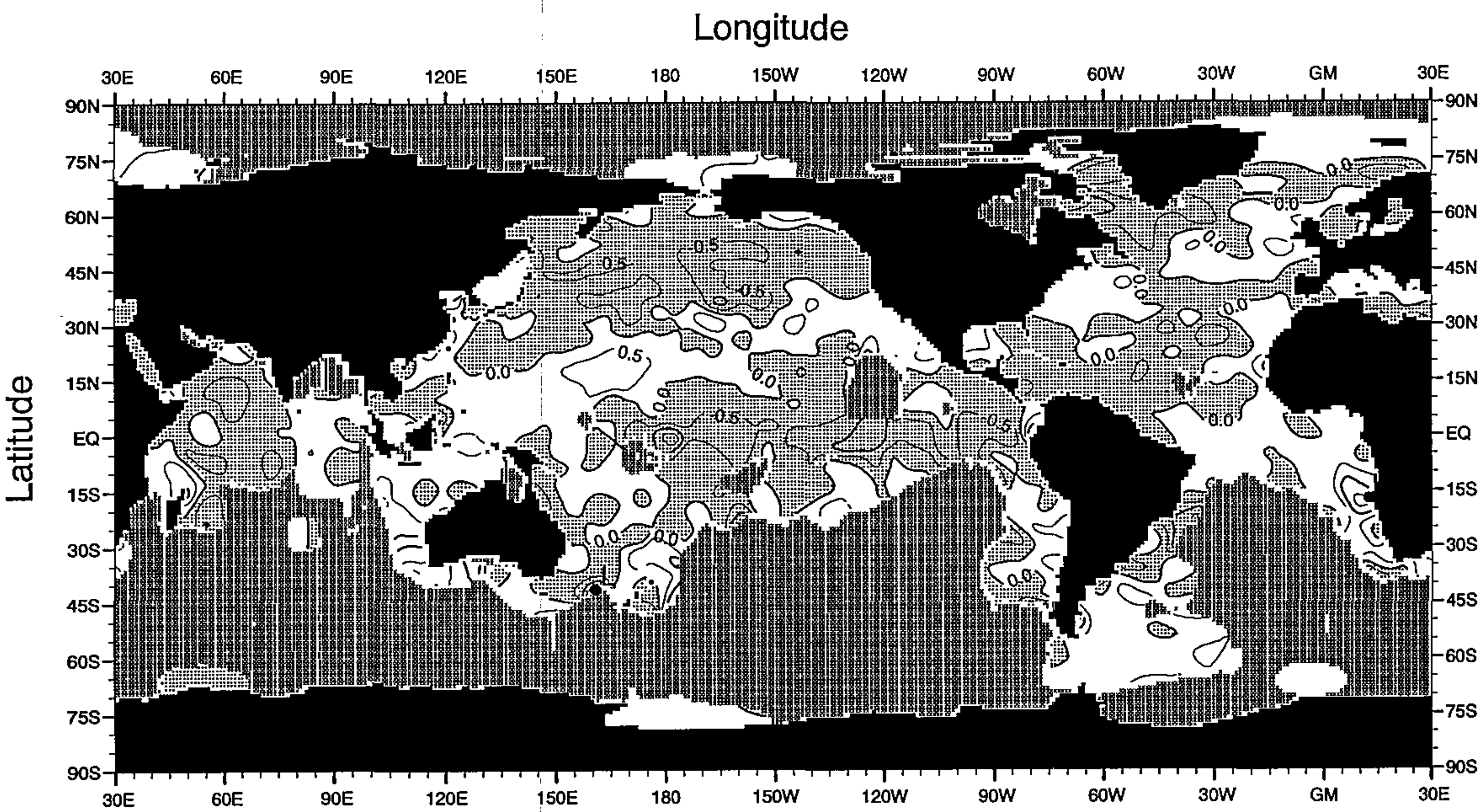


Minimum Value -2.08 Maximum Value 1.63 Contour Interval 0.50

Fig. B25 Temperature anomaly (°C) at the surface for year 1984

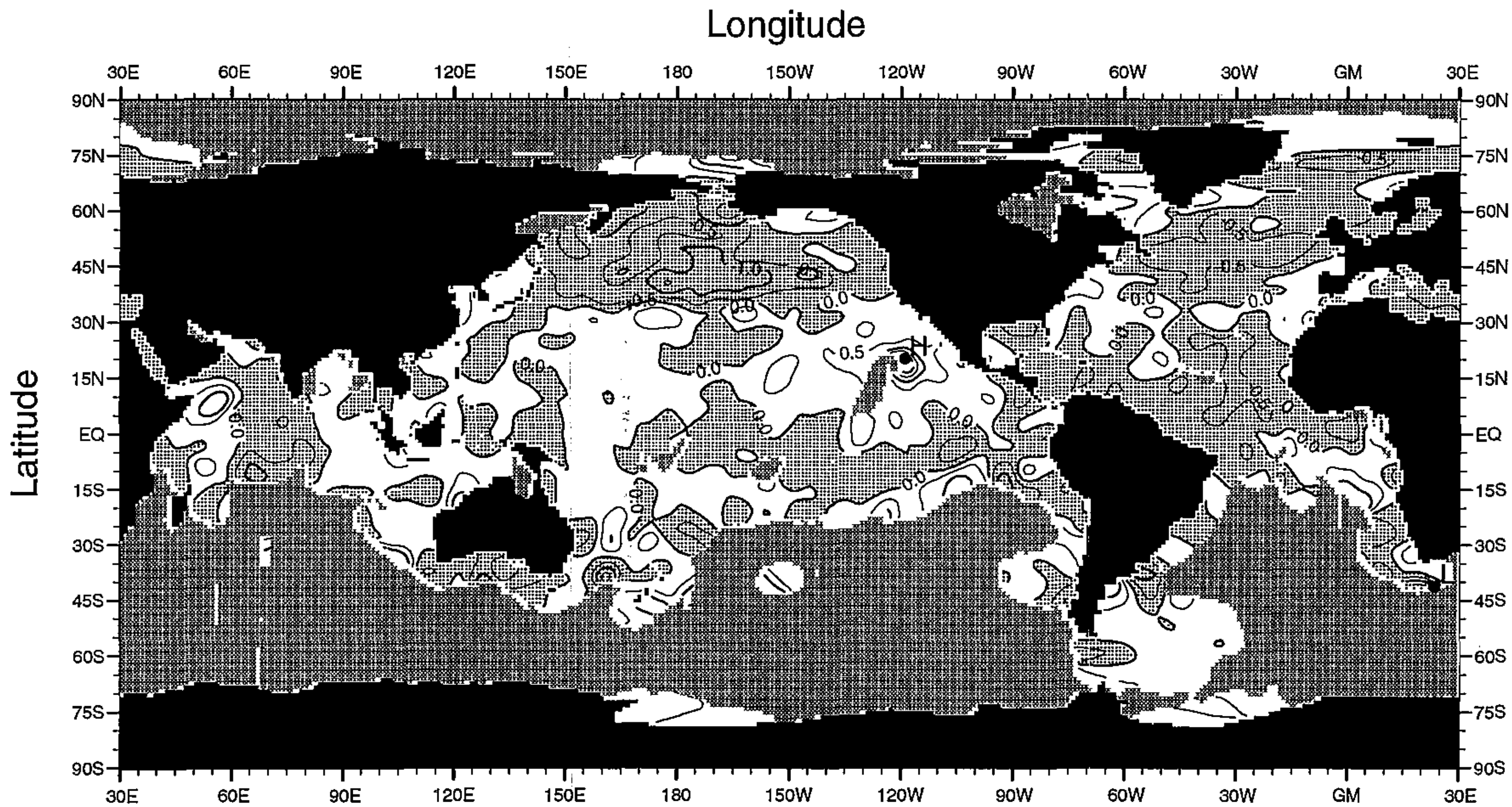


Minimum Value -1.85 Maximum Value 2.90 Contour Interval 0.50

Fig. B26 Temperature anomaly (°C) at the surface for year 1985

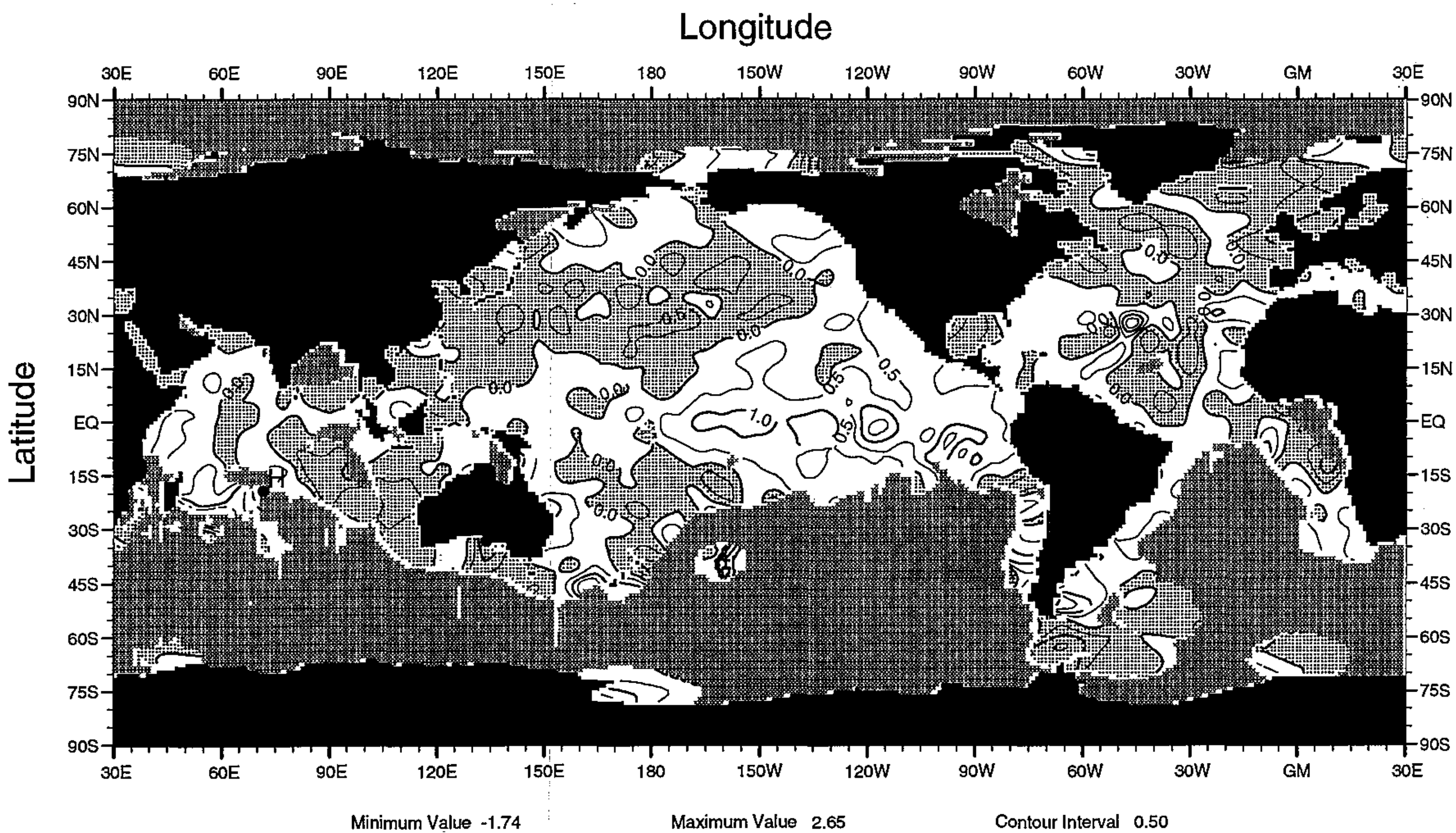


Fig. B27 Temperature anomaly (°C) at the surface for year 1986

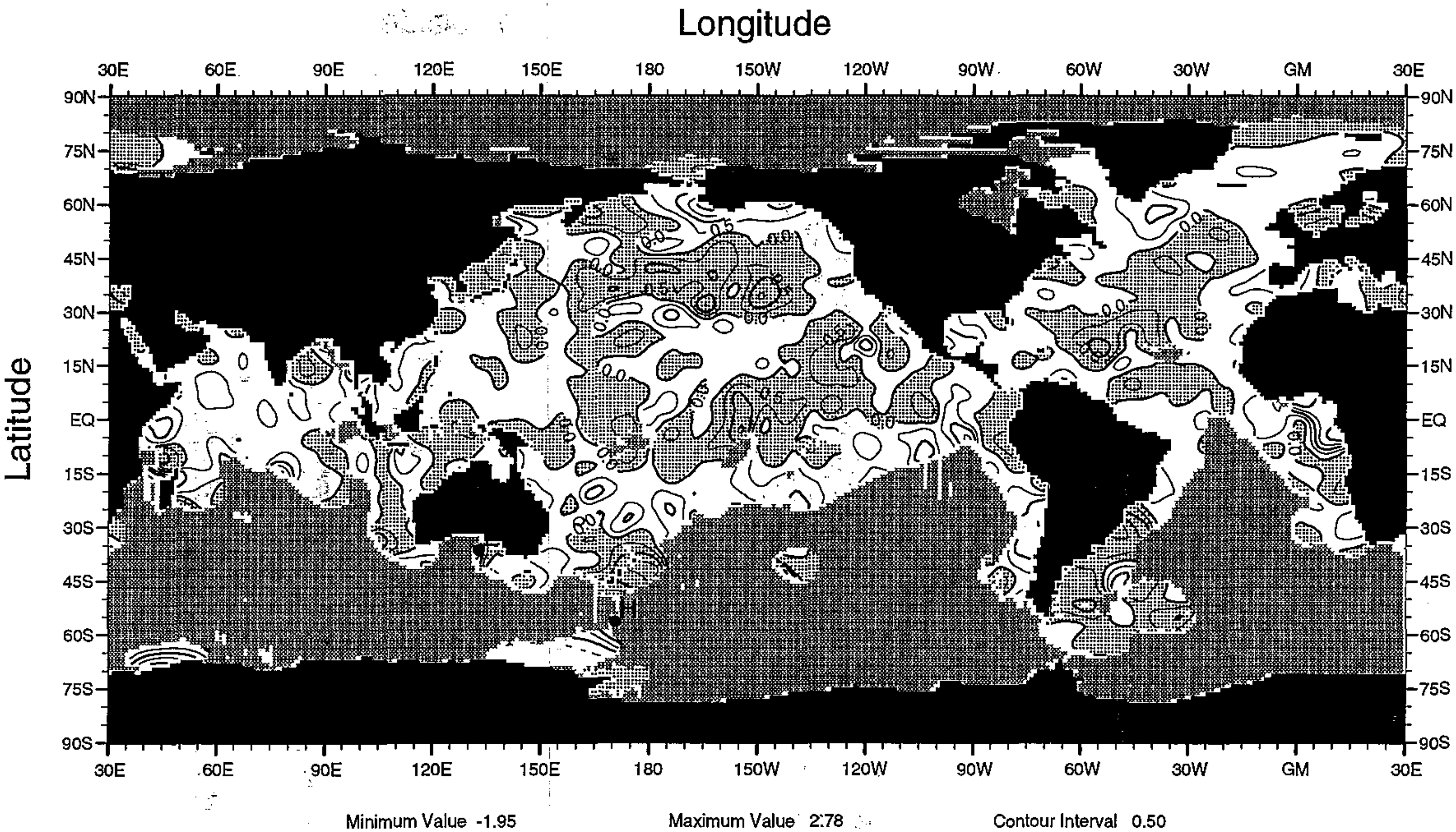


Fig. B28 Temperature anomaly (°C) at the surface for year 1987

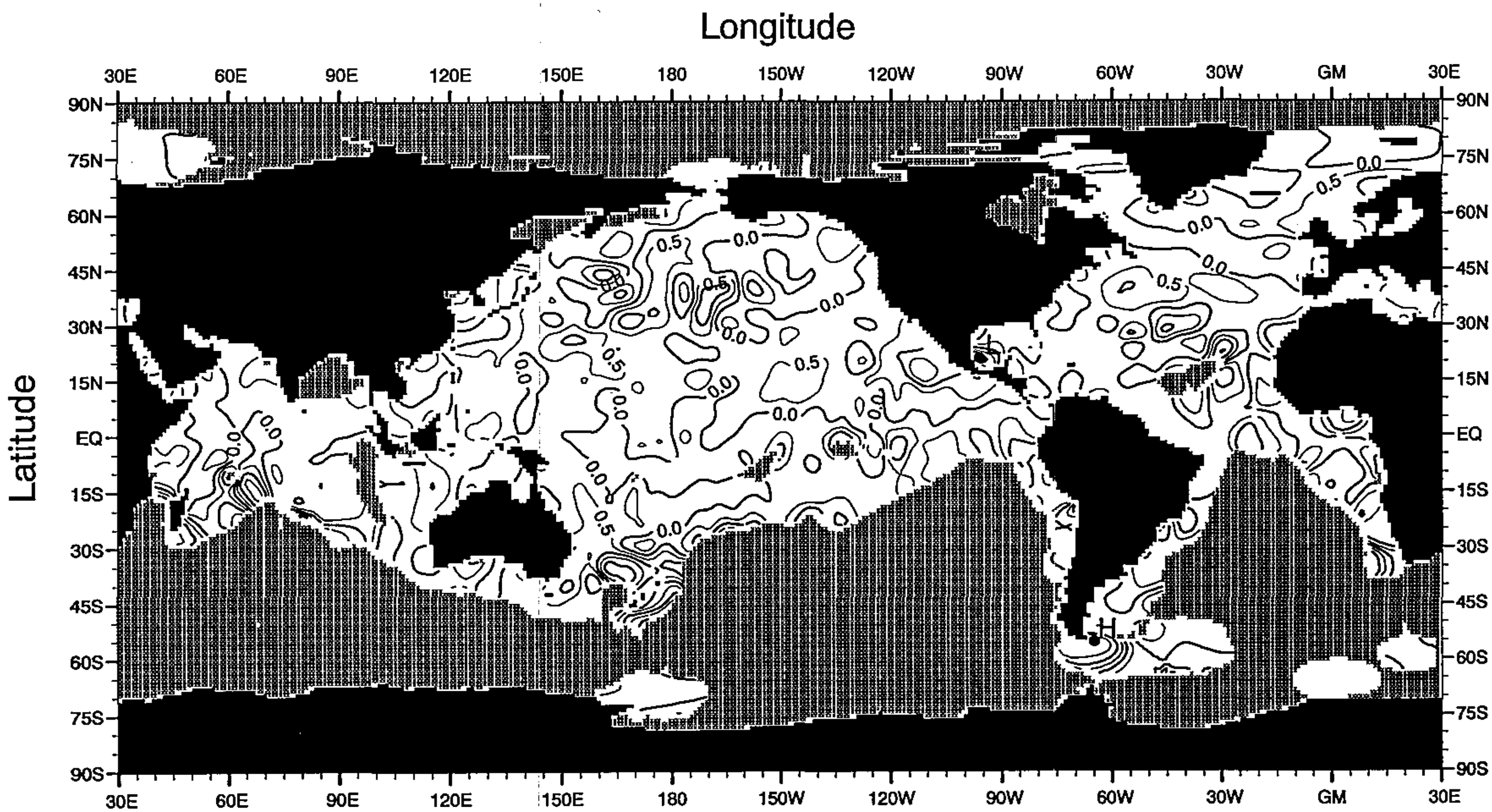


Minimum Value -3.05 Maximum Value 2.82 Contour Interval 0.50

Fig. B29 Temperature Anomaly (°C) at the surface for year 1988

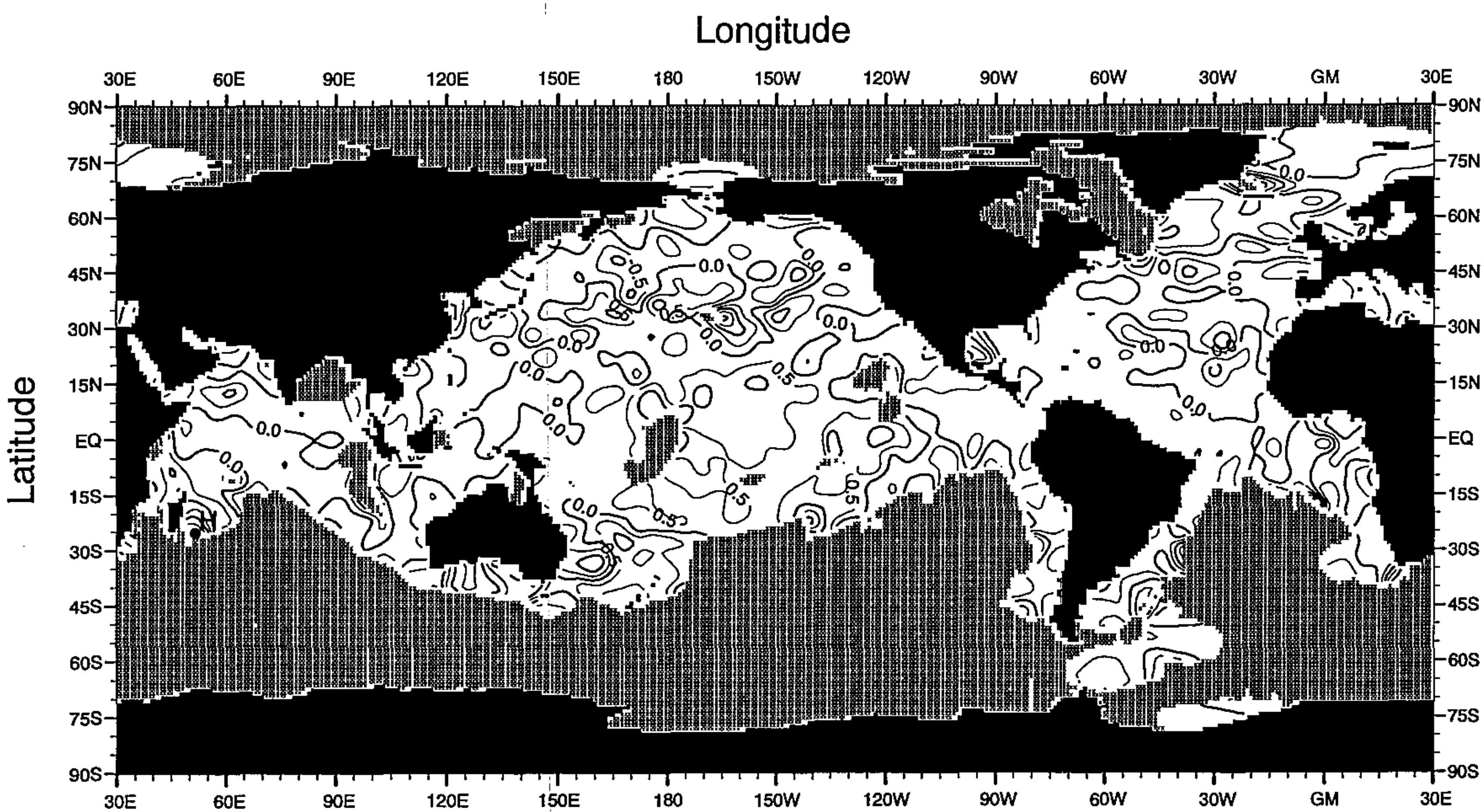


Minimum Value -2.77 Maximum Value 2.86 Contour Interval 0.50

Fig. B30 Temperature Anomaly (°C) at the surface for year 1989

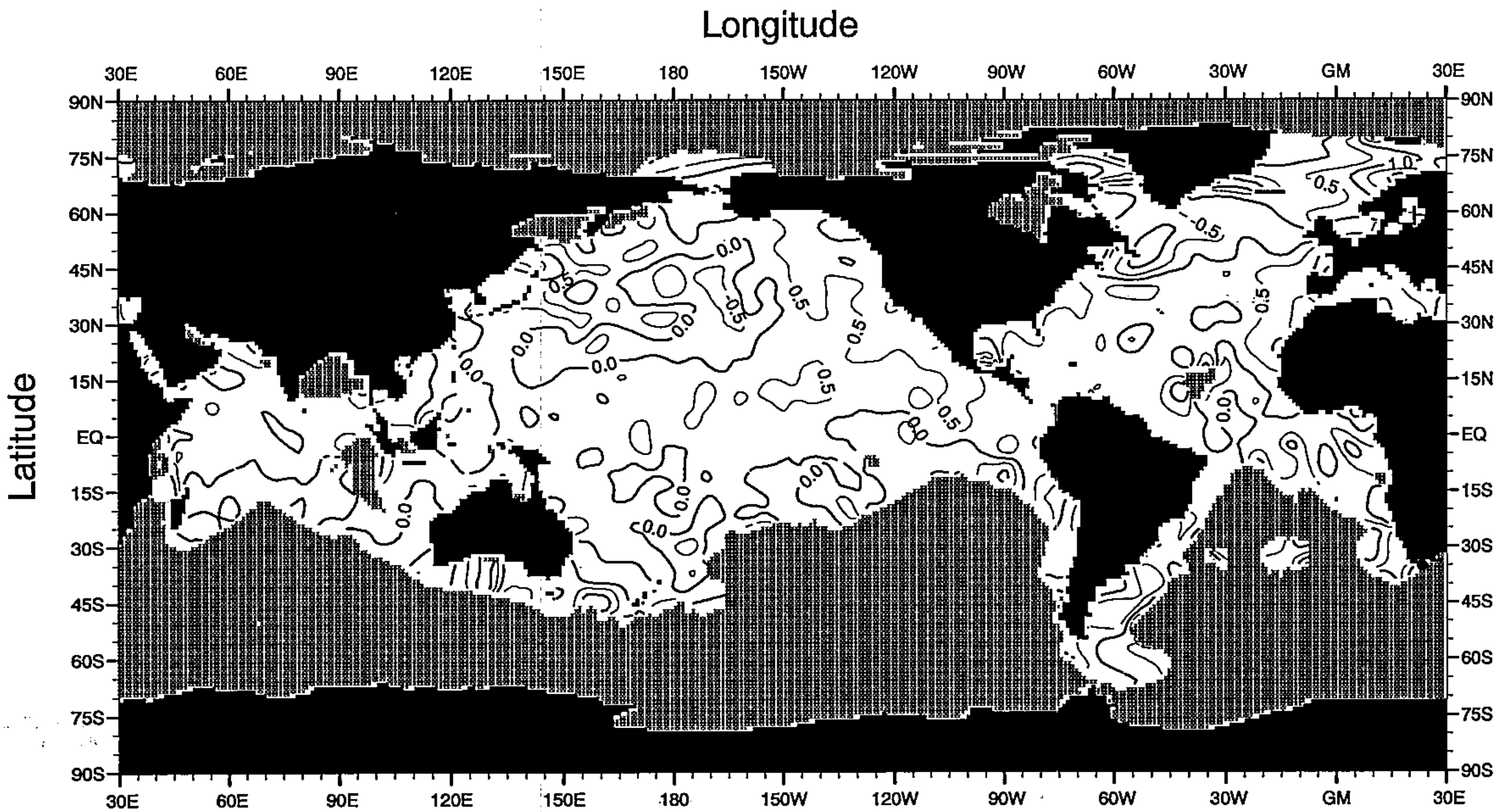


Minimum Value -1.89 Maximum Value 2.26 Contour Interval 0.50

Fig. B31 Temperature Anomaly (°C) at the surface for year 1990

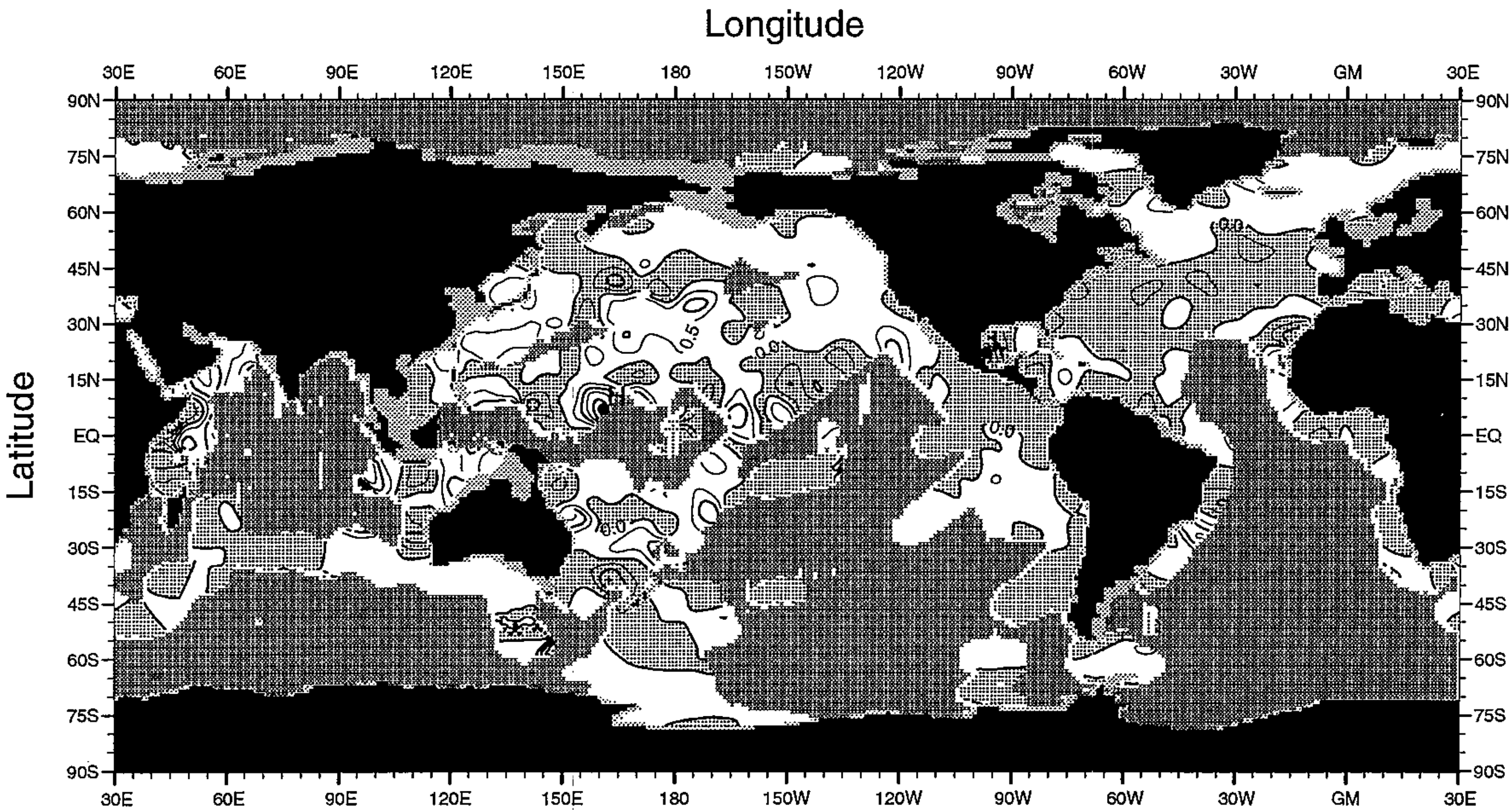


Minimum Value -2.34 Maximum Value 2.33 Contour Interval 0.50

Fig. C1 Temperature anomaly (°C) at 125 m depth for year 1960

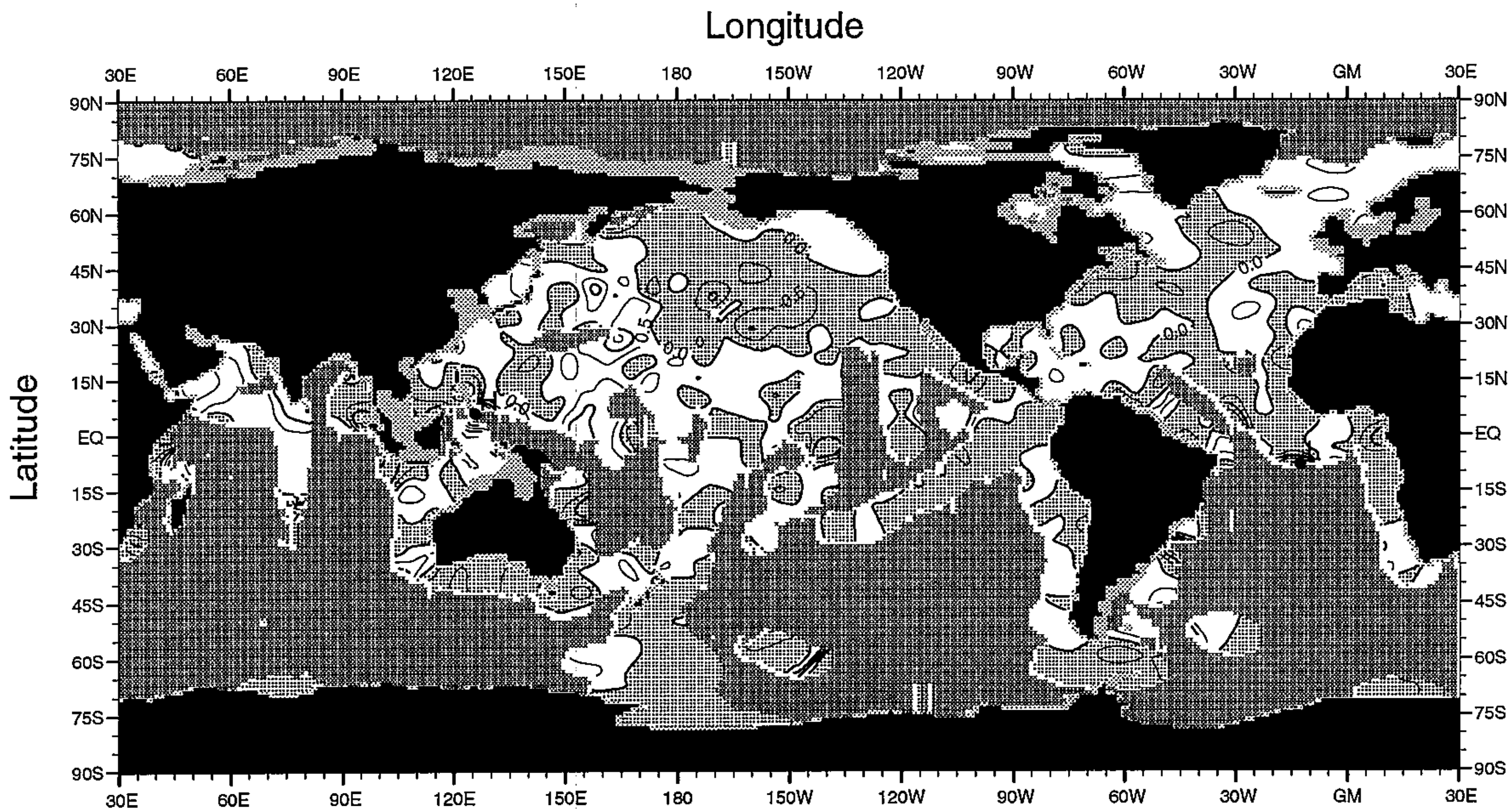


Minimum Value -2.37 Maximum Value 2.96 Contour Interval 0.50

Fig. C2 Temperature anomaly (°C) at 125 m depth for year 1961

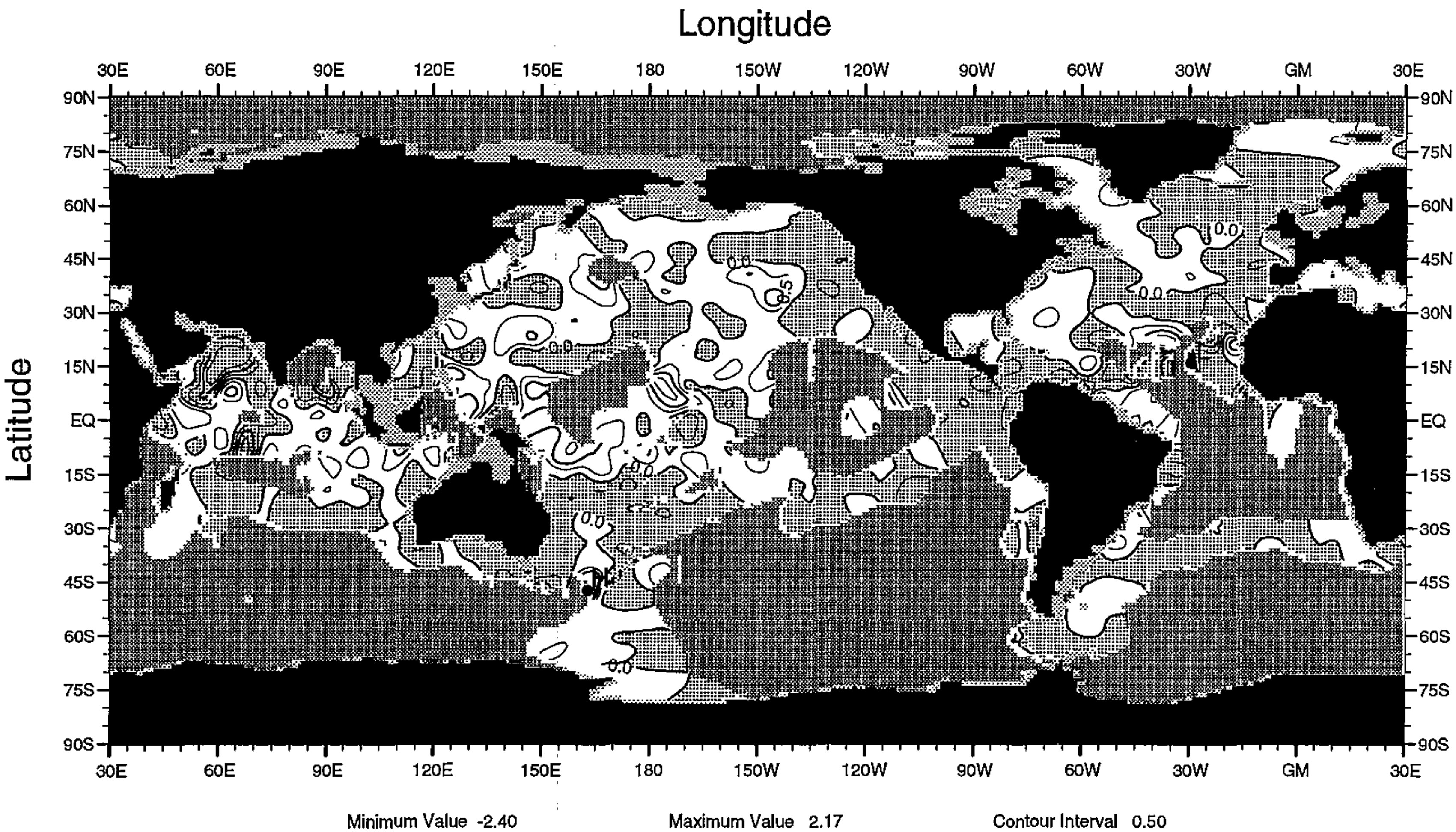


Fig. C3 Temperature anomaly (°C) at 125 m depth for year 1962

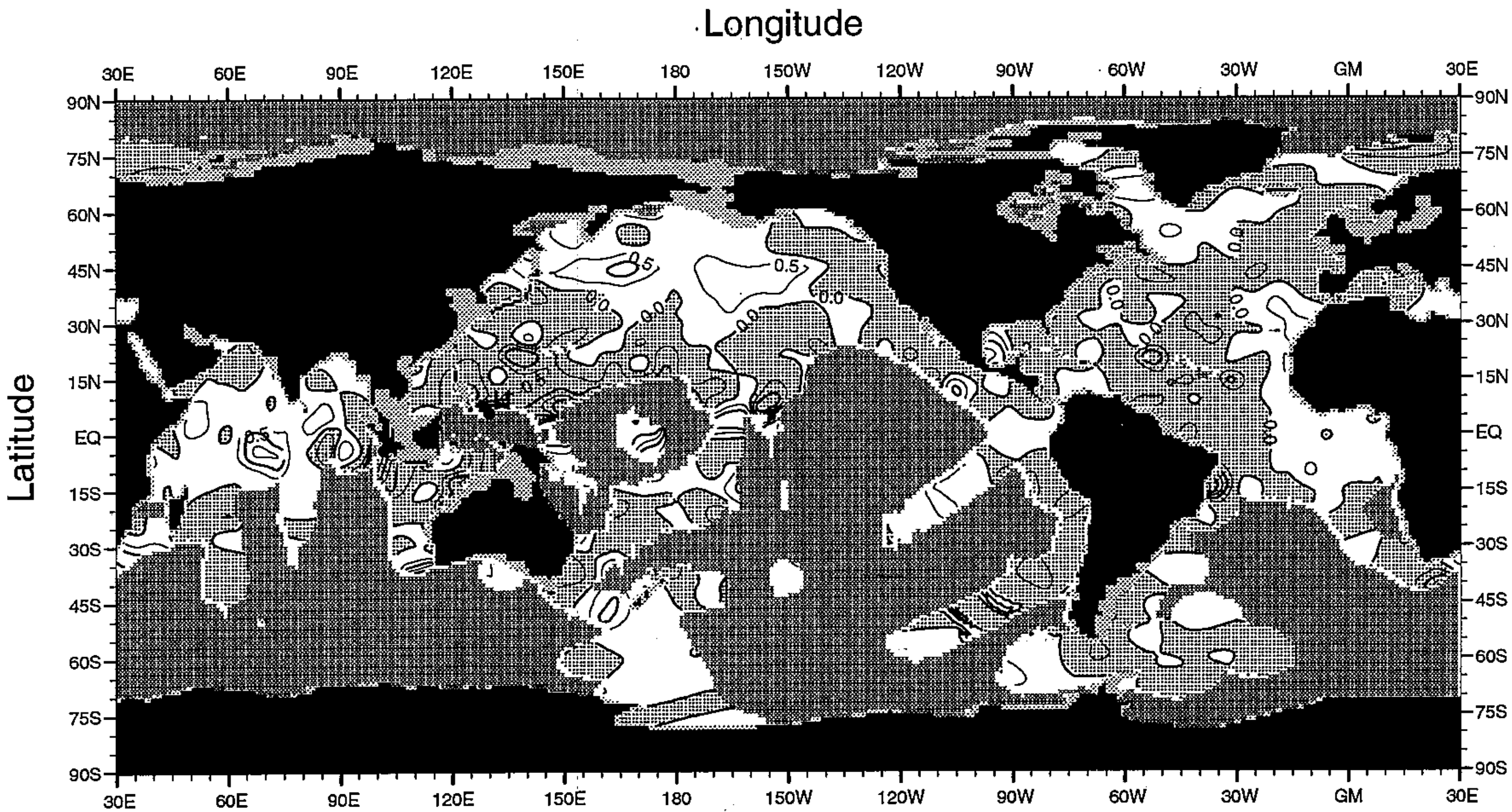


Minimum Value -2.83 Maximum Value 3.06 Contour Interval 0.50

Fig. C4 Temperature anomaly (°C) at 125 m depth for year 1963

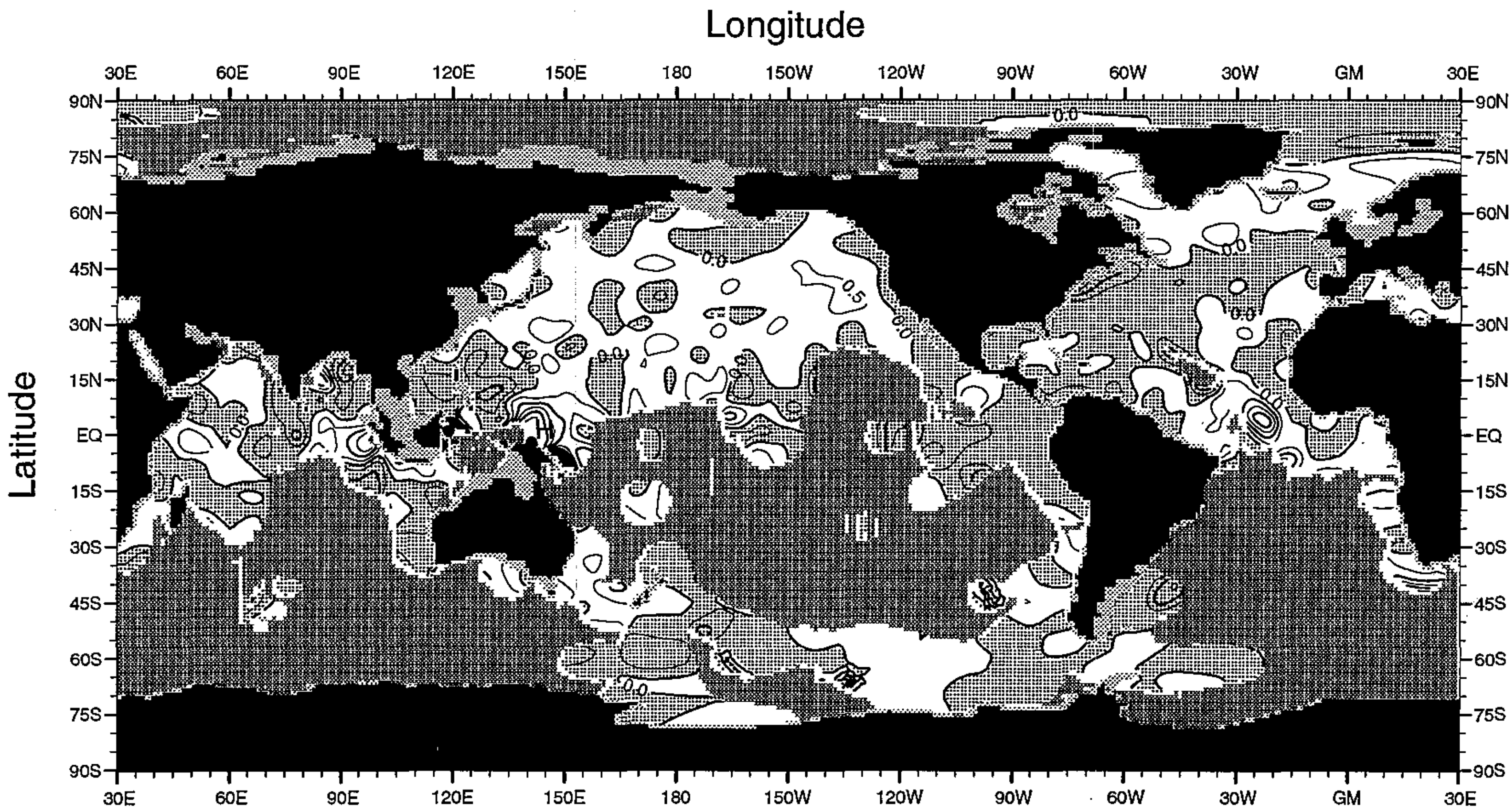


Minimum Value -3.37 Maximum Value 2.80 Contour Interval 0.50

Fig. C5 Temperature anomaly (°C) at 125 m depth for year 1964

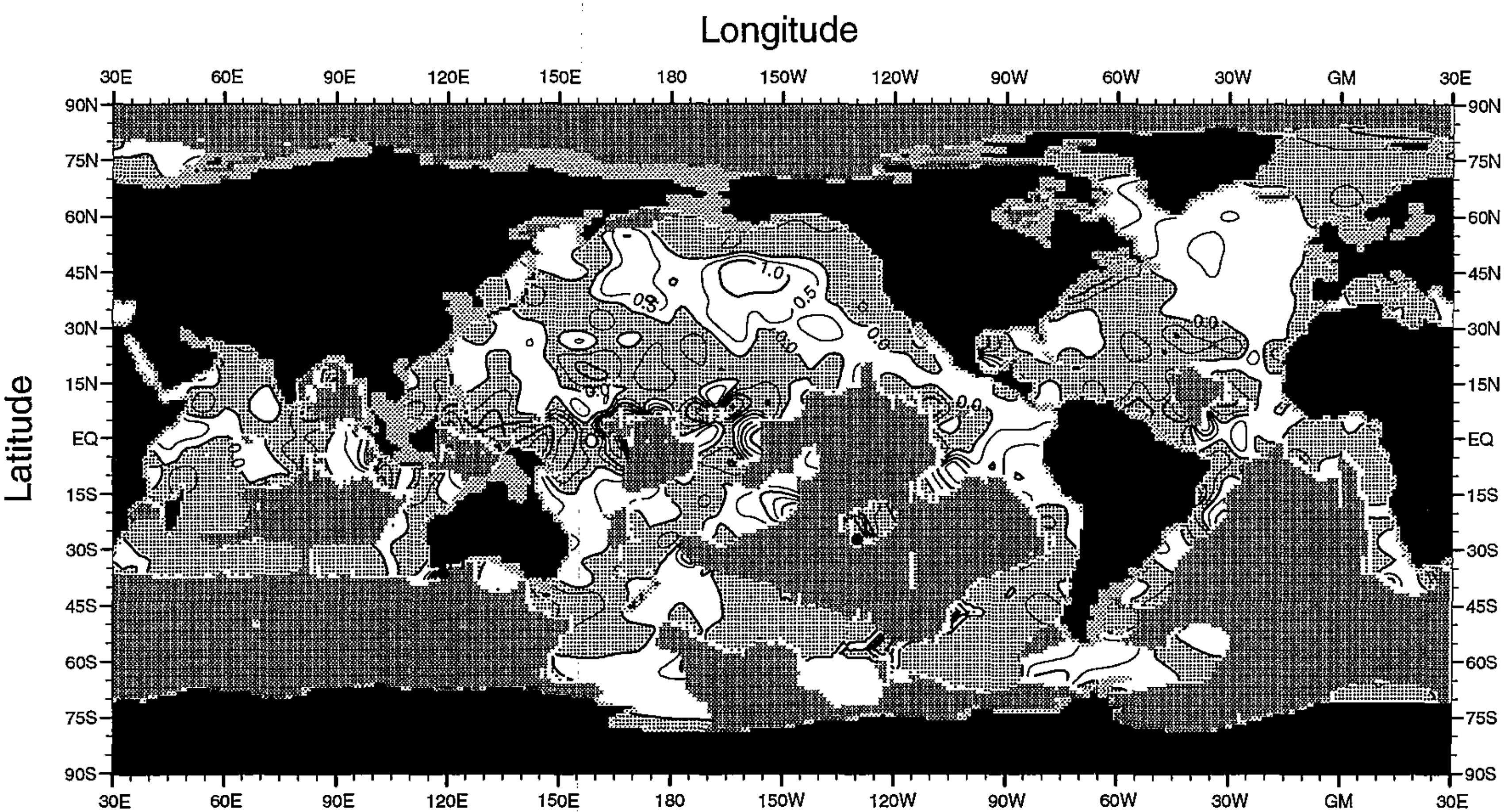


Minimum Value -3.46    Maximum Value 2.66    Contour Interval 0.50

Fig. C6 Temperature anomaly (°C) at 125 m depth for year 1965

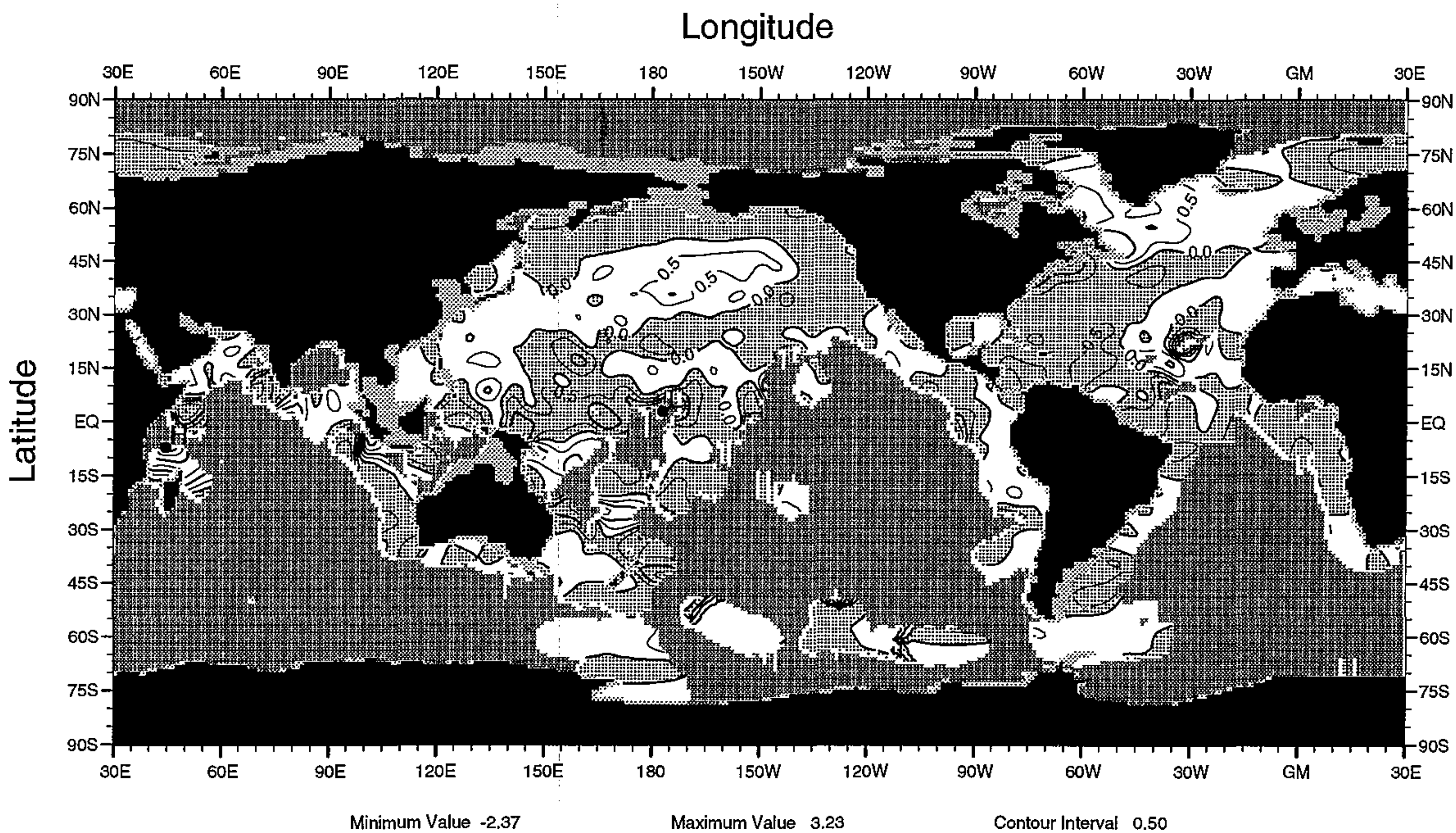


Fig. C7 Temperature anomaly (°C) at 125 m depth for year 1966

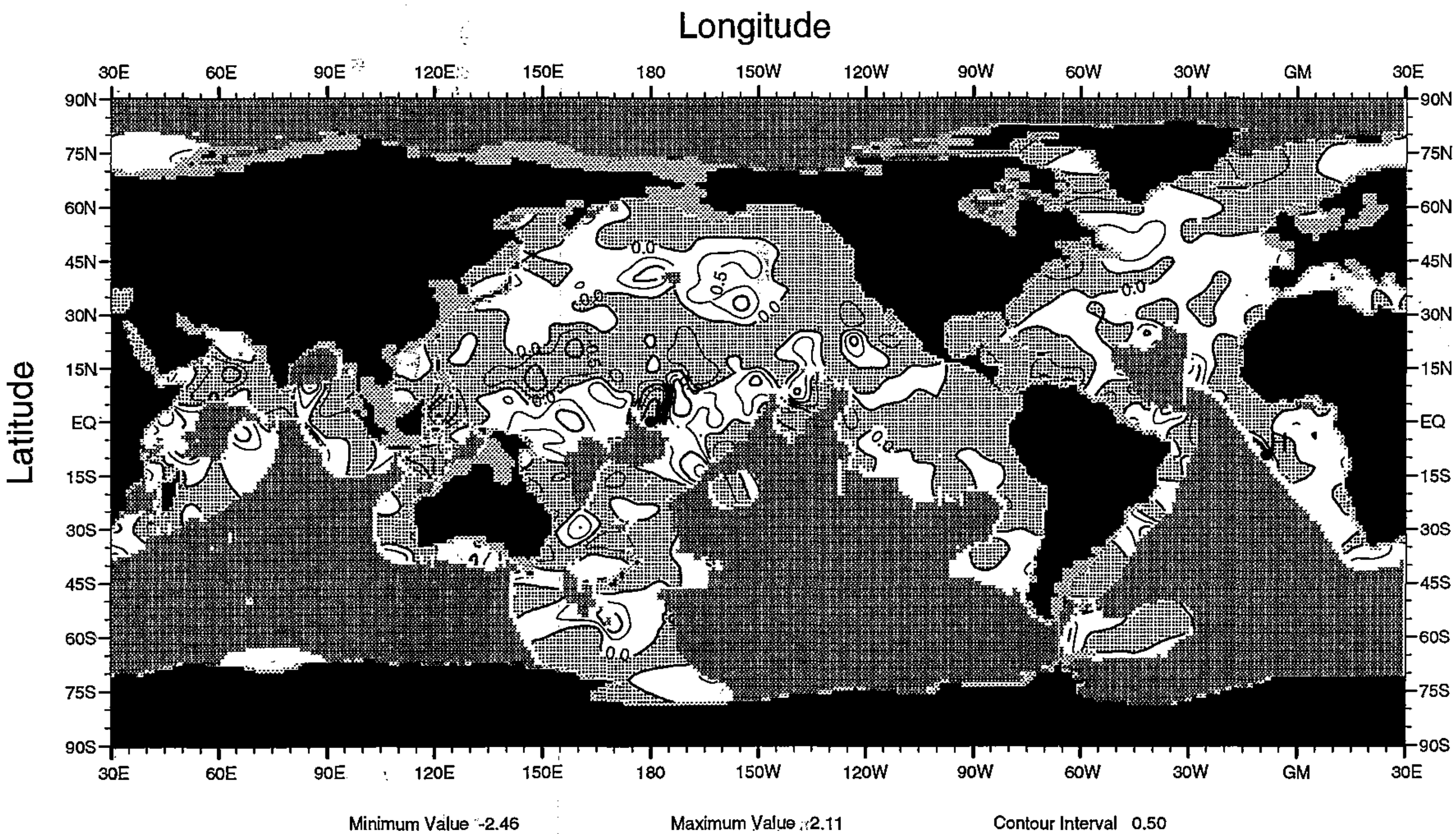


Fig. C8 : Temperature anomaly (°C) at 125 m depth for year 1967

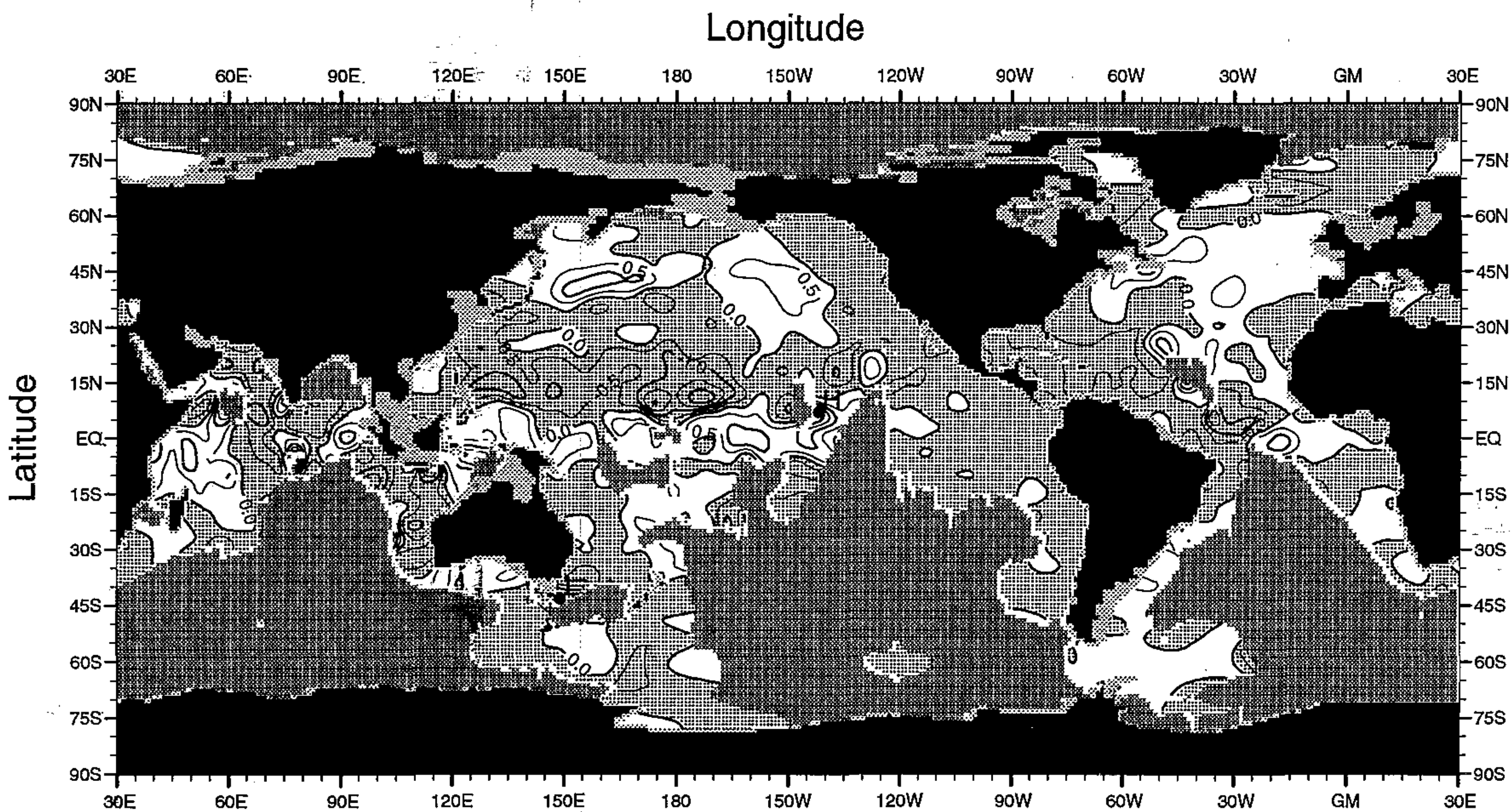


Minimum Value -2.94 Maximum Value 2.54 Contour Interval 0.50

Fig. C9 Temperature anomaly (°C) at 125 m depth for year 1968

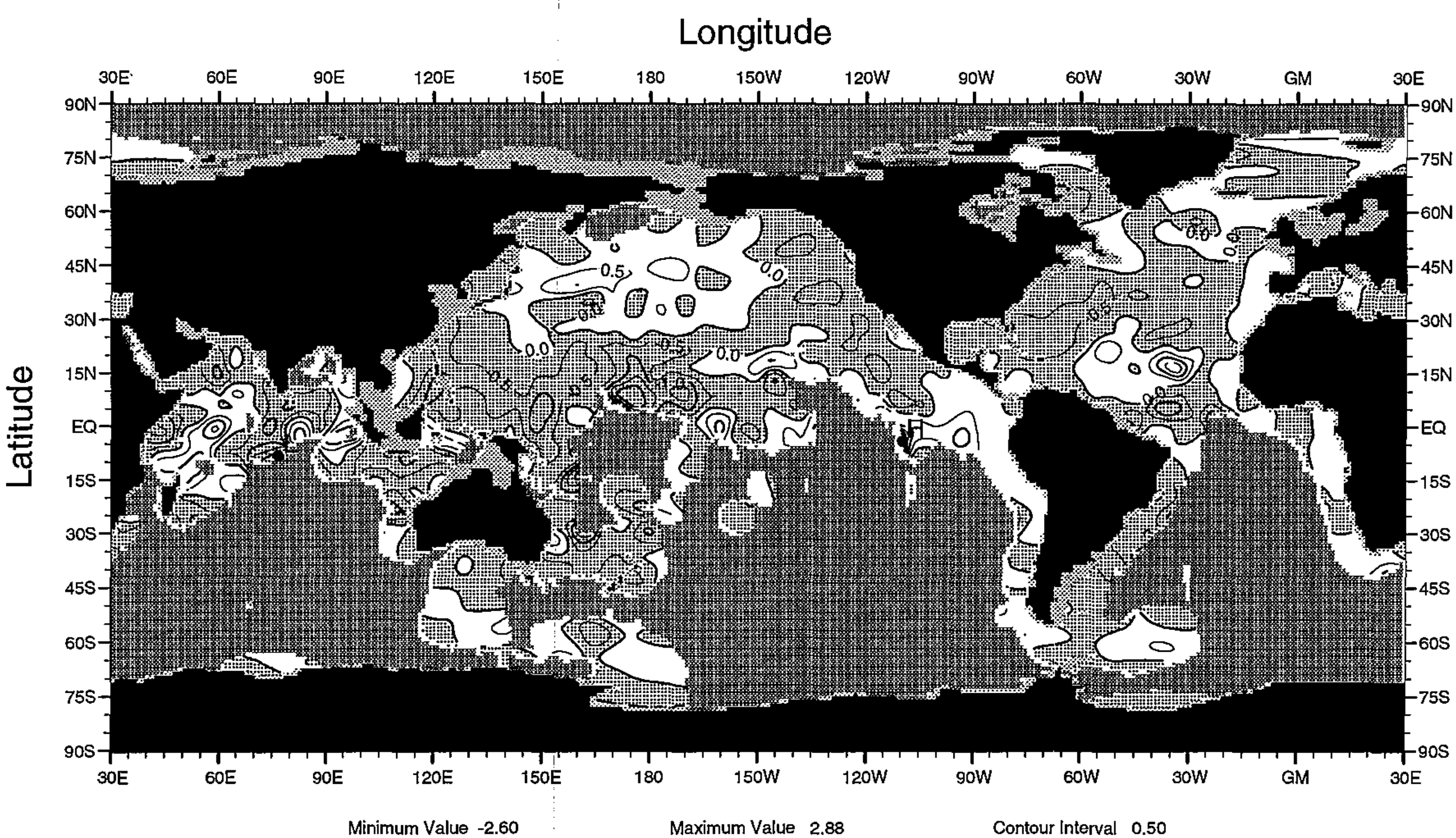


Fig. C10 Temperature anomaly (°C) at 125 m depth for year 1969

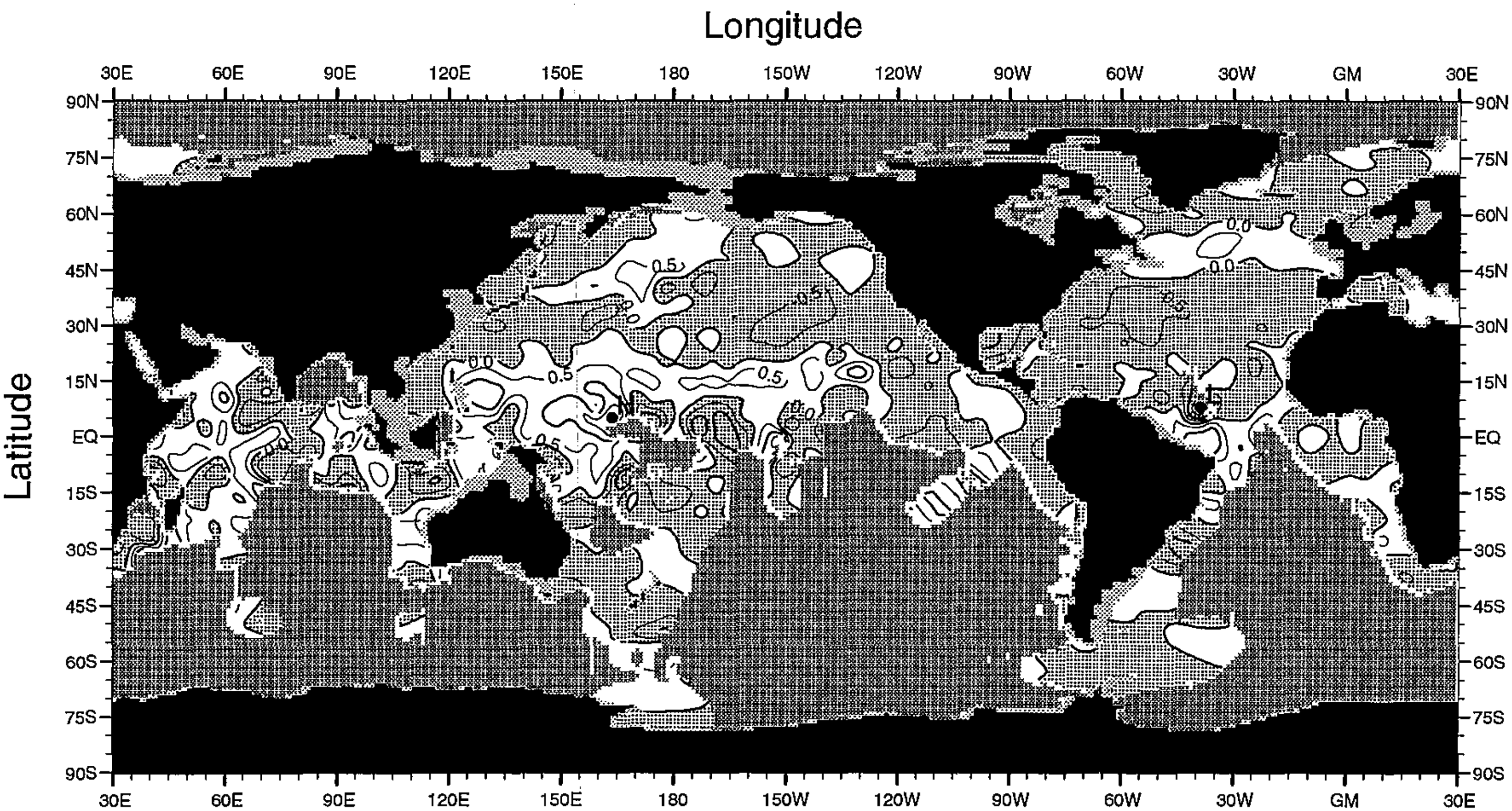


Minimum Value -1.87    Maximum Value 2.06    Contour Interval 0.50

Fig. C11 Temperature anomaly (°C) at 125 m depth for year 1970

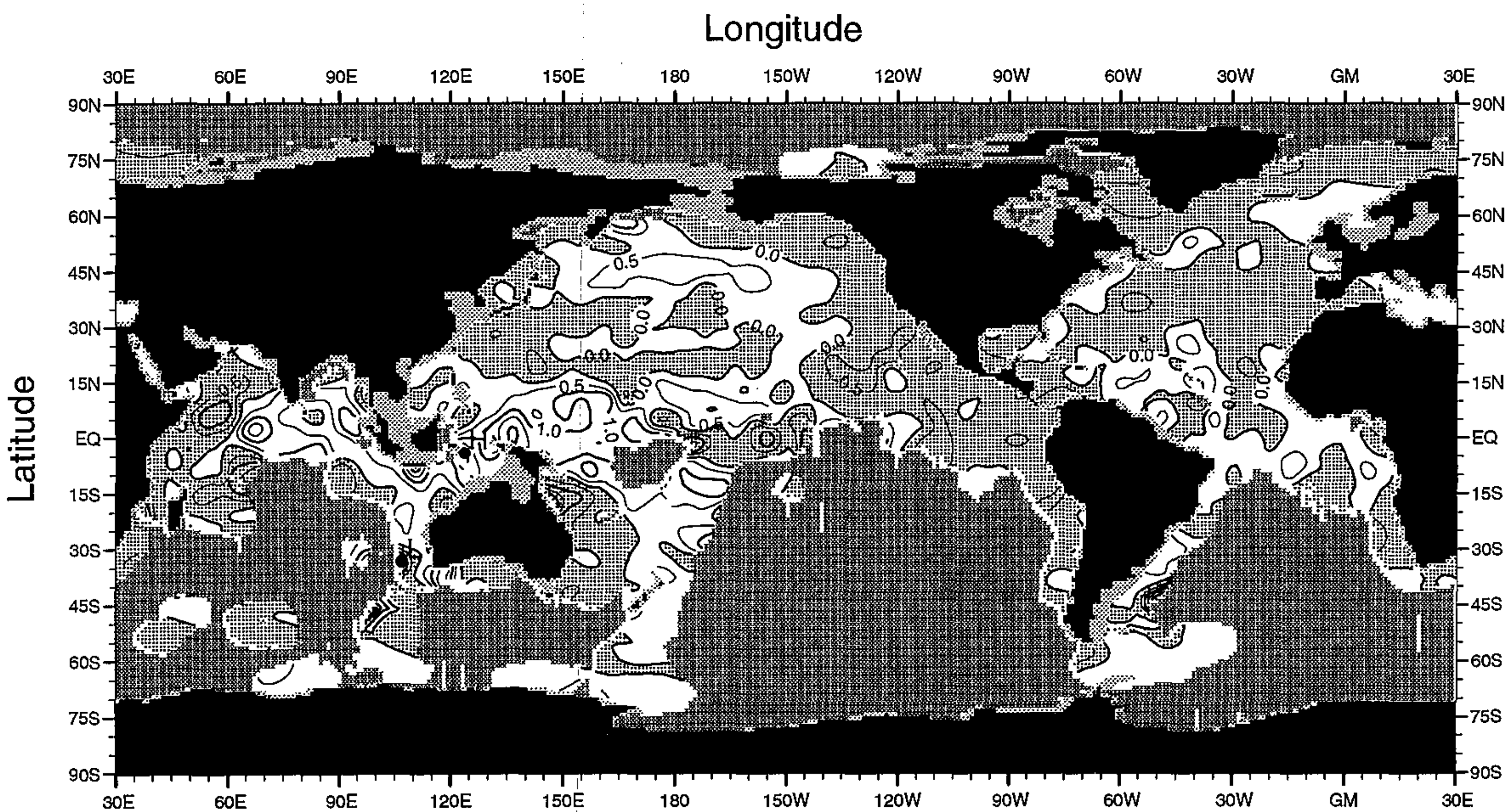


Minimum Value -2.45 Maximum Value 2.28 Contour Interval 0.50

Fig. C12 Temperature anomaly (°C) at 125 m depth for year 1971

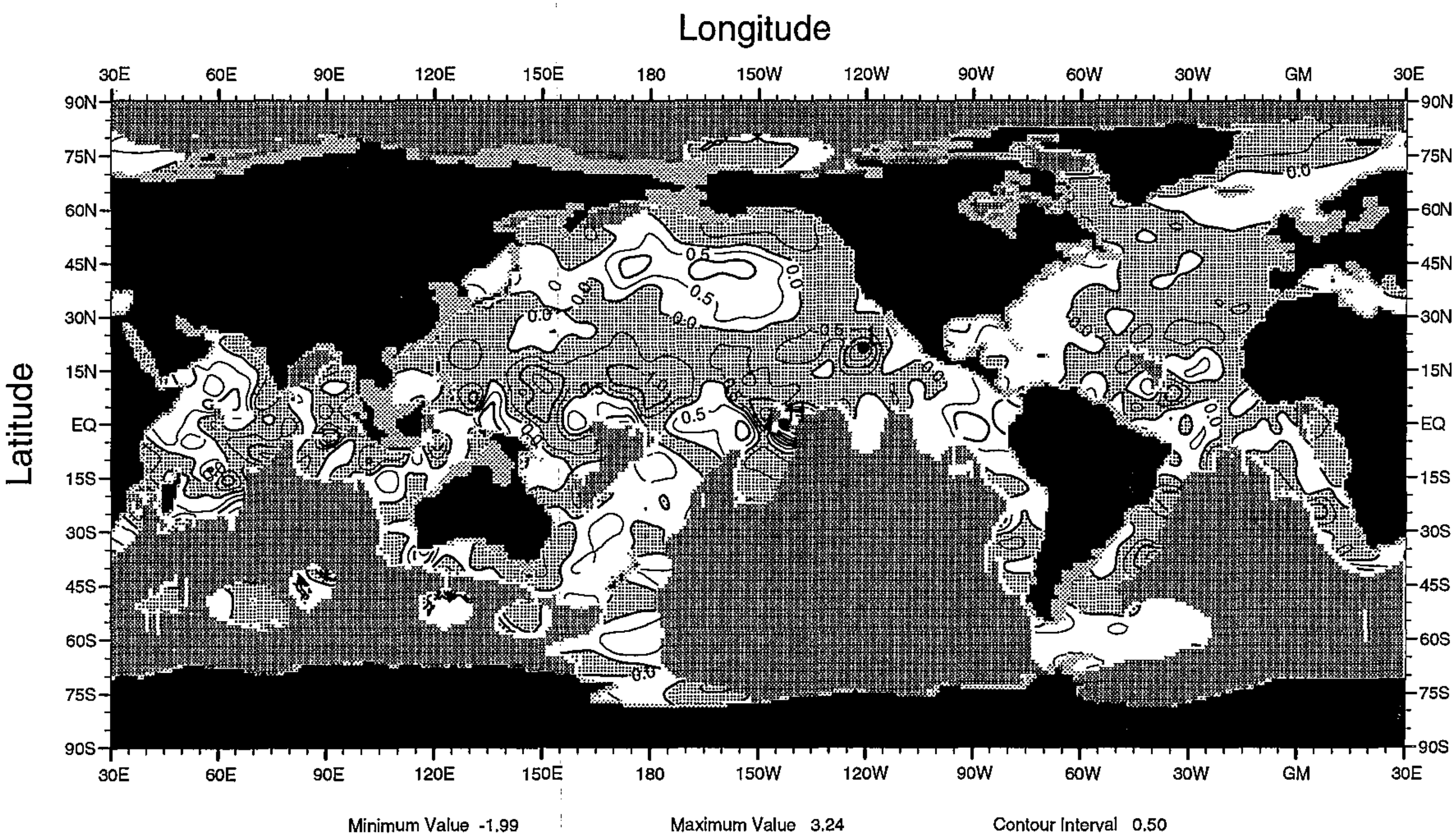


Fig. C13 Temperature anomaly (°C) at 125 m depth for year 1972

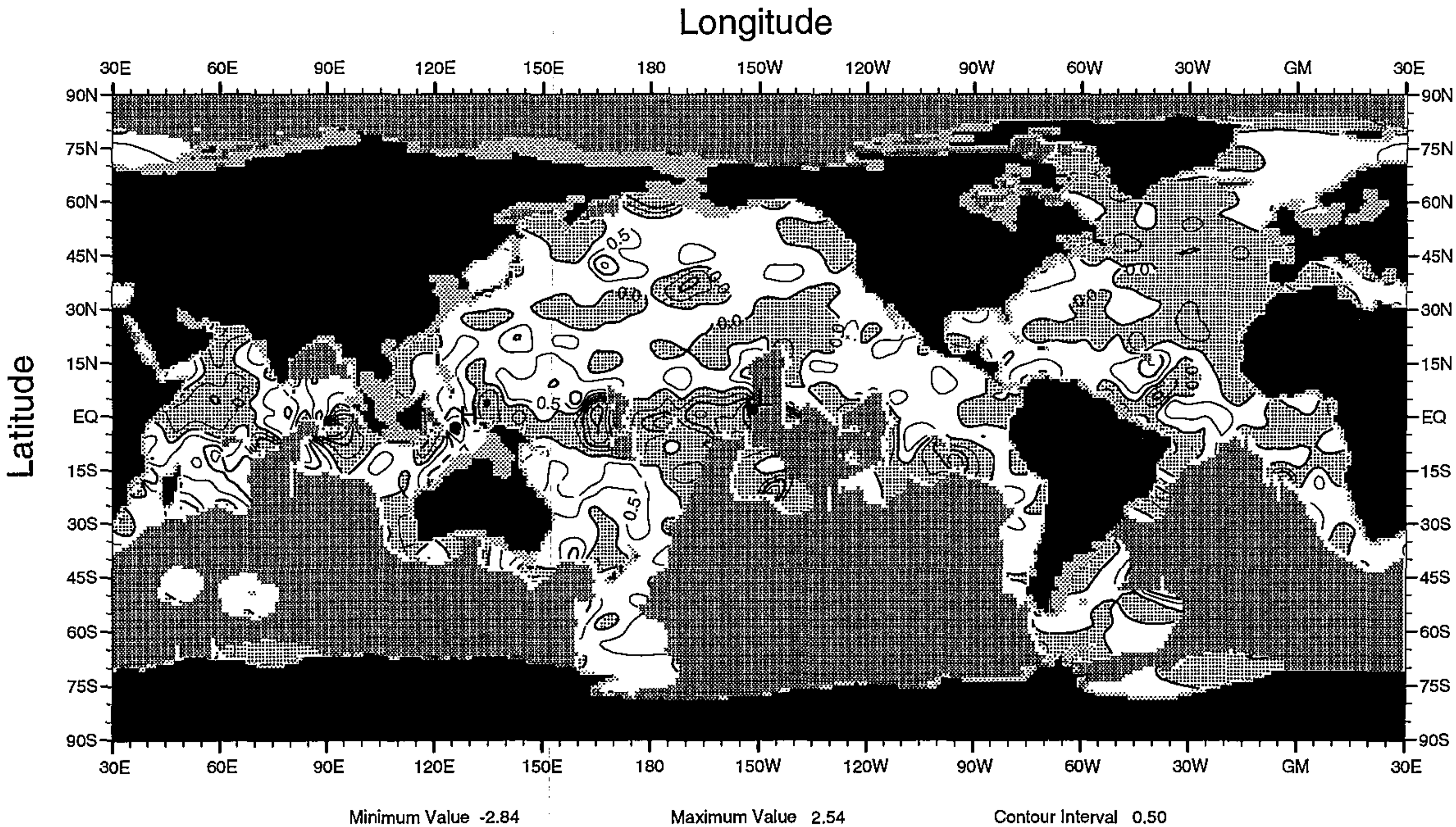


Fig. C14 Temperature anomaly (°C) at 125 m depth for year 1973

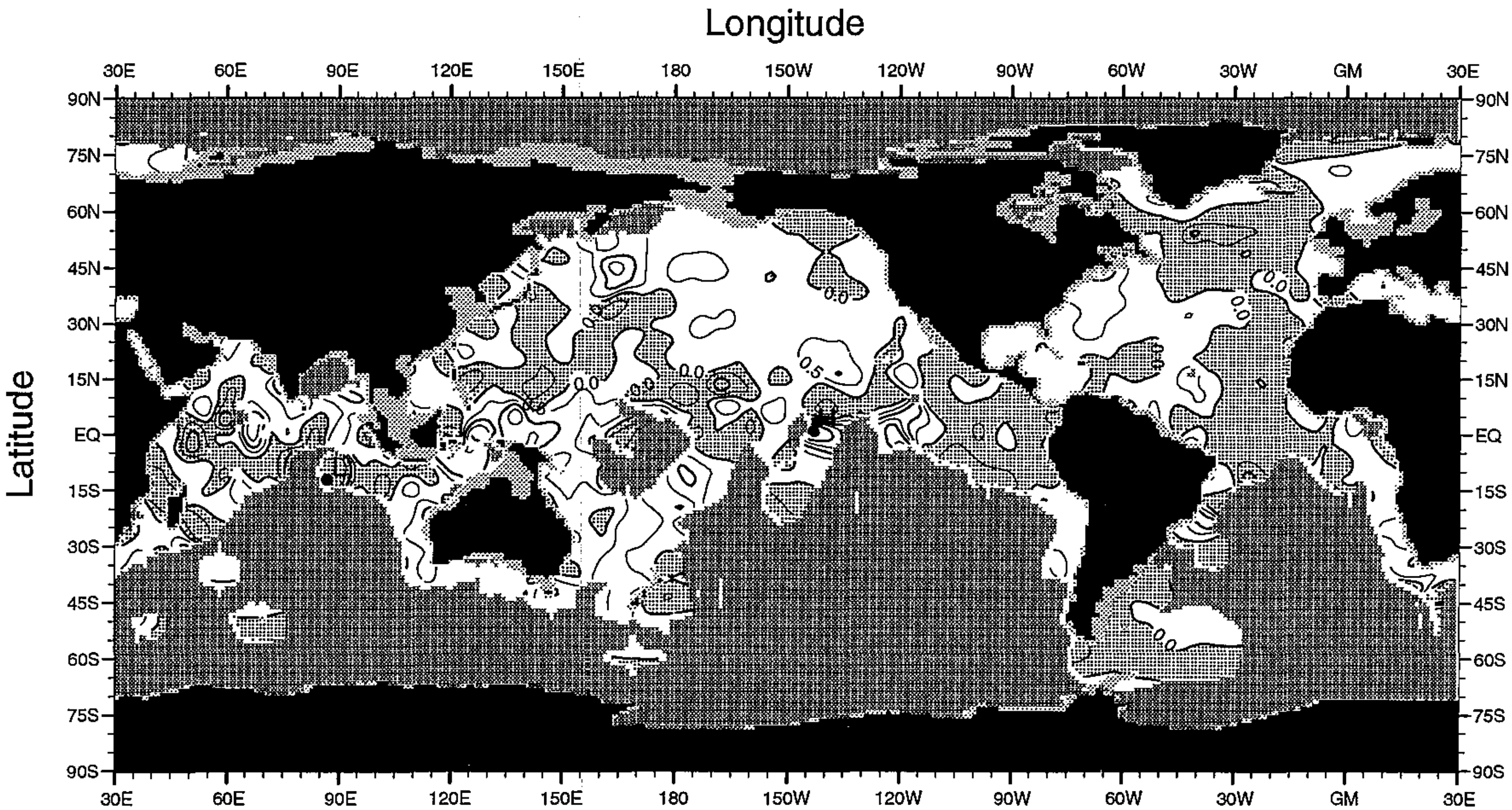


Minimum Value -1.67 Maximum Value 2.76 Contour Interval 0.50

Fig. C15 Temperature anomaly (°C) at 125 m depth for year 1974

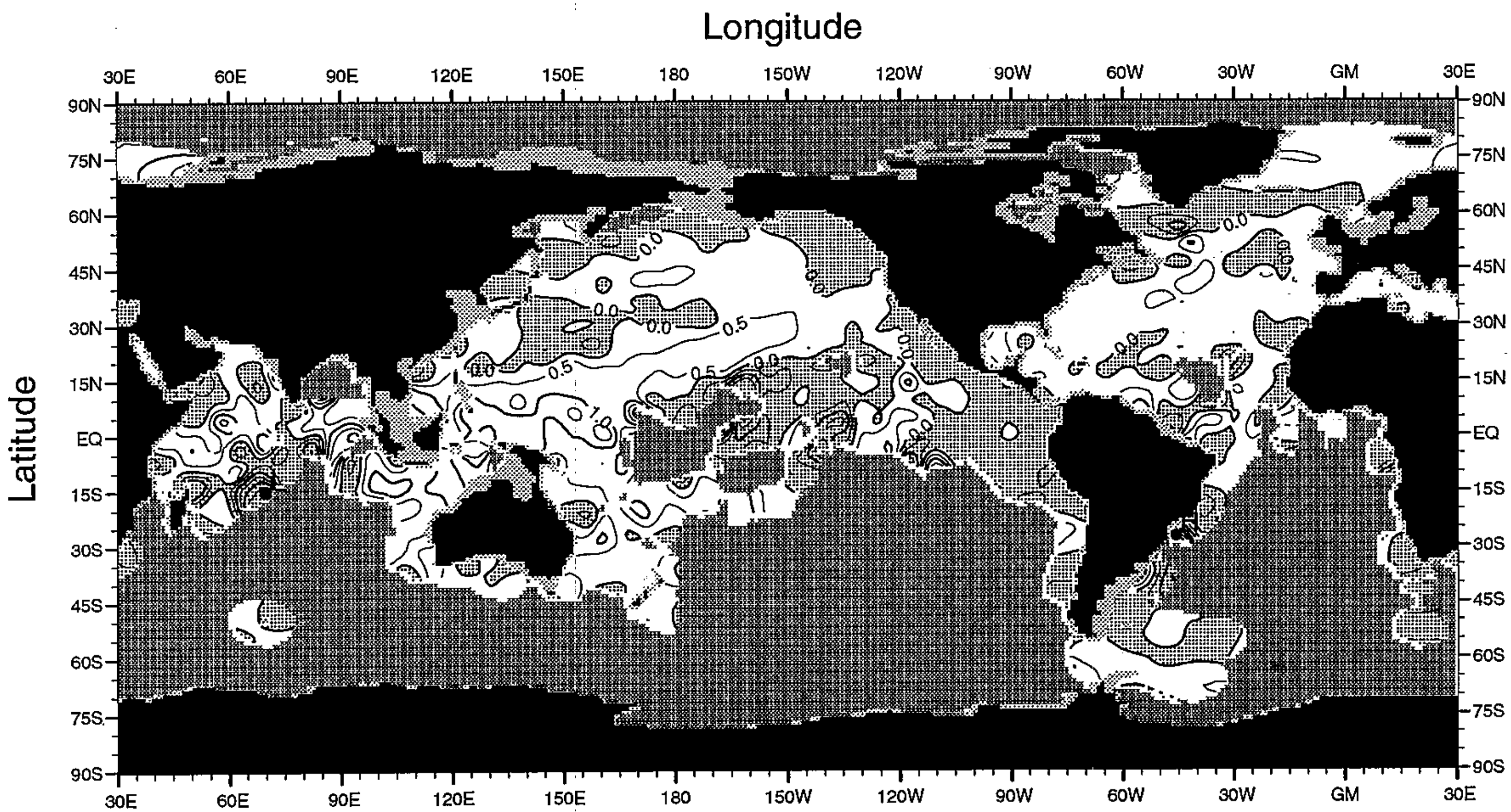


Minimum Value -2.99 Maximum Value 3.28 Contour Interval 0.50

Fig. C16 Temperature anomaly (°C) at 125 m depth for year 1975

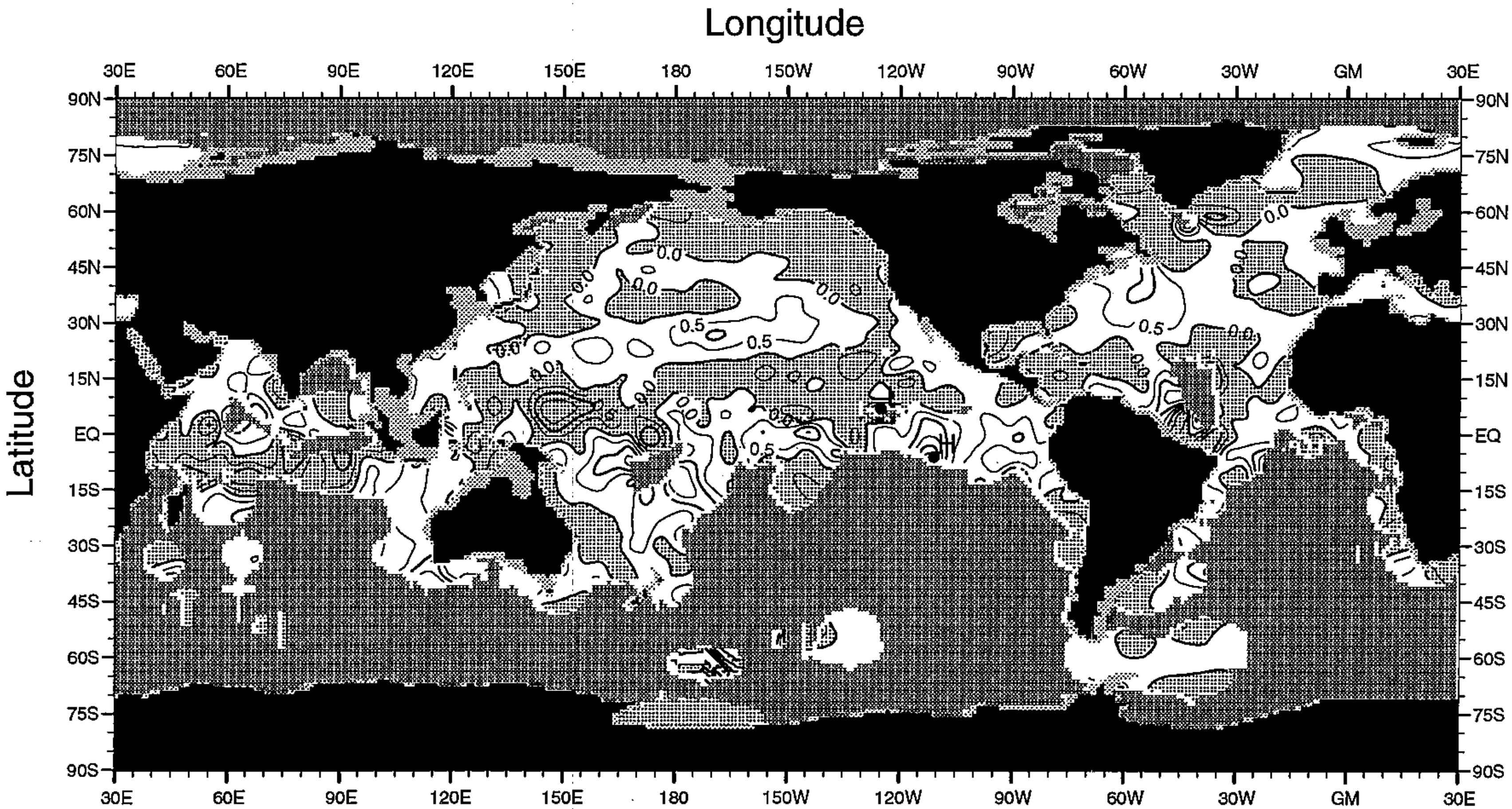


Minimum Value -1.90 Maximum Value 2.75 Contour Interval 0.50

Fig. C17 Temperature anomaly (°C) at 125 m depth for year 1976

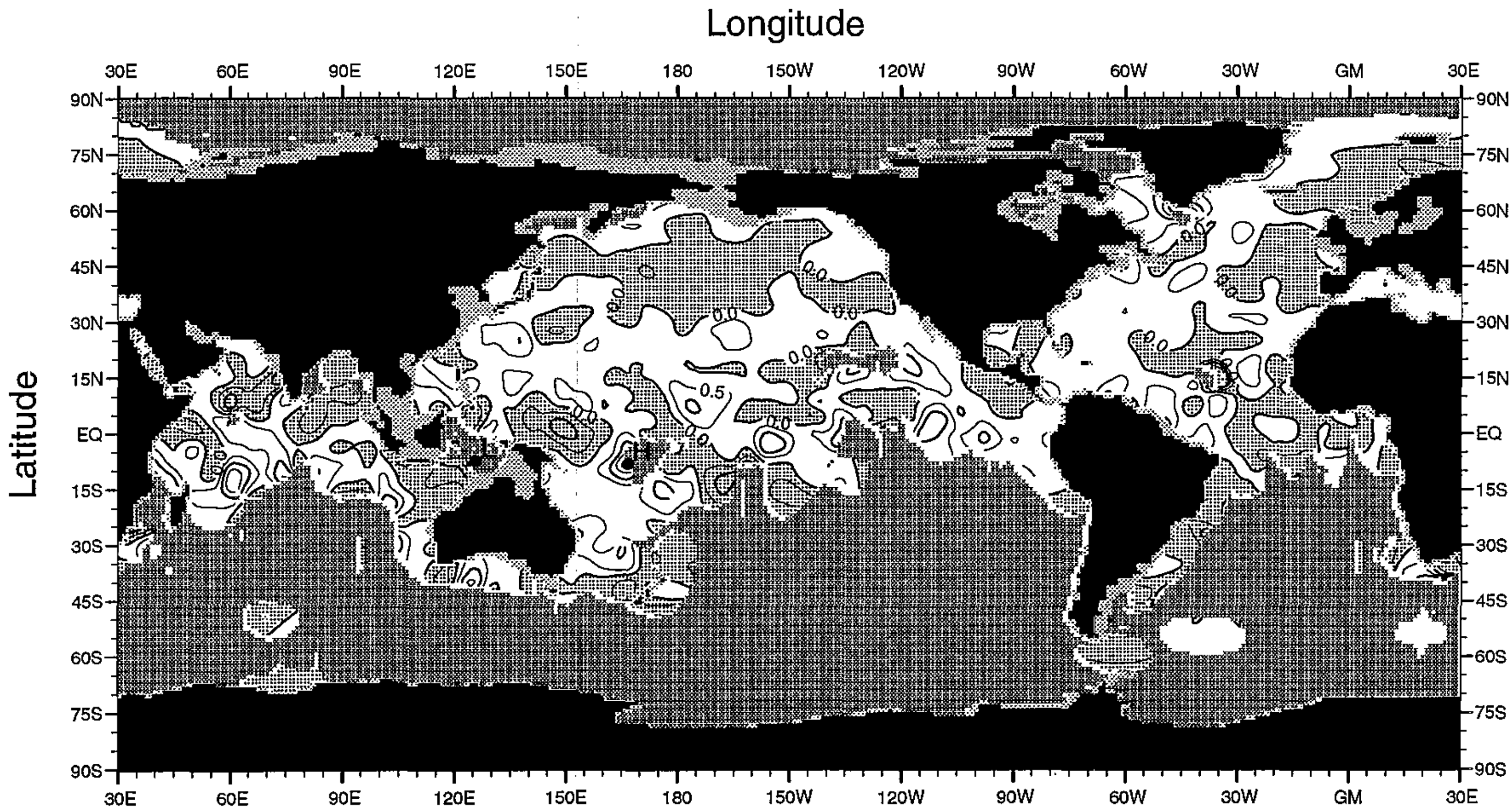


Minimum Value -2.93 Maximum Value 2.20 Contour Interval 0.50

Fig. C18 Temperature anomaly (°C) at 125 m depth for year 1977

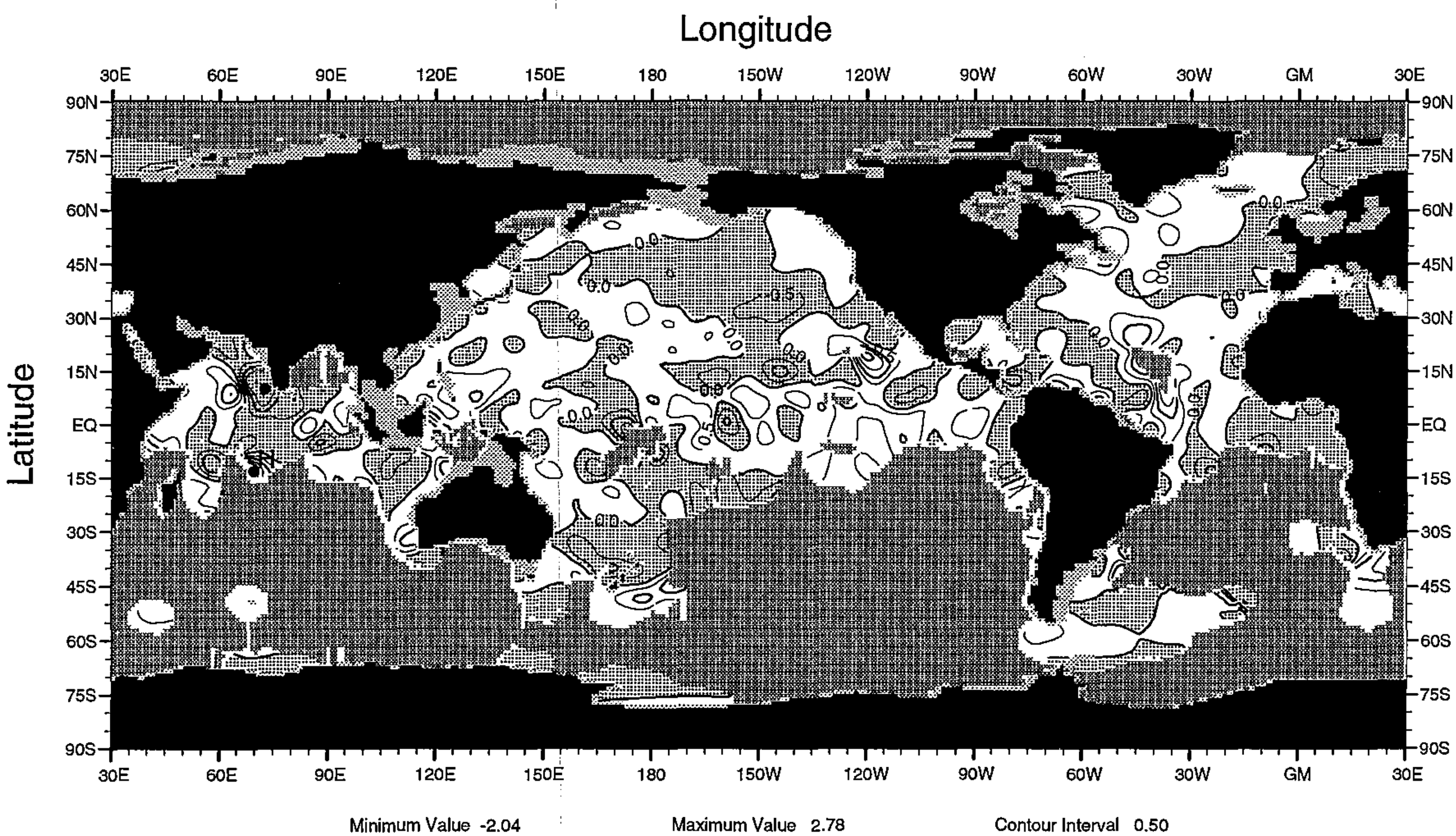


Fig. C19 Temperature anomaly (°C) at 125 m depth for year 1978

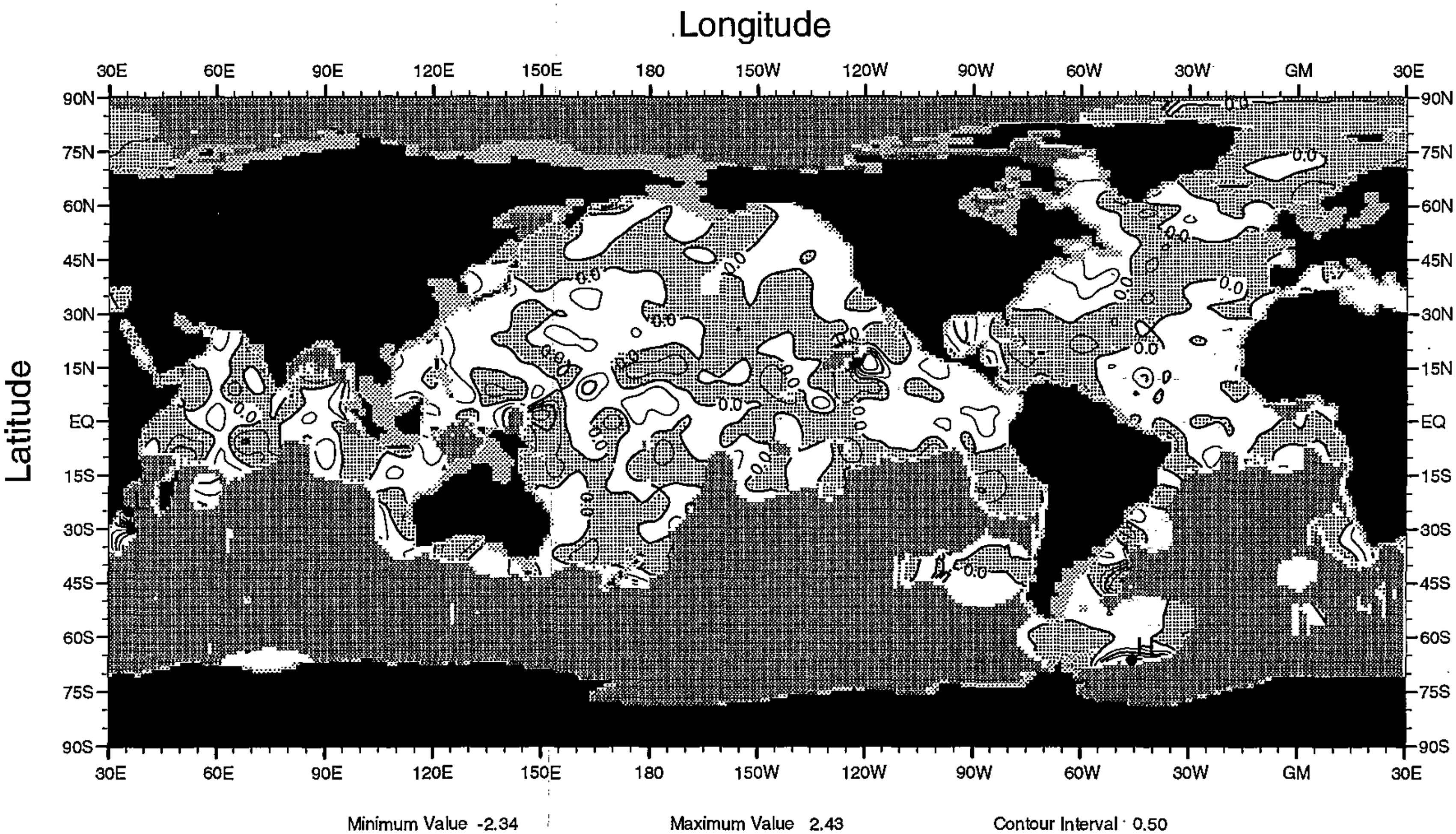


Fig. C20 Temperature anomaly (°C) at 125 m depth for year 1979

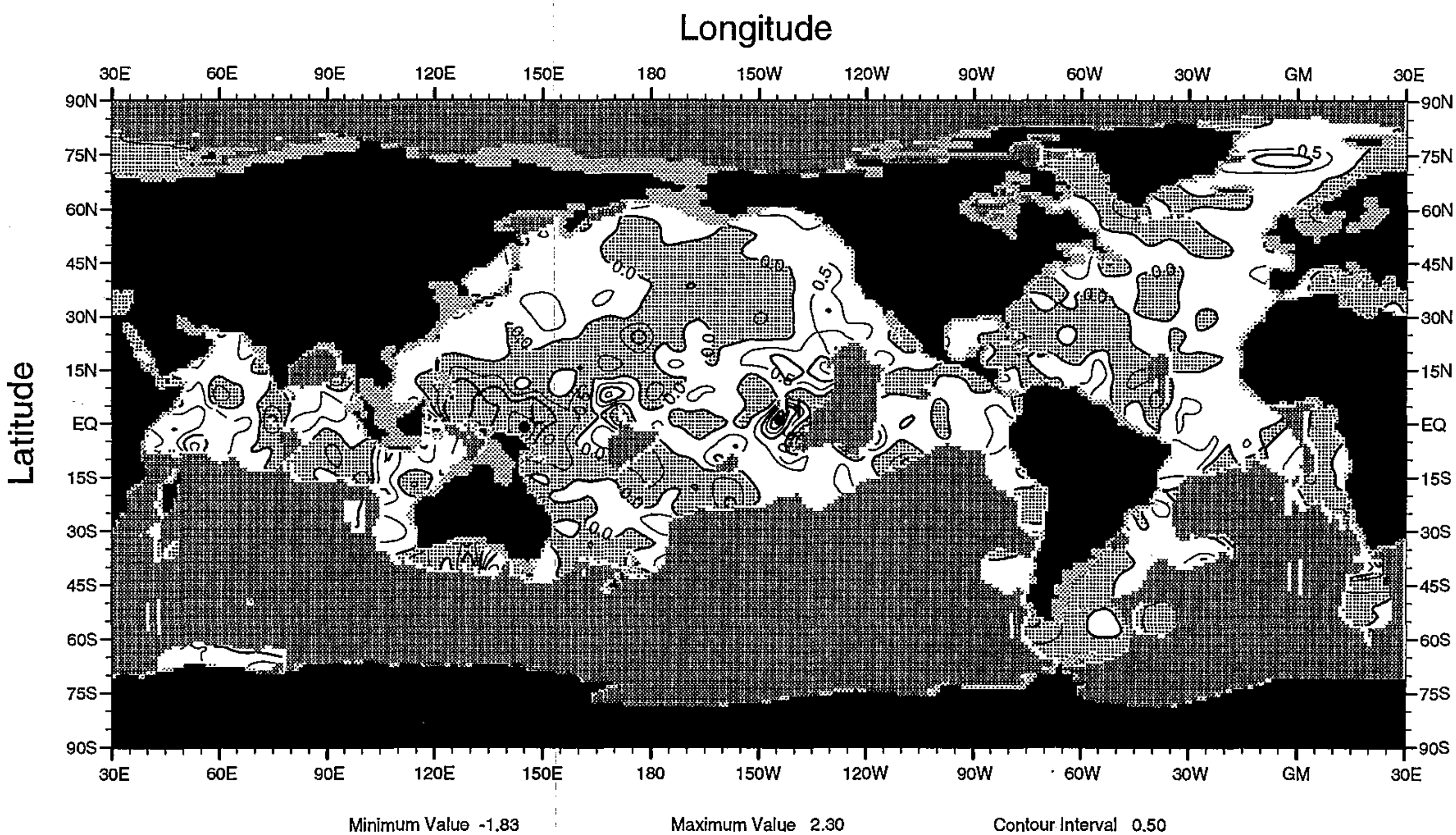


Fig. C21 Temperature anomaly (°C) at 125 m depth for year 1980

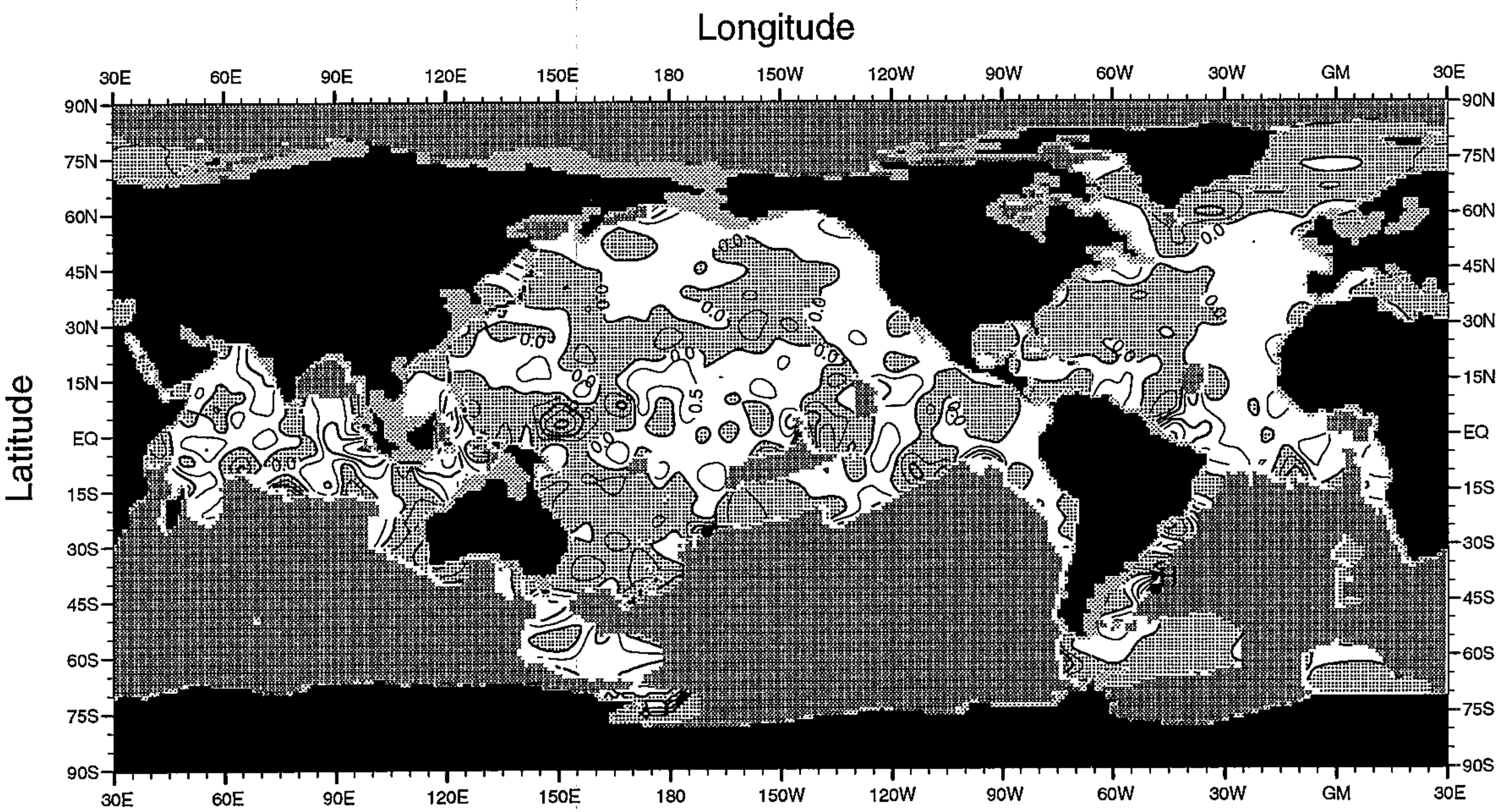


Minimum Value -2.43 Maximum Value 2.72 Contour Interval 0.50

Fig. C22 Temperature anomaly (°C) at 125 m depth for year 1981

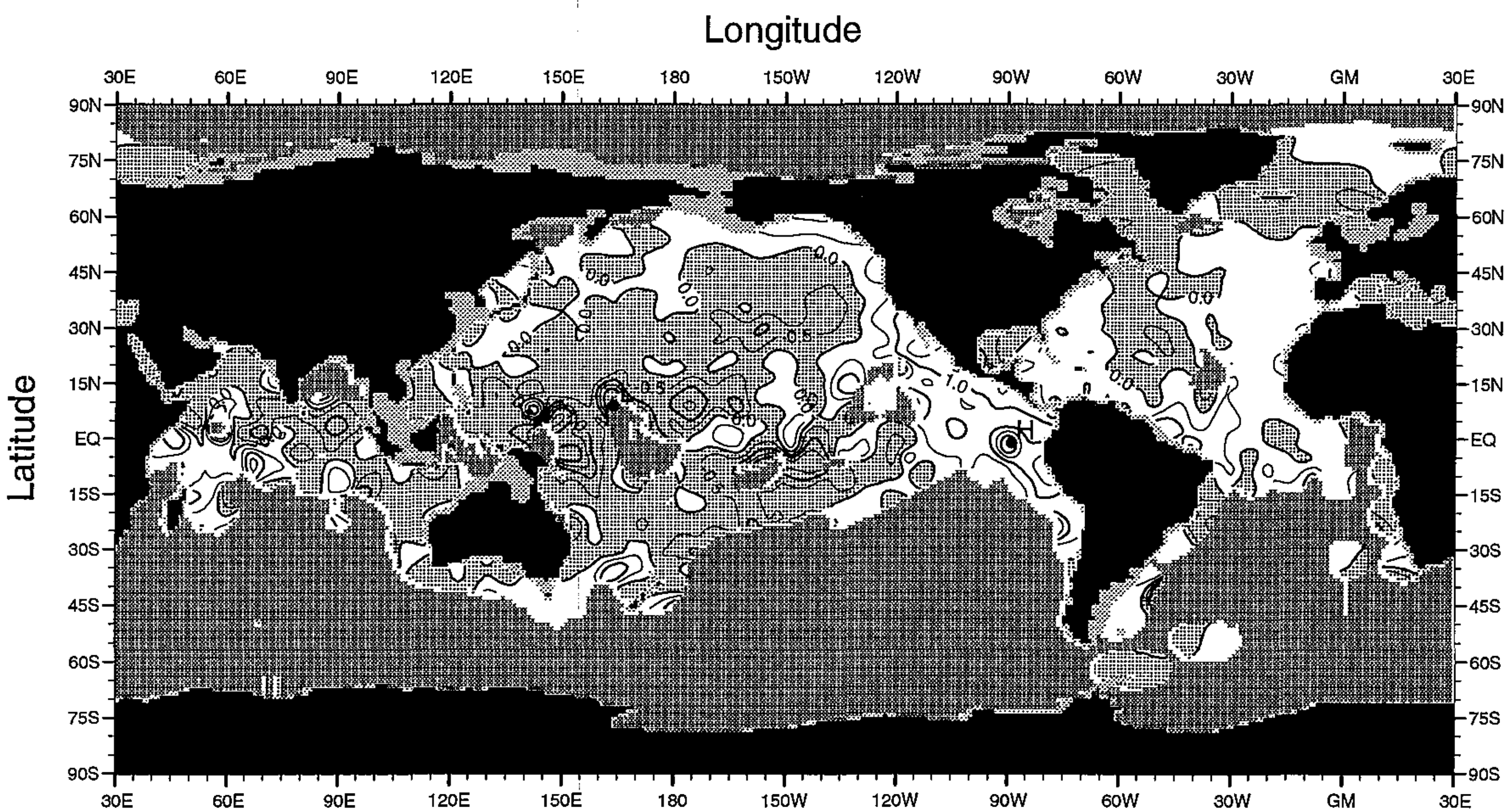


Minimum Value -2.67 Maximum Value 2.49 Contour Interval 0.50

Fig. C23 Temperature anomaly (°C) at 125 m depth for year 1982

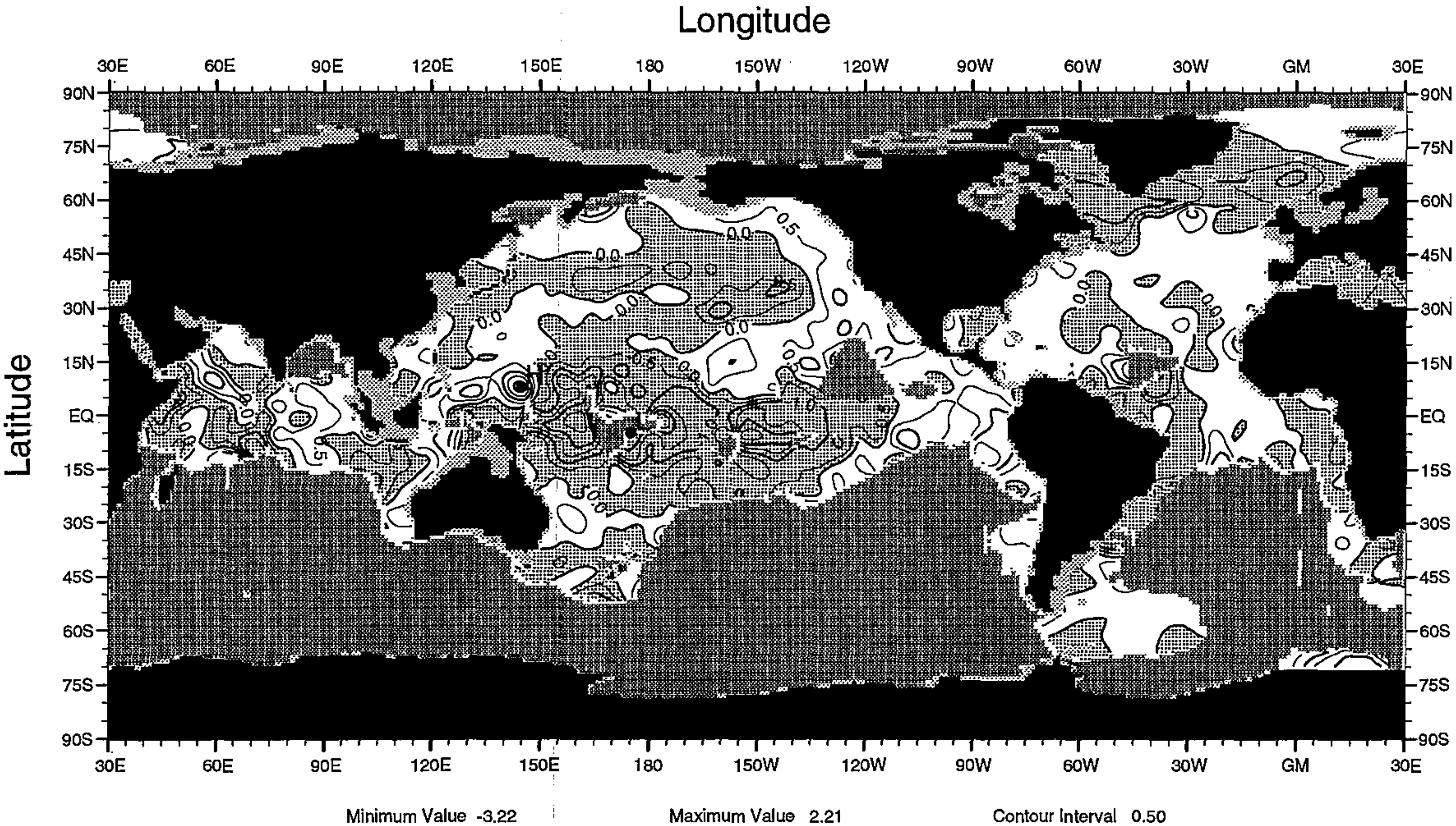


Fig. C24. Temperature anomaly (°C) at 125 m depth for year 1983

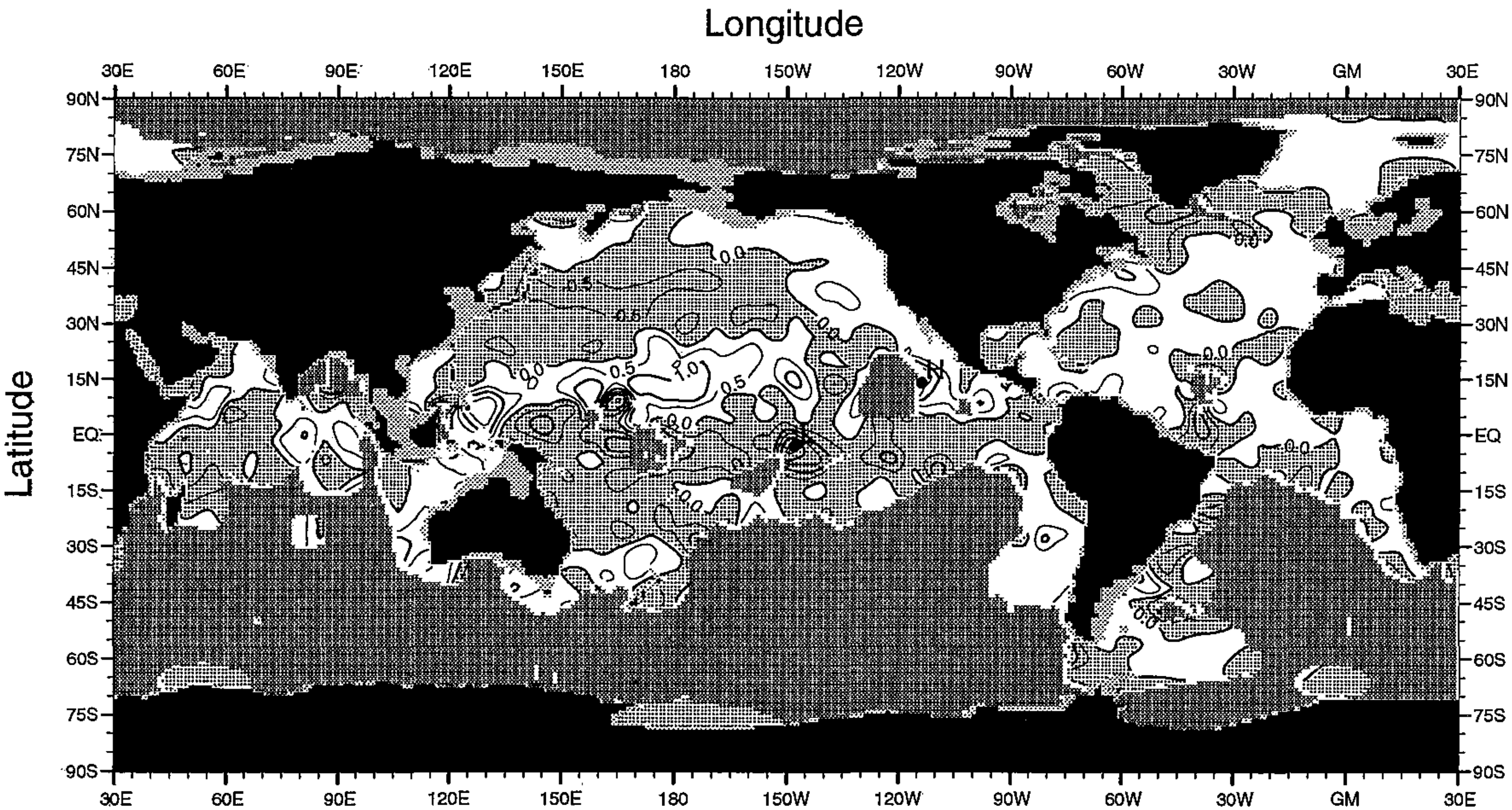


Minimum Value -2.64 Maximum Value 2.12 Contour Interval 0.50

Fig. C25 Temperature anomaly (°C) at 125 m depth for year 1984

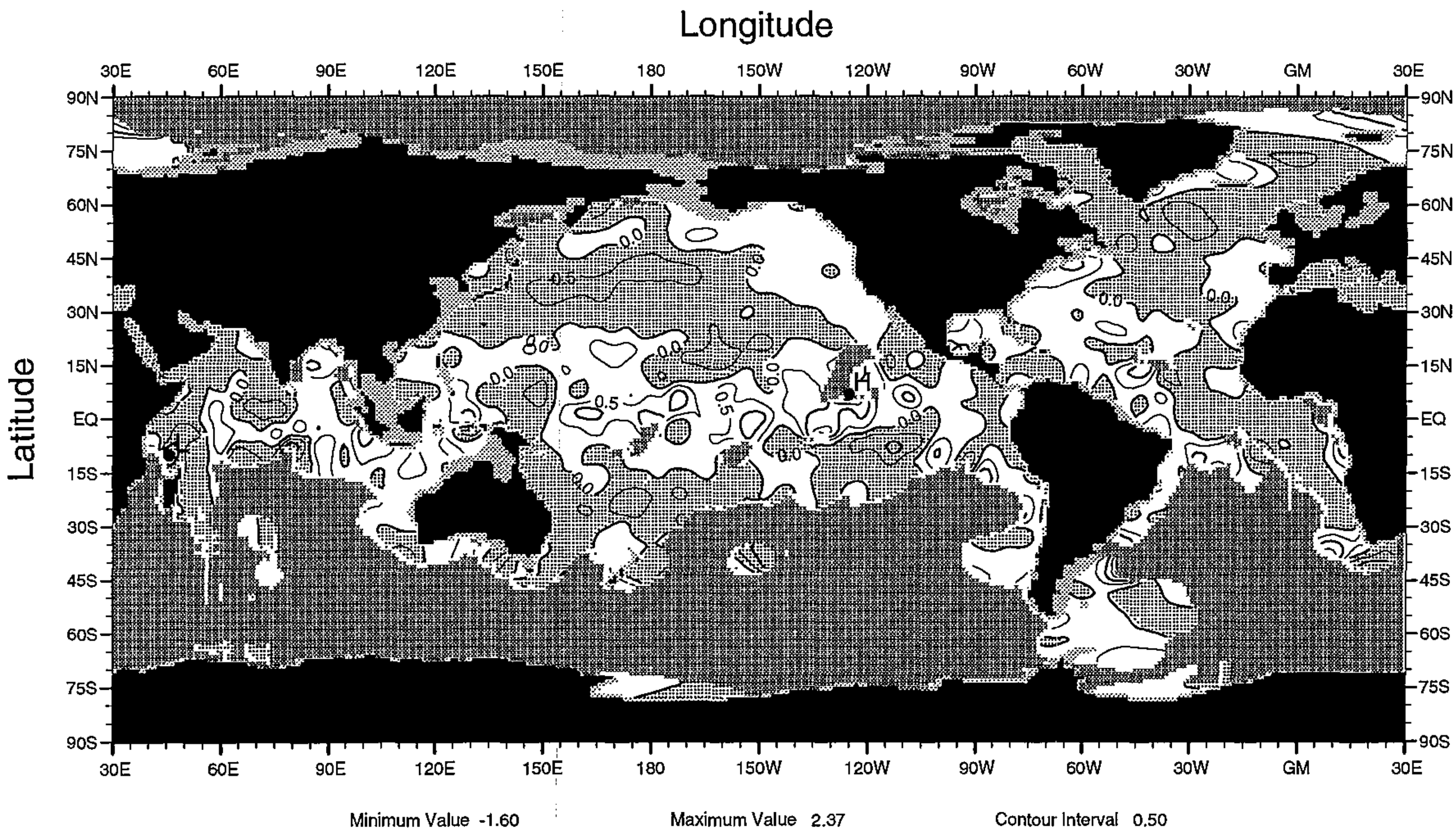


Fig. C26 Temperature anomaly (°C) at 125 m depth for year 1985

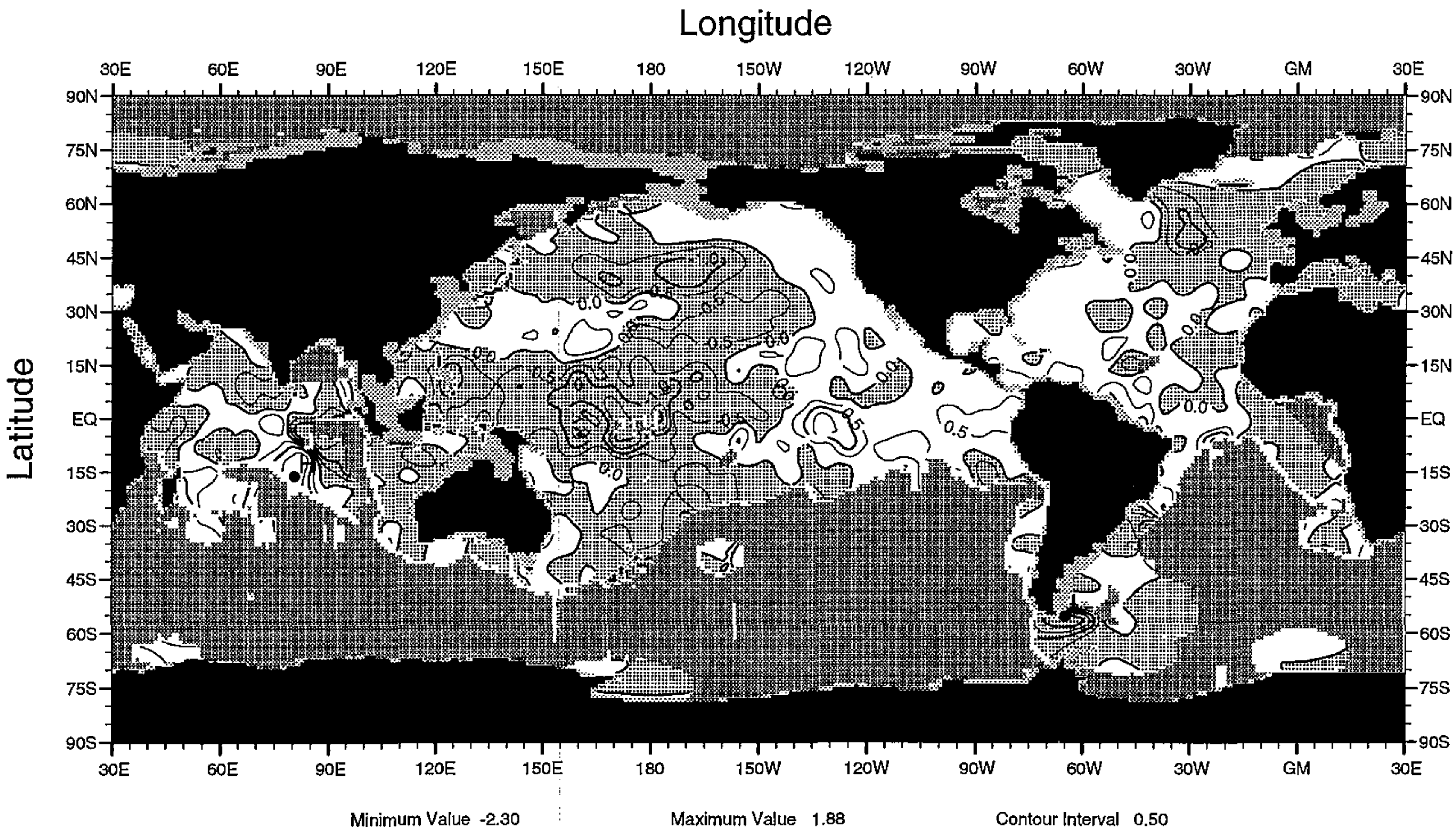


Fig. C27 Temperature anomaly (°C) at 125 m depth for year 1986

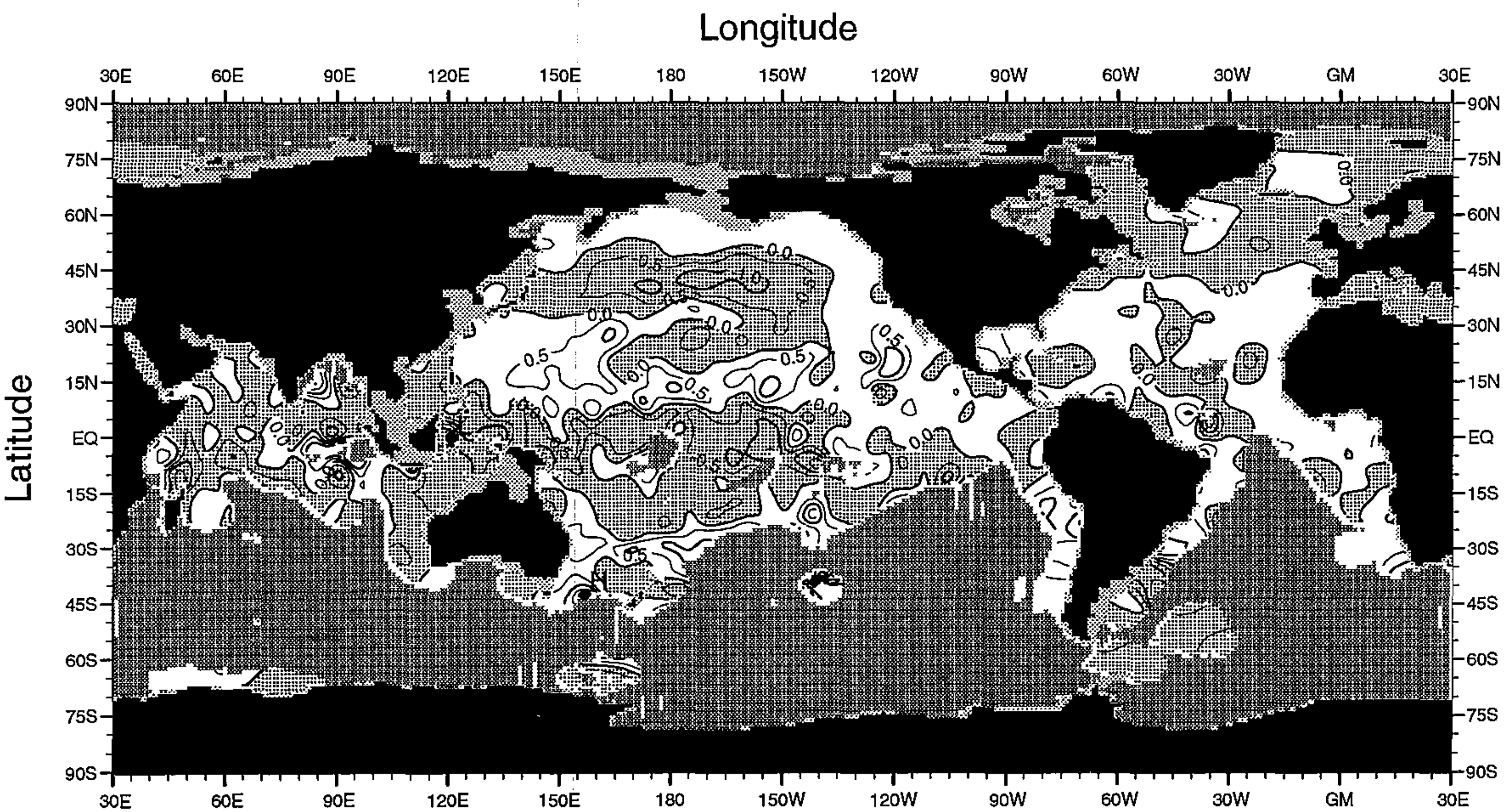


Minimum Value -2.31 Maximum Value 2.46 Contour Interval 0.50

Fig. C28 Temperature anomaly (°C) at 125 m depth for year 1987

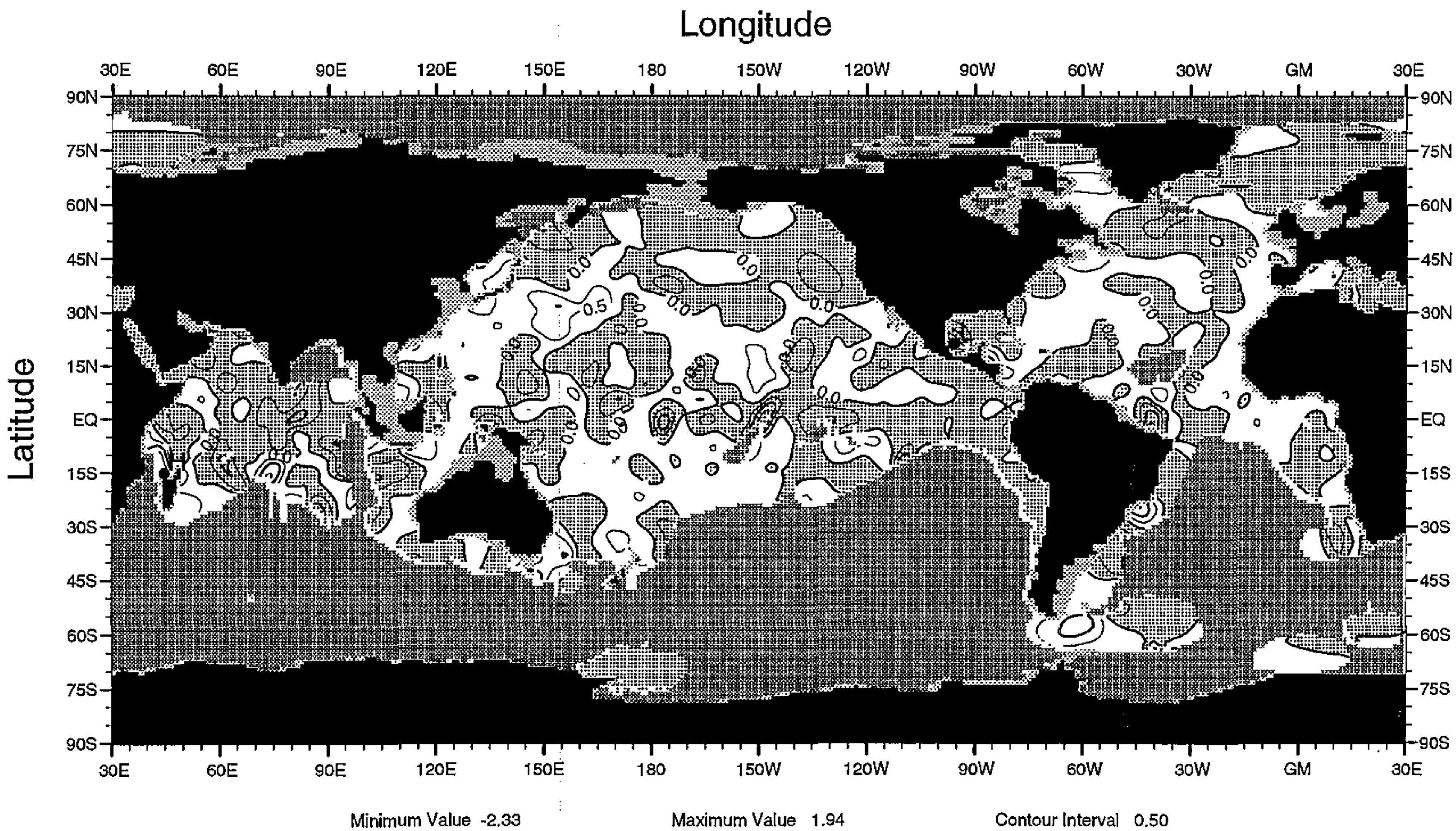


Fig. C29 Temperature anomaly (°C) at 125 m depth for year 1988

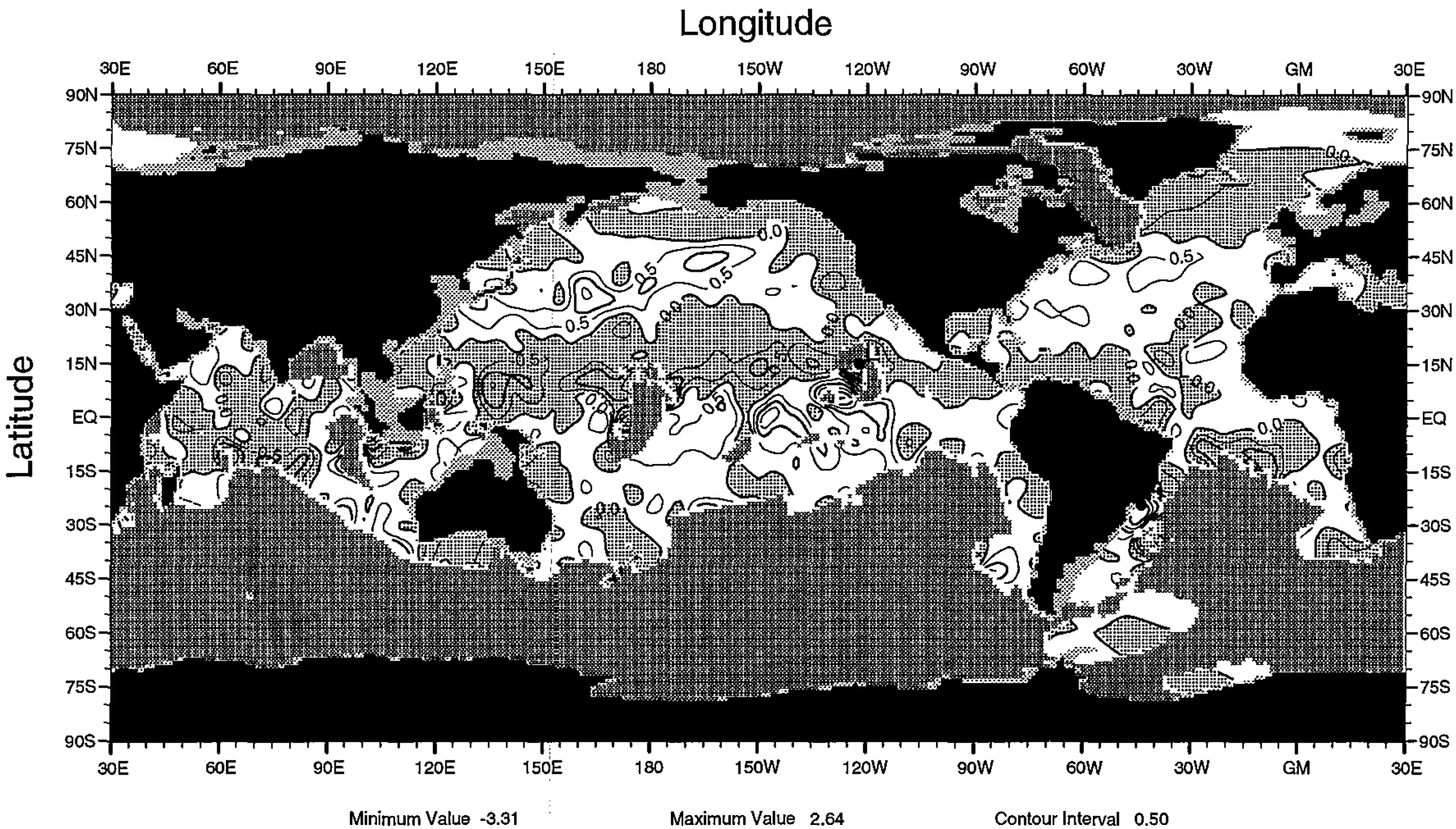


Fig. C30 Temperature anomaly (°C) at 125 m depth for year 1989

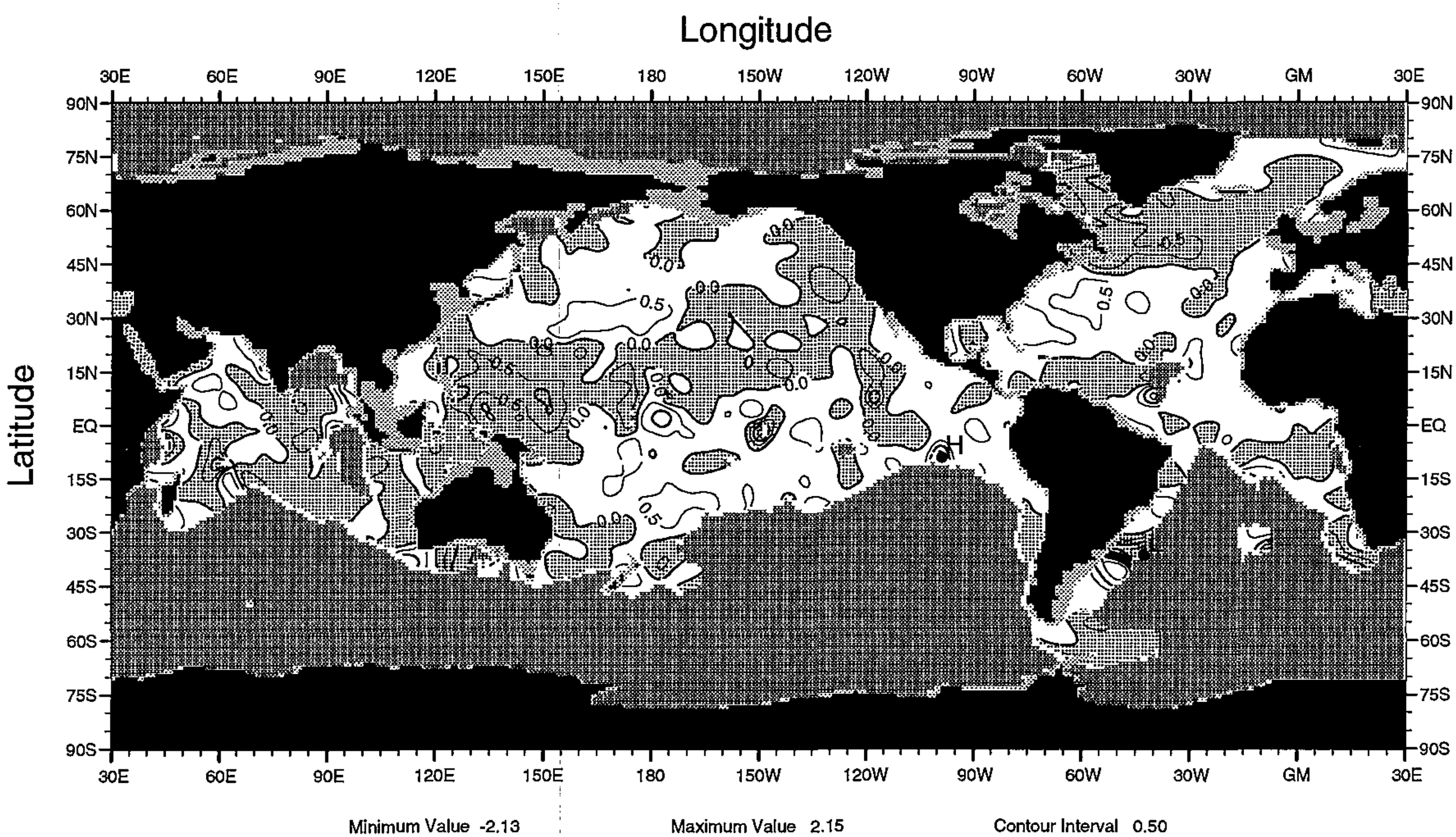


Fig. C31 Temperature anomaly (°C) at 125 m depth for year 1990

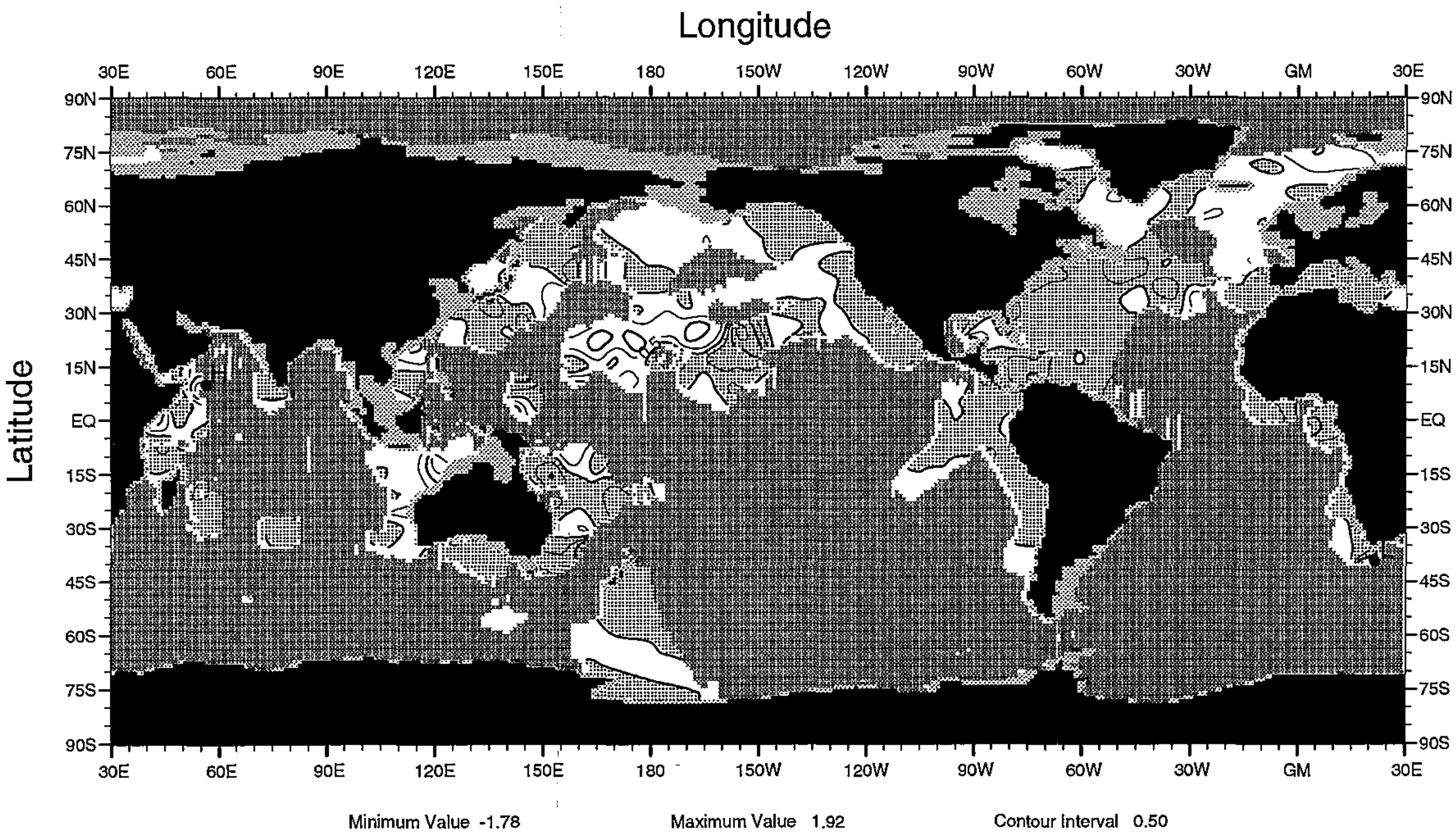


Fig. D1 Temperature anomaly (°C) at 250 m depth for year 1960

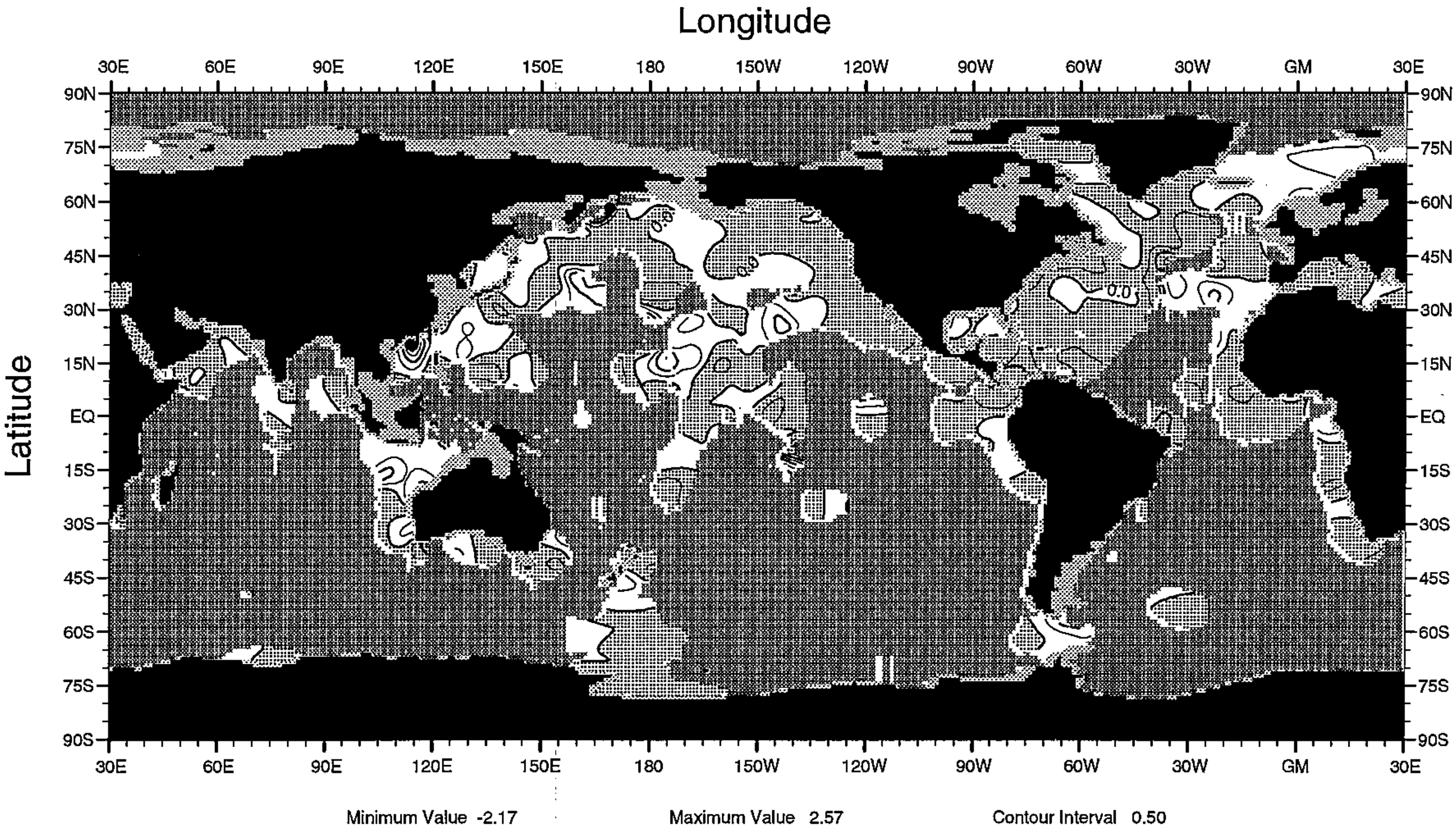


Fig. D2 Temperature anomaly (°C) at 250 m depth for year 1961

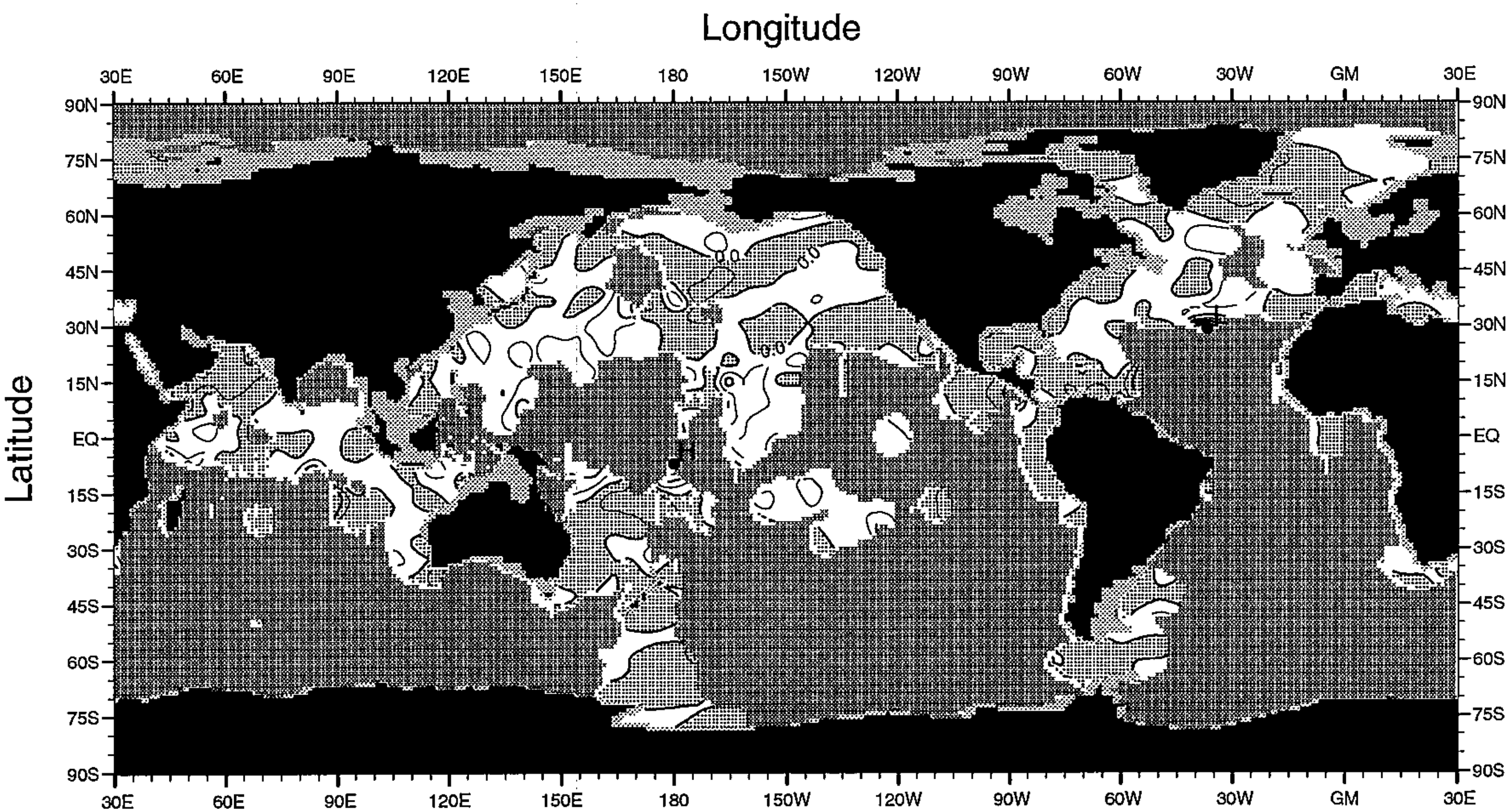


Minimum Value -3.05 Maximum Value 2.15 Contour Interval 0.50

Fig. D3 Temperature anomaly (°C) at 250 m depth for year 1962

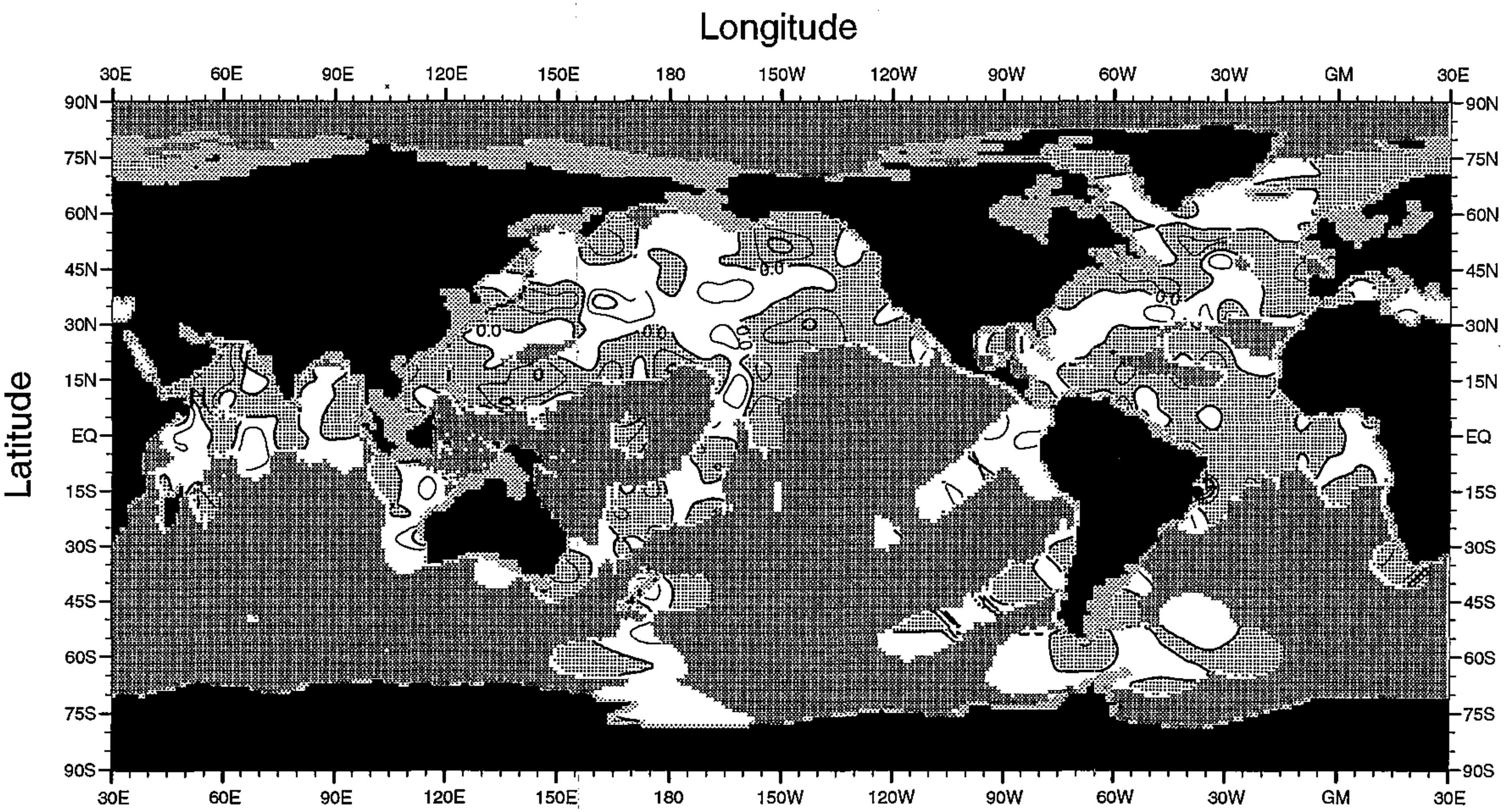


Minimum Value -2.13 Maximum Value 1.71 Contour Interval 0.50

Fig. D4 Temperature anomaly (°C) at 250 m depth for year 1963

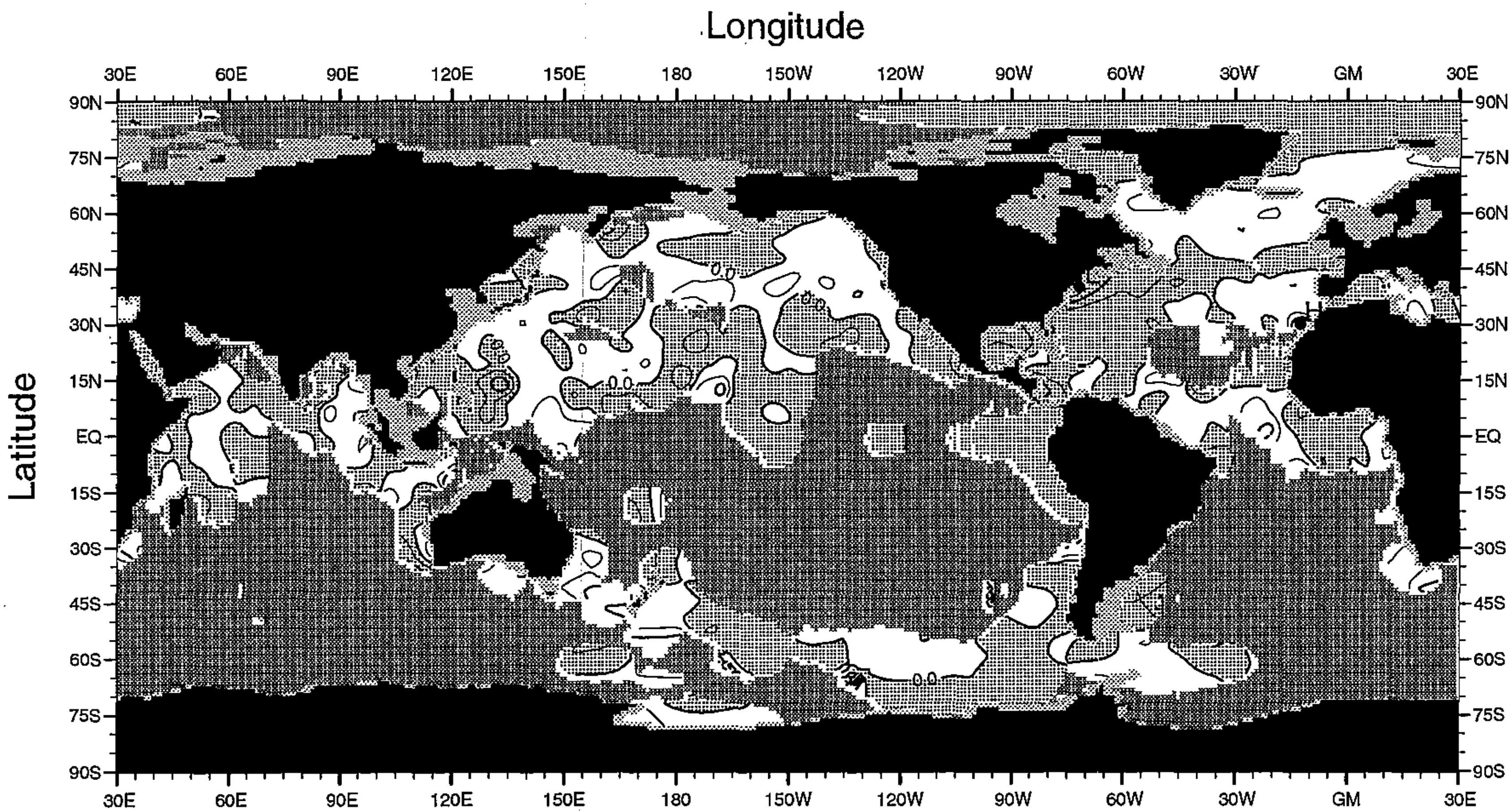


Minimum Value -1.91    Maximum Value 2.07    Contour Interval 0.50

Fig. D5 Temperature anomaly (°C) at 250 m depth for year 1964

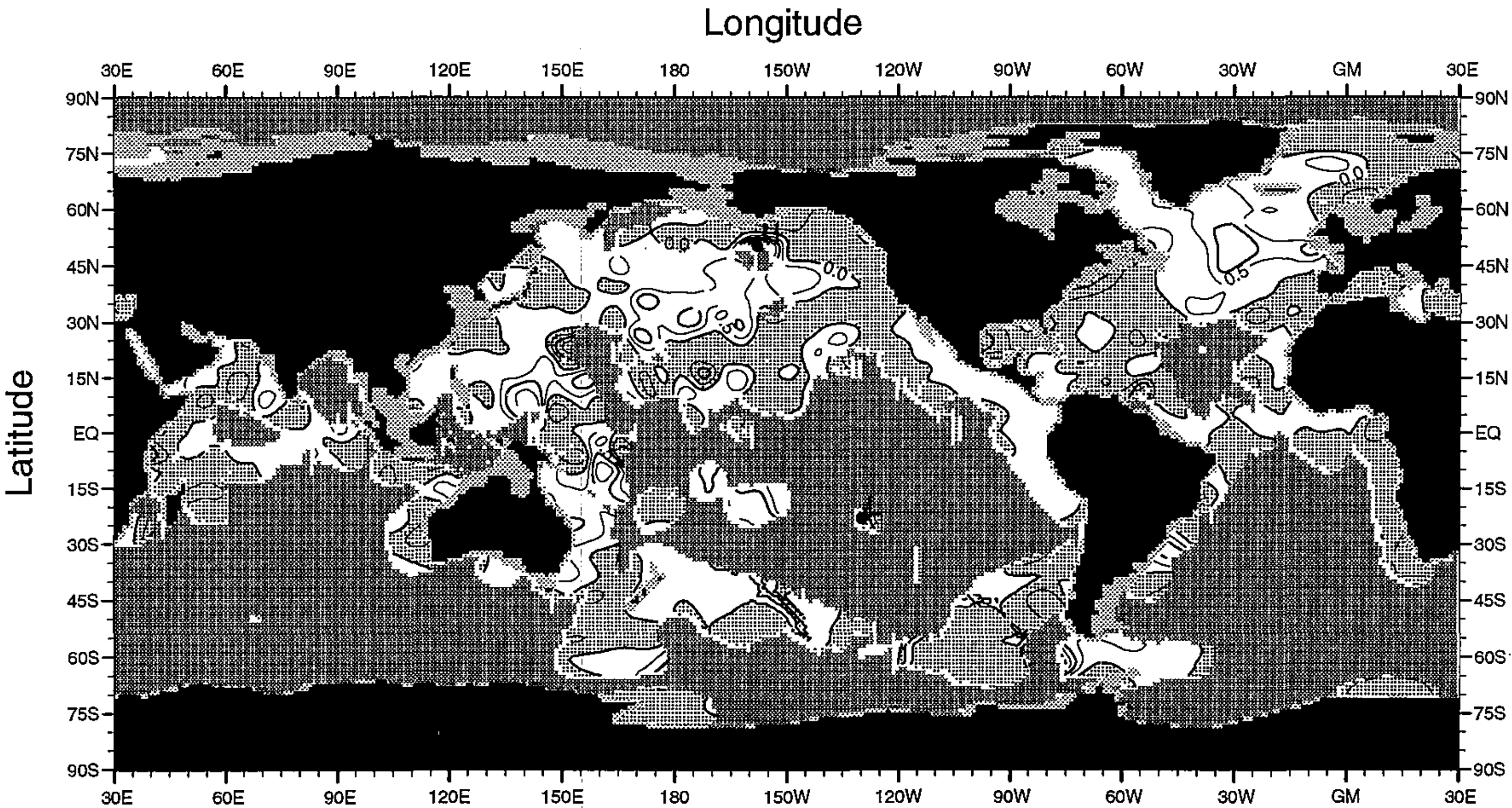


Minimum Value -2.76 Maximum Value 2.78 Contour Interval 0.50

Fig. D6 Temperature anomaly (°C) at 250 m depth for year 1965

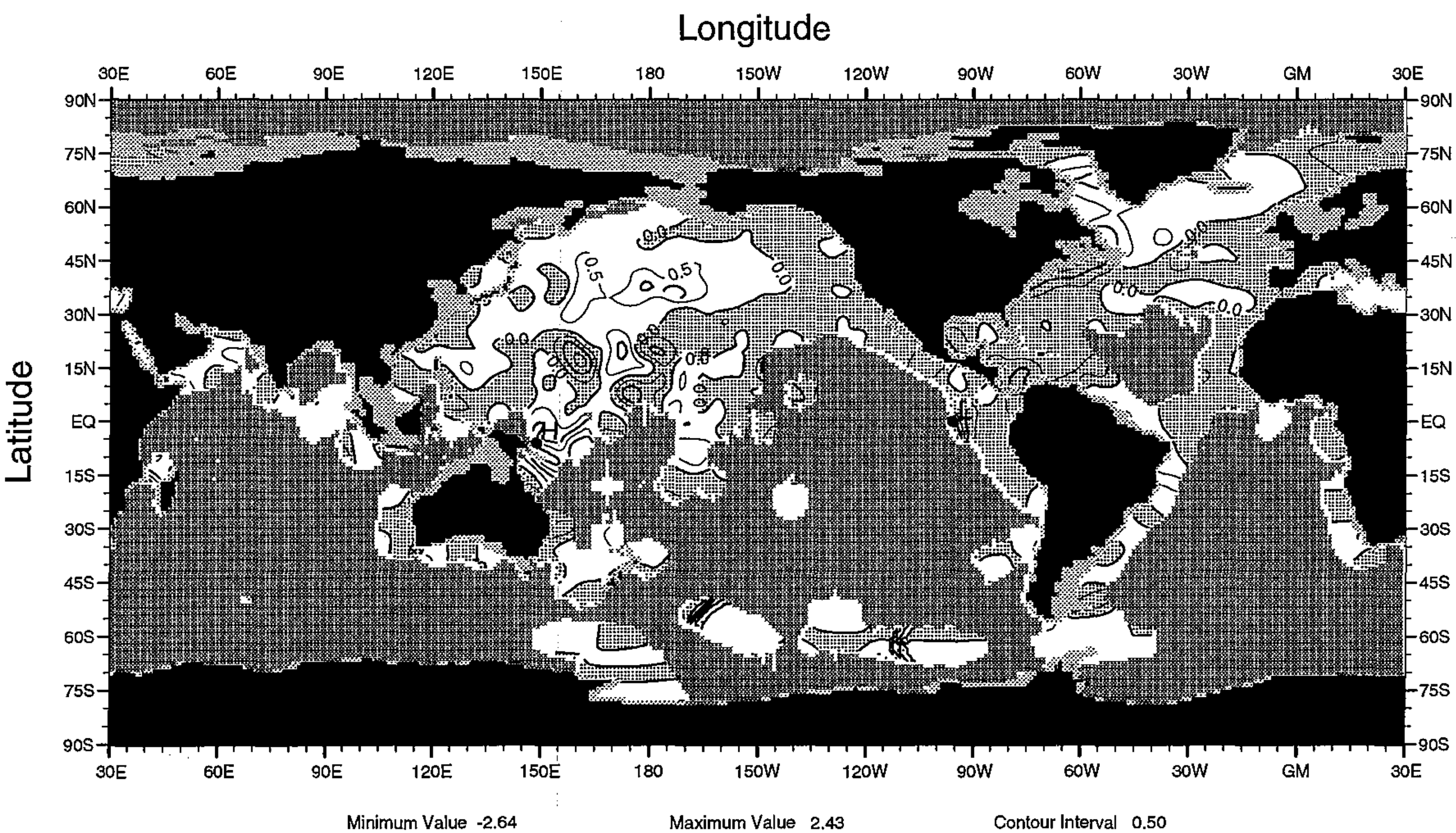


Fig. D7 Temperature anomaly (°C) at 250 m depth for year 1966

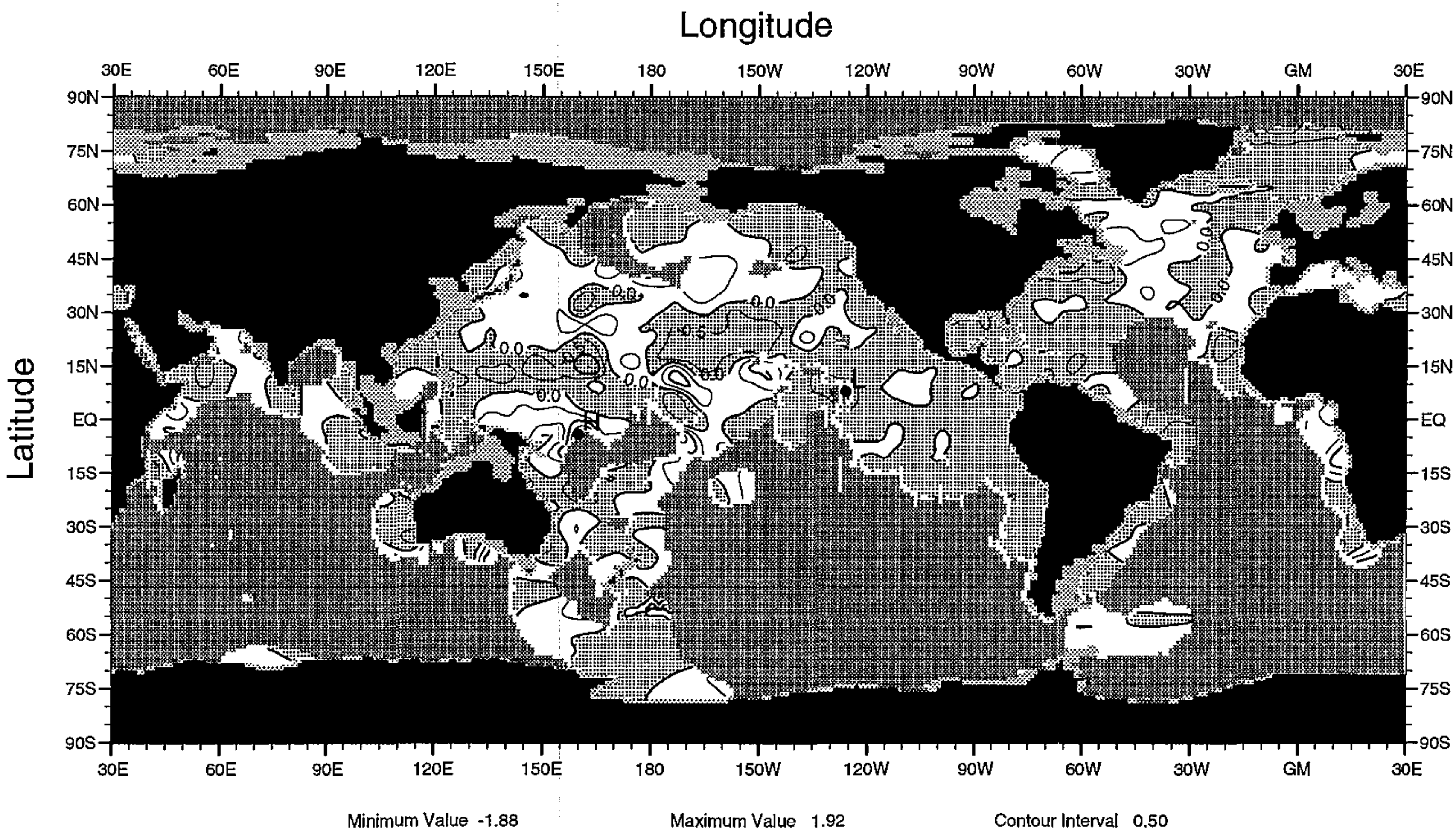


Fig. D8 Temperature anomaly (°C) at 250 m depth for year 1967

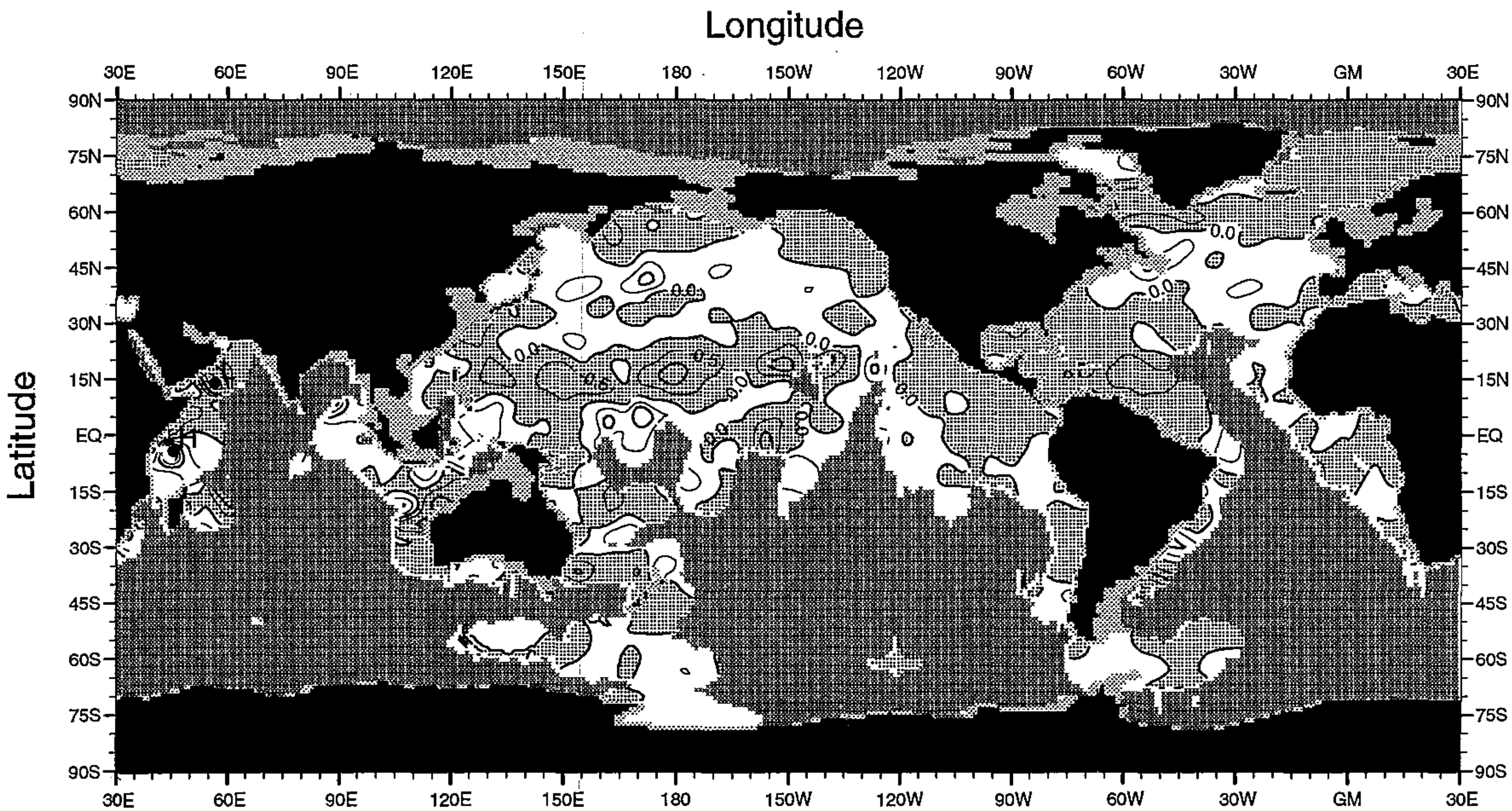


Minimum Value -1.74 Maximum Value 2.43 Contour Interval 0.50

Fig. D9 Temperature anomaly (°C) at 250 m depth for year 1968

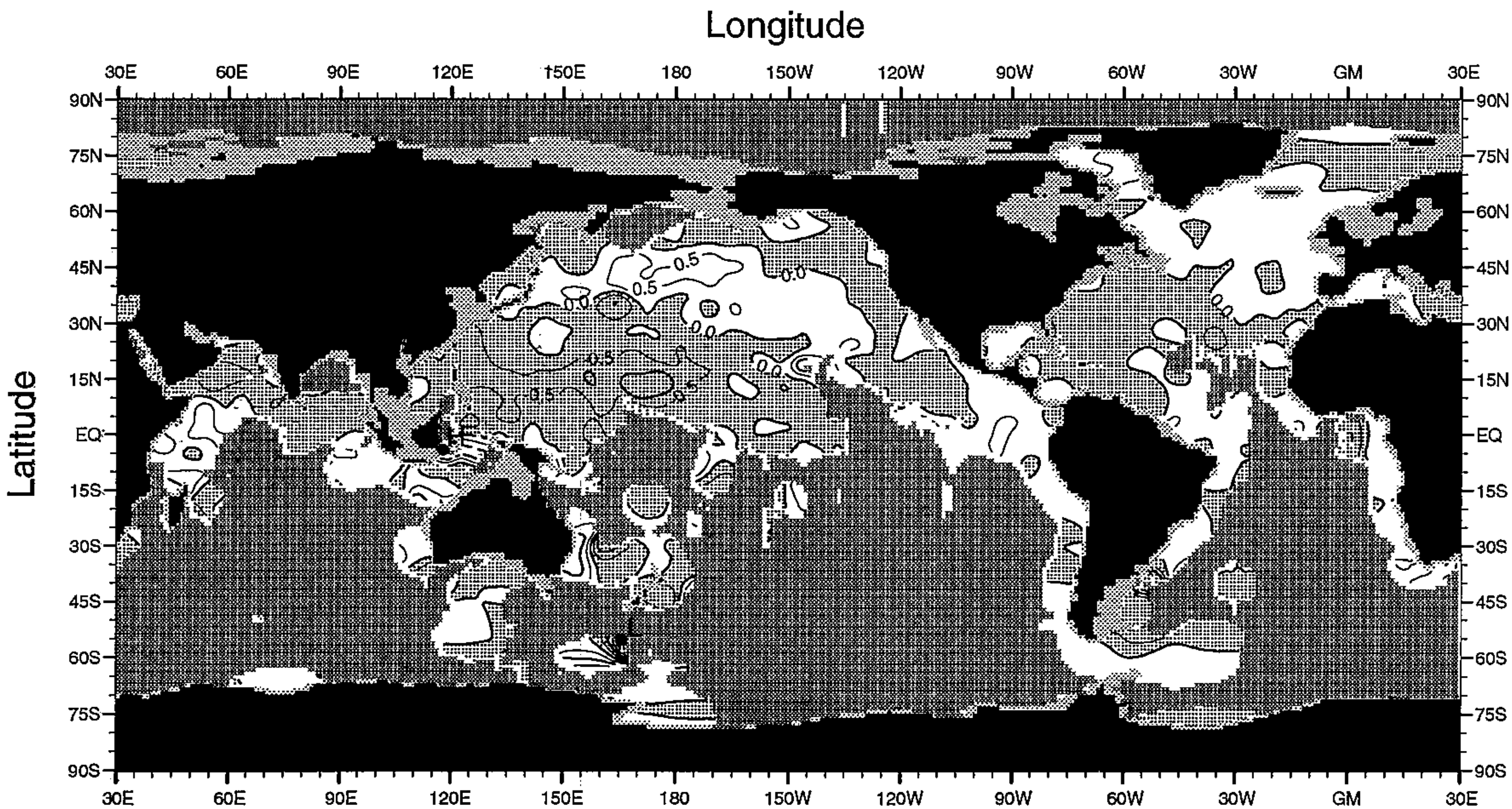


Minimum Value -2.54 Maximum Value 2.17 Contour Interval 0.50

Fig. D10 Temperature anomaly (°C) at 250 m depth for year 1969

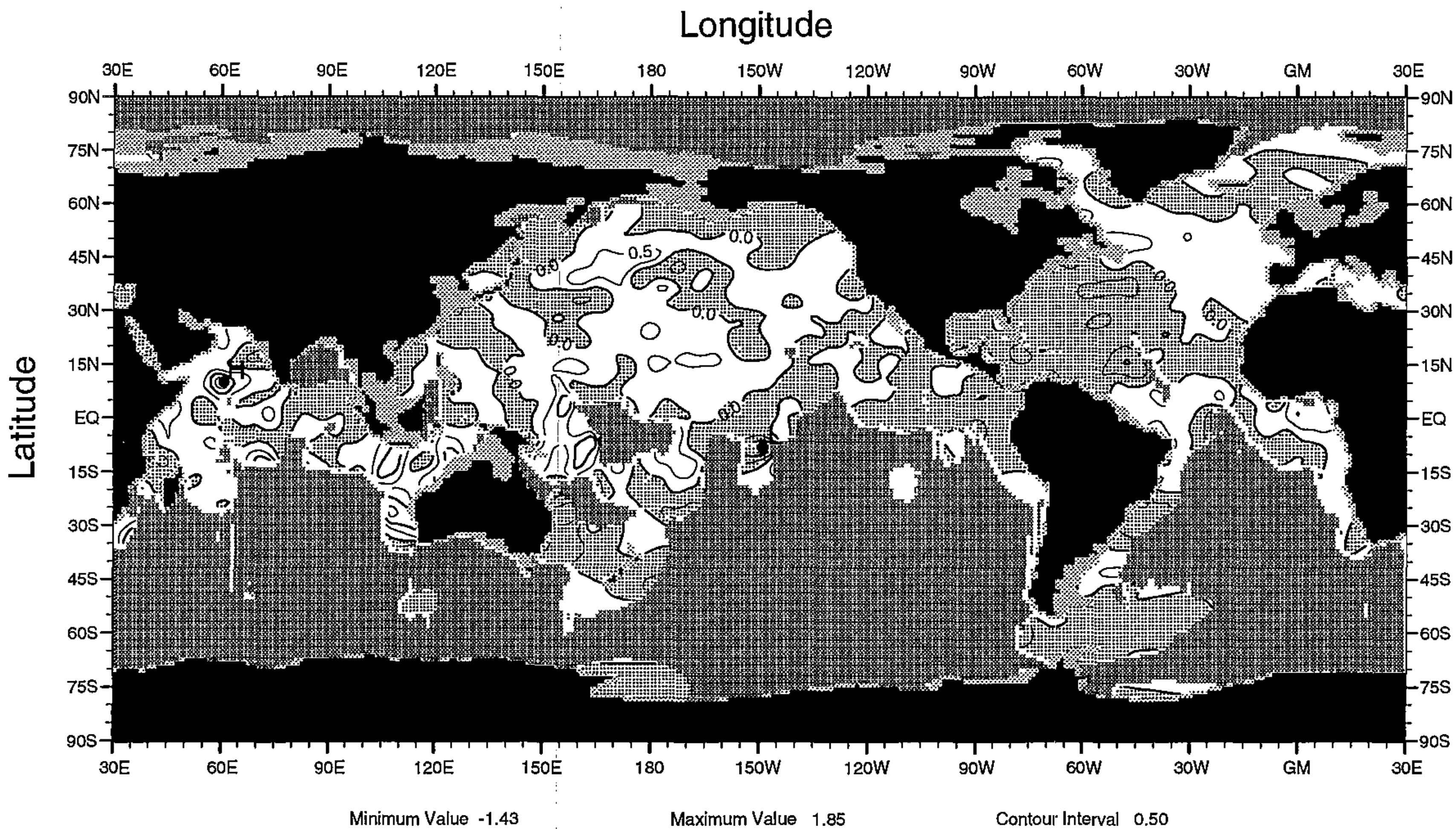


Fig. D11 Temperature anomaly (°C) at 250 m depth for year 1970

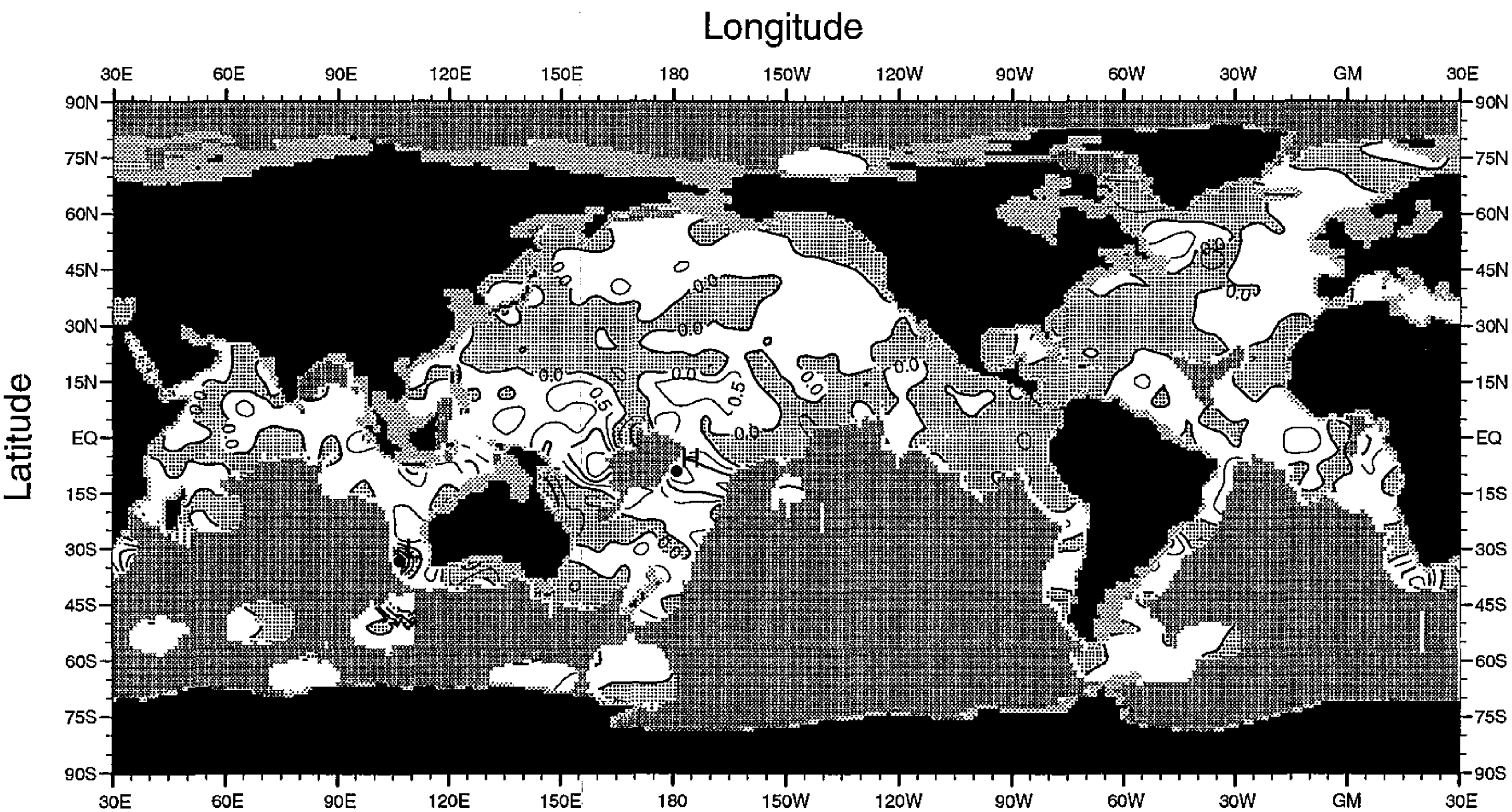


Minimum Value -2.53 Maximum Value 1.99 Contour Interval 0.50

Fig. D12 Temperature anomaly (°C) at 250 m depth for year 1971

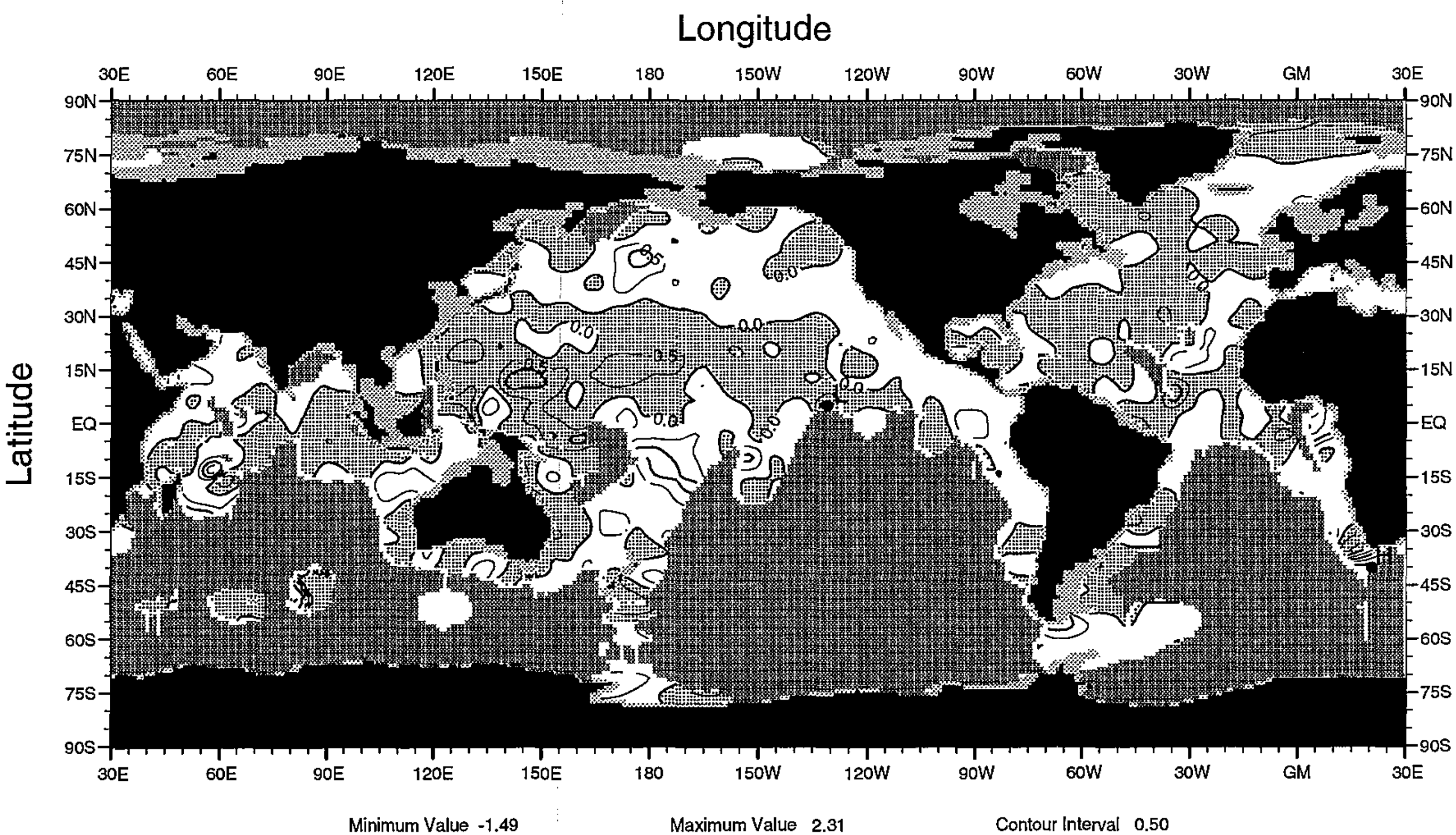


Fig. D13 Temperature anomaly (°C) at 250 m depth for year 1972

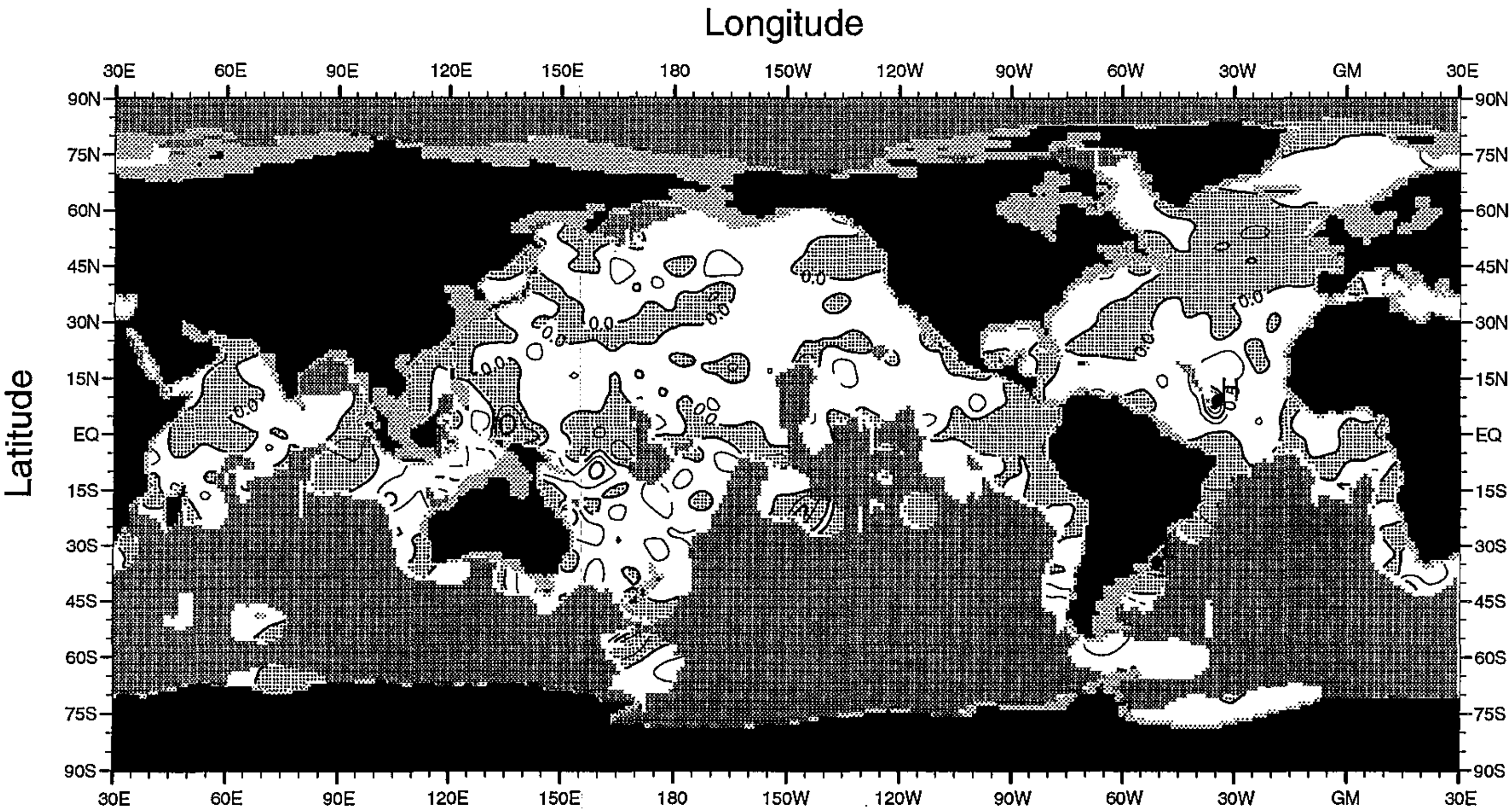


Minimum Value -1.52 Maximum Value 2.39 Contour Interval 0.50

Fig. D14 Temperature anomaly (°C) at 250 m depth for year 1973

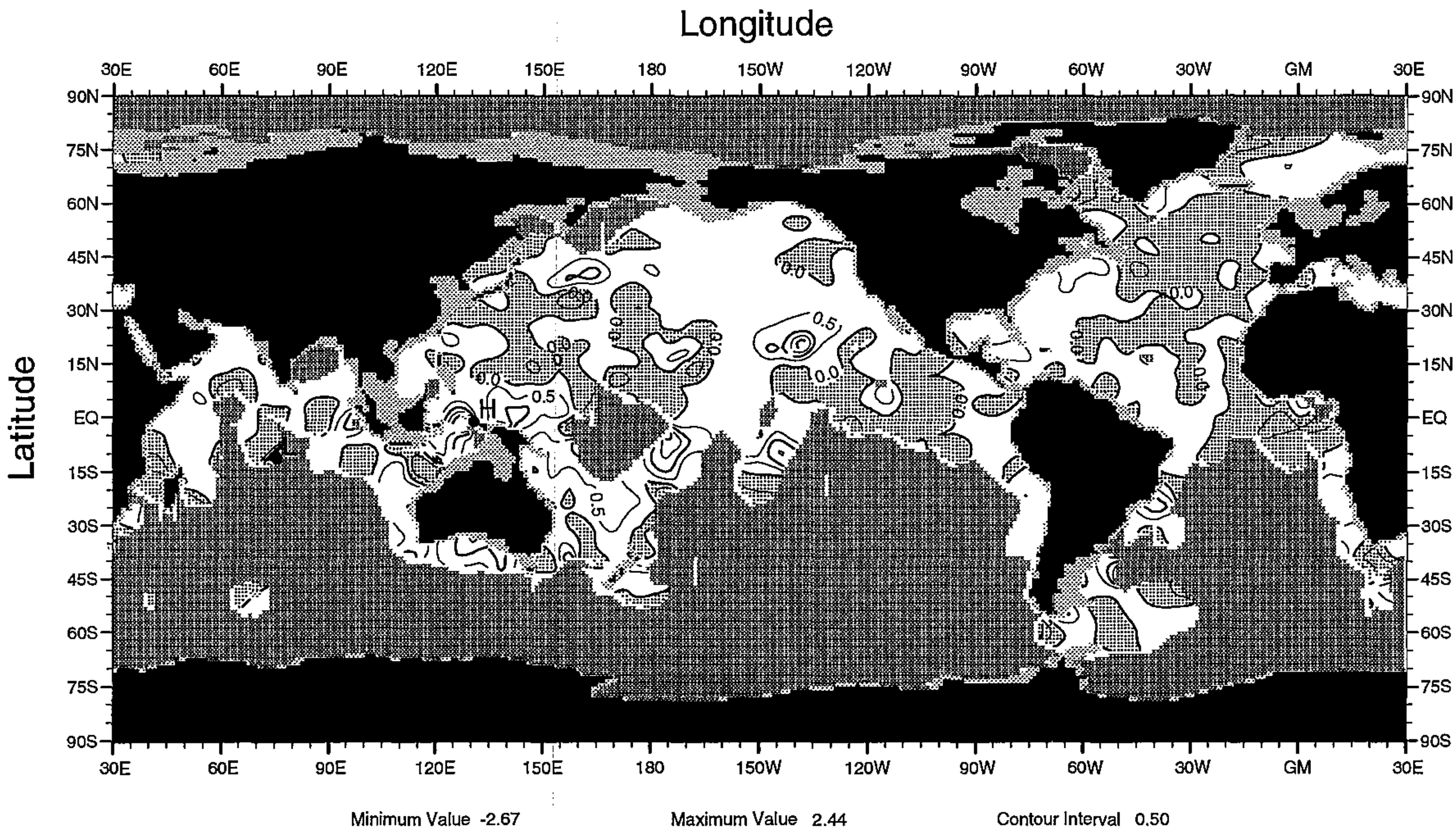


Fig. D15 Temperature anomaly (°C) at 250 m depth for year 1974

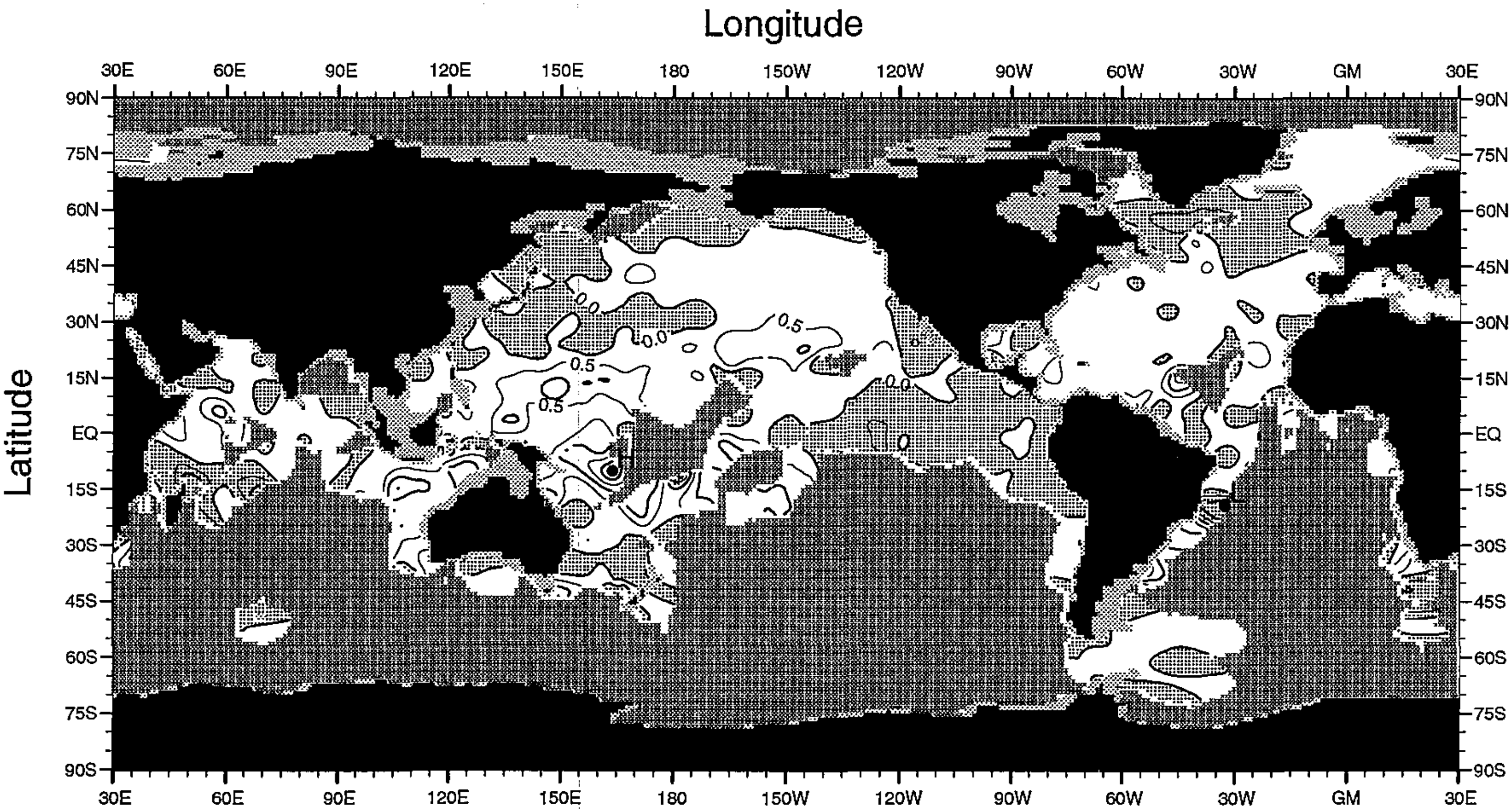


Minimum Value -1.50 Maximum Value 2.37 Contour Interval 0.50

Fig. D16 Temperature anomaly (°C) at 250 m depth for year 1975

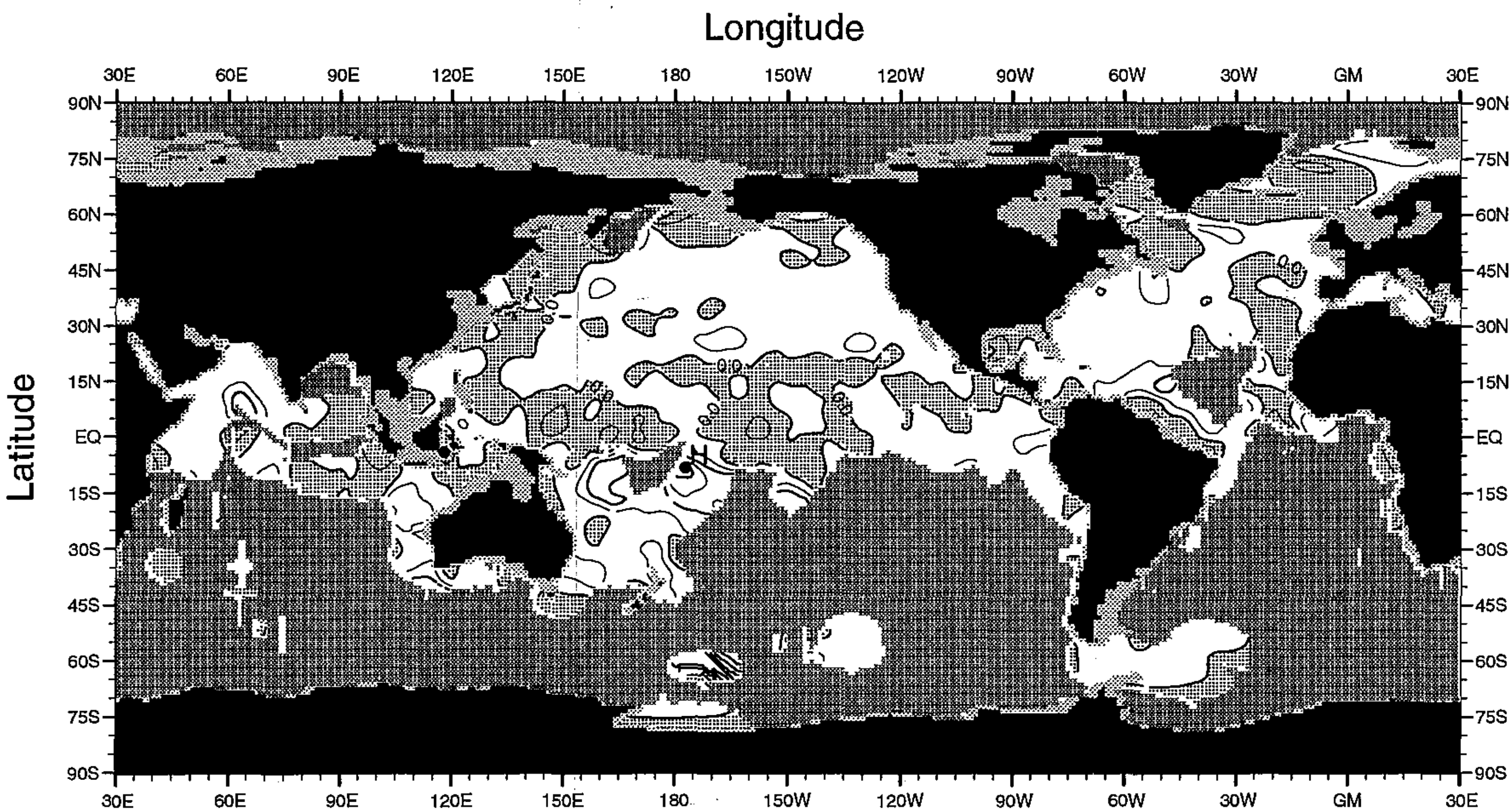


Minimum Value -1.53 Maximum Value 2.23 Contour Interval 0.50

Fig. D17 Temperature anomaly (°C) at 250 m depth for year 1976

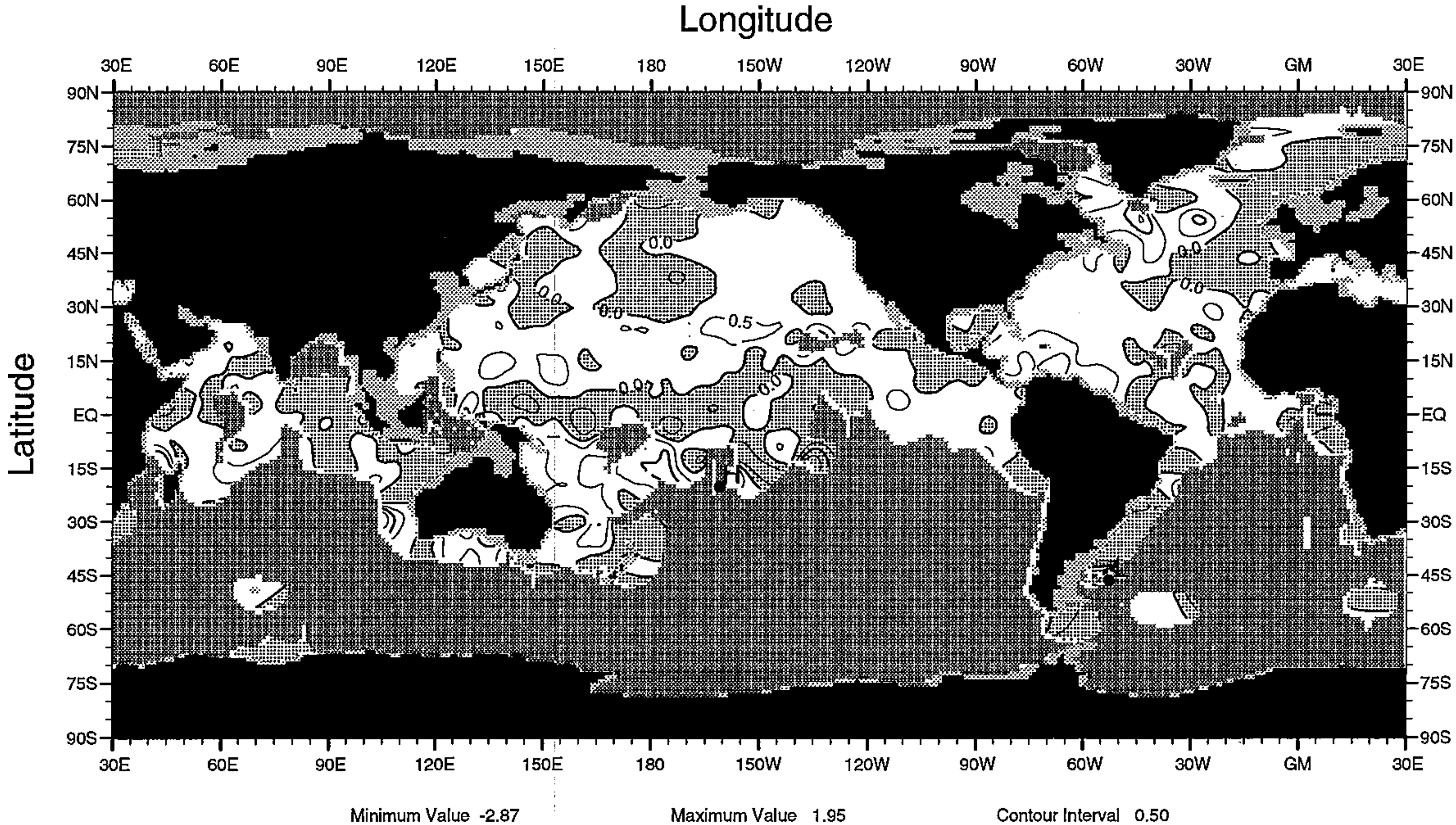


Fig. D18 Temperature anomaly (°C) at 250 m depth for year 1977

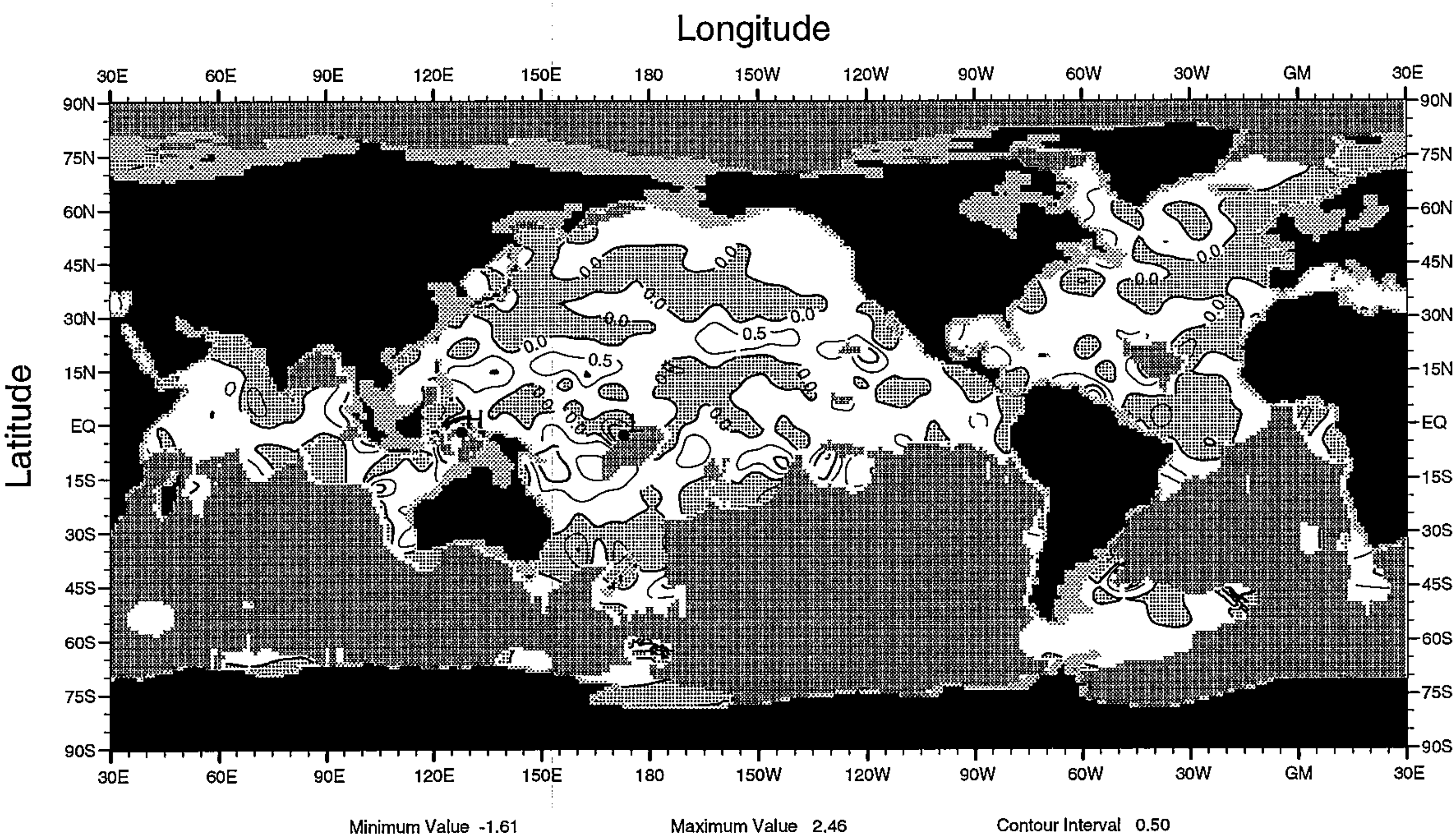


Fig. D19 Temperature anomaly (°C) at 250 m depth for year 1978

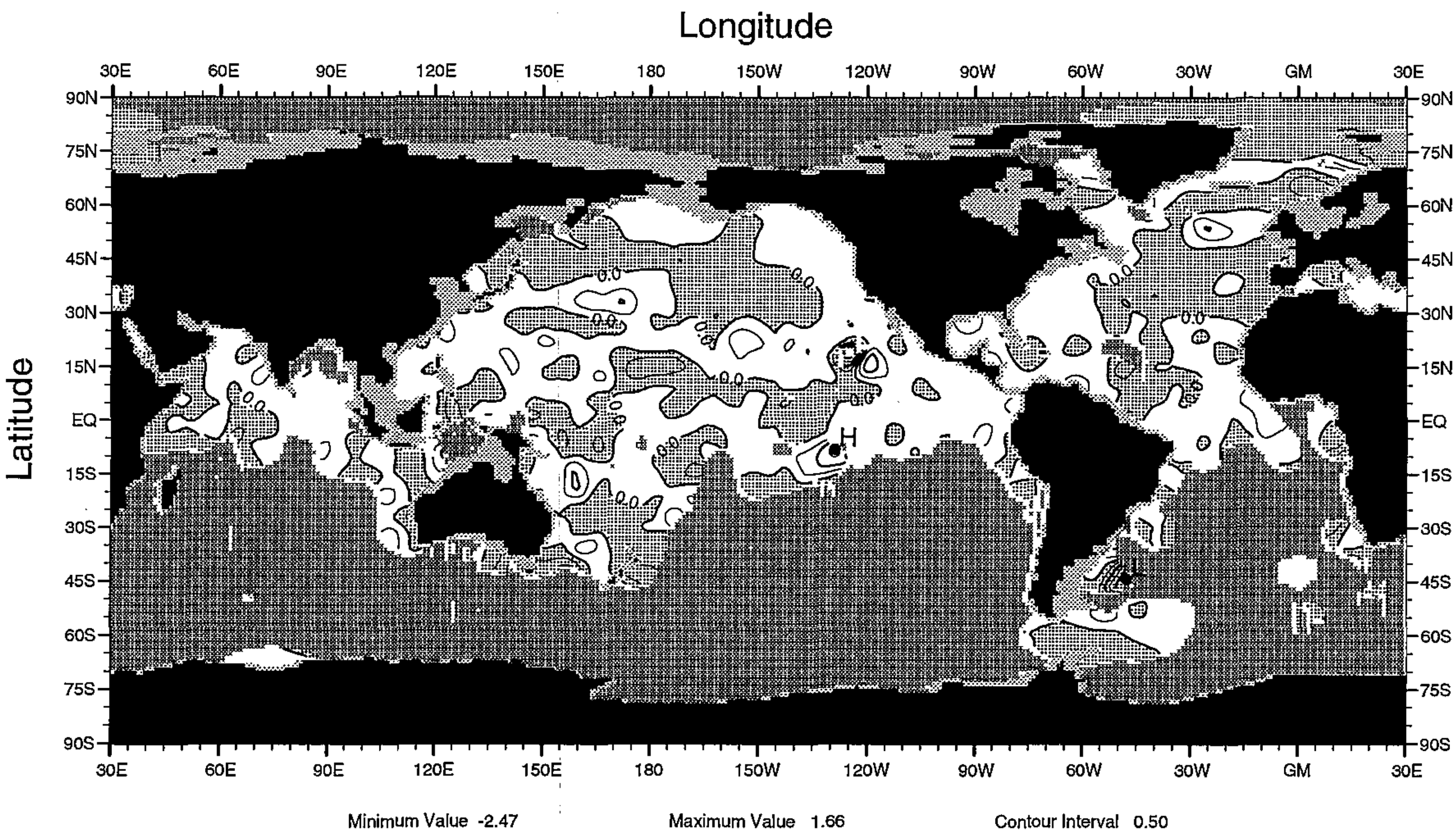


Fig. D20 Temperature anomaly (°C) at 250 m depth for year 1979

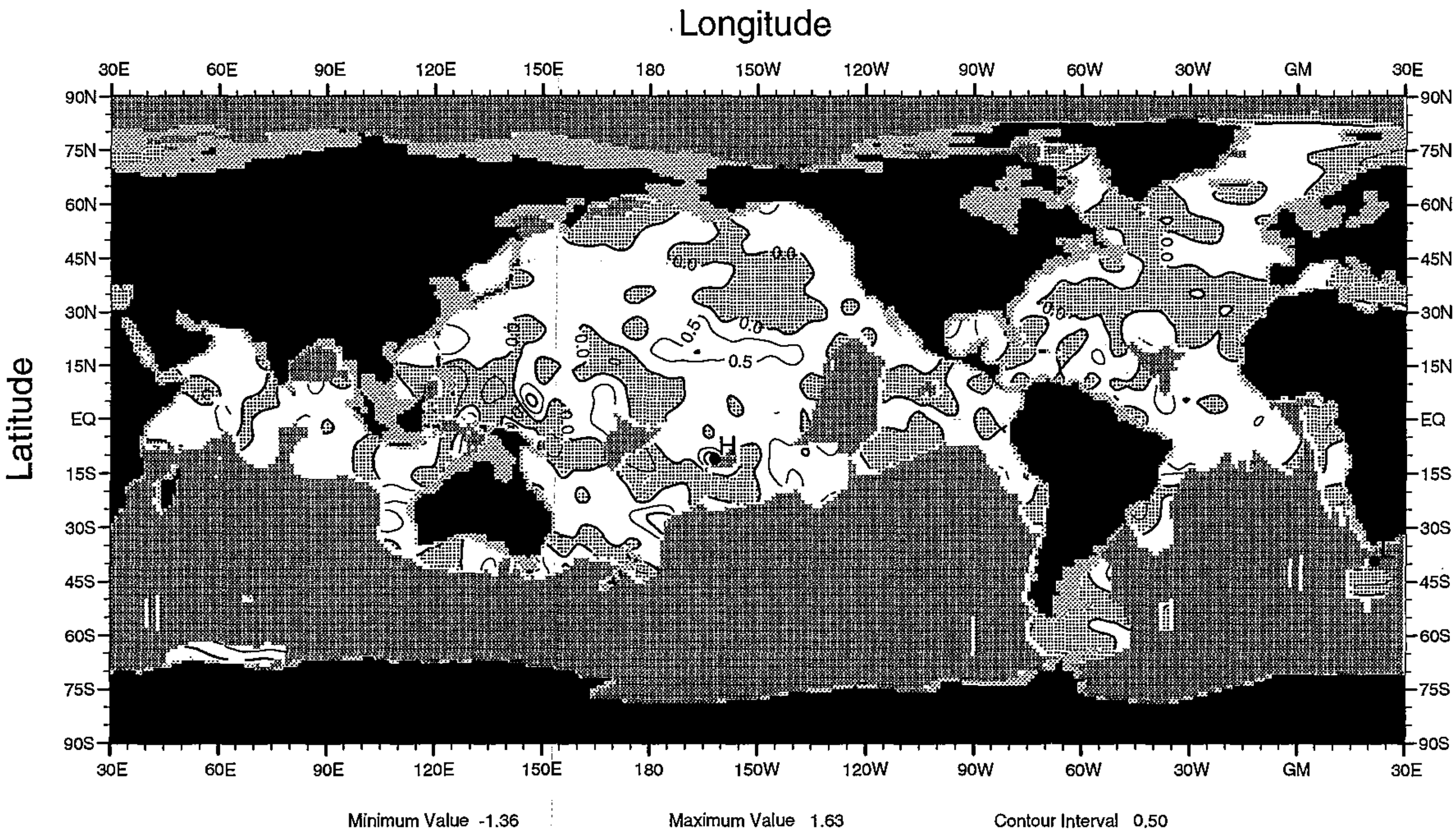


Fig. D21 Temperature anomaly (°C) at 250 m depth for year 1980

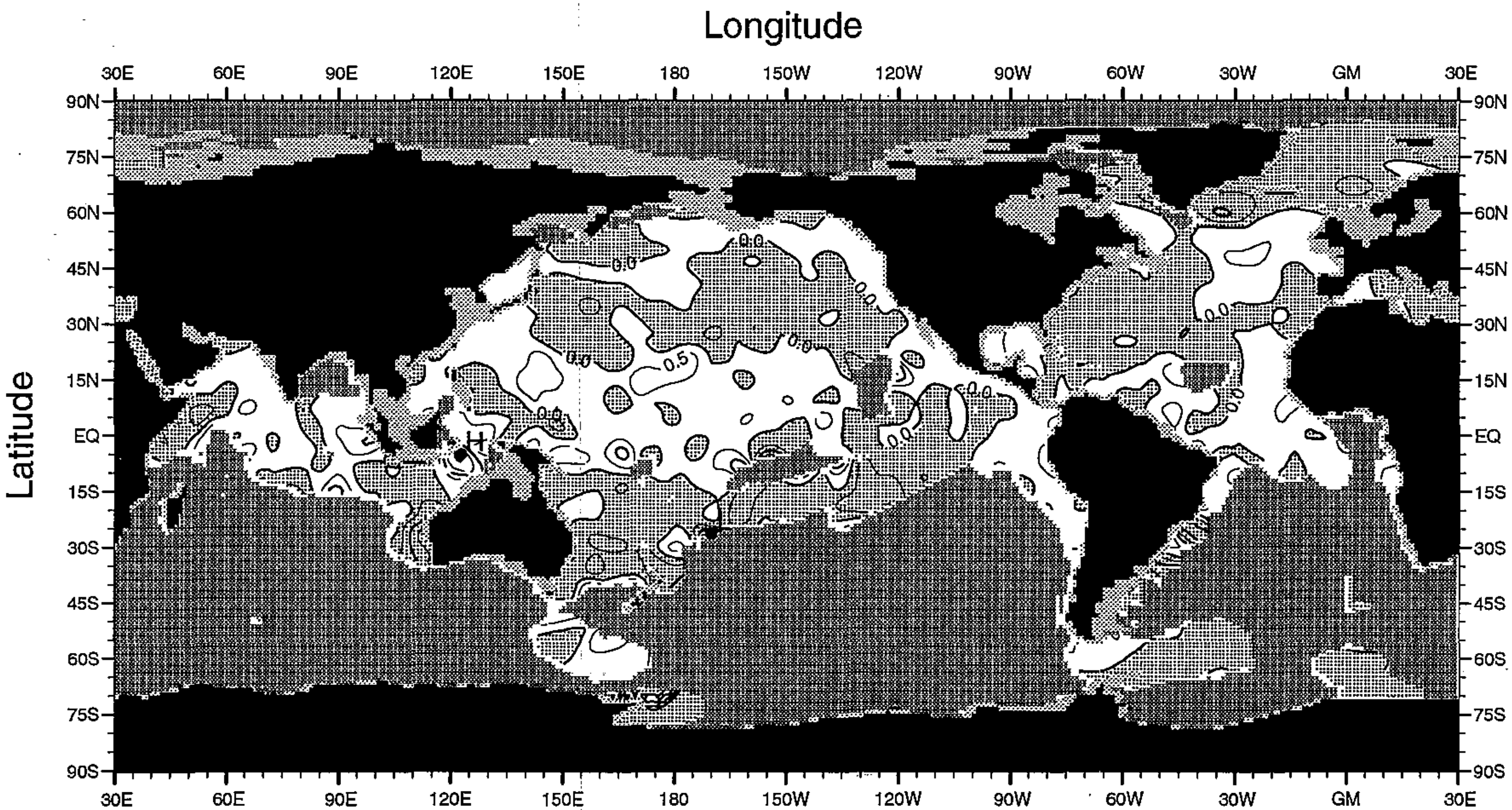


Minimum Value -2.03 Maximum Value 2.12 Contour Interval 0.50

Fig. D22 Temperature anomaly (°C) at 250 m depth for year 1981

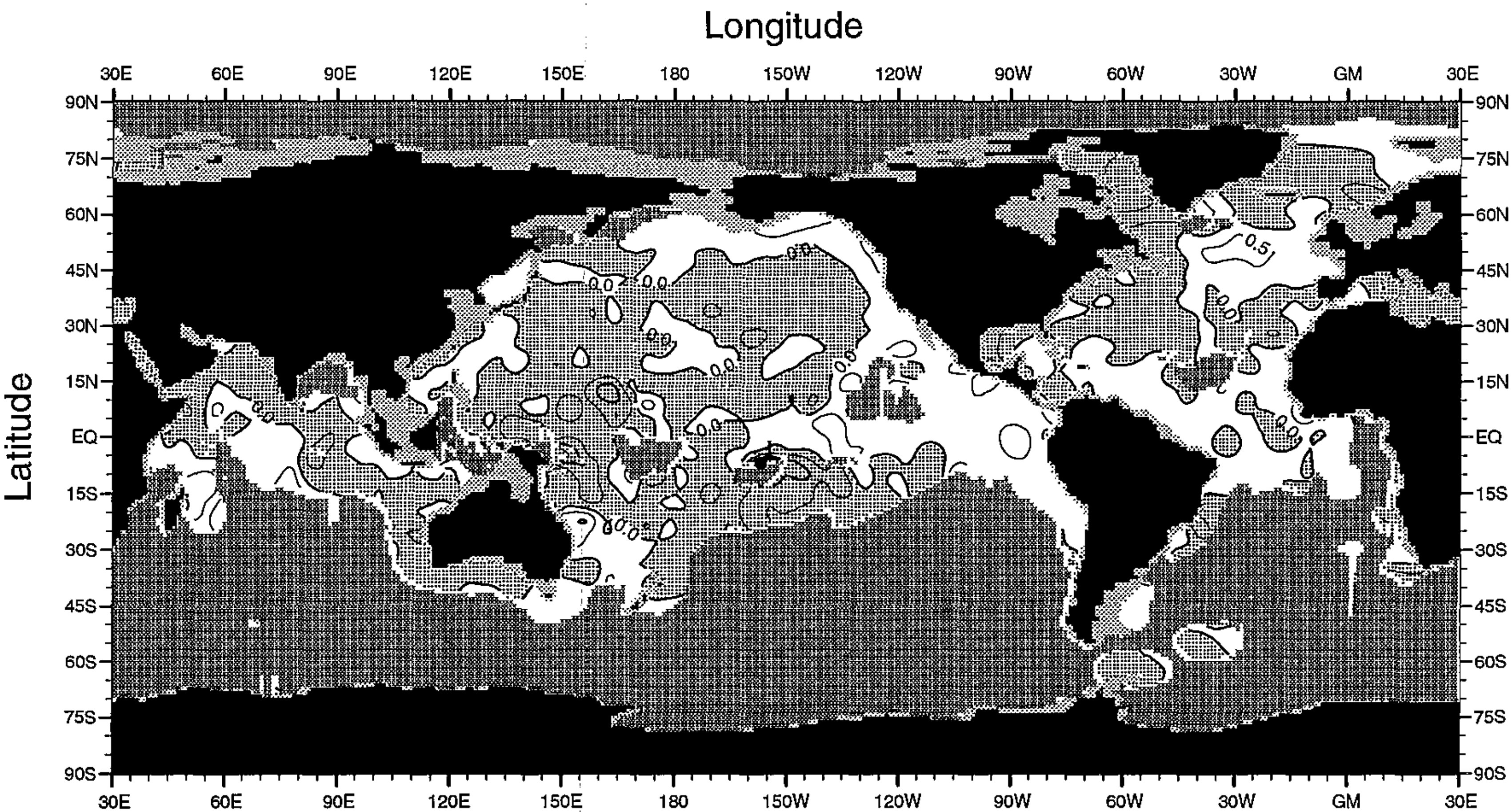


Minimum Value -2.12 Maximum Value 1.22 Contour Interval 0.50

Fig. D23 Temperature anomaly (°C) at 250 m depth for year 1982

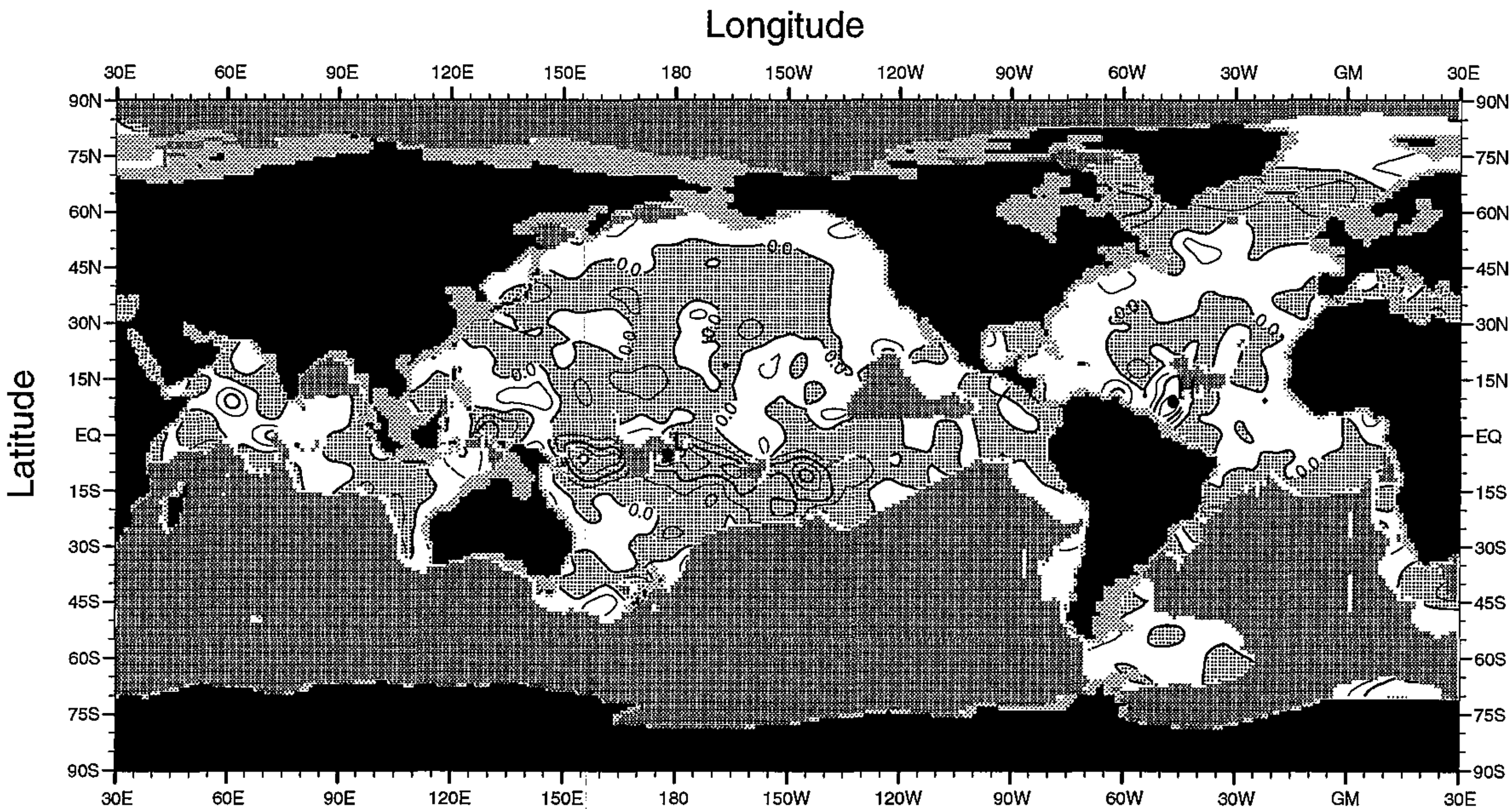


Minimum Value -2.71 Maximum Value 1.95 Contour Interval 0.50

Fig. D24 Temperature anomaly (°C) at 250 m depth for year 1983

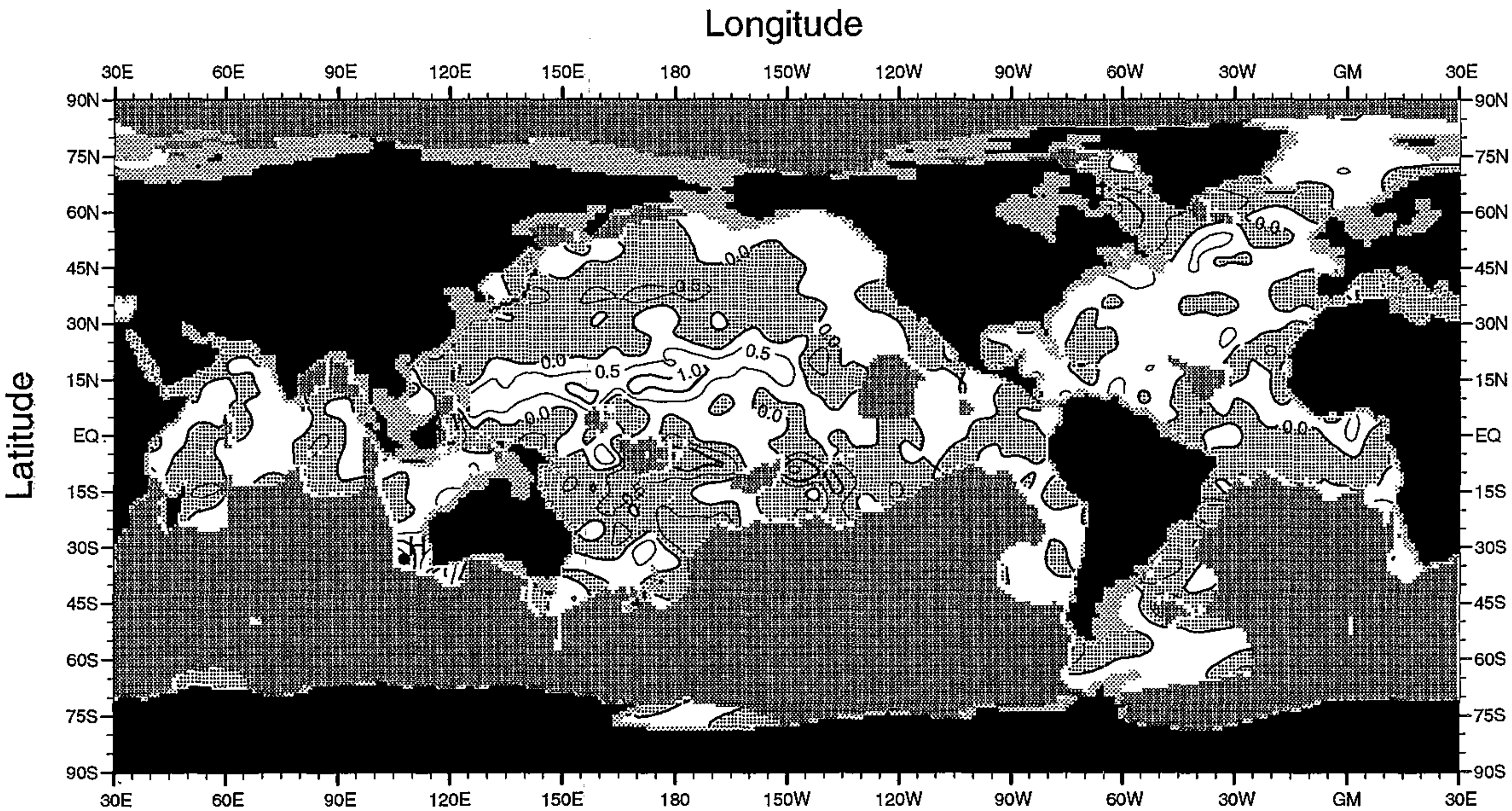


Minimum Value -2.50 Maximum Value 1.77 Contour Interval 0.50

Fig. D25 Temperature anomaly (°C) at 250 m depth for year 1984

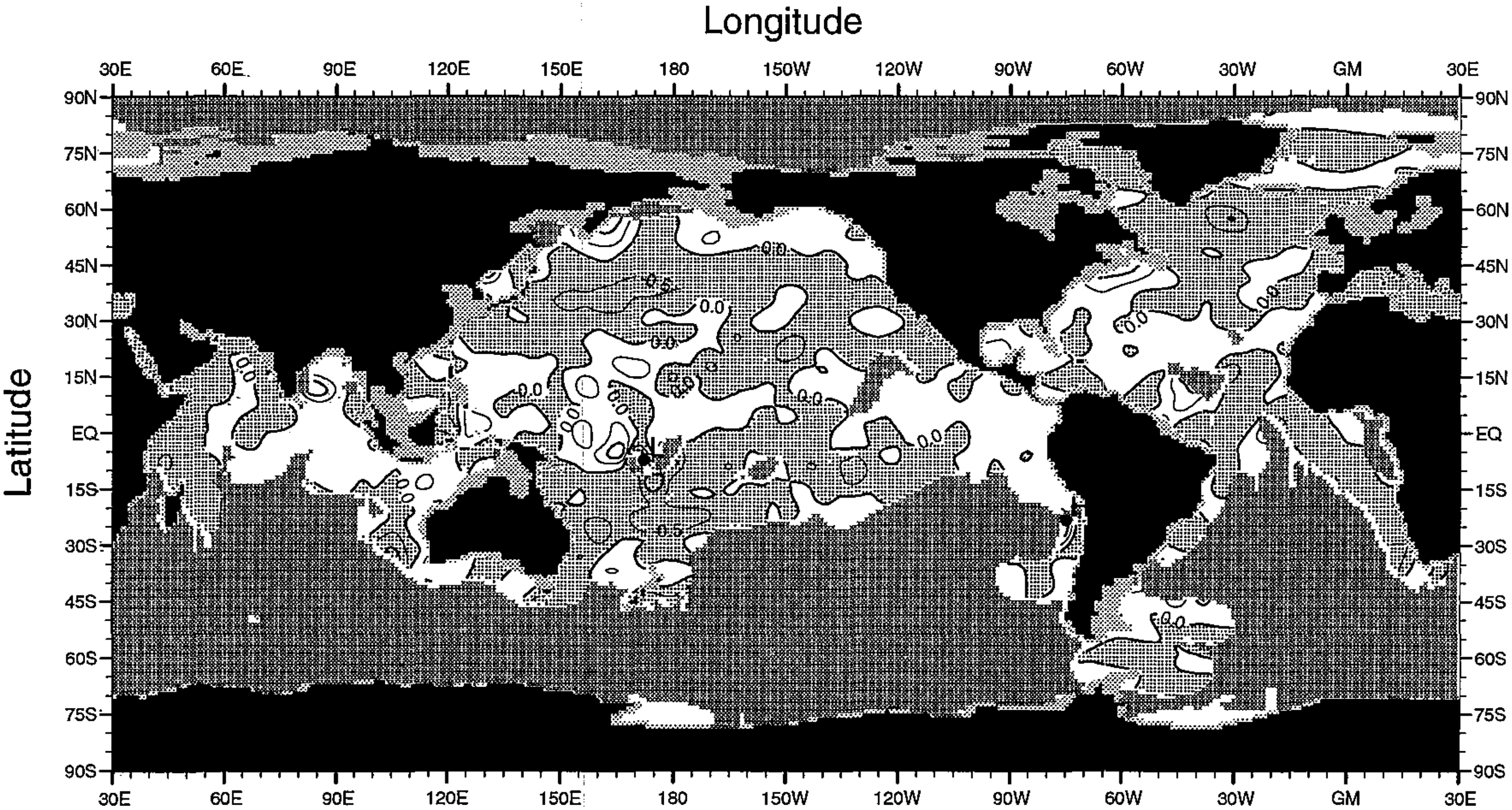


Minimum Value -1.37 Maximum Value 1.47 Contour Interval 0.50

Fig. D26 Temperature anomaly (°C) at 250 m depth for year 1985

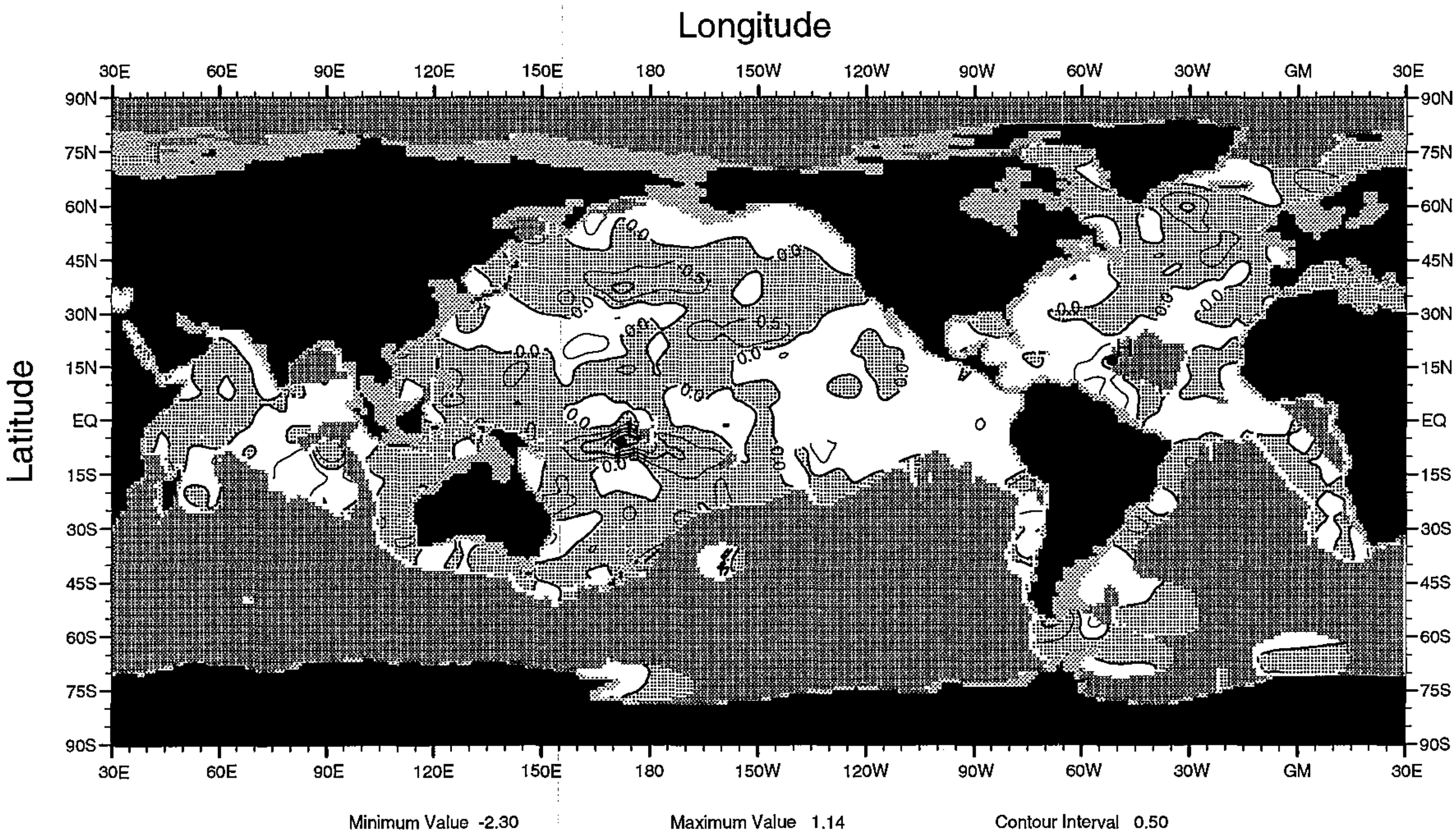


Fig. D27 Temperature anomaly (°C) at 250 m depth for year 1986

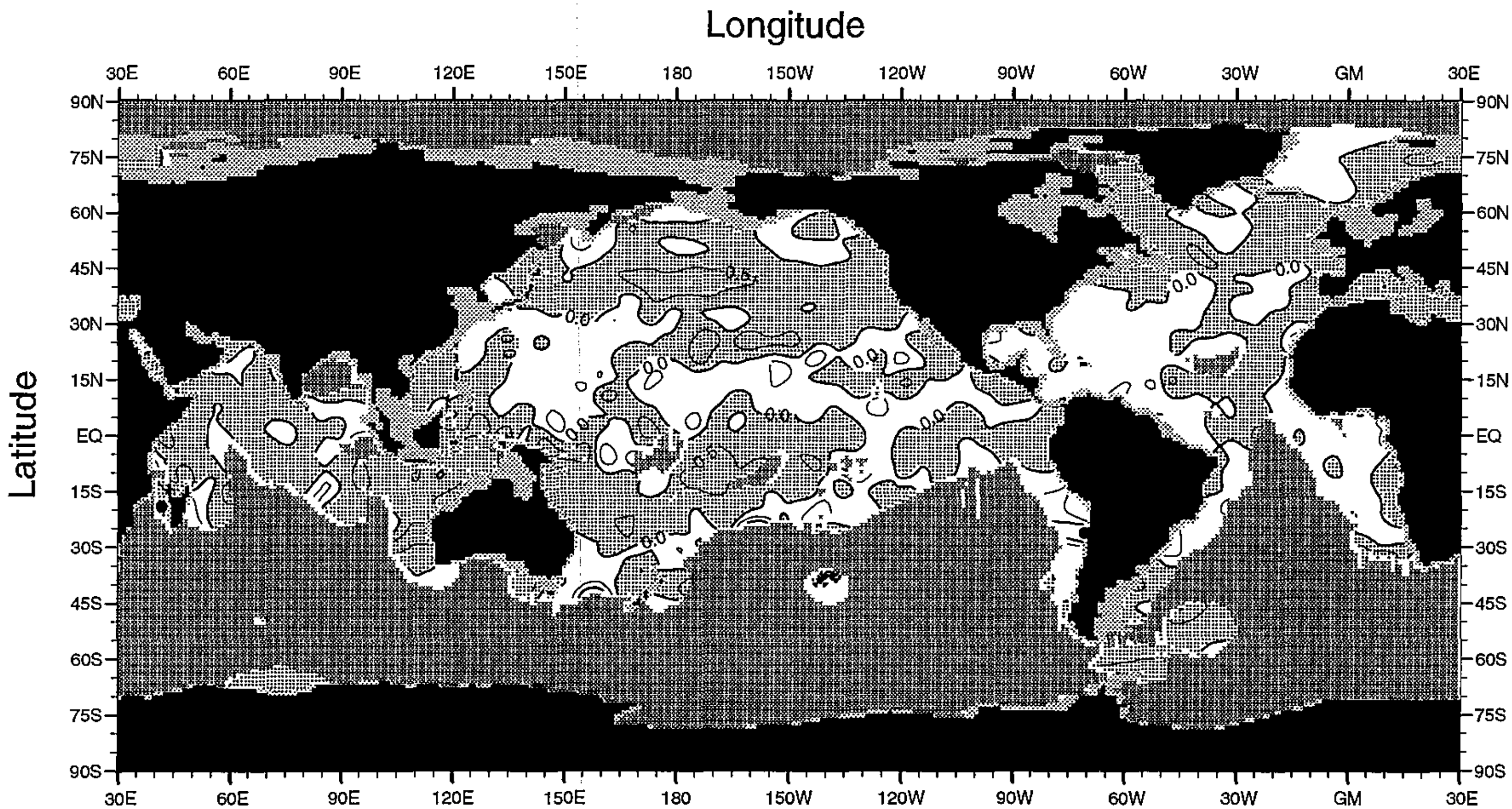


Minimum Value -1.96 Maximum Value 1.64 Contour Interval 0.50

Fig. D28 Temperature anomaly (°C) at 250 m depth for year 1987

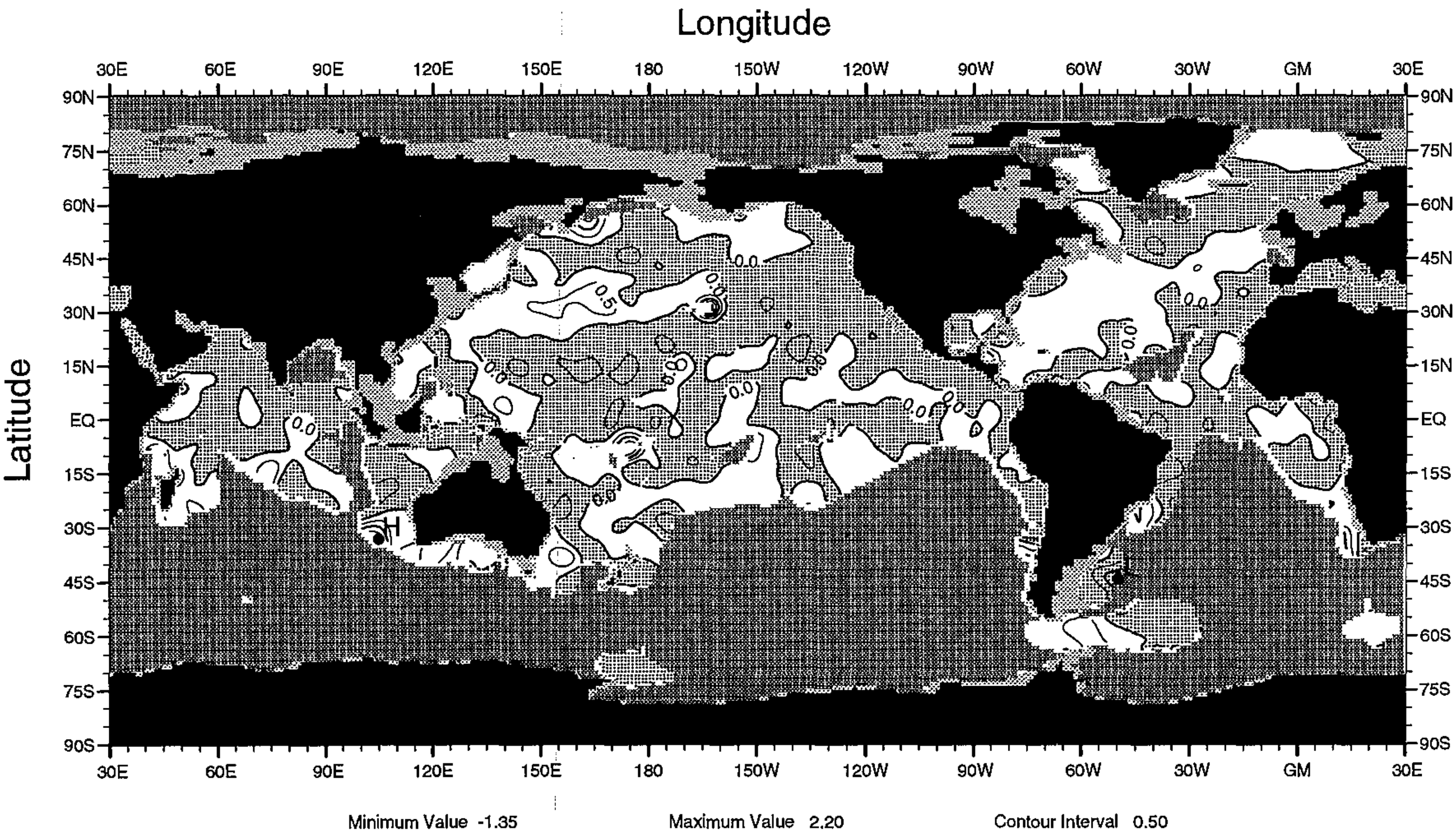


Fig. D29 Temperature anomaly (°C) at 250 m depth for year 1988

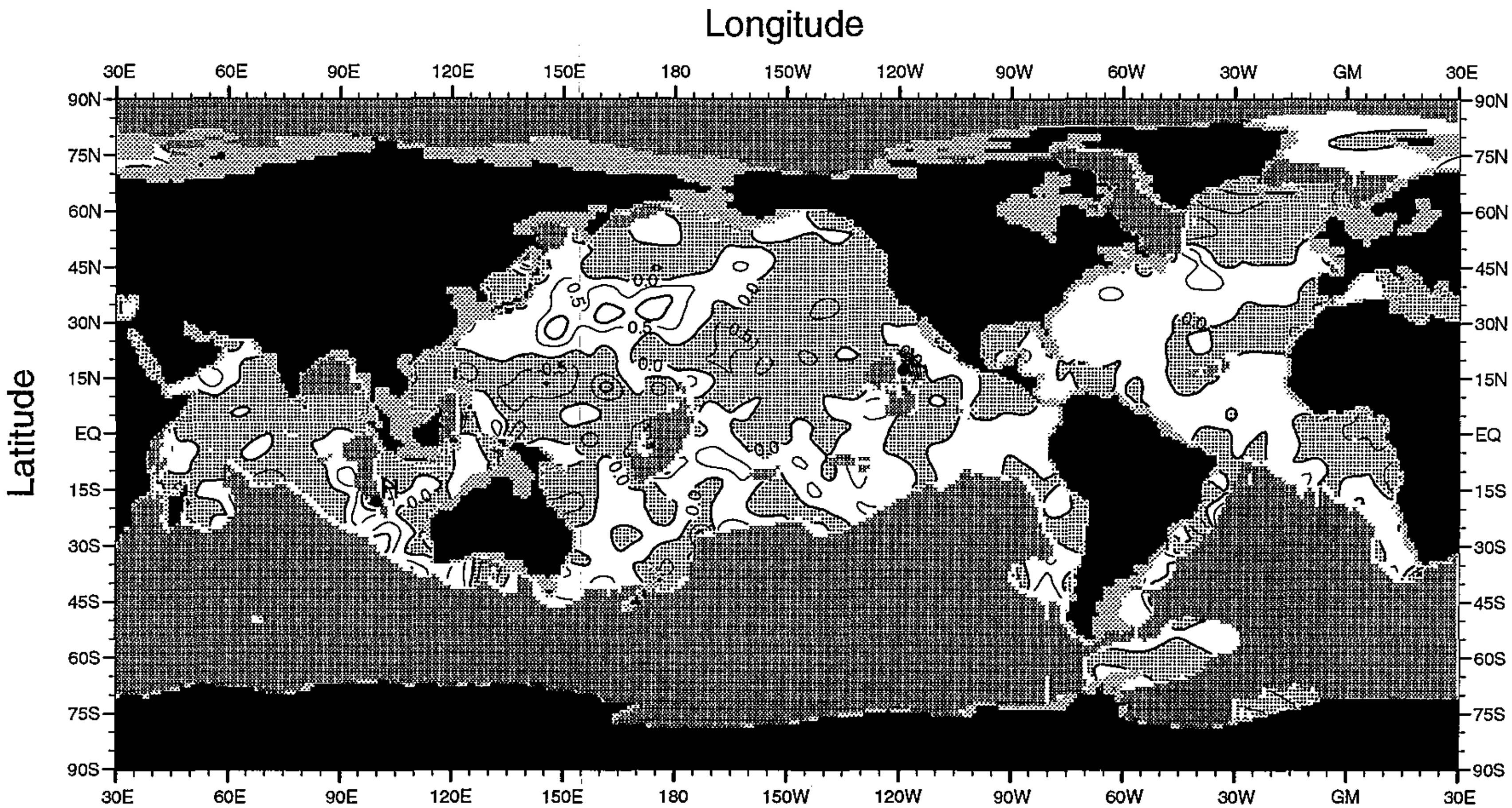


Minimum Value -2.38 Maximum Value 1.79 Contour Interval 0.50

Fig. D30 Temperature anomaly (°C) at 250 m depth for year 1989

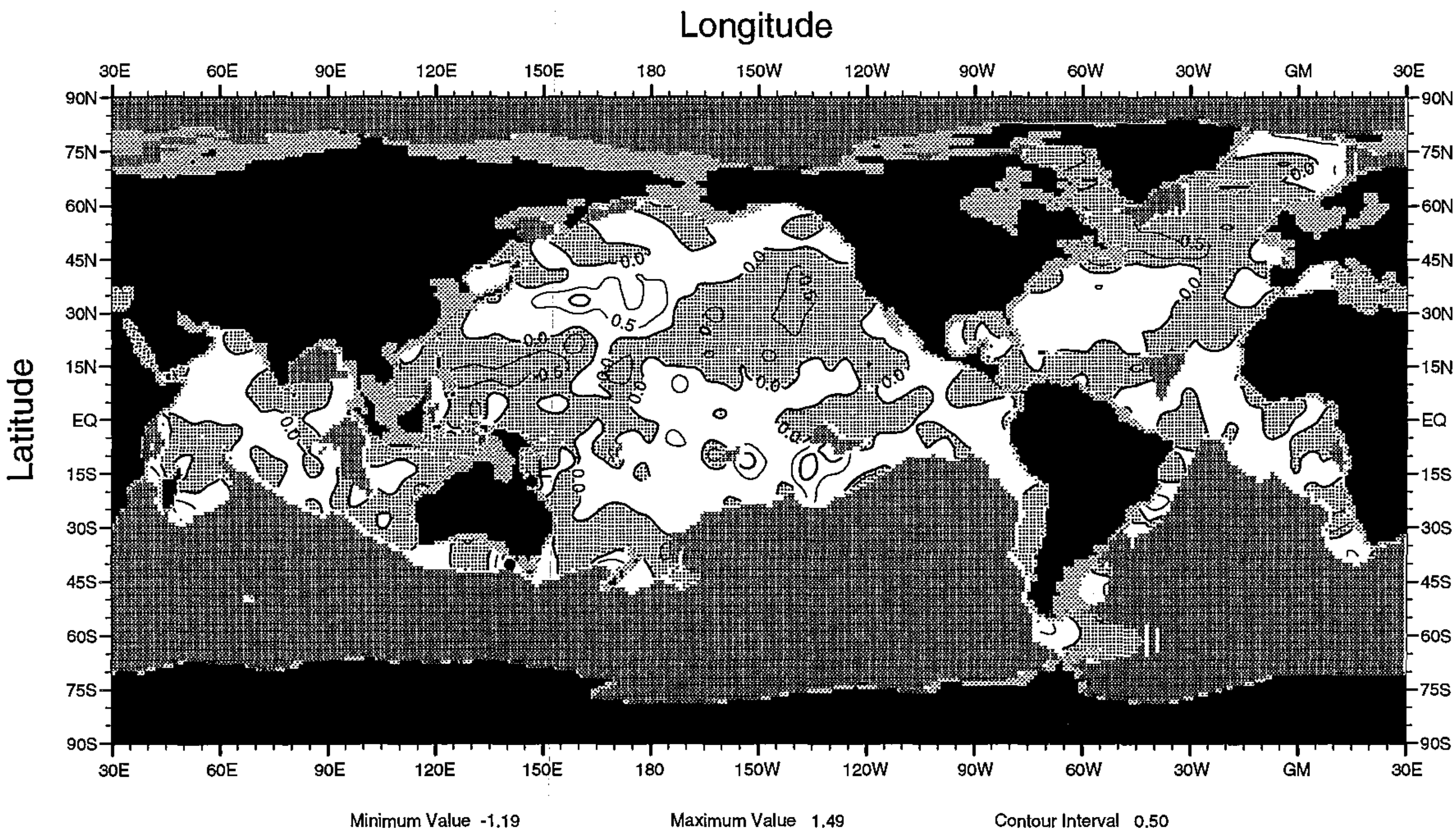


Fig. D31 Temperature anomaly (°C) at 250 m depth for year 1990

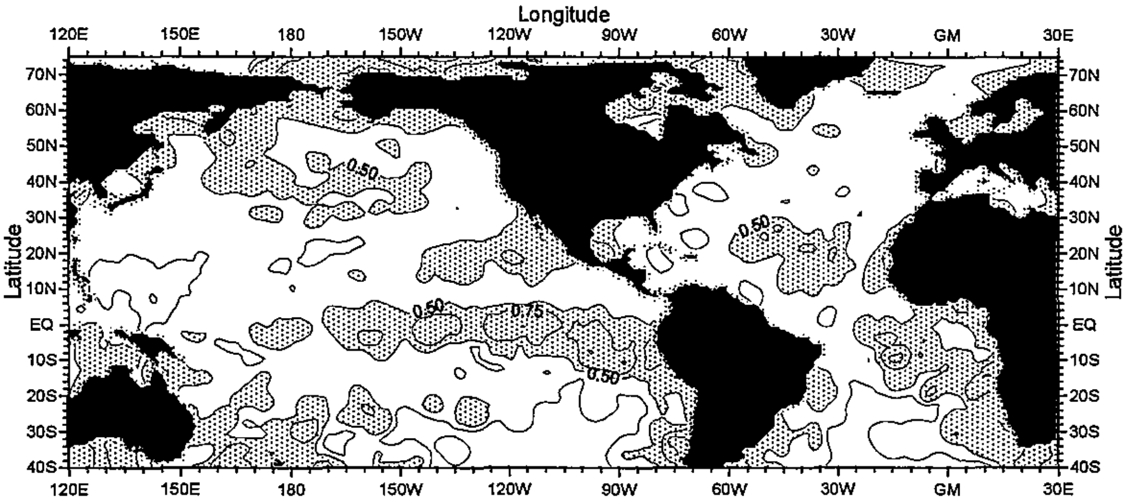


Fig.E1 Standard deviation of yearly temperature anomalies (C) at the surface

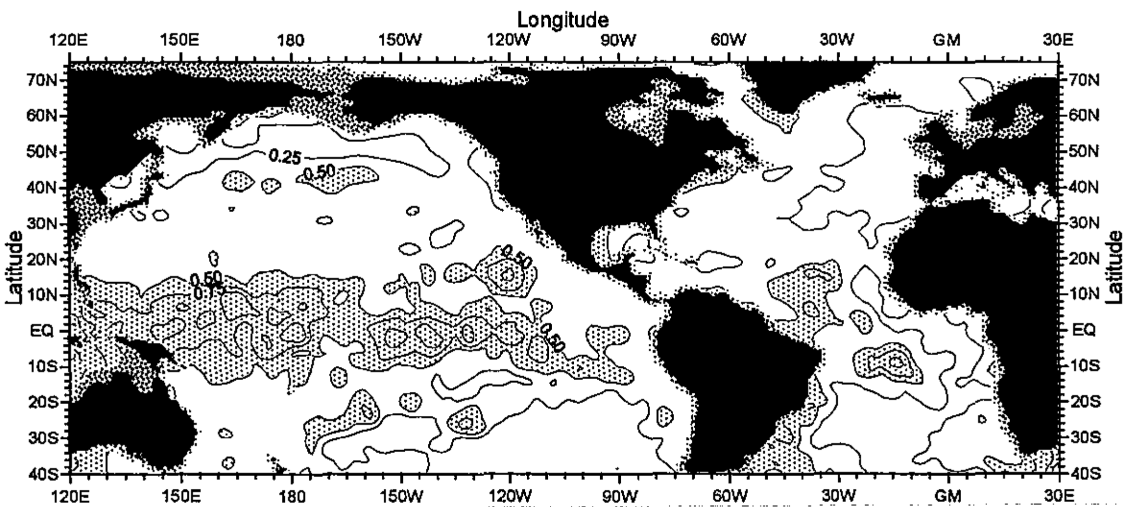


Fig.E2 Standard deviation of yearly temperature anomalies (C) at 125 m depth

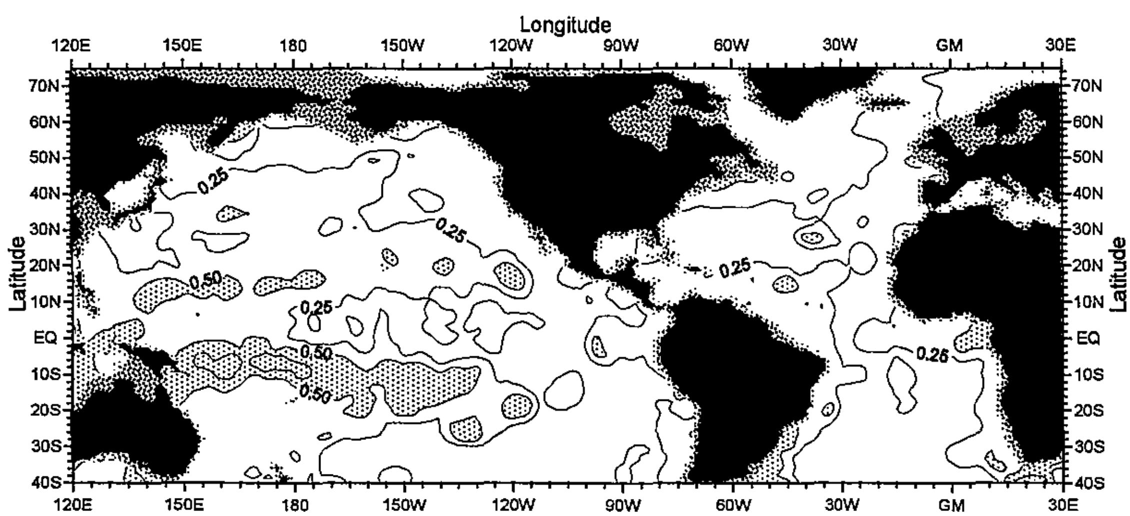


Fig.E3 Standard deviation of yearly temperature anomalies (C) at 250 m depth

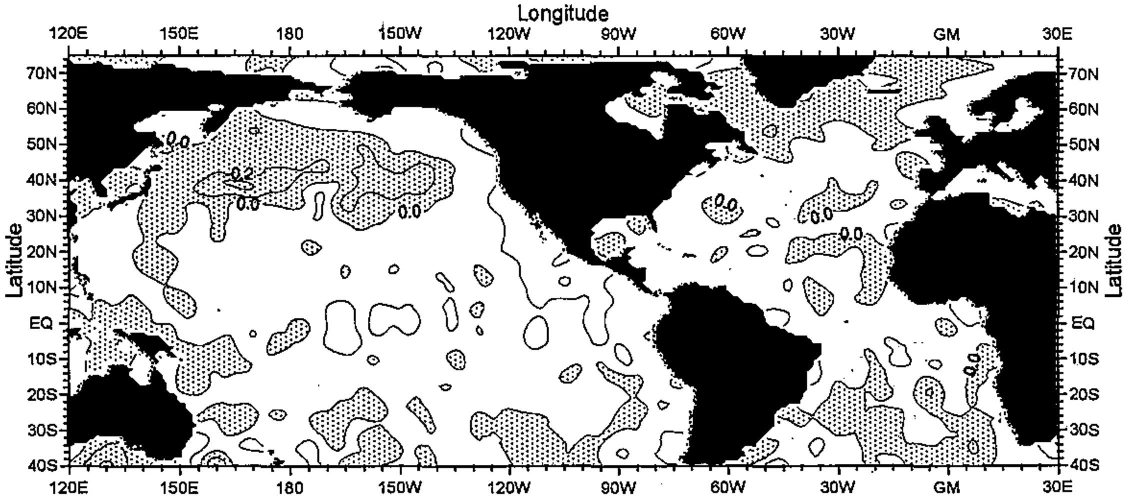


Fig.E4 Temperature anomaly trend for 1960-1990 period (C/10 YR) at the surface

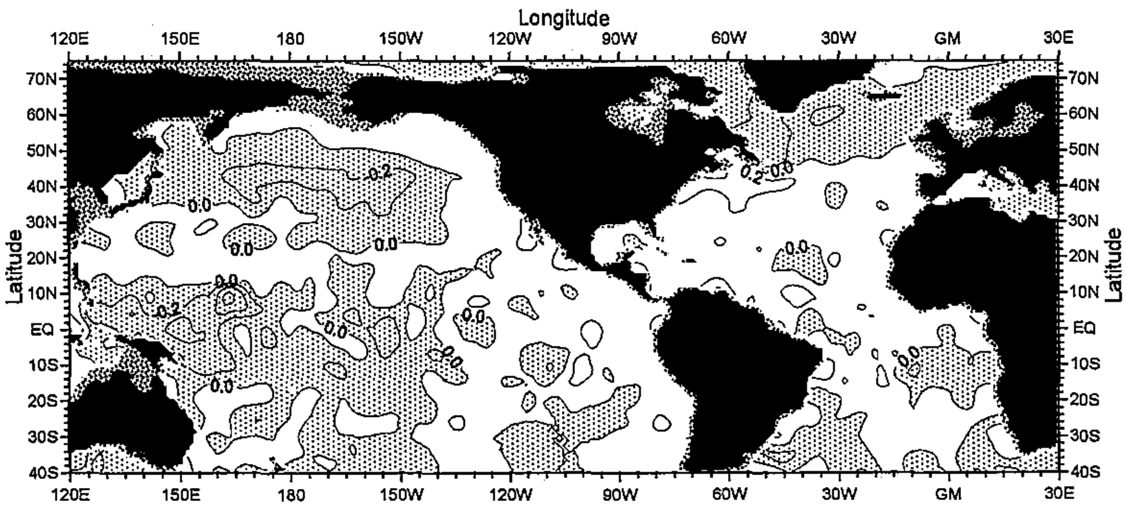


Fig.E5 Temperature anomaly trend for 1960-1990 period (C/10 YR) at 125 m depth

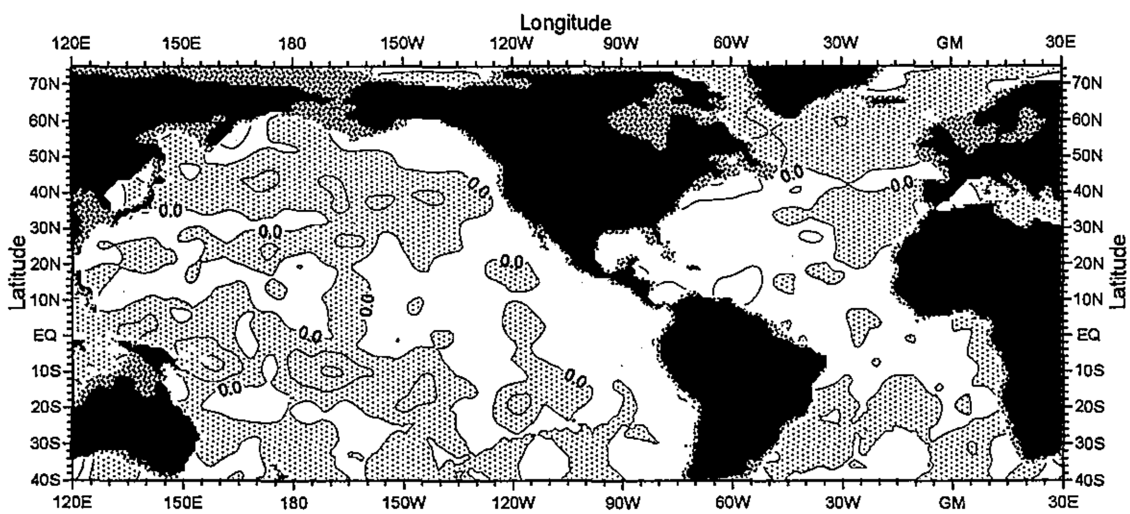


Fig.E6 Temperature anomaly trend for 1960-1990 period (C/10 YR) at 250 m depth

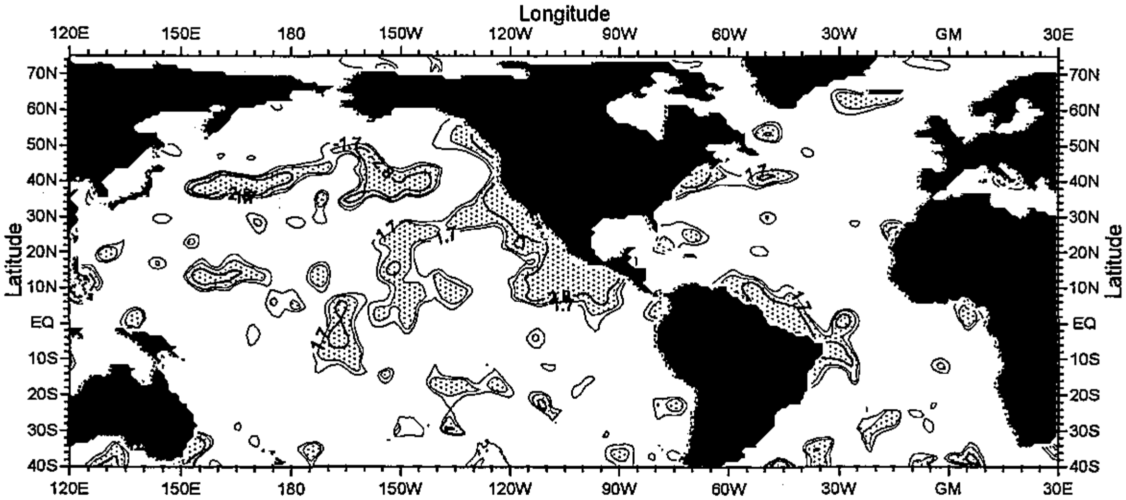


Fig.E7 Trend significance at 10%, 5%, and 1% levels (t-test) at the surface

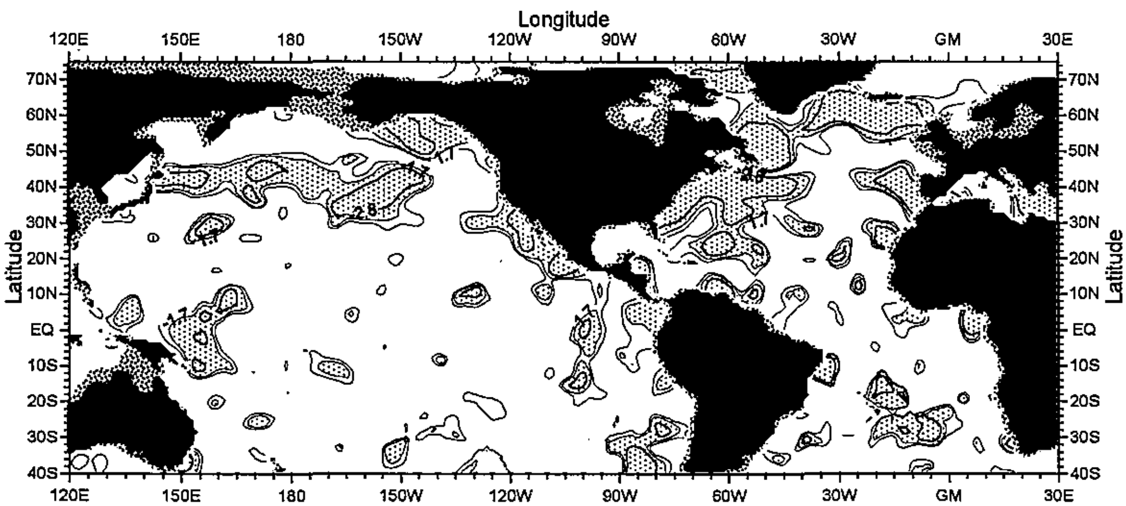


Fig.E8 Trend significance at 10%, 5%, and 1% levels (t-test) at 125 m depth

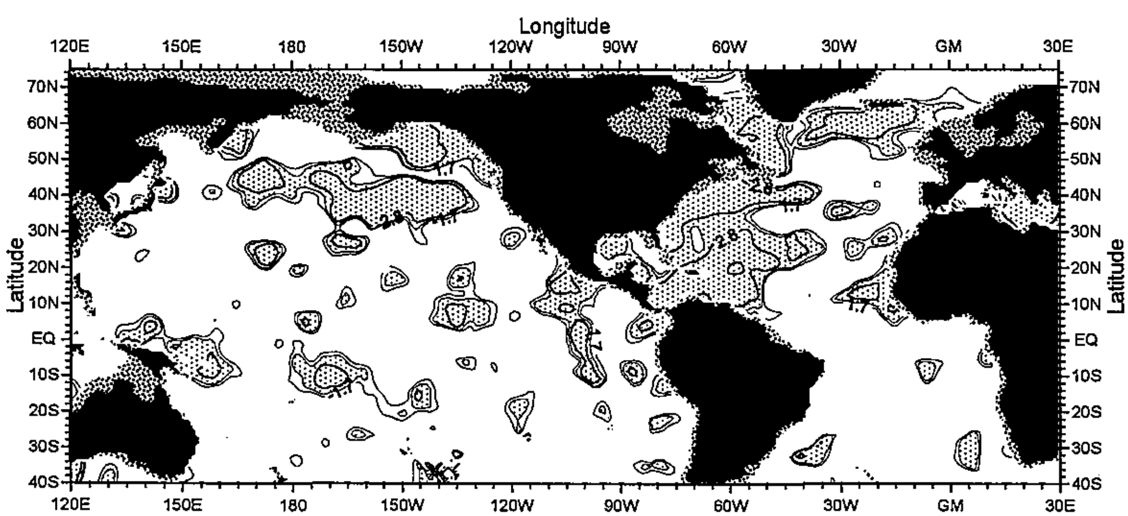


Fig.E9 Trend significance at 10%, 5%, and 1% levels (t-test) at 250 m depth

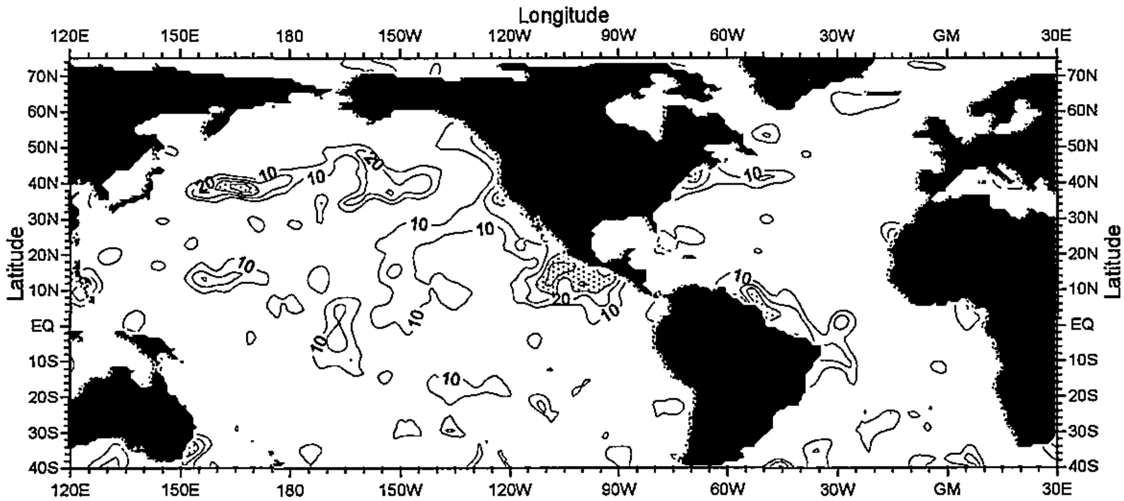


Fig.E10 Percent of variance explained by linear trend at the surface

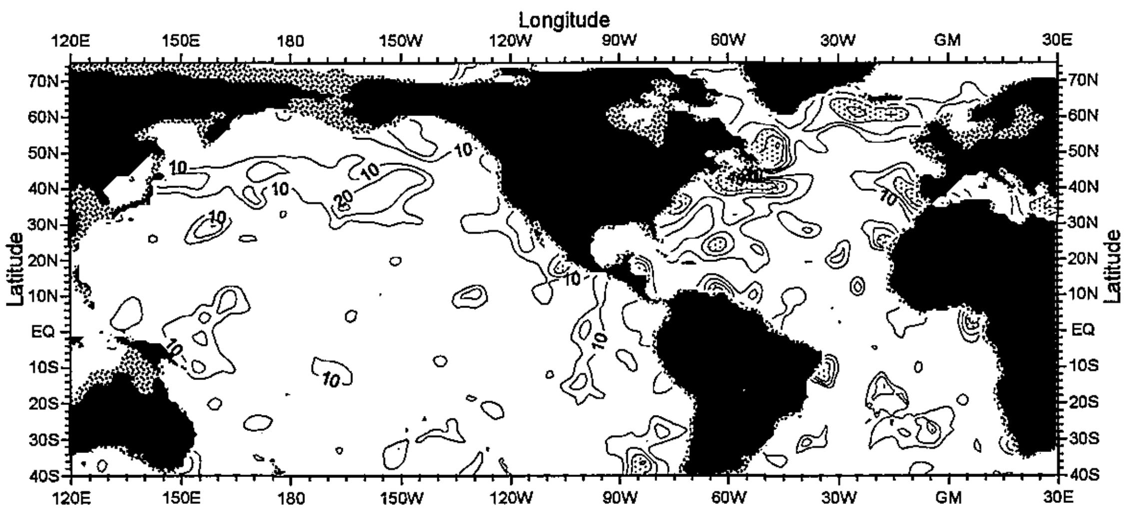


Fig.E11 Percent of variance explained by linear trend at 125 m depth

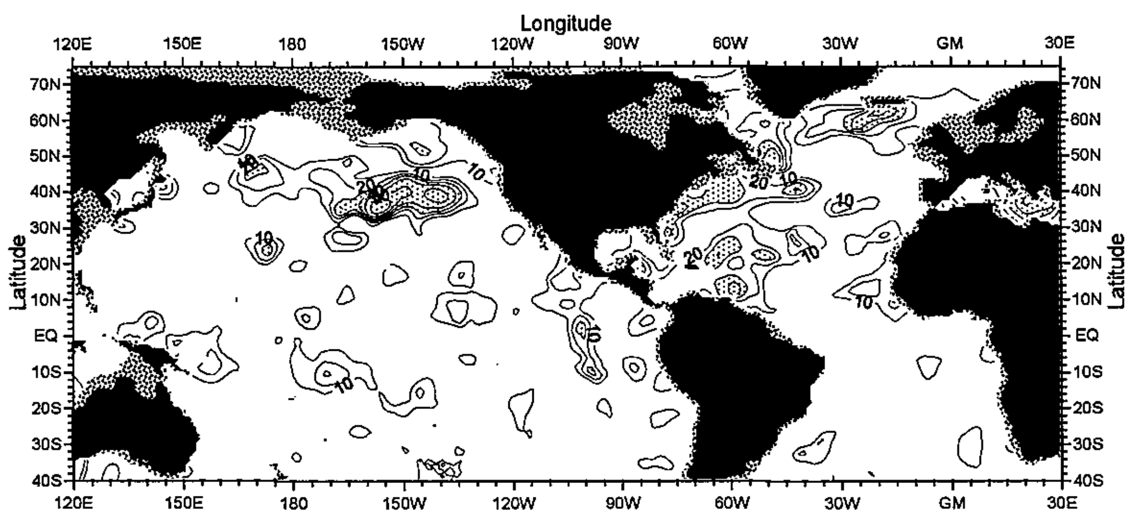


Fig.E12 Percent of variance explained by linear trend at 250 m depth

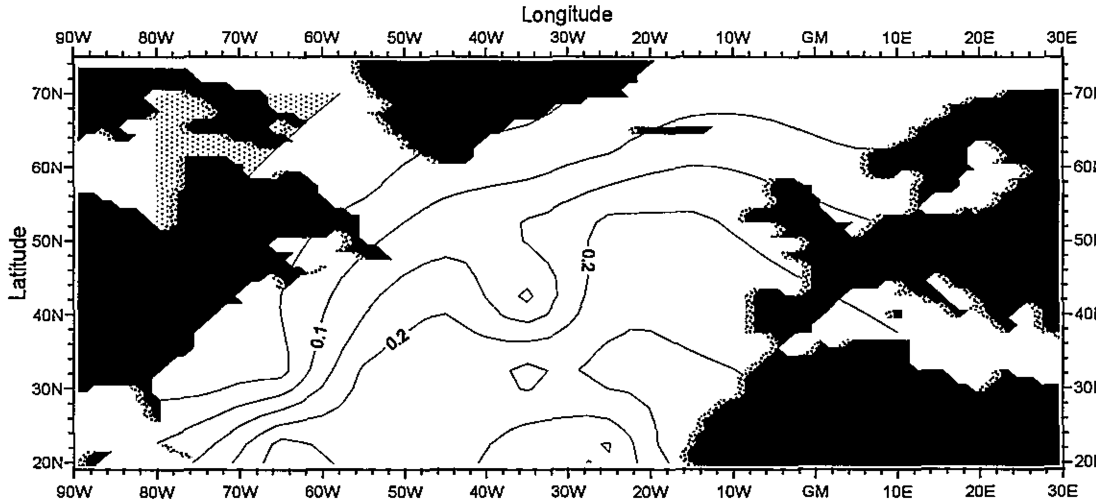

Fig.F1 1ST EOF of North Atlantic temperature anomalies for 1960-90 period at the surface

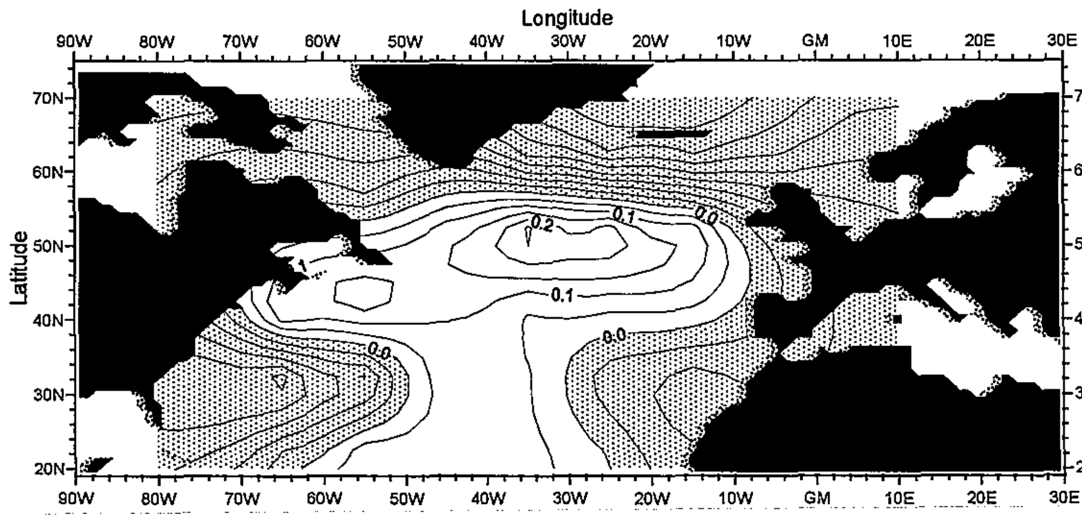

Fig.F2 2ND EOF of North Atlantic temperature anomalies for 1960-90 period at the surface

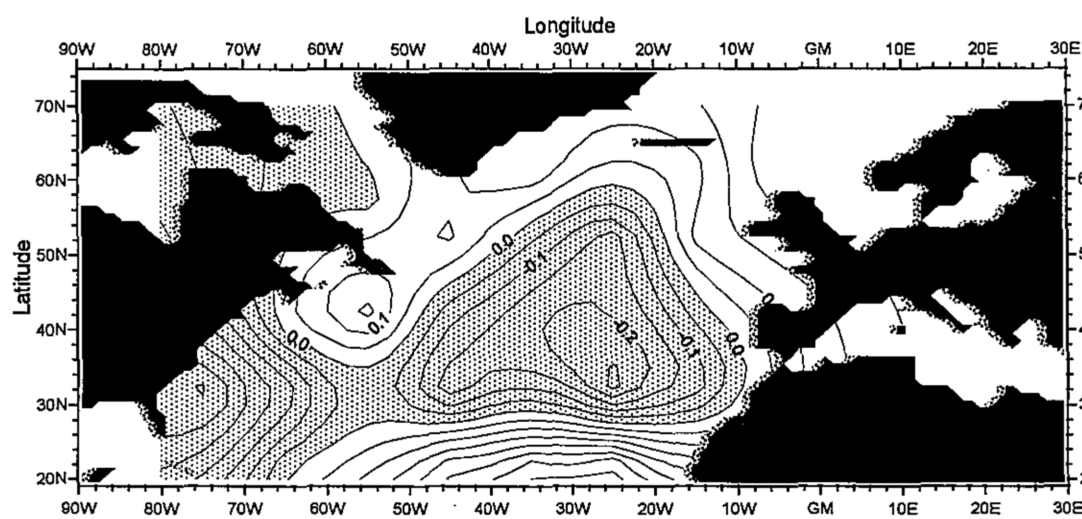

Fig.F3 3RD EOF of North Atlantic temperature anomalies for 1960-90 period at the surface

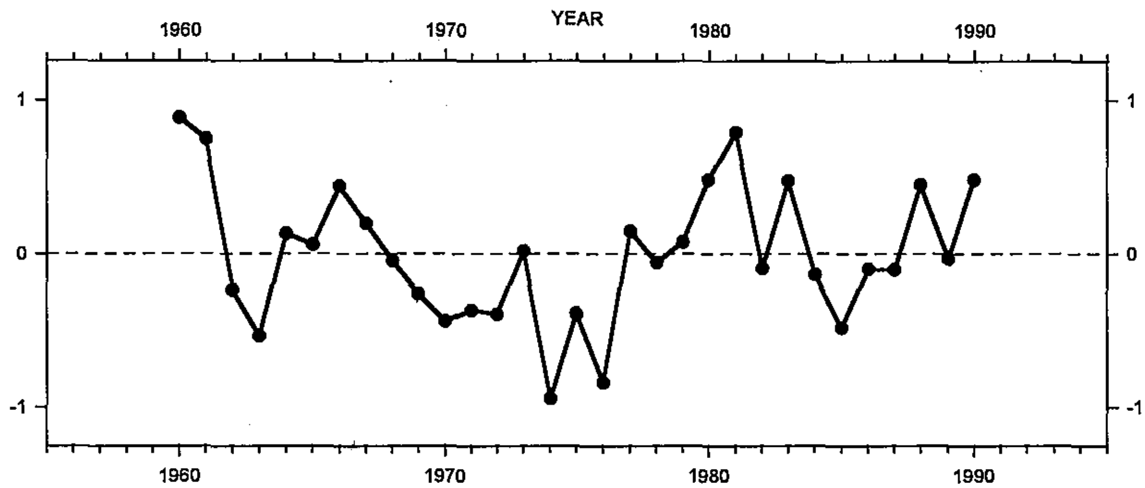


Fig.F4 1ST EOF time series of North Atlantic temperature anomalies at the surface (20.2%)

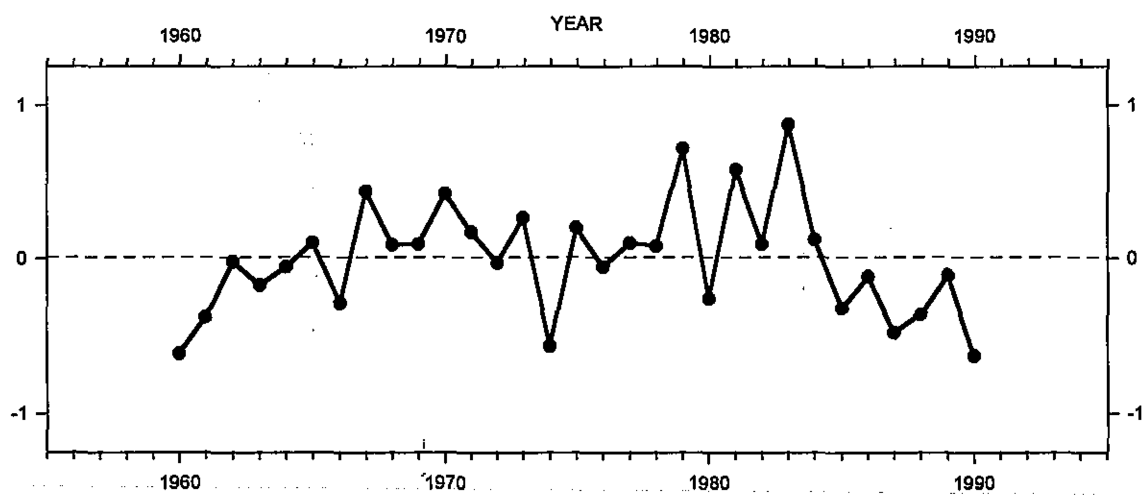


Fig.F5 2ND EOF time series of North Atlantic temperature anomalies at the surface (13.7%)

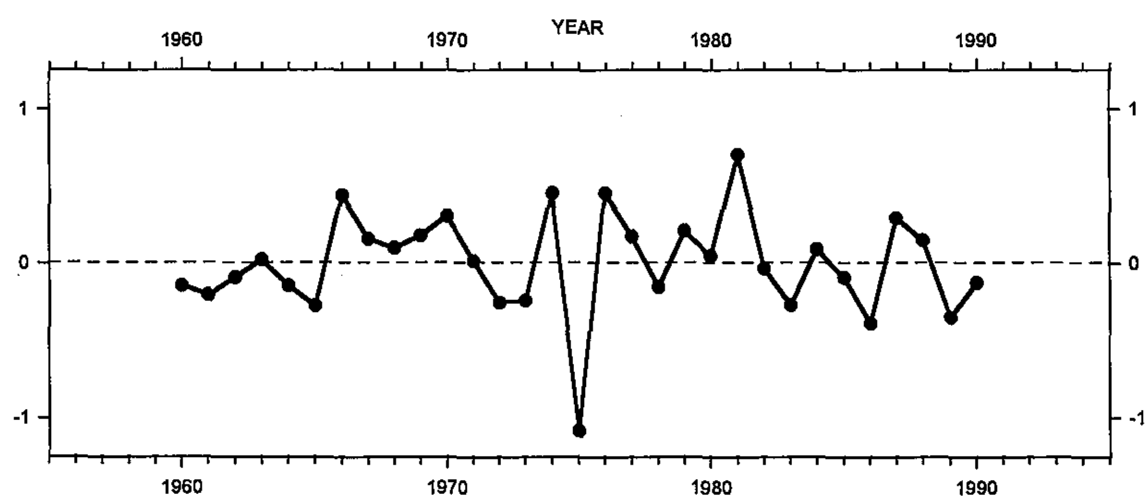


Fig.F6 3RD EOF time series of North Atlantic temperature anomalies at the surface (11.0%)

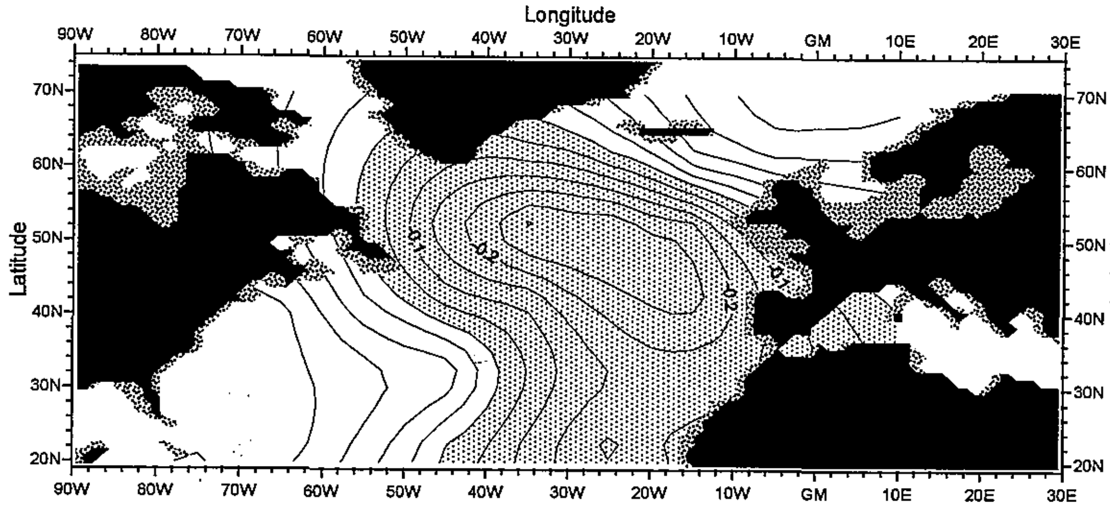

Fig.F7 1ST EOF of North Atlantic temperature anomalies for 1960-90 period at 125 m depth

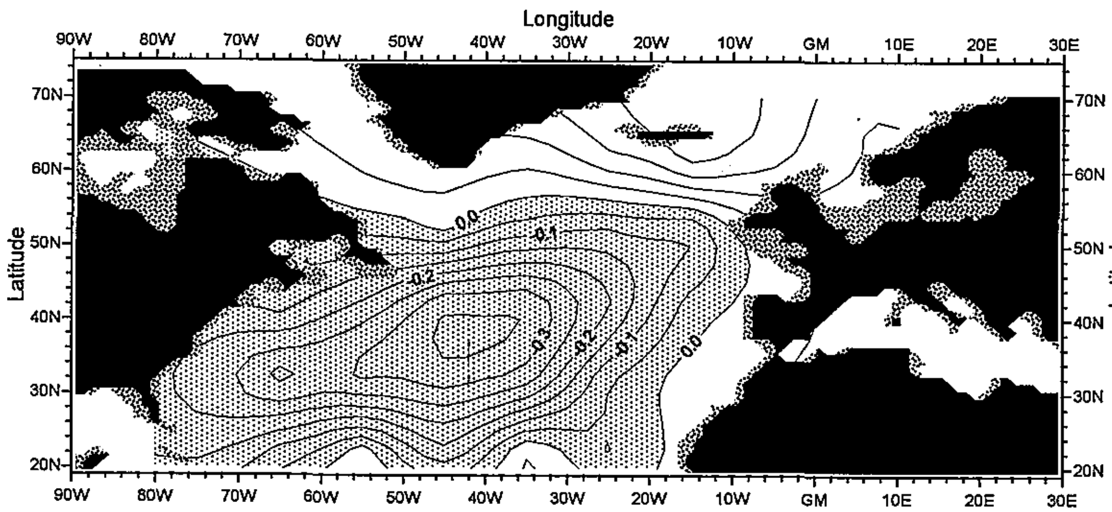

Fig.F8 2ND EOF of North Atlantic temperature anomalies for 1960-90 period at 125 m depth

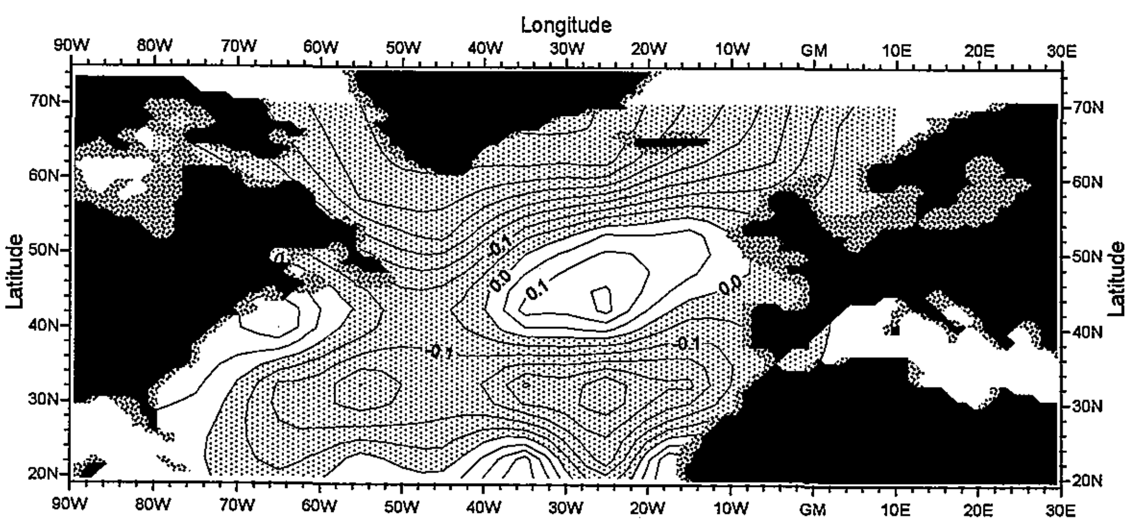

Fig.F9 3RD EOF of North Atlantic temperature anomalies for 1960-90 period at 125 m depth

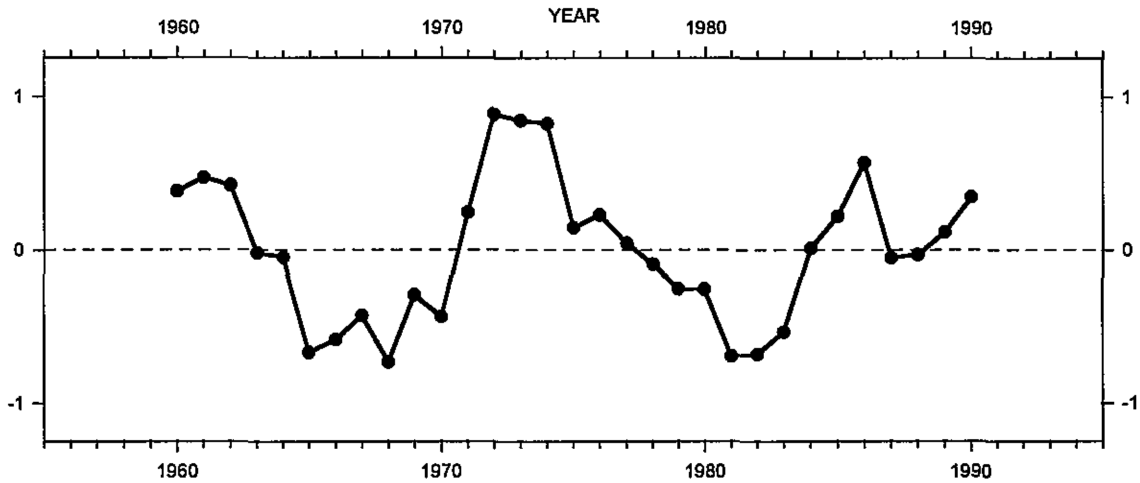


Fig.F10 1ST EOF time series of North Atlantic temperature anomalies at 125 m depth (21.7%)

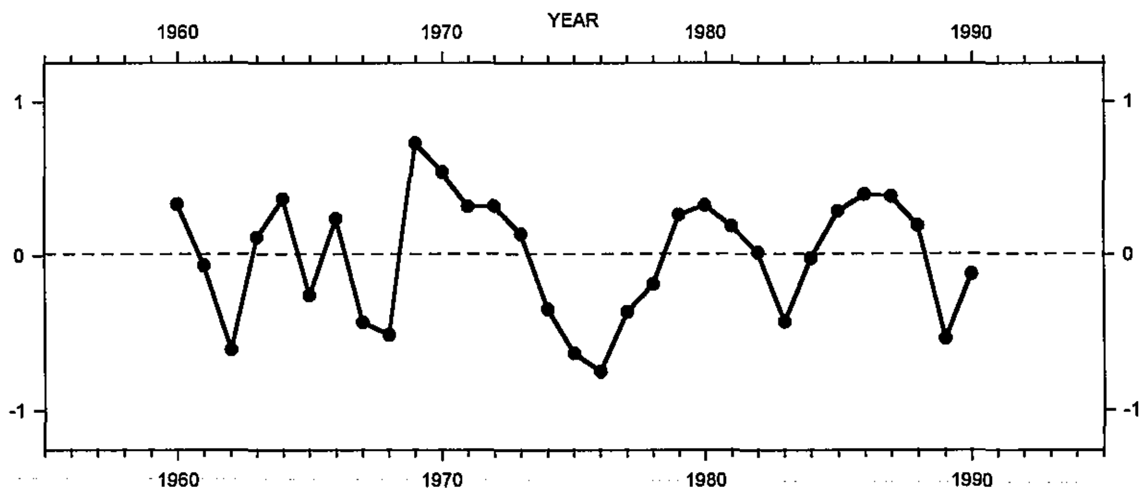


Fig.F11 2ND EOF time series of North Atlantic temperature anomalies at 125 m depth (15.5%)

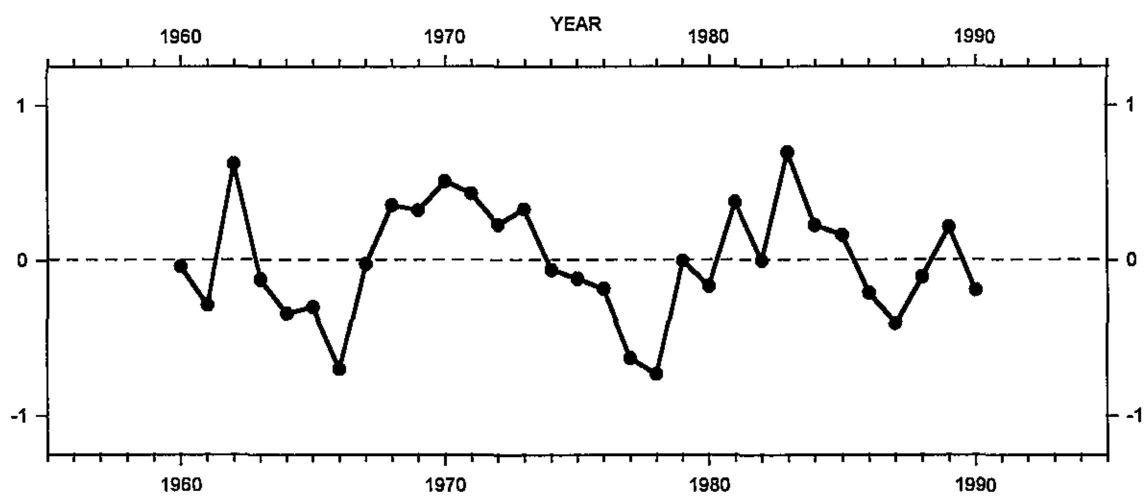


Fig.F12 3RD EOF time series of North Atlantic temperature anomalies at 125 m depth (13.3%)

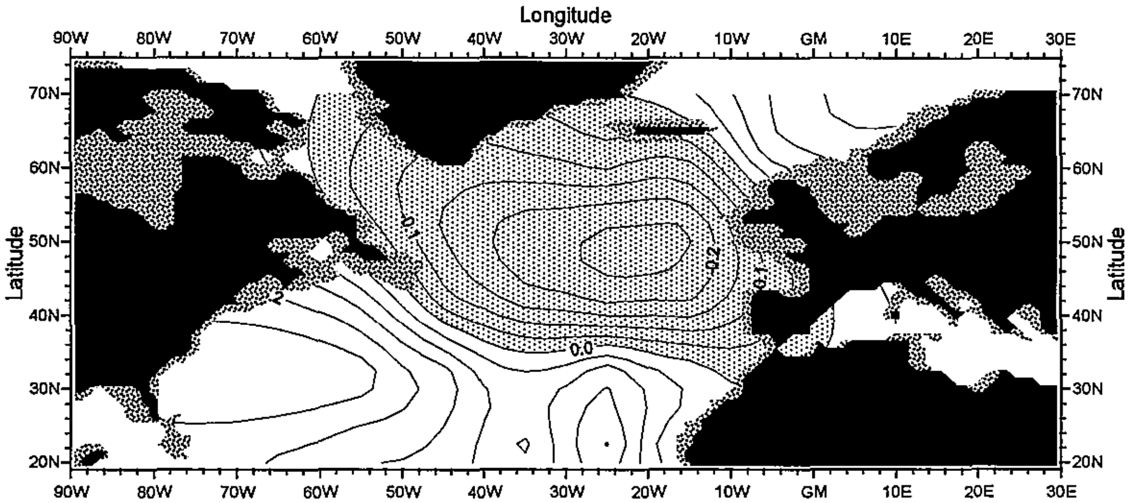


Fig.F13 1ST EOF of North Atlantic temperature anomalies for 1960-90 period at 250 m depth

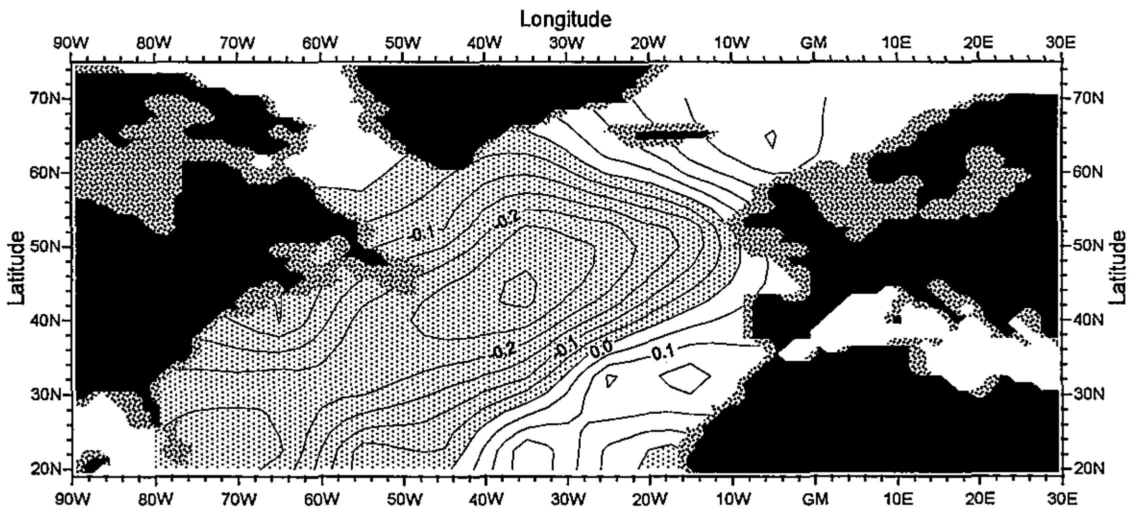


Fig.F14 2ND EOF of North Atlantic temperature anomalies for 1960-90 period at 250 m depth

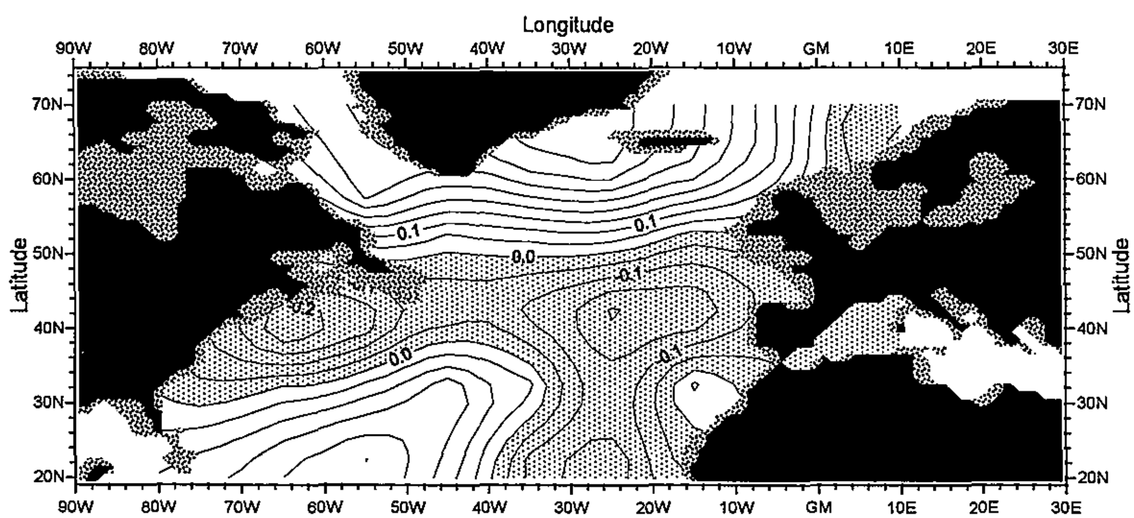


Fig.F15 3RD EOF of North Atlantic temperature anomalies for 1960-90 period at 250 m depth

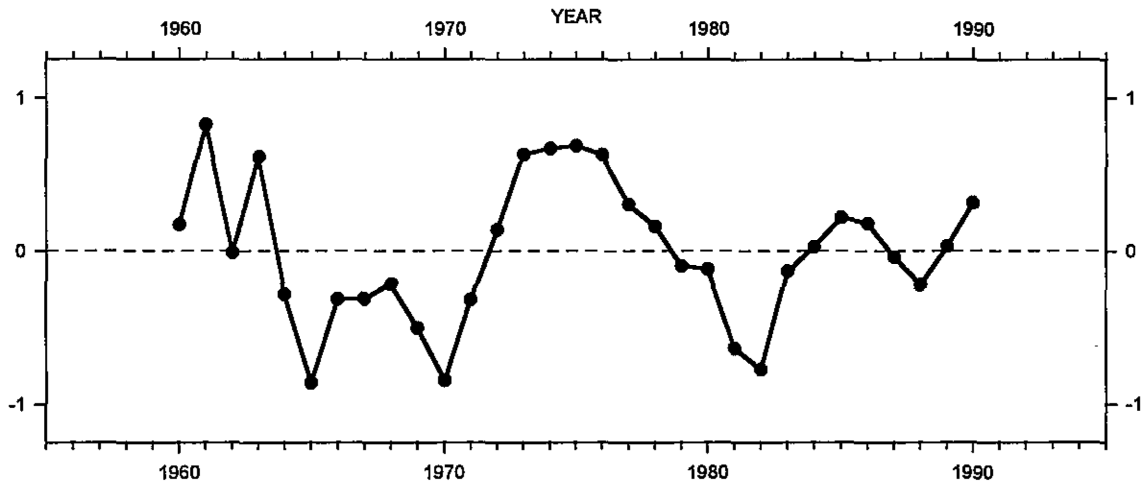

Fig.F16 1ST EOF time series of North Atlantic temperature anomalies at 250 m depth (21.1%)

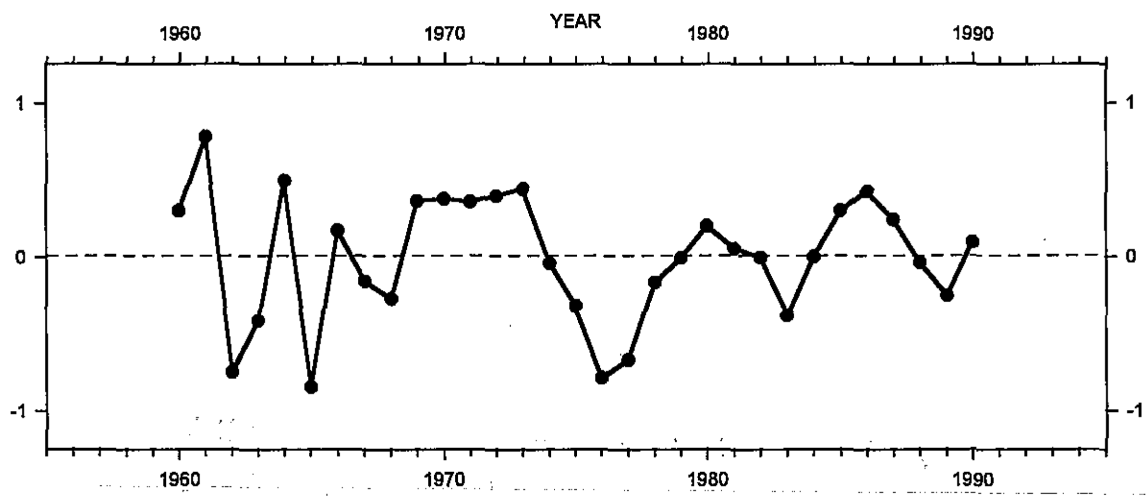

Fig.F17 .2ND EOF time series of North Atlantic temperature anomalies at 250 m depth (16.9%)

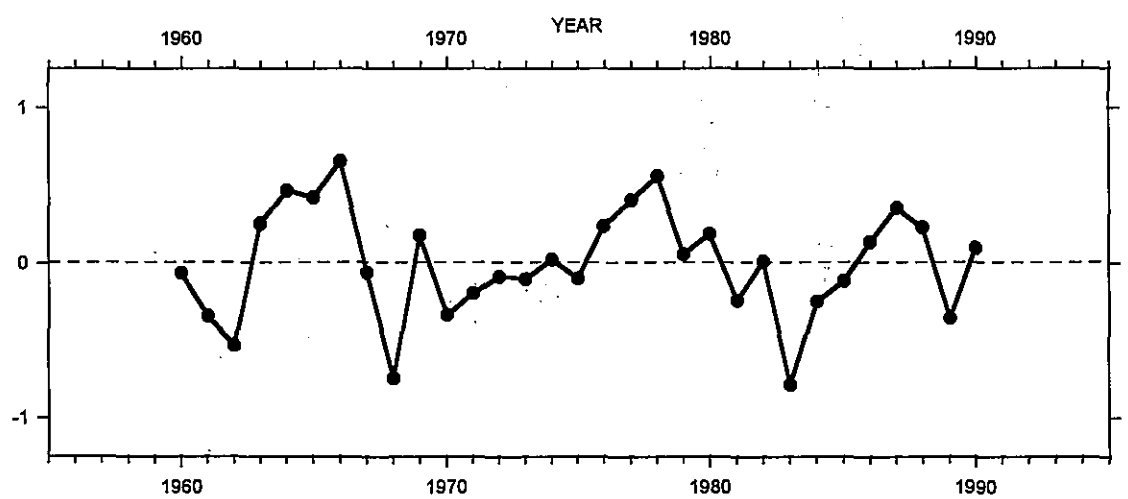

Fig.F18 3RD EOF time series of North Atlantic temperature anomalies at 250 m depth (12.3%)

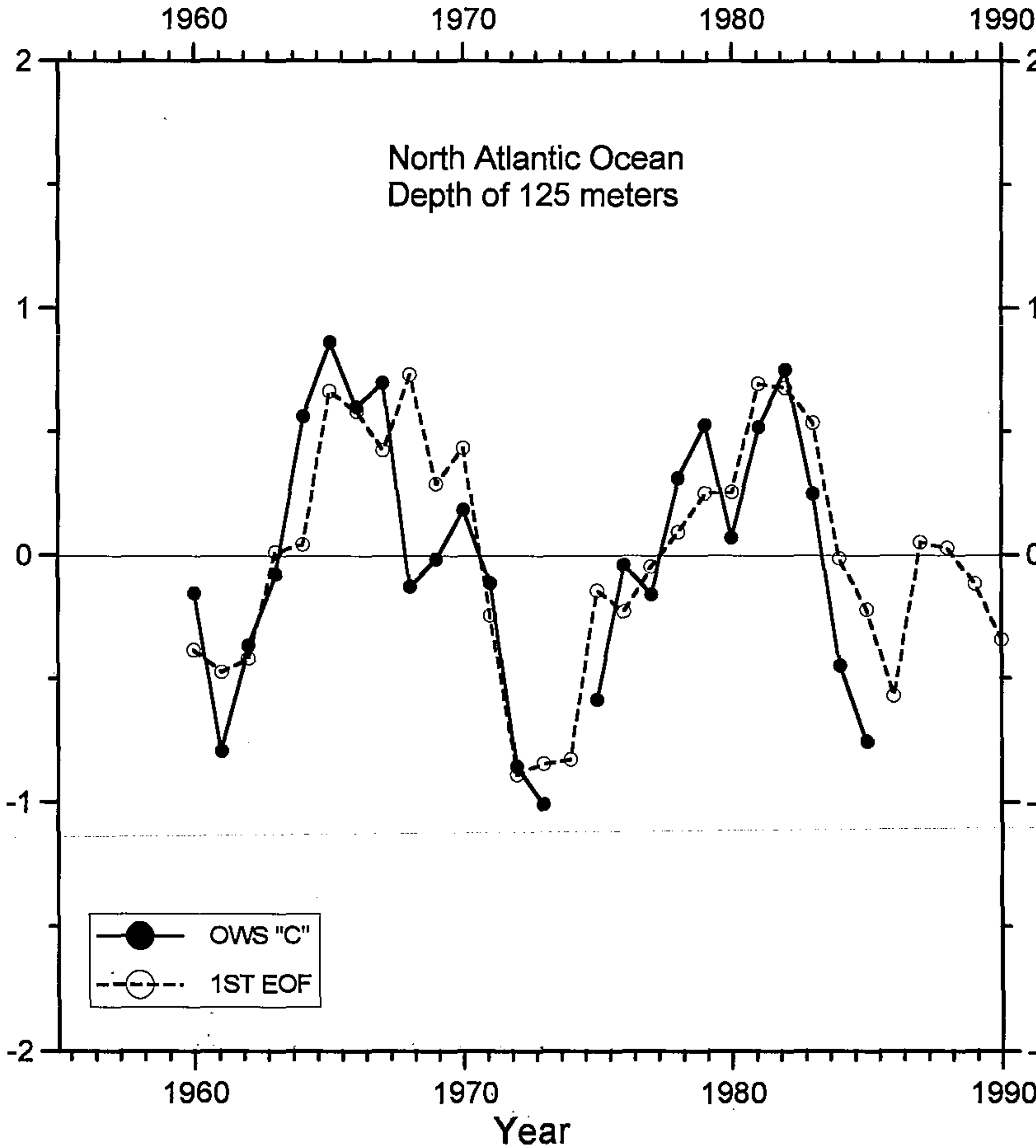


Fig.F19 Time series of 1ST EOF (multiplied by -1) of North Atlantic temperature anomalies and temperature residuals about linear trend for 1960-85 at OWS "C" at 125 m depth

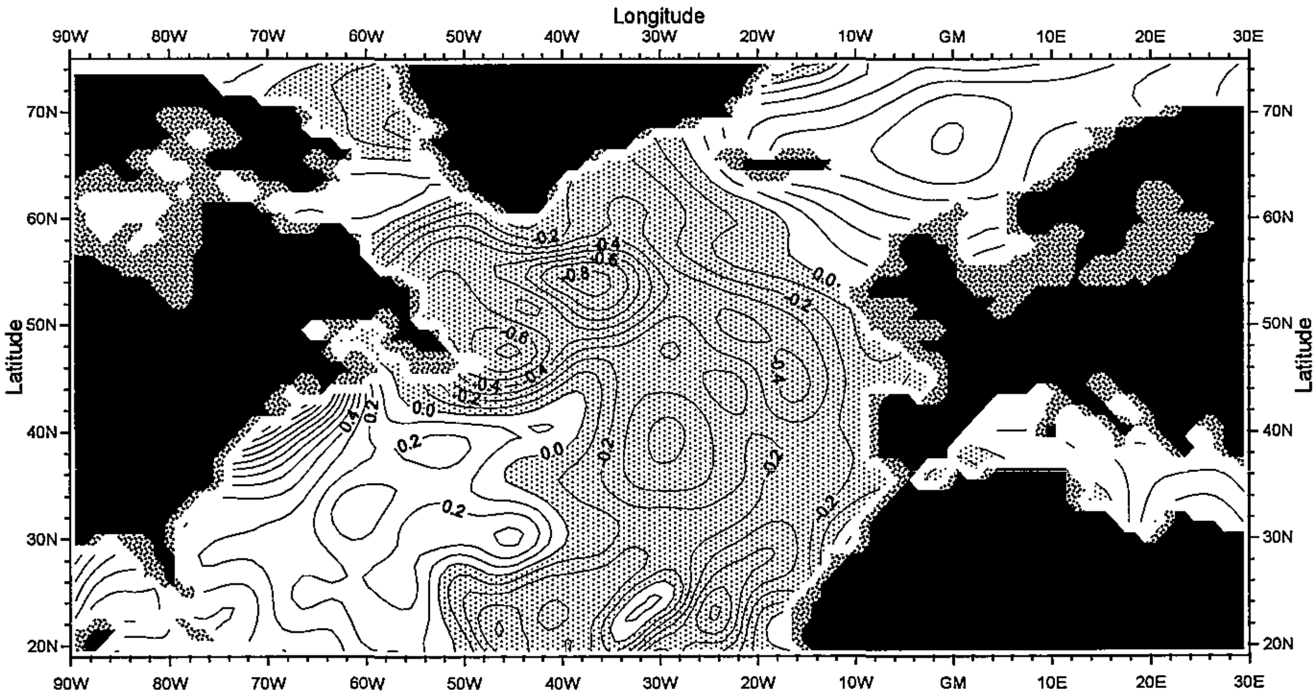


Fig.F20 Temperature anomaly (C) difference field (1972-75 minus 1965-68) at 125 m depth

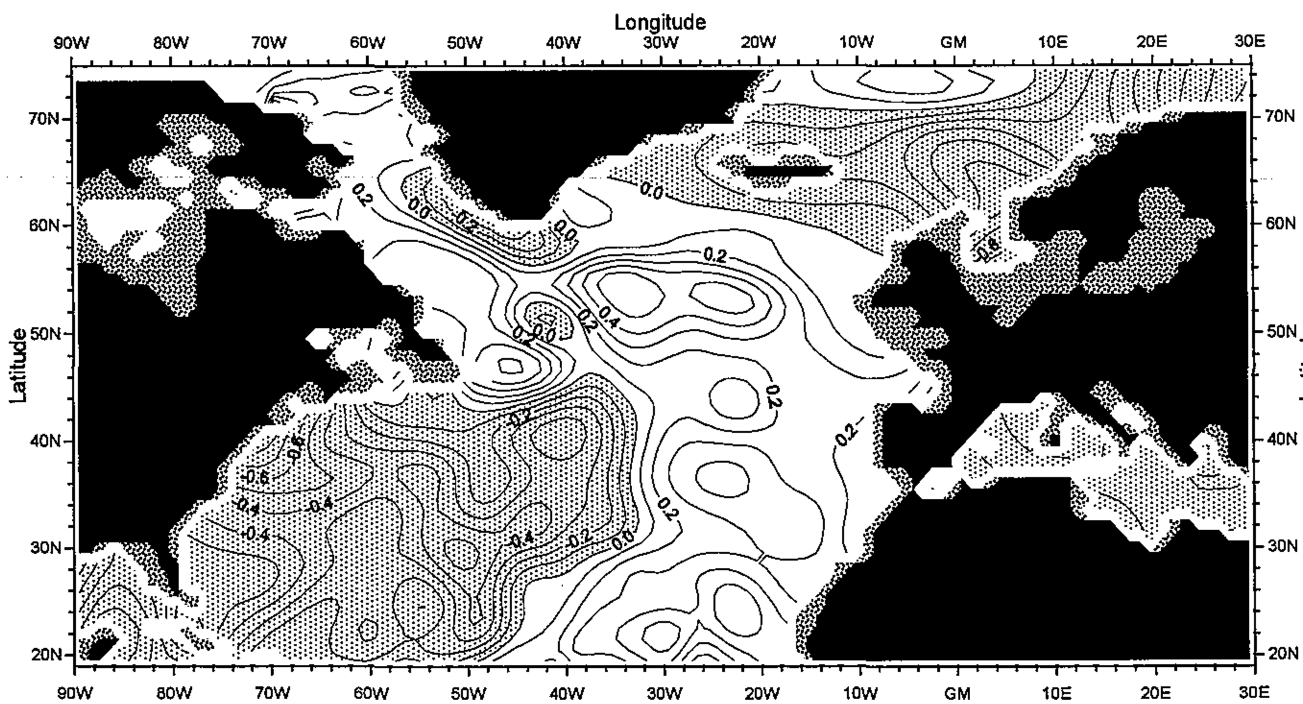


Fig.F21 Temperature anomaly (C) difference field (1979-82 minus 1972-75) at 125 m depth

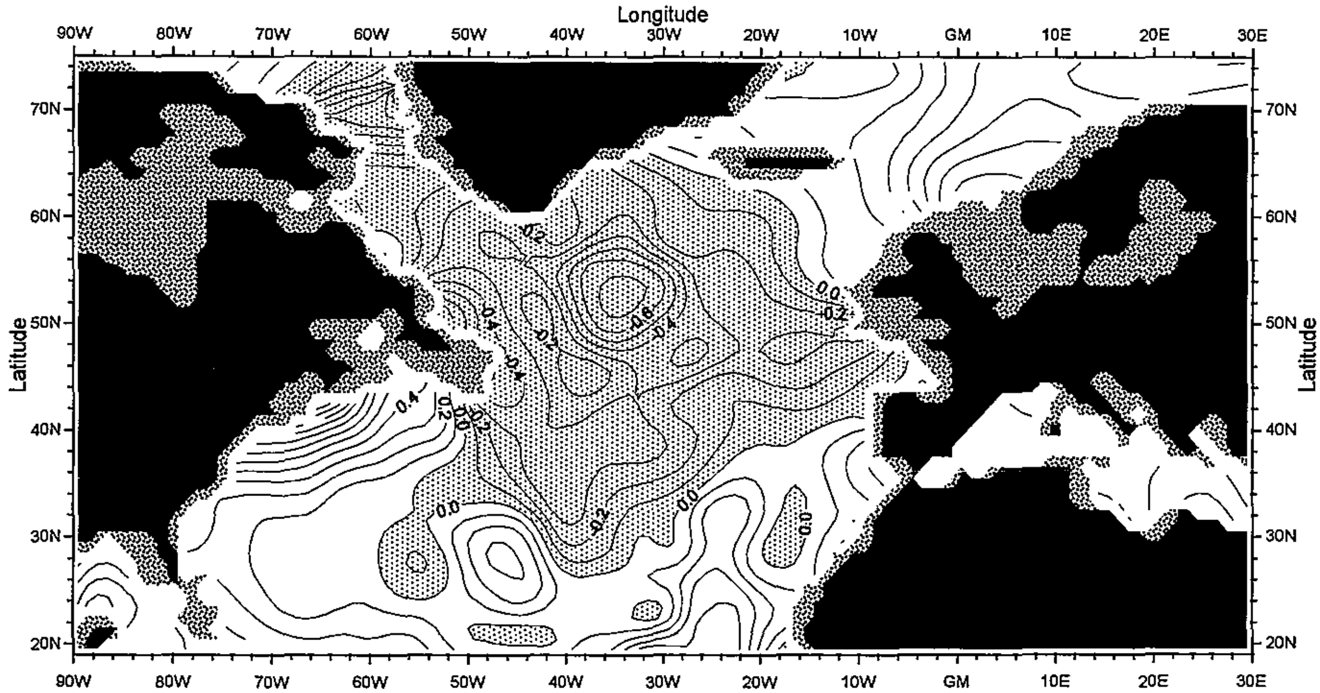


Fig.F22 Temperature anomaly (C) difference field (1972-75 minus 1965-68) at 250 m depth

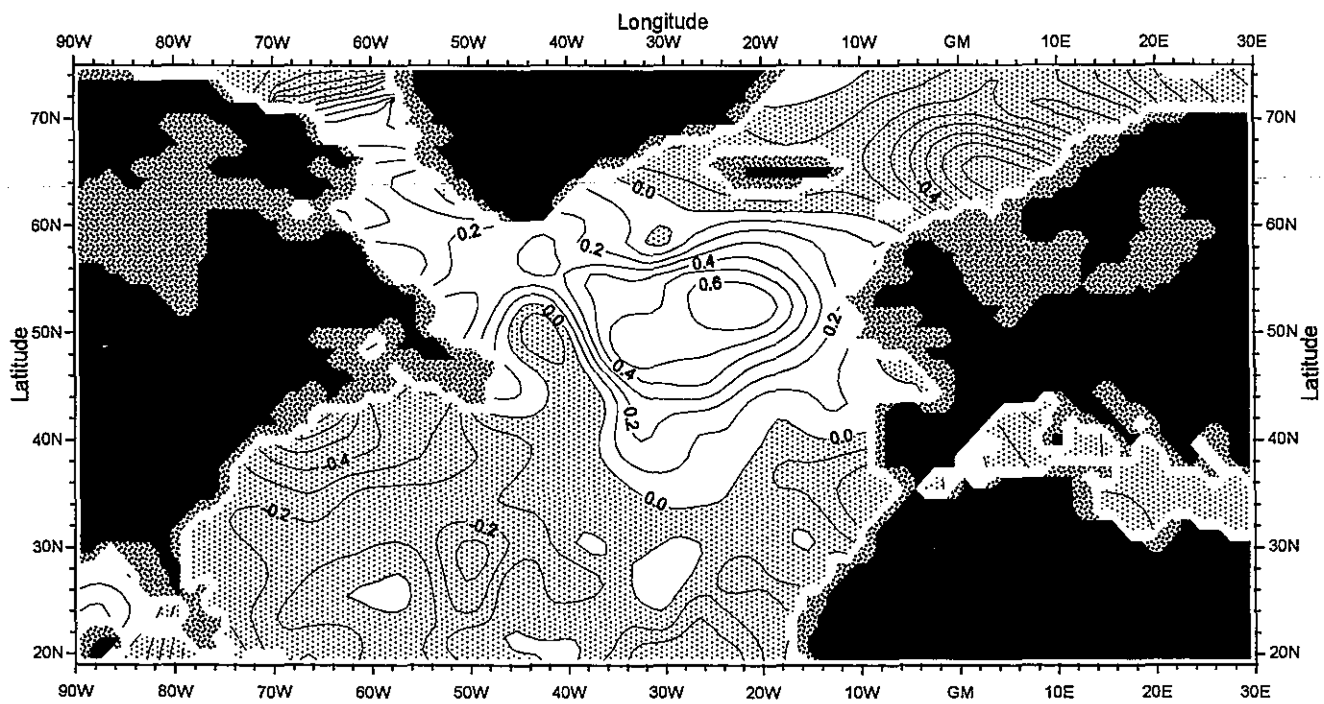


Fig.F23 Temperature anomaly (C) difference field (1979-82 minus 1972-75) at 250 m depth

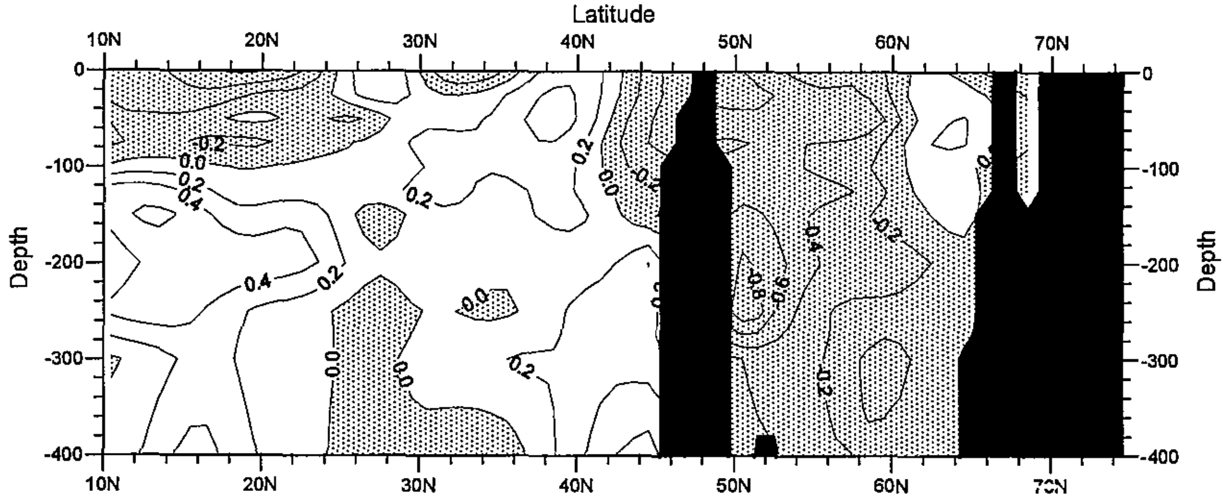


Fig.F24 Temperature anomaly (C) difference field (1972-75 minus 1965-68) at 53.5W

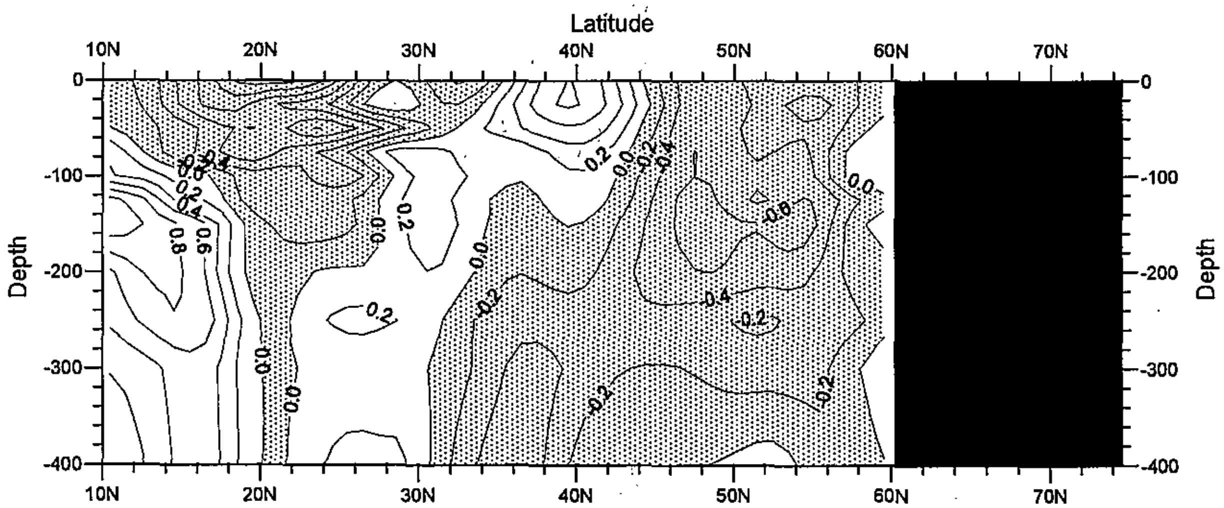


Fig.F25 Temperature anomaly (C) difference field (1972-75 minus 1965-68) at 43.5W

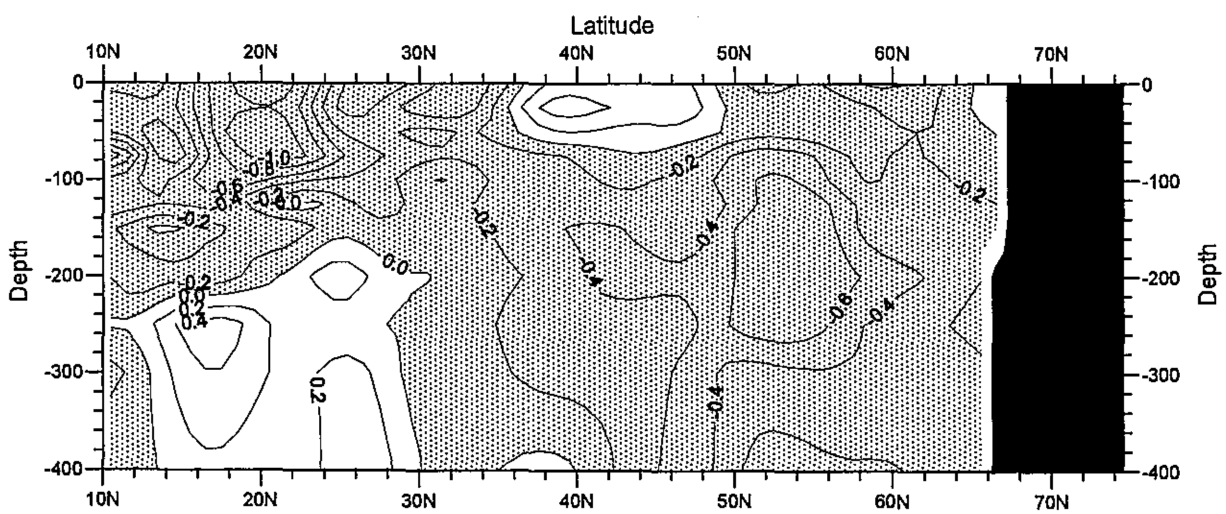


Fig.F26 Temperature anomaly (C) difference field (1972-75 minus 1965-68) at 33.5W

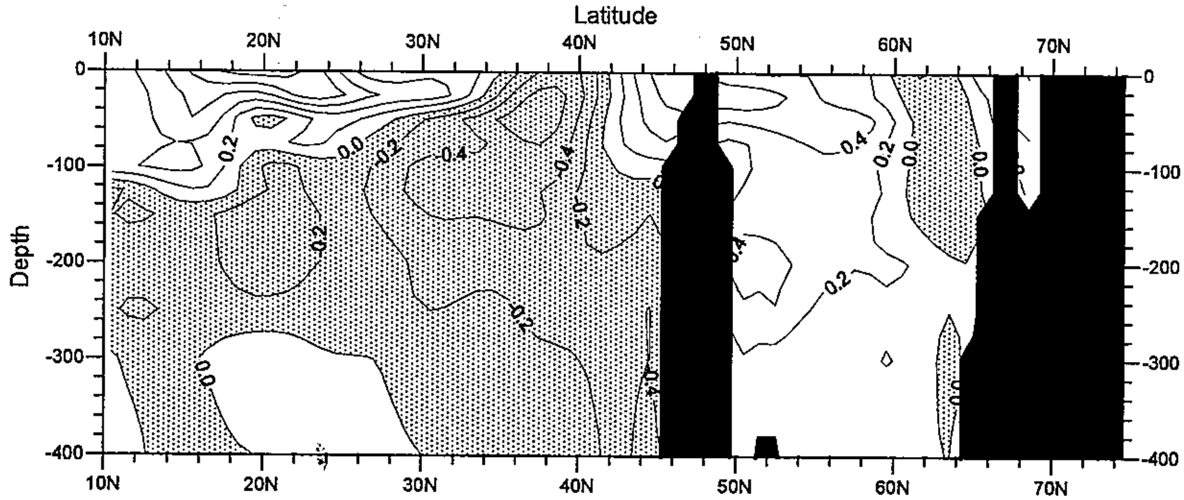


Fig.F27 Temperature anomaly (C) difference field (1979-82 minus 1972-75) at 53.5W

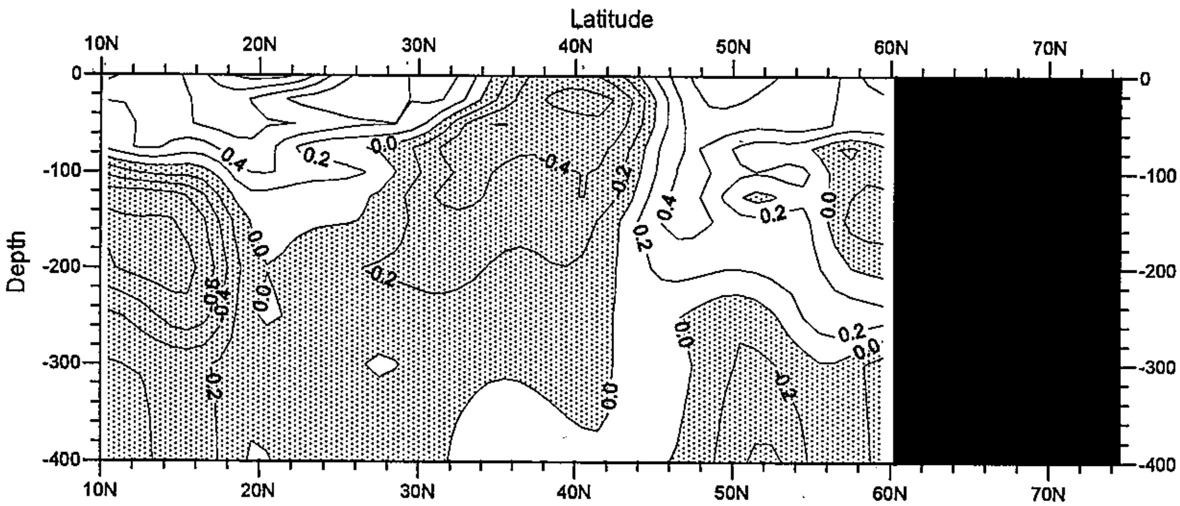


Fig.F28 Temperature anomaly (C) difference field (1979-82 minus 1972-75) at 43.5W

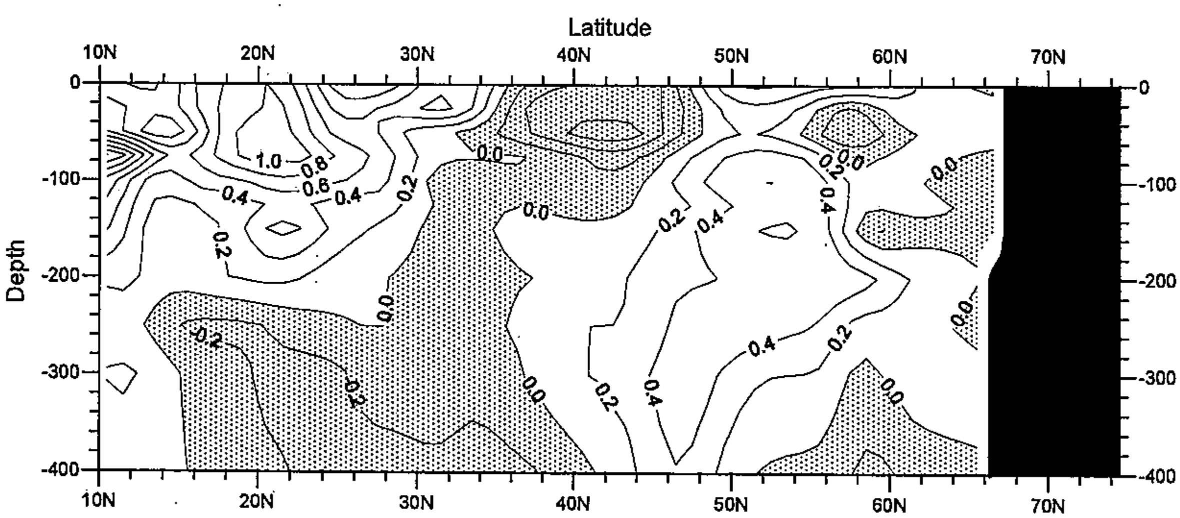


Fig.F29 Temperature anomaly (C) difference field (1979-82 minus 1972-75) at 33.5W

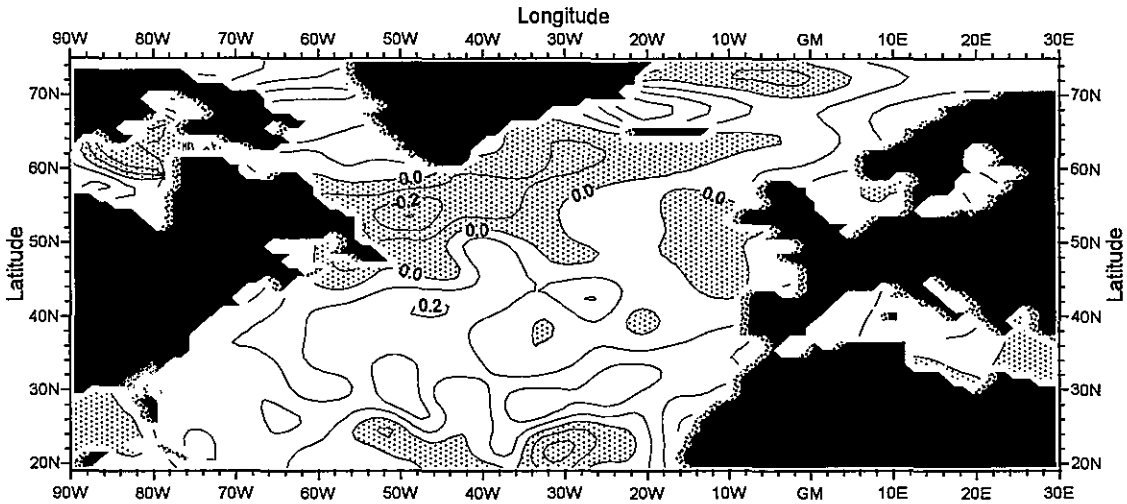


Fig.G1 Temperature anomaly trend (C/10 YR) for 1966-1990 period at the surface

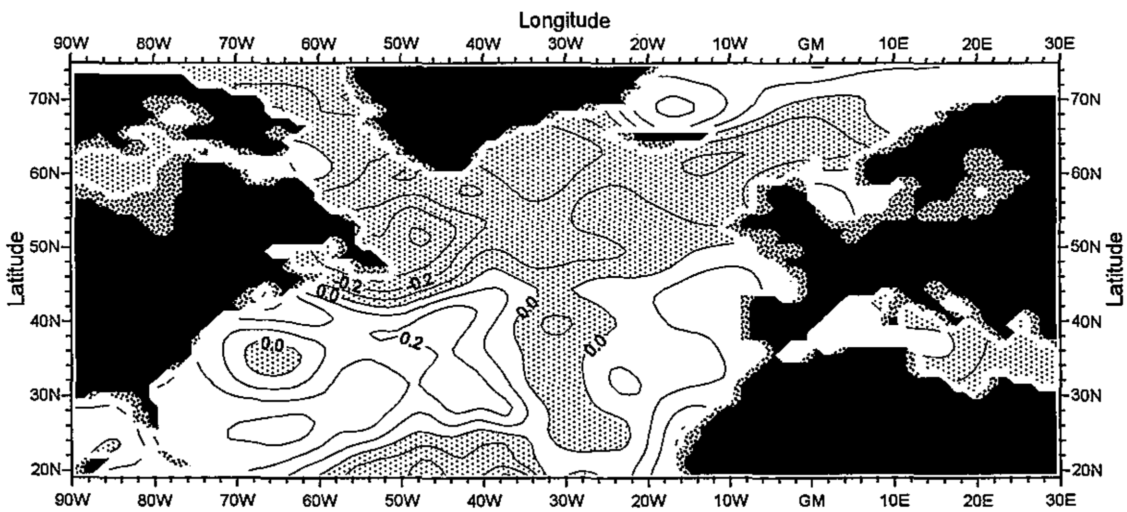


Fig.G2 Temperature anomaly trend (C/10 YR) for 1966-1990 period at 75 m depth

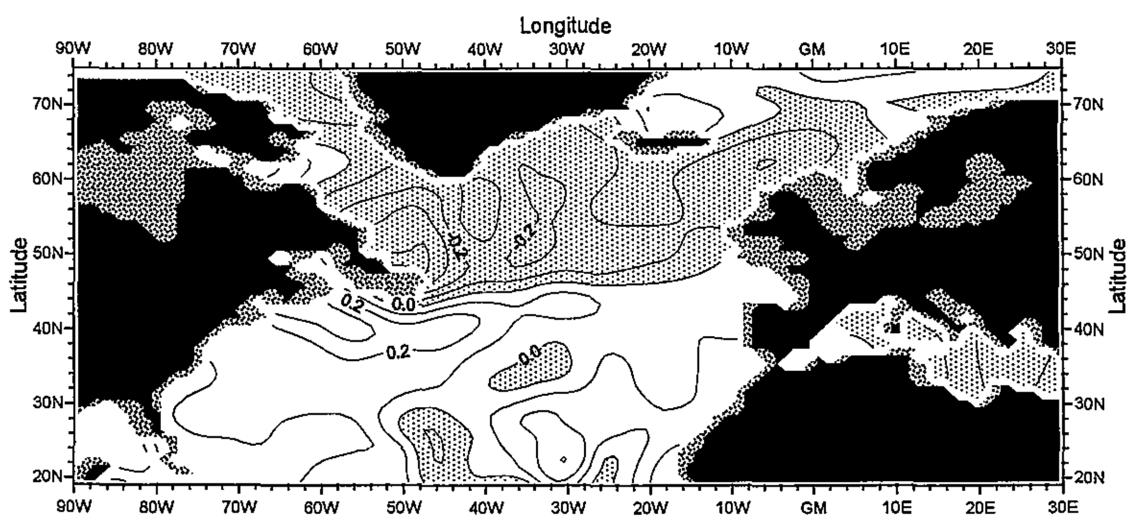


Fig.G3 Temperature anomaly trend (C/10 YR) for 1966-1990 period at 150 m depth

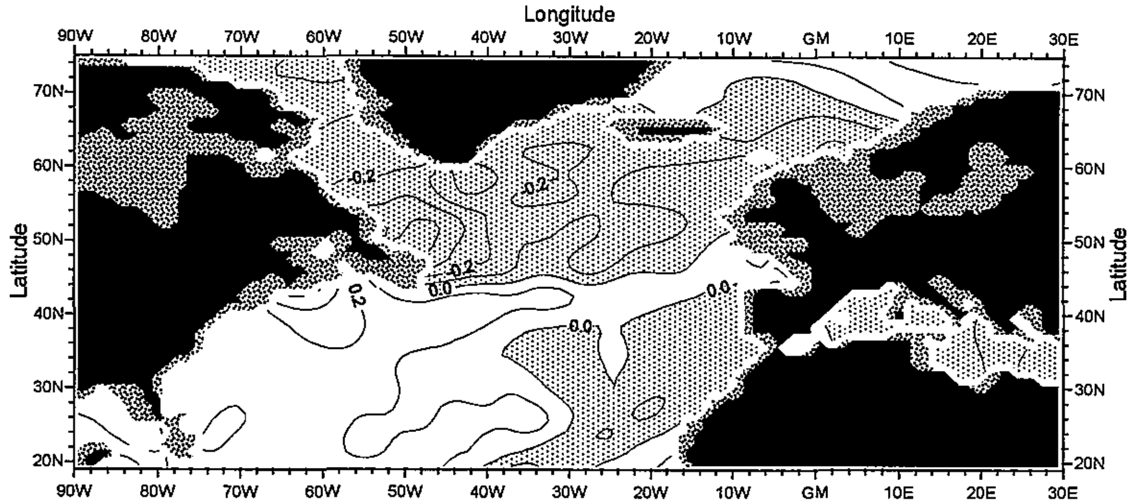


Fig.G4 Temperature anomaly trend (C/10 YR) for 1966-1990 period at 250 m depth

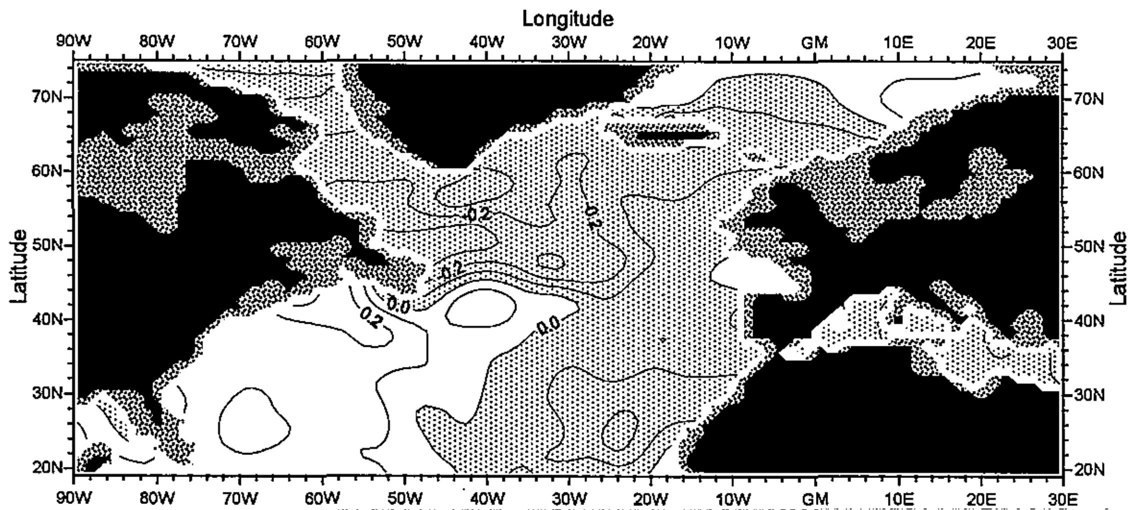


Fig.G5 Temperature anomaly trend (C/10 YR) for 1966-1990 period at 300 m depth

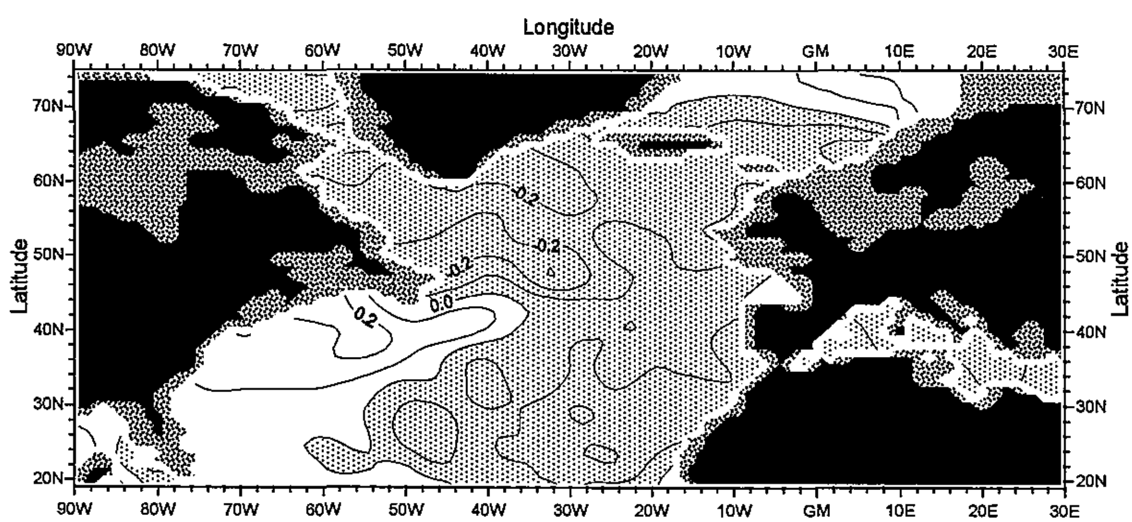


Fig.G6 Temperature anomaly trend (C/10 YR) for 1966-1990 period at 400 m depth

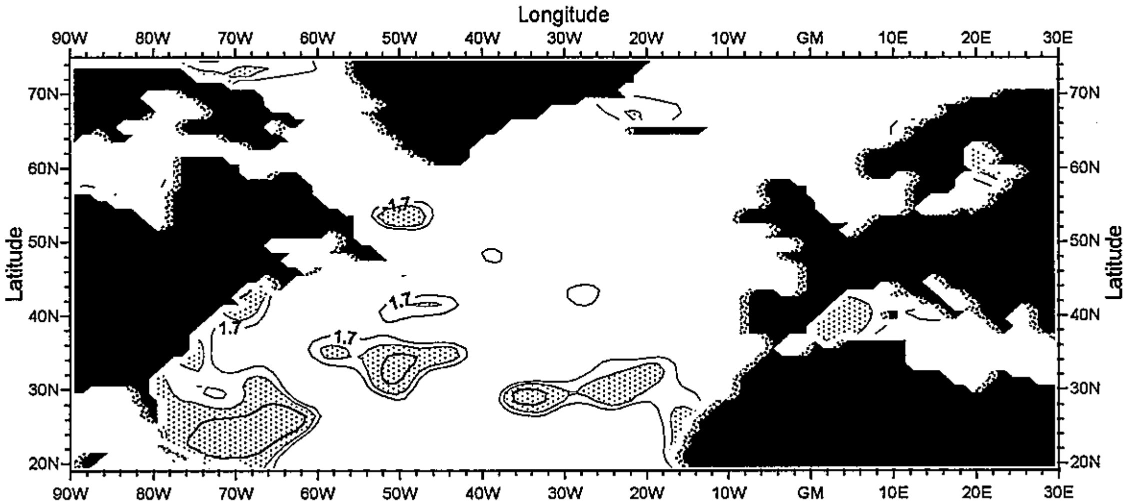


Fig.G7 Trend significance at 10%, 5%, and 1% levels (t-test) at the surface

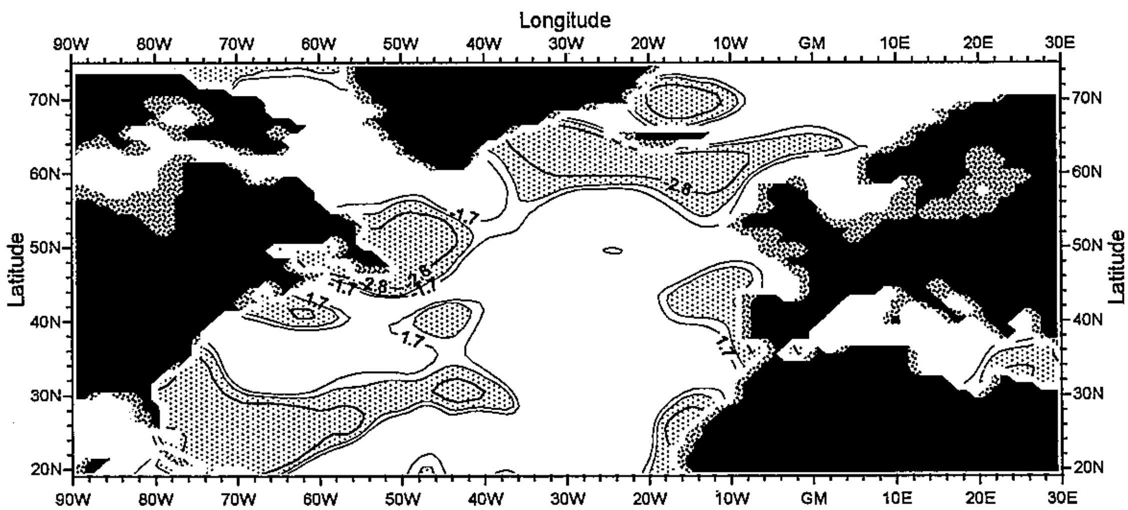


Fig.G8 Trend significance at 10%, 5%, and 1% levels (t-test) at 75 m depth

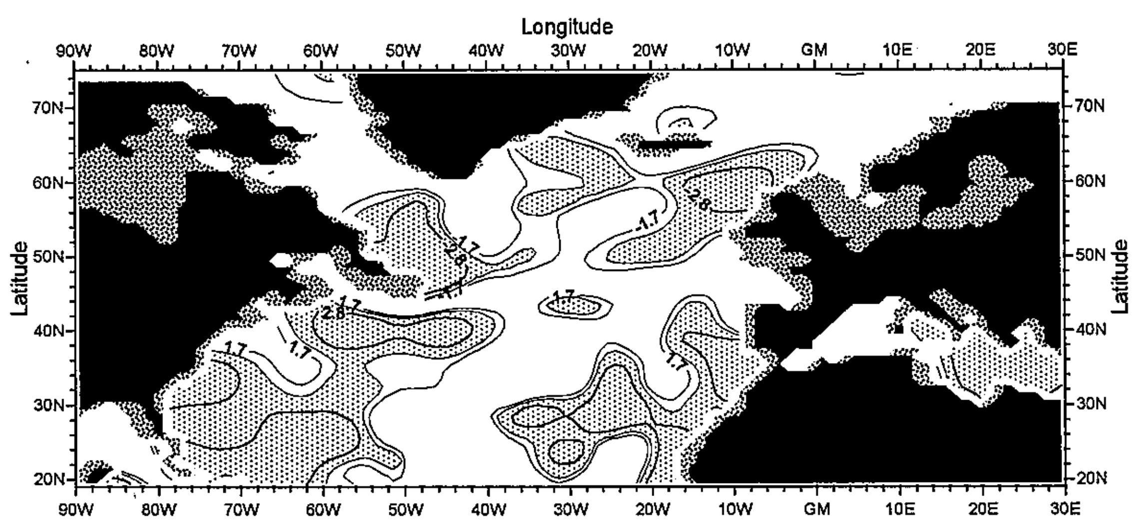


Fig.G9 Trend significance at 10%, 5%, and 1% levels (t-test) at 150 m depth

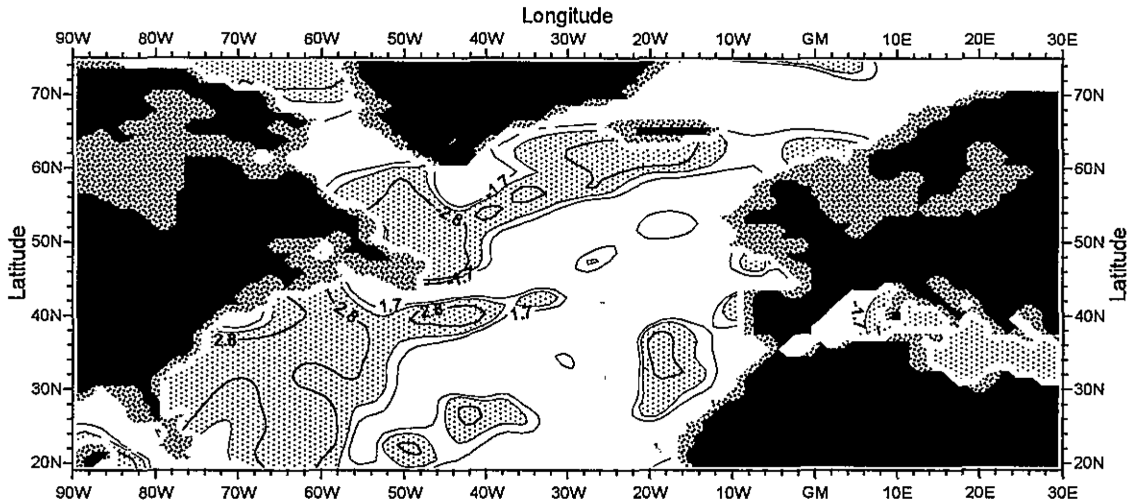


Fig.G10 Trend significance at 10%, 5%, and 1% levels (t-test) at 250 m depth

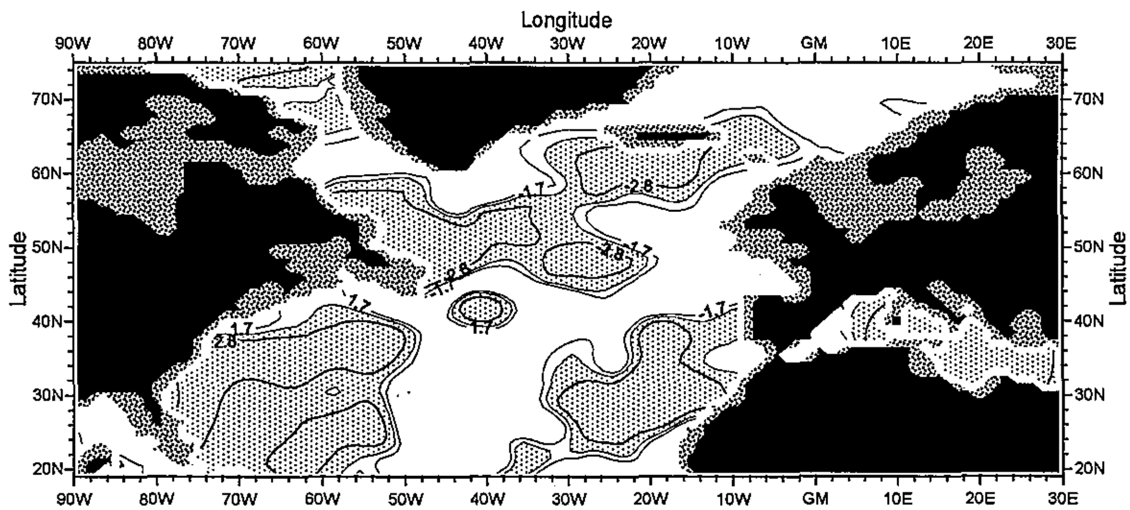


Fig.G11 Trend significance at 10%, 5%, and 1% levels (t-test) at 300 m depth

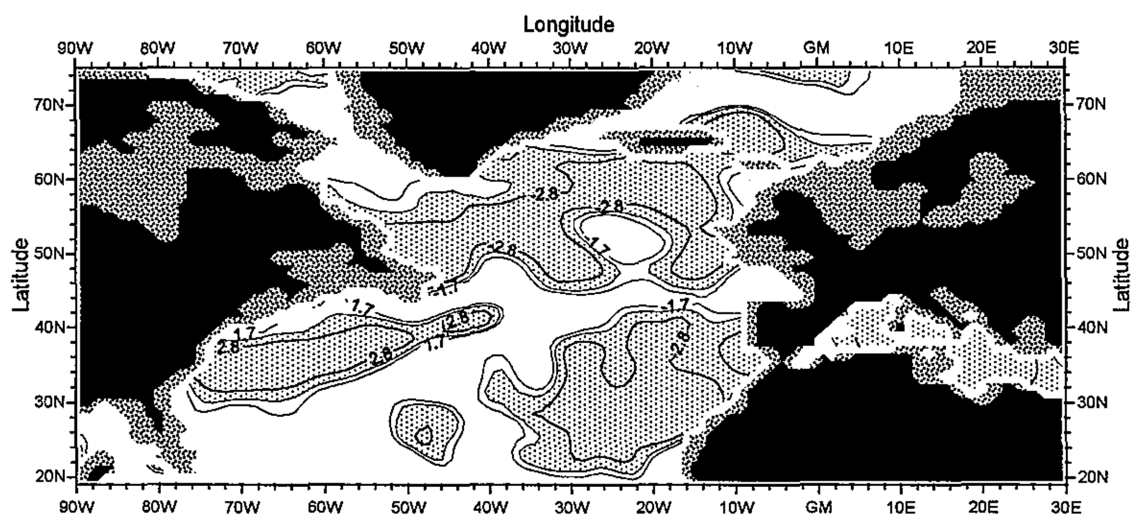


Fig.G12 Trend significance at 10%, 5%, and 1% levels (t-test) at 400 m depth

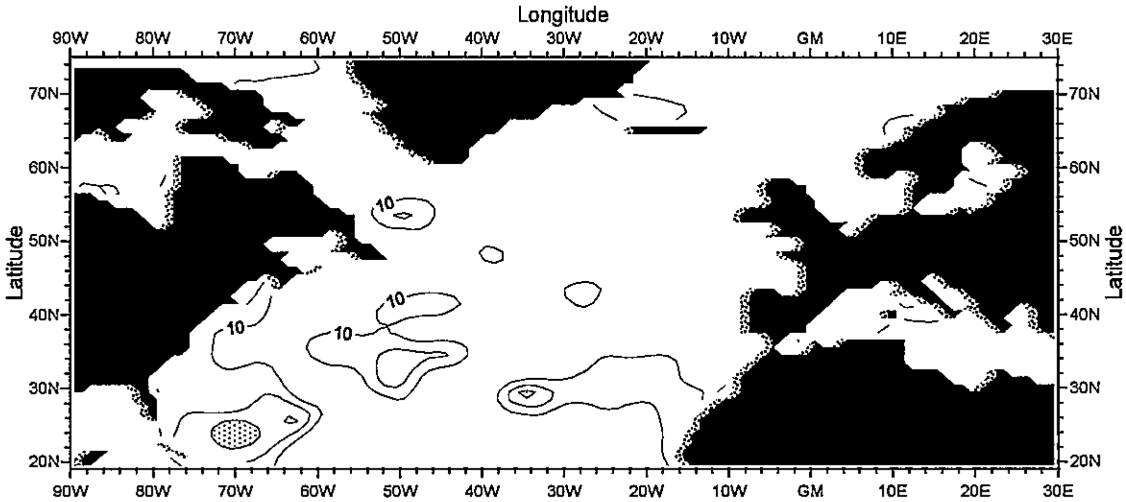


Fig.G13 Percent of variance explained by linear trend for 1966-90 period at the surface

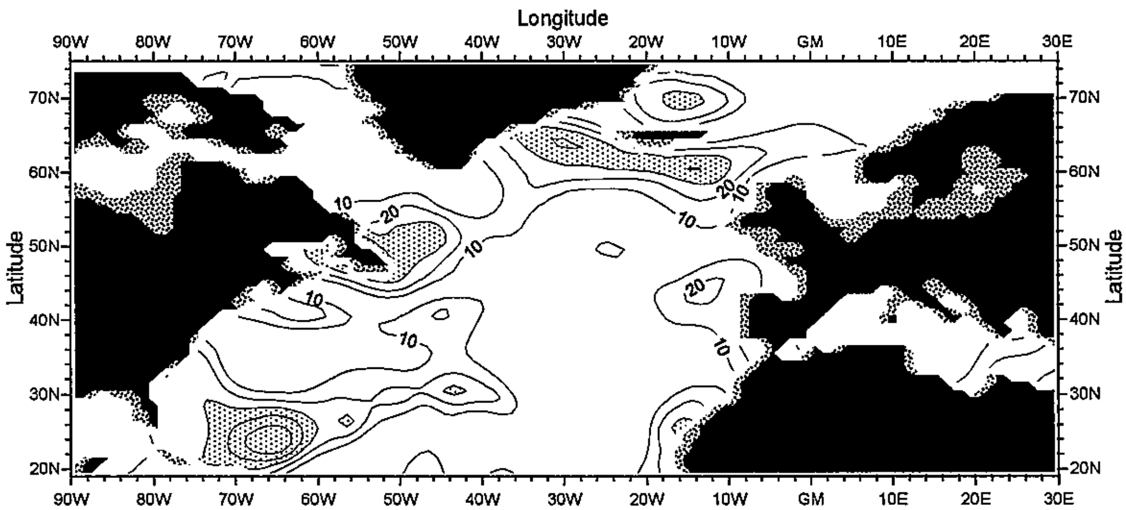


Fig.G14 Percent of variance explained by linear trend for 1966-90 period at 75 m depth

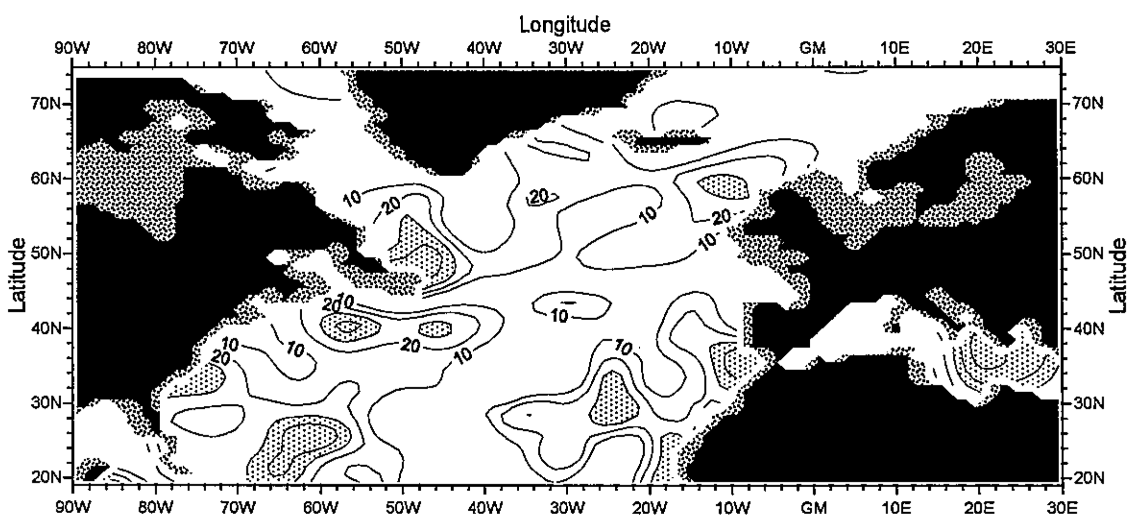


Fig.G15 Percent of variance explained by linear trend for 1966-90 period at 150 m depth

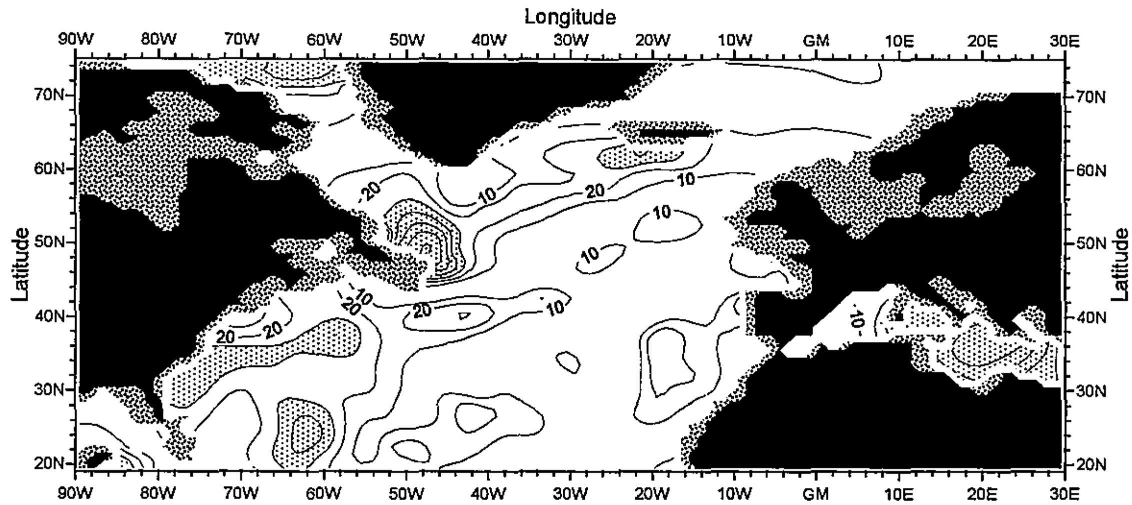


Fig.G16 Percent of variance explained by linear trend for 1966-90 period at 250 m depth

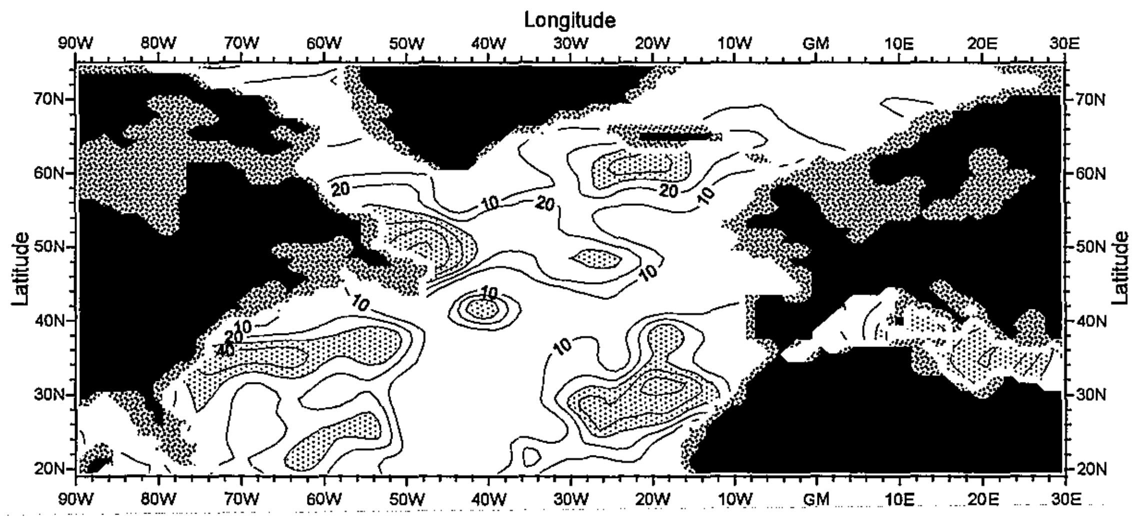


Fig.G17 Percent of variance explained by linear trend for 1966-90 period at 300 m depth

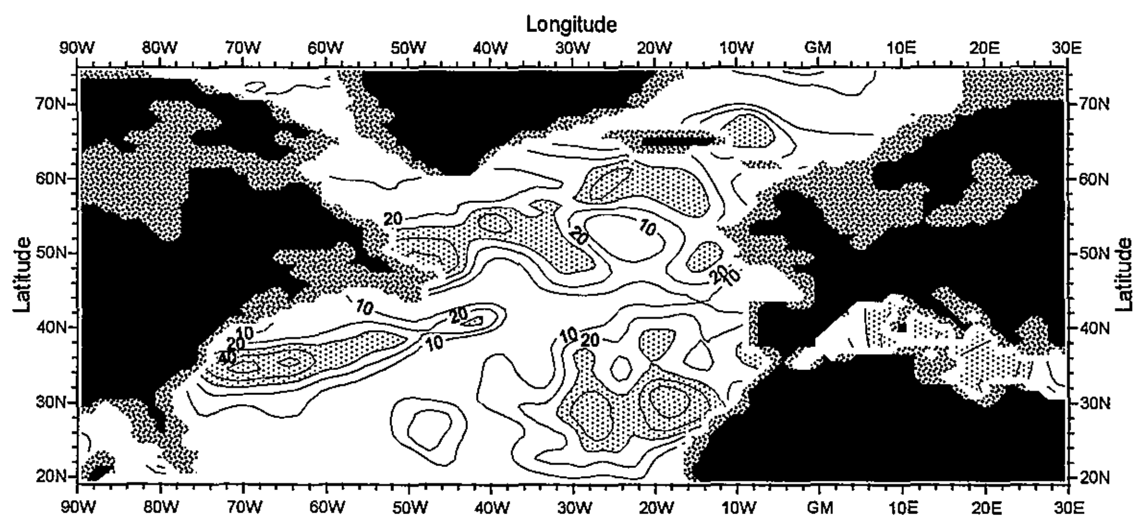


Fig.G18 Percent of variance explained by linear trend for 1966-90 period at 400 m depth

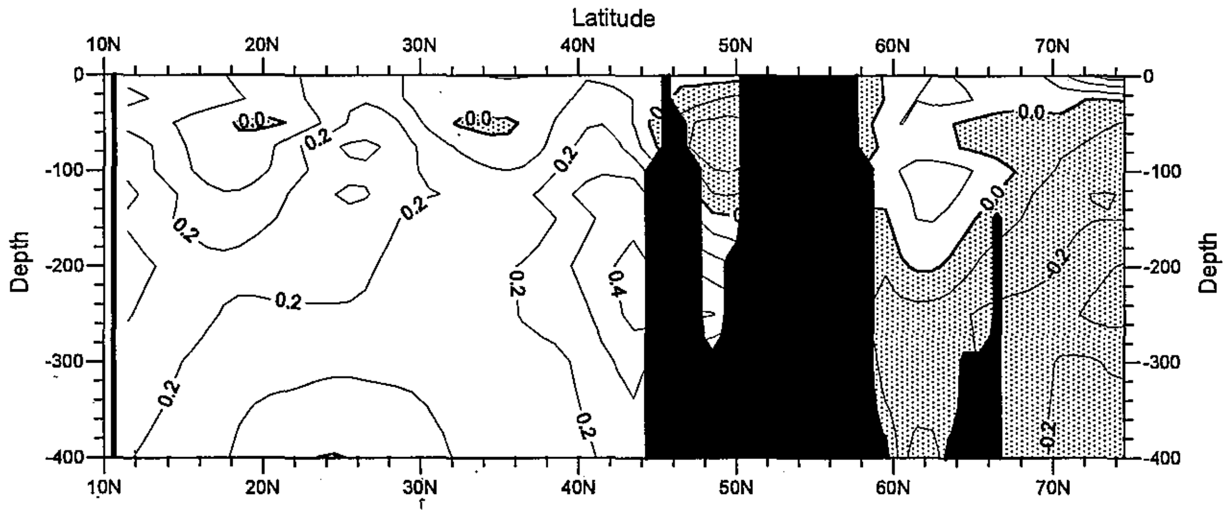


Fig.G19 Temperature anomaly trend (C/10 YR) for 1966-1990 period at 61.5W

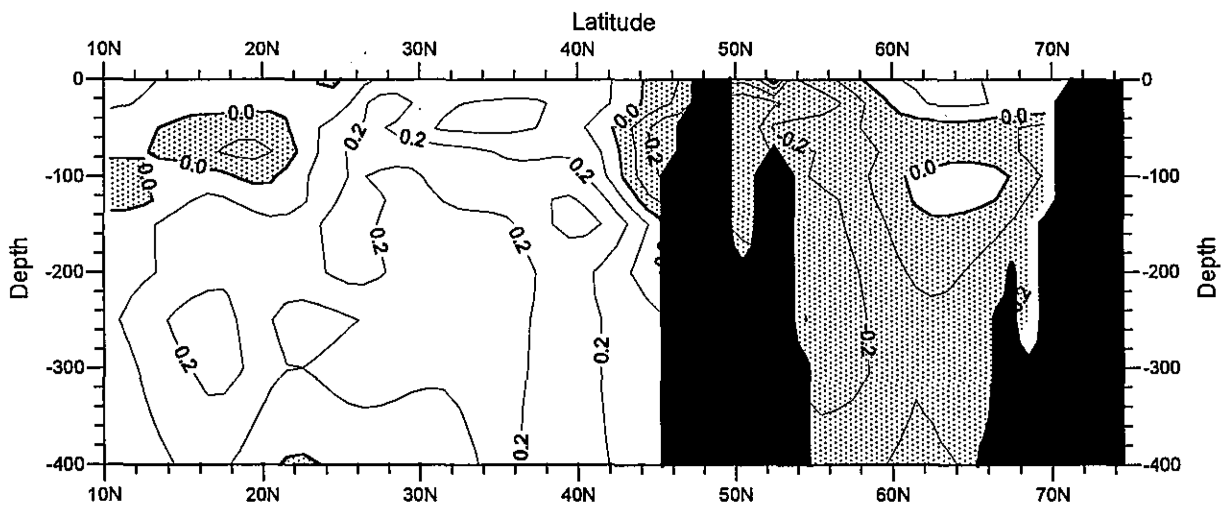


Fig.G20 Temperature anomaly trend (C/10 YR) for 1966-1990 period at 55.5W

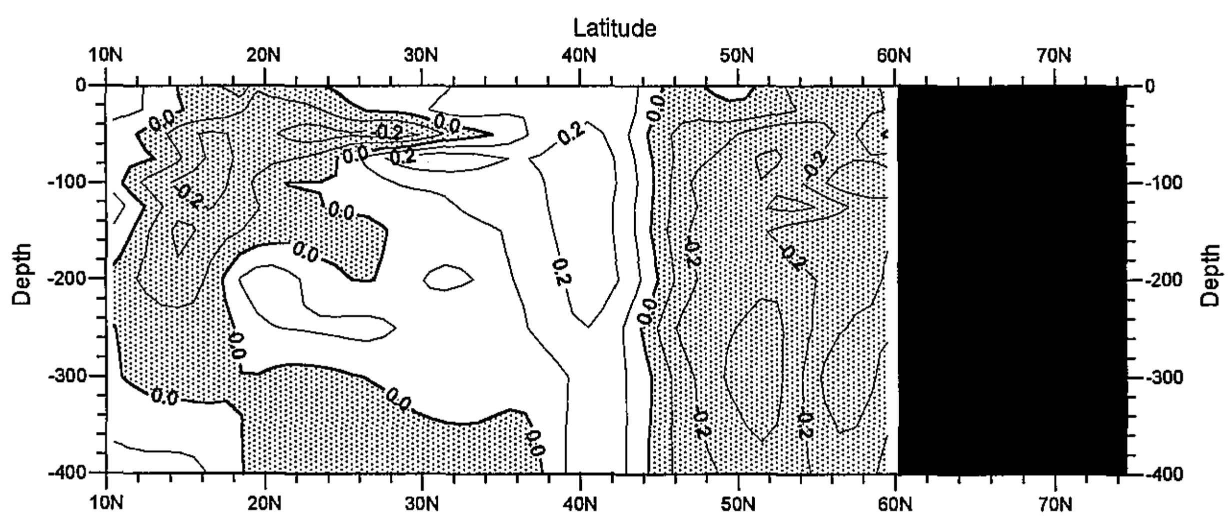


Fig.G21 Temperature anomaly trend (C/10 YR) for 1966-1990 period at 43.5W

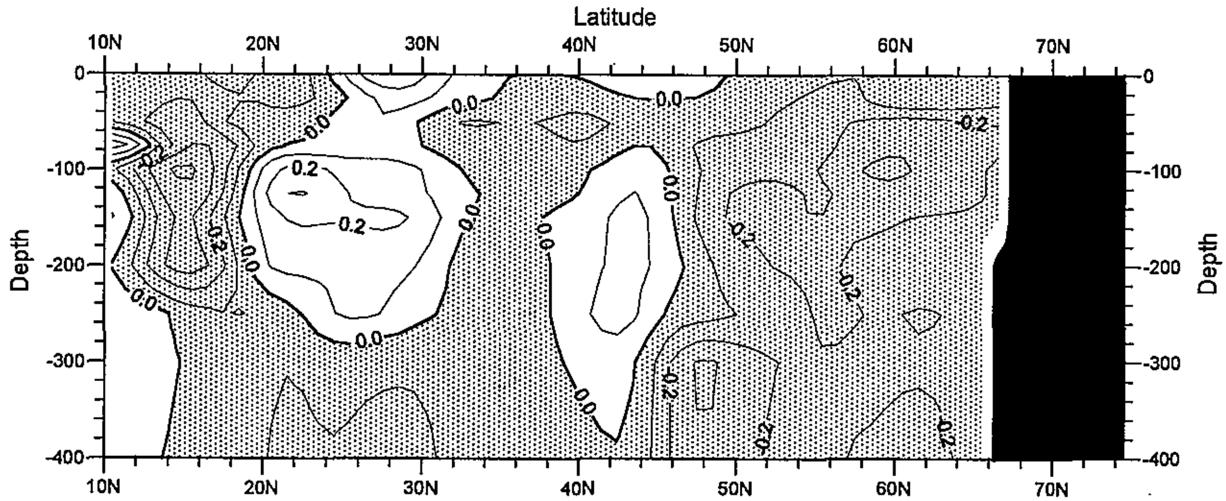


Fig.G22 Temperature anomaly trend (C/10 YR) for 1966-1990 period at 33.5W

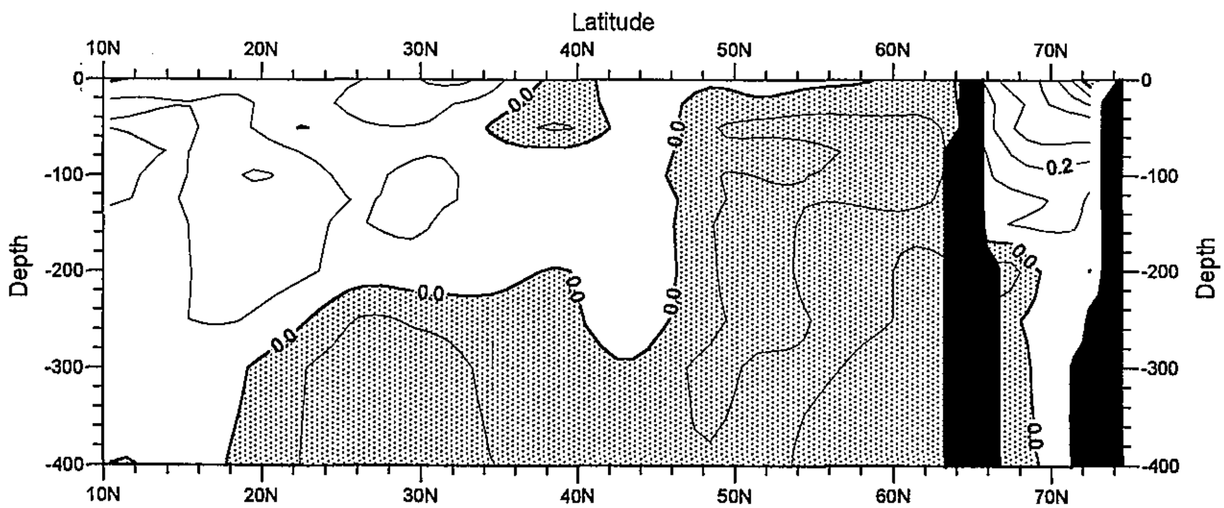


Fig.G23 Temperature anomaly trend (C/10 YR) for 1966-1990 period at 20.5W

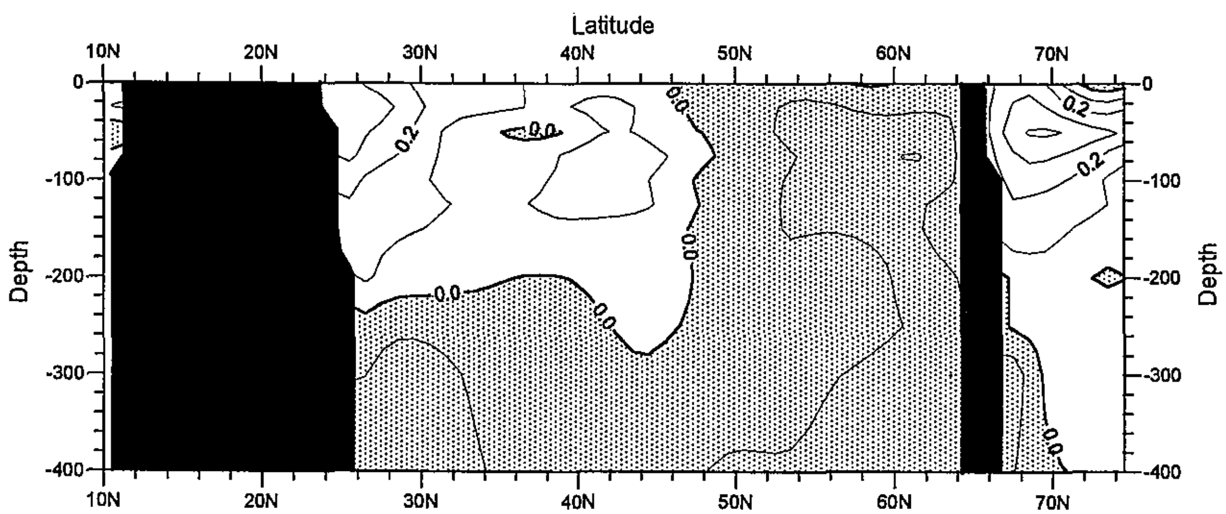


Fig.G24 Temperature anomaly trend (C/10 YR) for 1966-1990 period at 15.5W

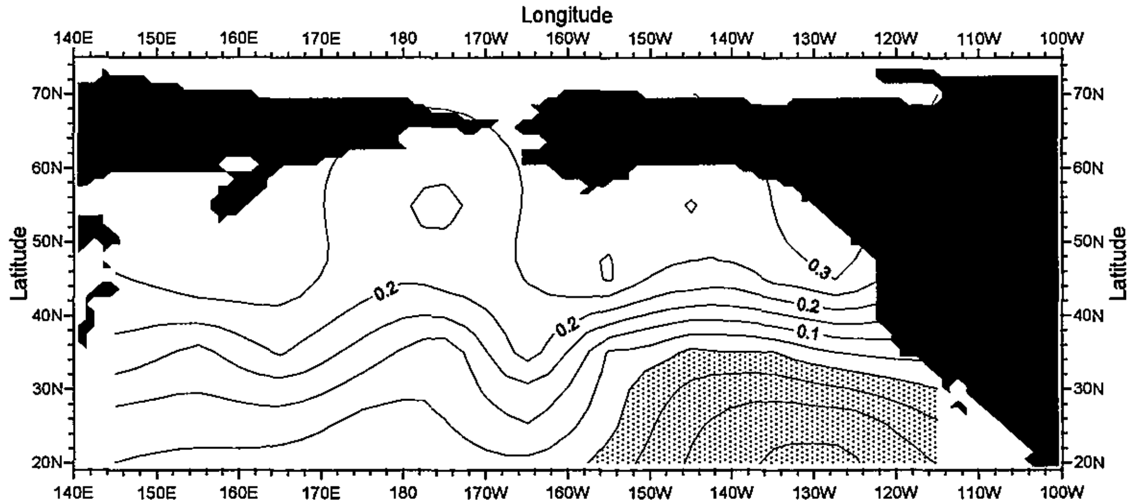


Fig.H1 1ST EOF of North Pacific temperature anomalies for 1960-90 period at the surface

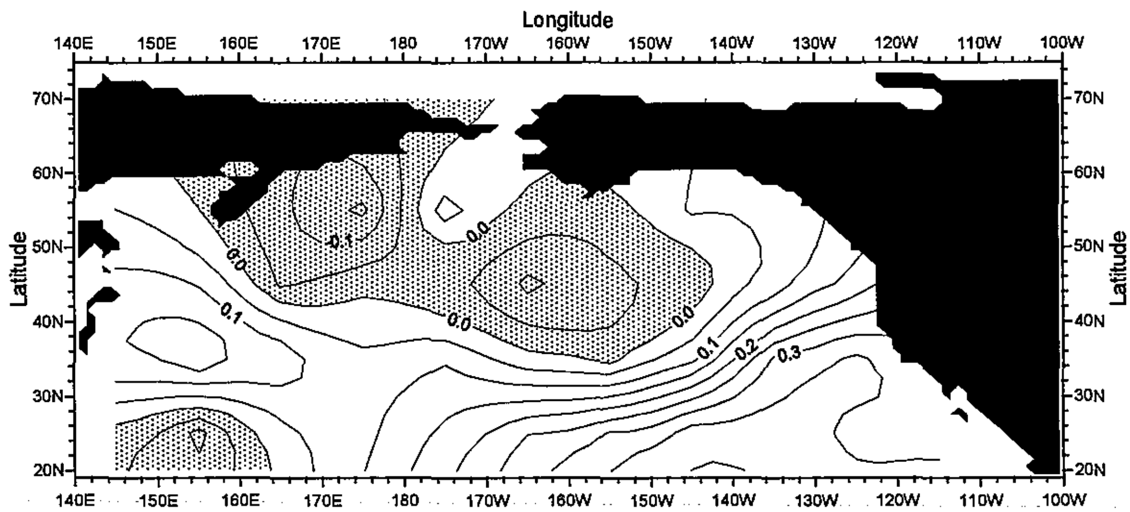


Fig.H2 2ND EOF of North Pacific temperature anomalies for 1960-90 period at the surface

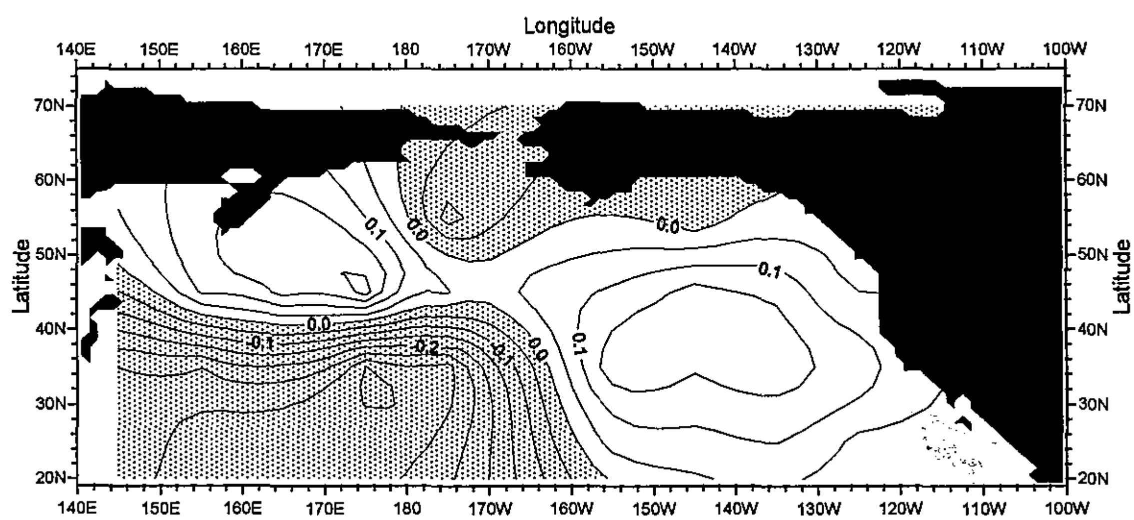


Fig.H3 3RD EOF of North Pacific temperature anomalies for 1960-90 period at the surface

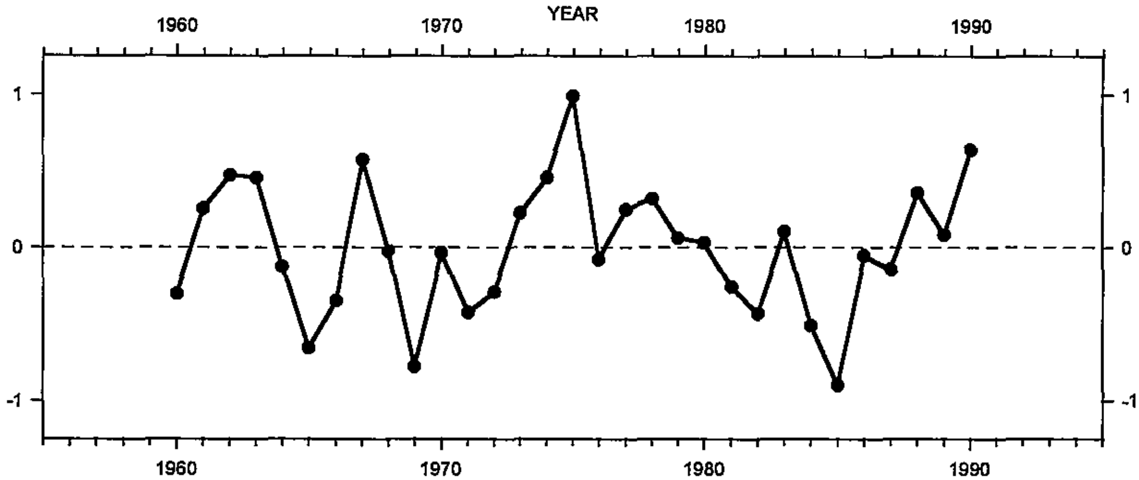


Fig.H4 1ST EOF time series of North Pacific temperature anomalies at the surface (18.8%)

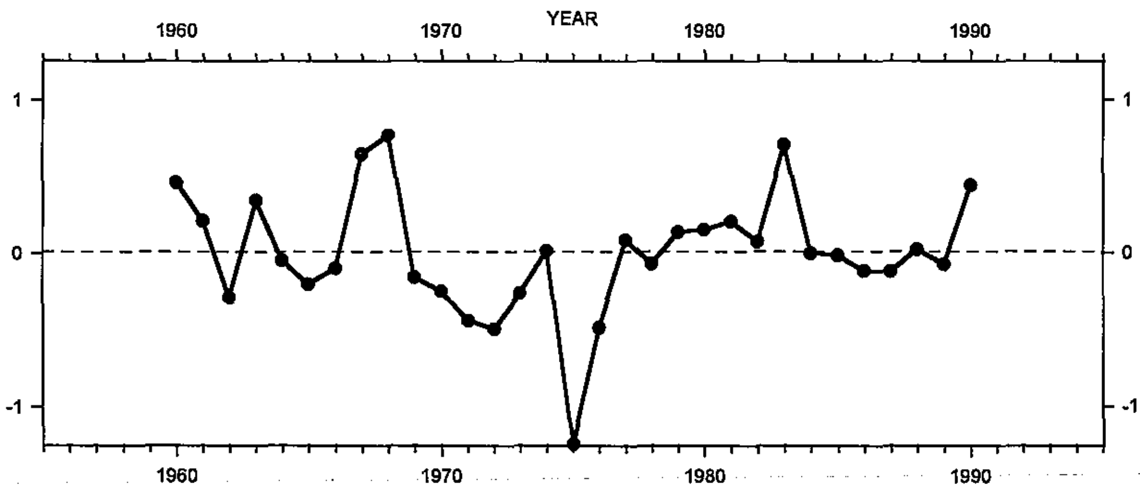


Fig.H5 2ND EOF time series of North Pacific temperature anomalies at the surface (15.8%)

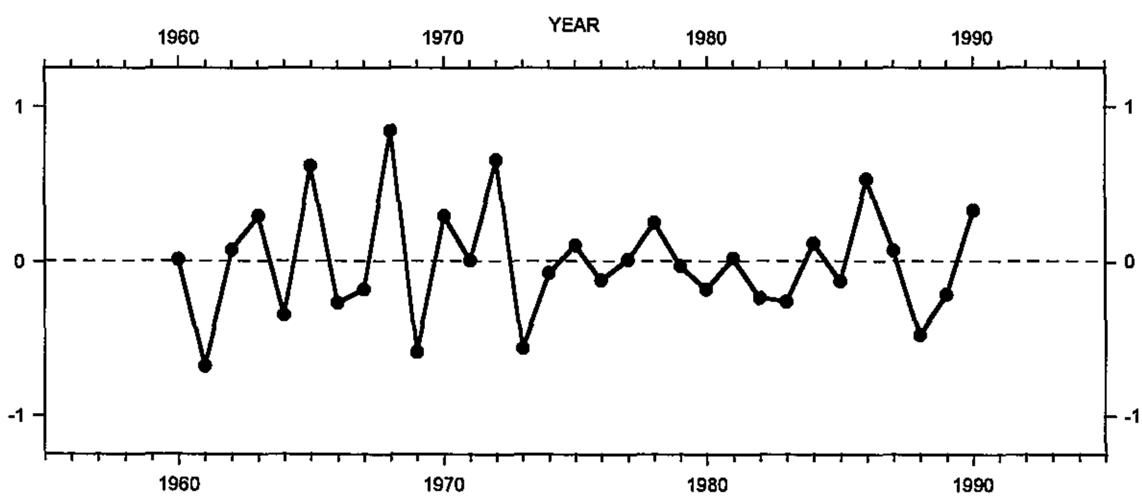


Fig.H6 3RD EOF time series of North Pacific temperature anomalies at the surface (13.2%)

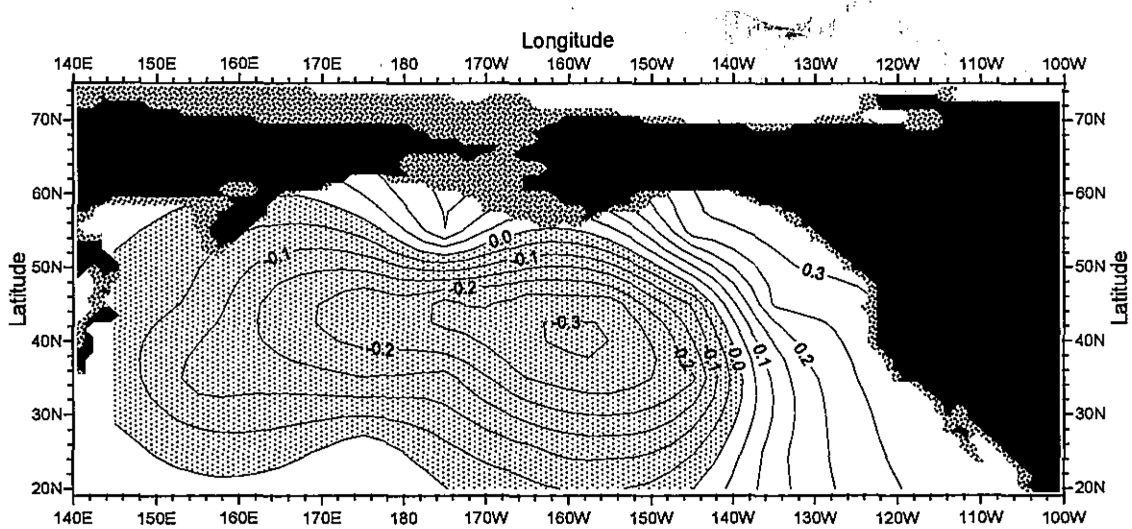


Fig.H7 1ST EOF of North Pacific temperature anomalies for 1960-90 period at 125 m depth

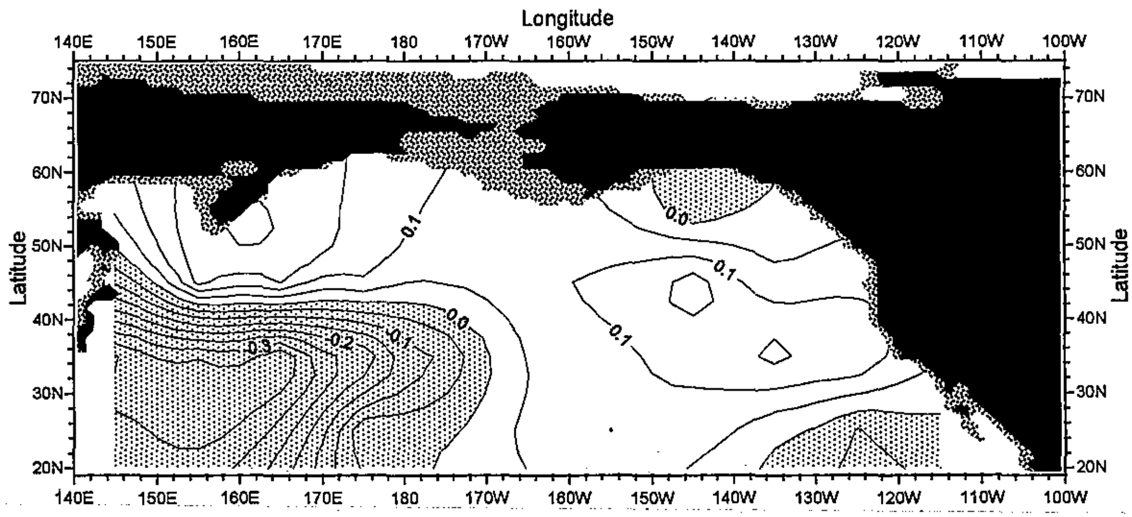


Fig.H8 2ND EOF of North Pacific temperature anomalies for 1960-90 period at 125 m depth

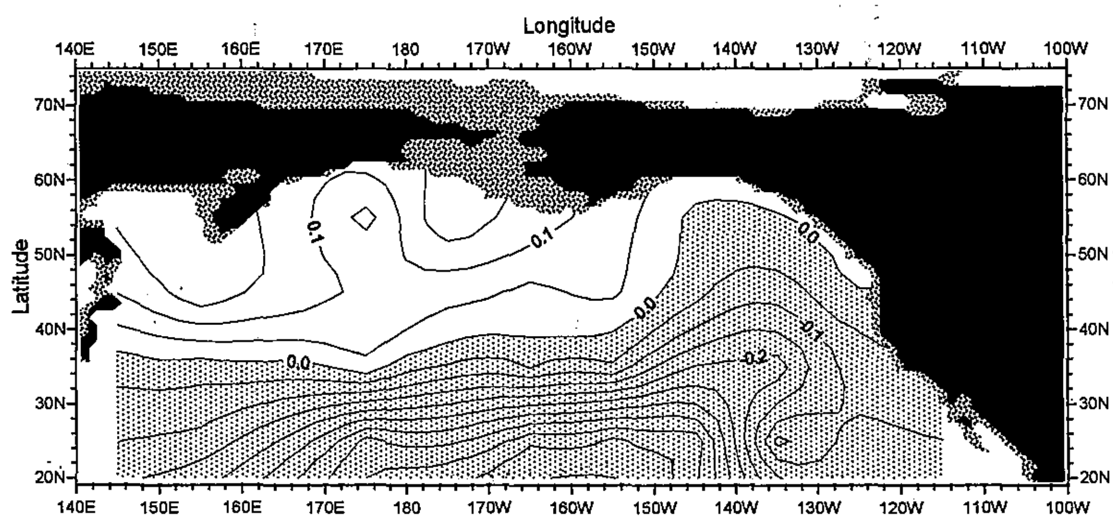


Fig.H9 3RD EOF of North Pacific temperature anomalies for 1960-90 period at 125 m depth

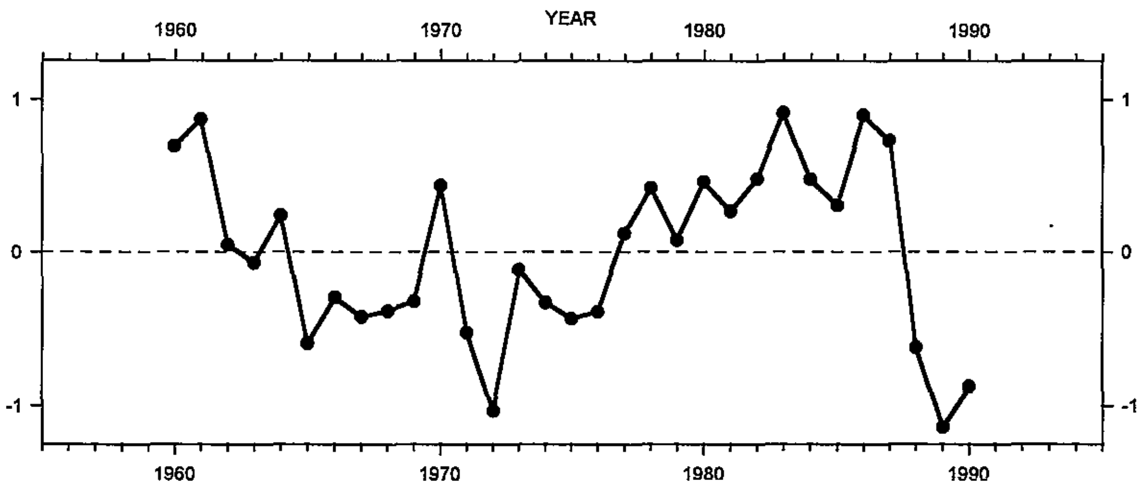

Fig.H10 1ST EOF time series of North Pacific temperature anomalies at 125 m depth (32.7%)

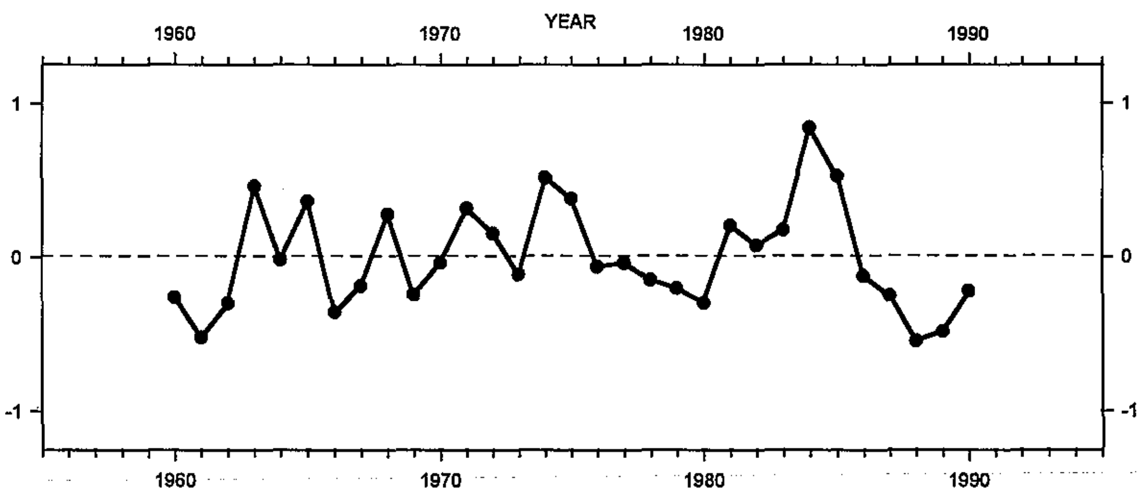

Fig.H11 2ND EOF time series of North Pacific temperature anomalies at 125 m depth (11.8%)

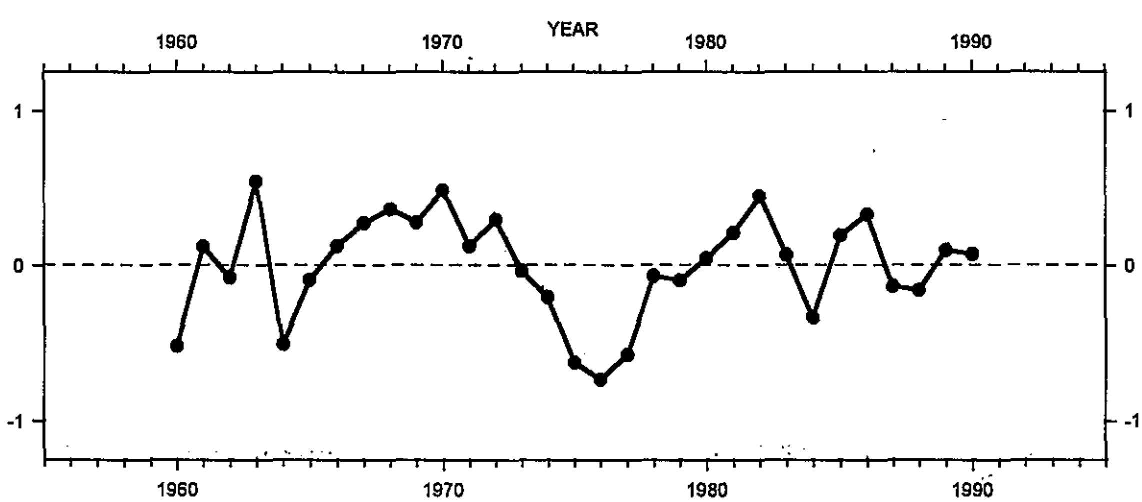

Fig.H12 3RD EOF time series of North Pacific temperature anomalies at 125 m depth (11.2%)

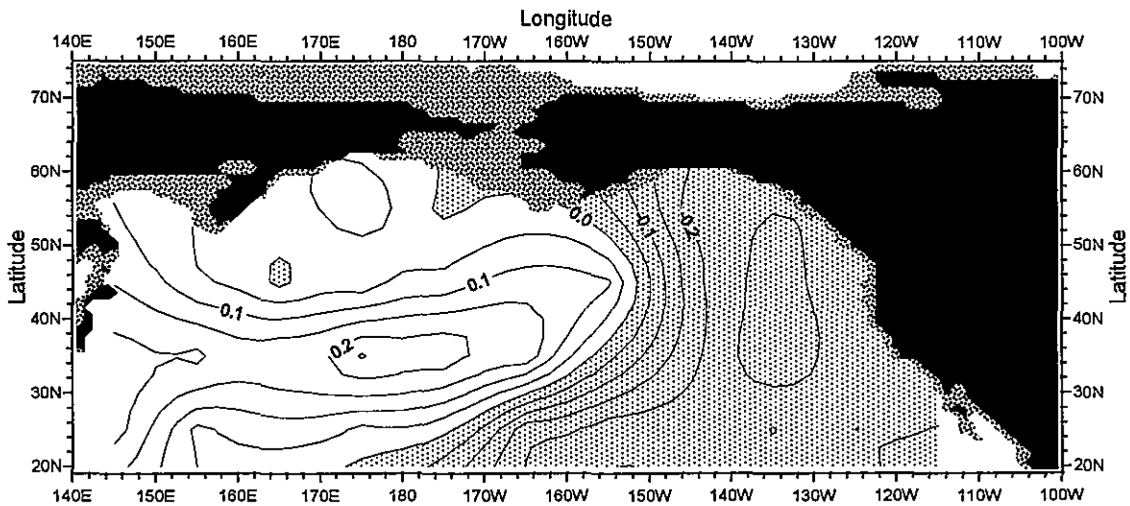


Fig.H13 1ST EOF of North Pacific temperature anomalies for 1960-90 period at 250 m depth

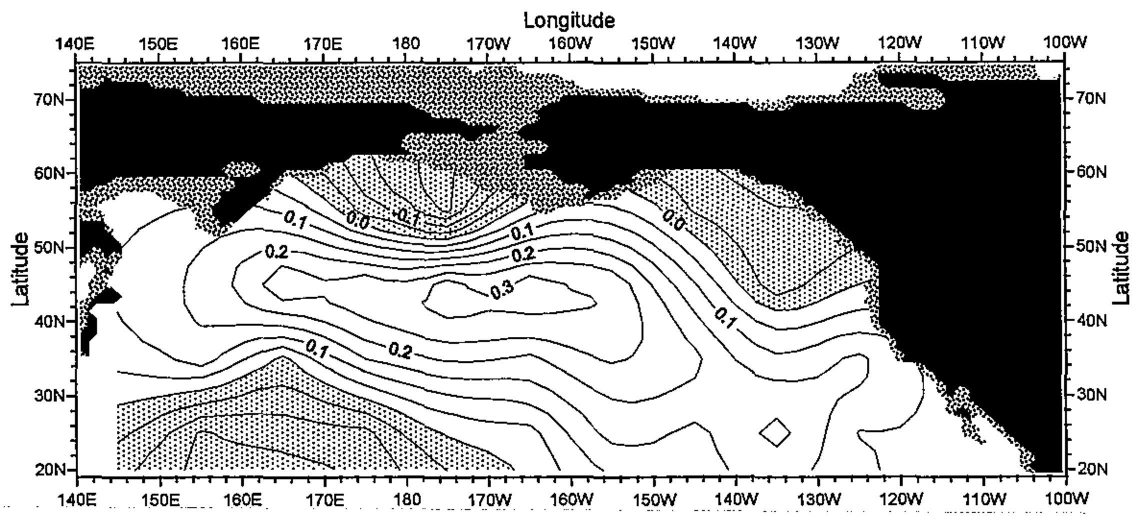


Fig.H14 2ND EOF of North Pacific temperature anomalies for 1960-90 period at 250 m depth

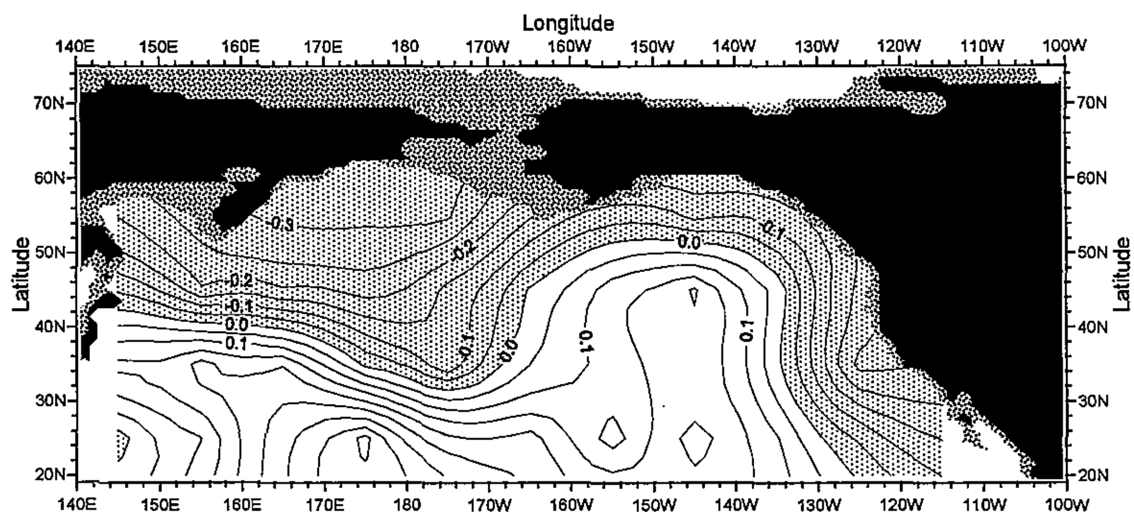


Fig.H15 3RD EOF of North Pacific temperature anomalies for 1960-90 period at 250 m depth

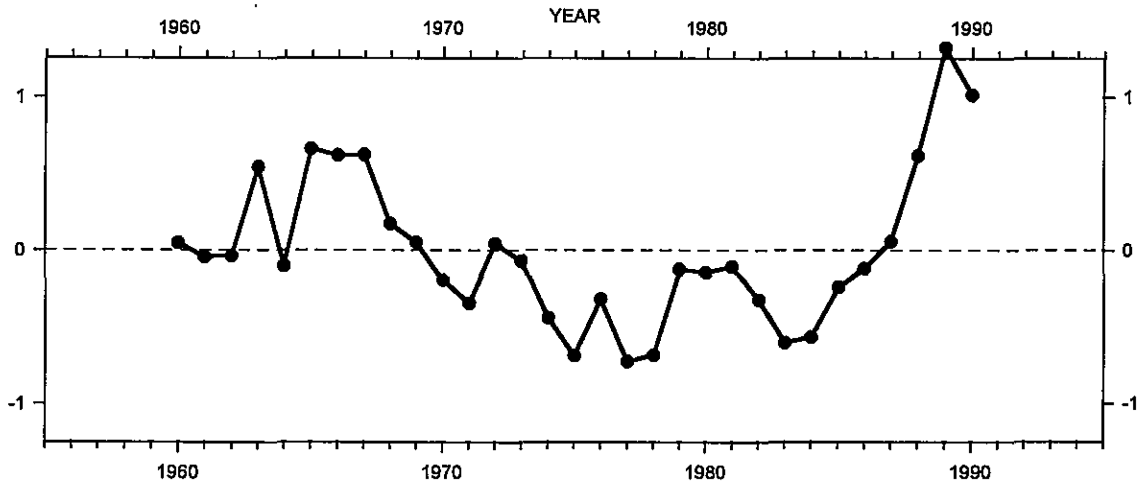

Fig.H16 1ST EOF time series of North Pacific temperature anomalies at 250 m depth (25.1%)

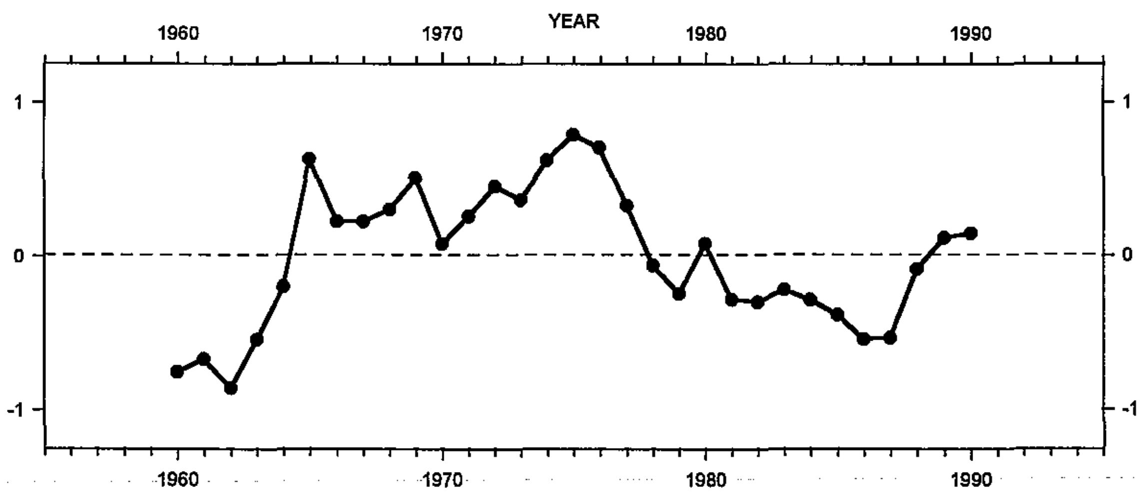

Fig.H17 2ND EOF time series of North Pacific temperature anomalies at 250 m depth (20.4%)

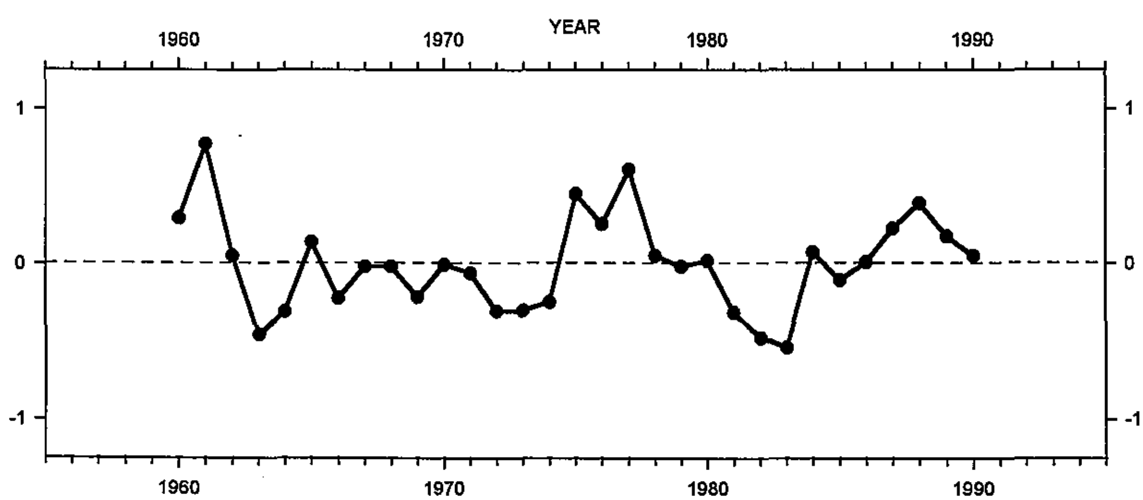

Fig.H18 3RD EOF time series of North Pacific temperature anomalies at 250 m depth (9.5%)

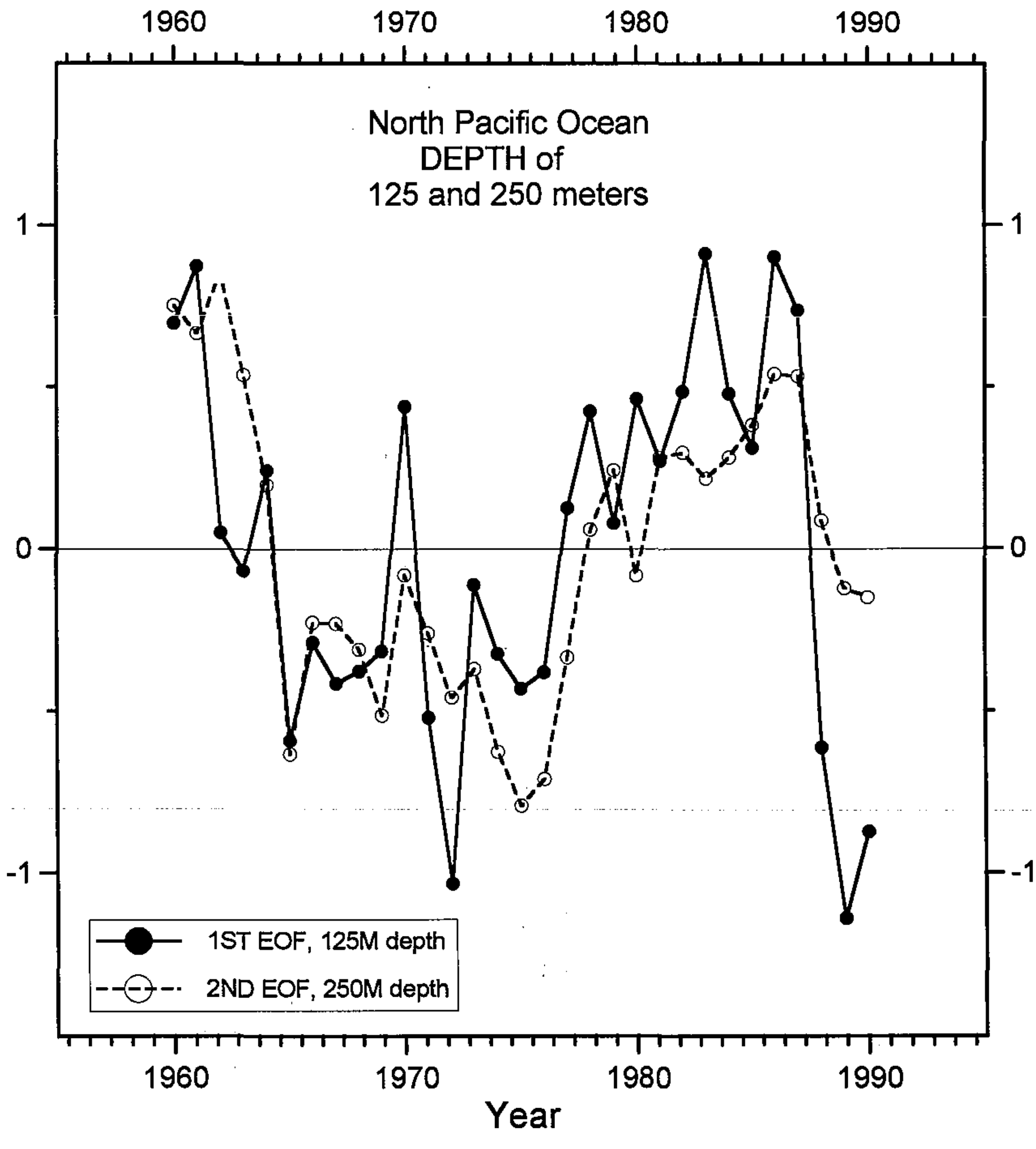


Fig.H19 Time series of EOFs of temperature anomalies in the North Pacific ocean at depths of 125 m (1ST EOF) and 250 m (2ND EOF multiplied by -1)

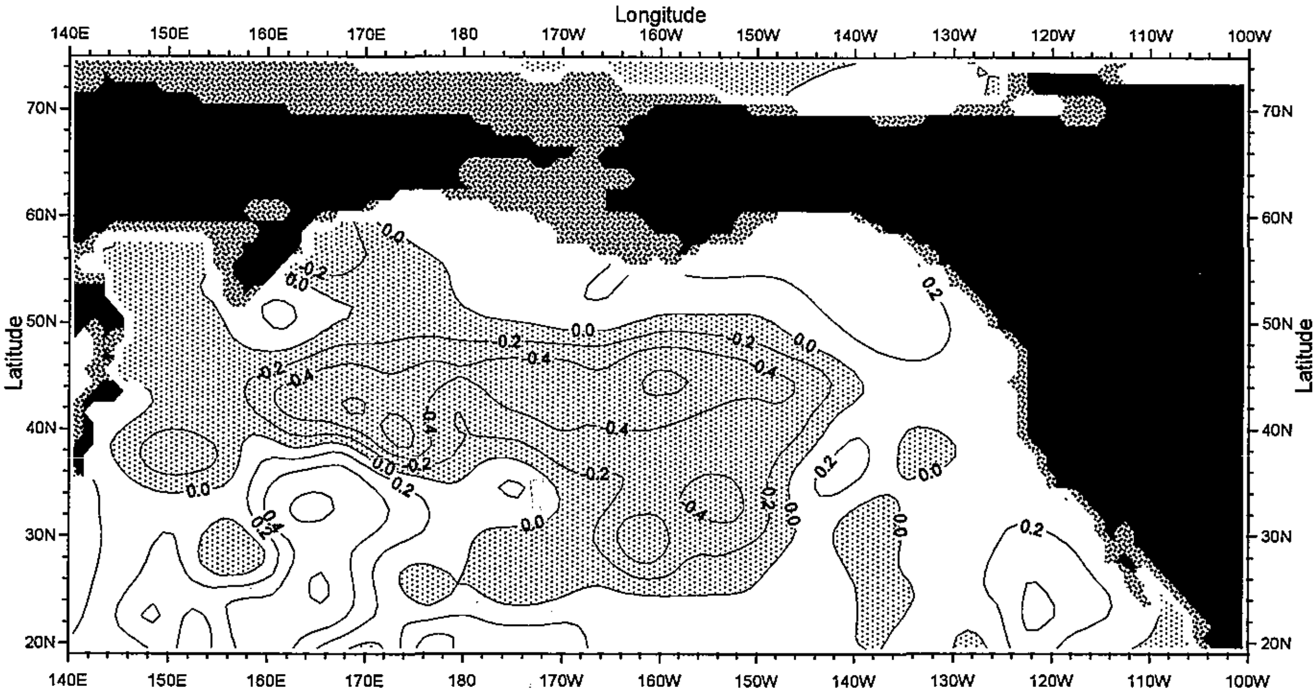


Fig.H20 Mean (1960-1962) temperature anomaly ( C) field at 125 m depth

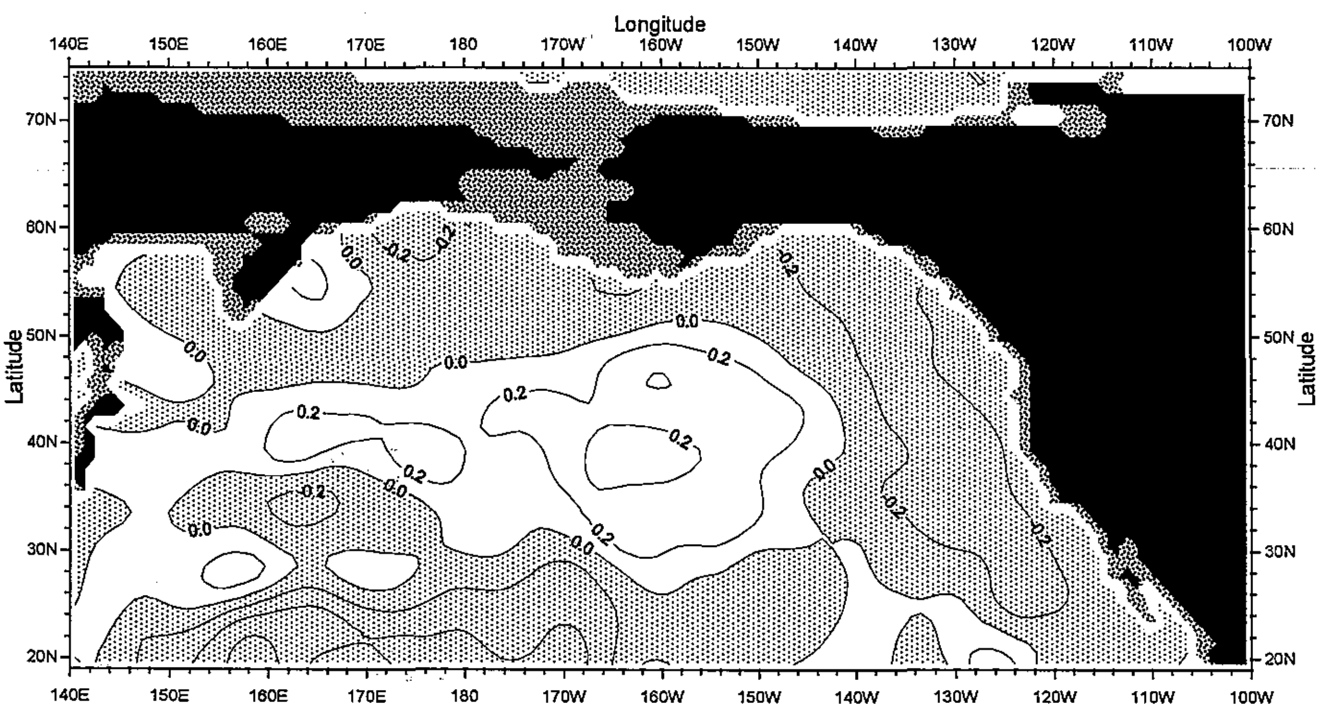


Fig.H21 Mean (1965-1969) temperature anomaly ( C) field at 125 m depth

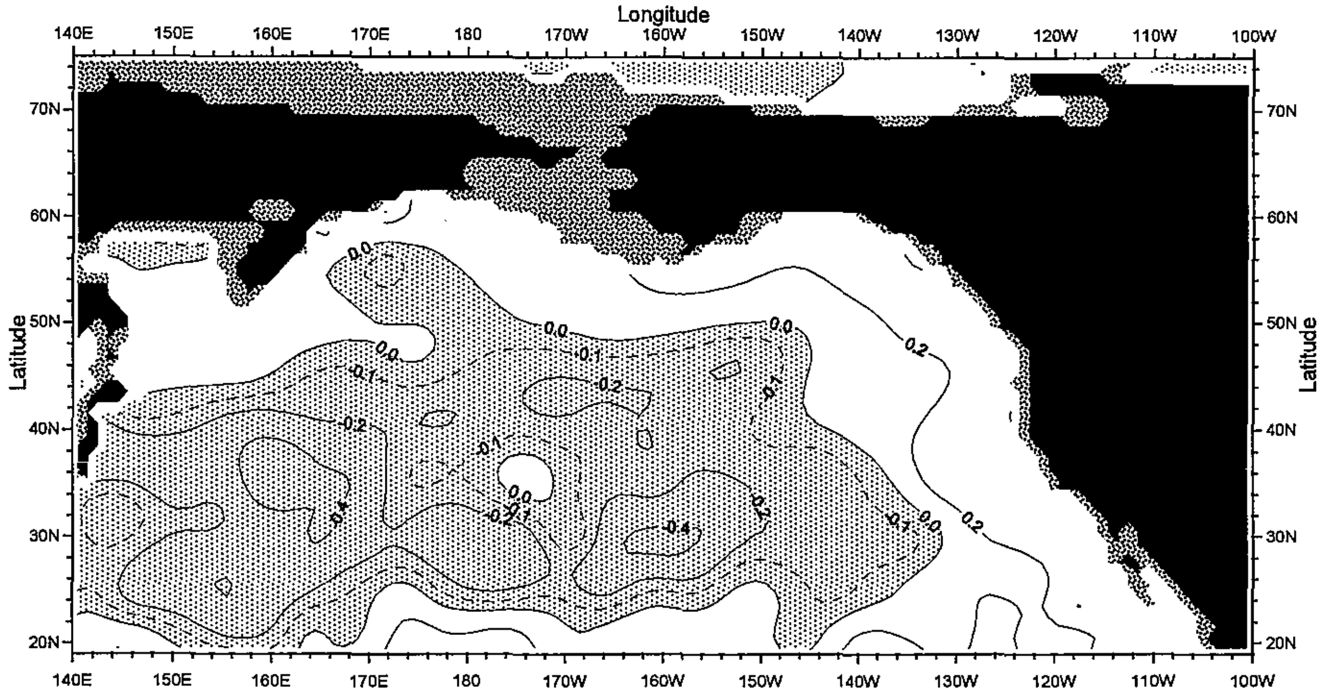


Fig.H22 Mean (1981-1985) temperature anomaly ( C) field at 125 m depth

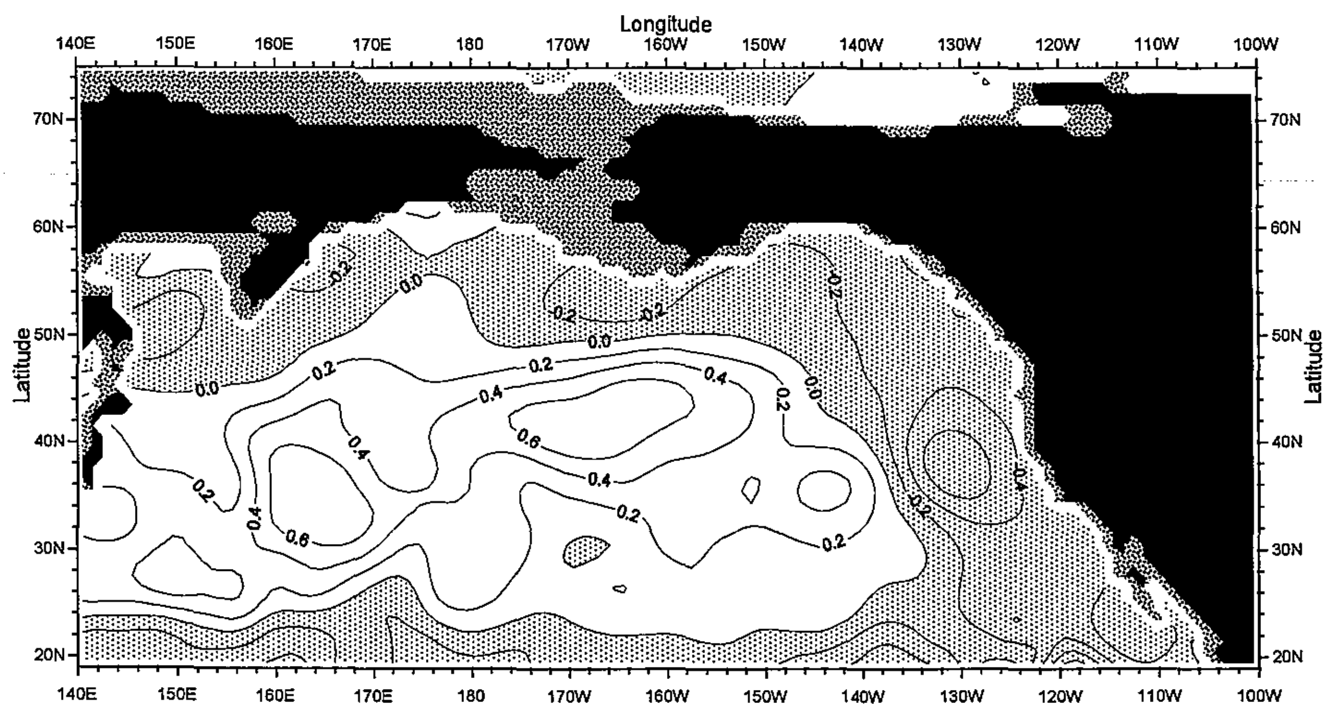


Fig.H23 Mean (1988-1990) temperature anomaly ( C) field at 125 m depth

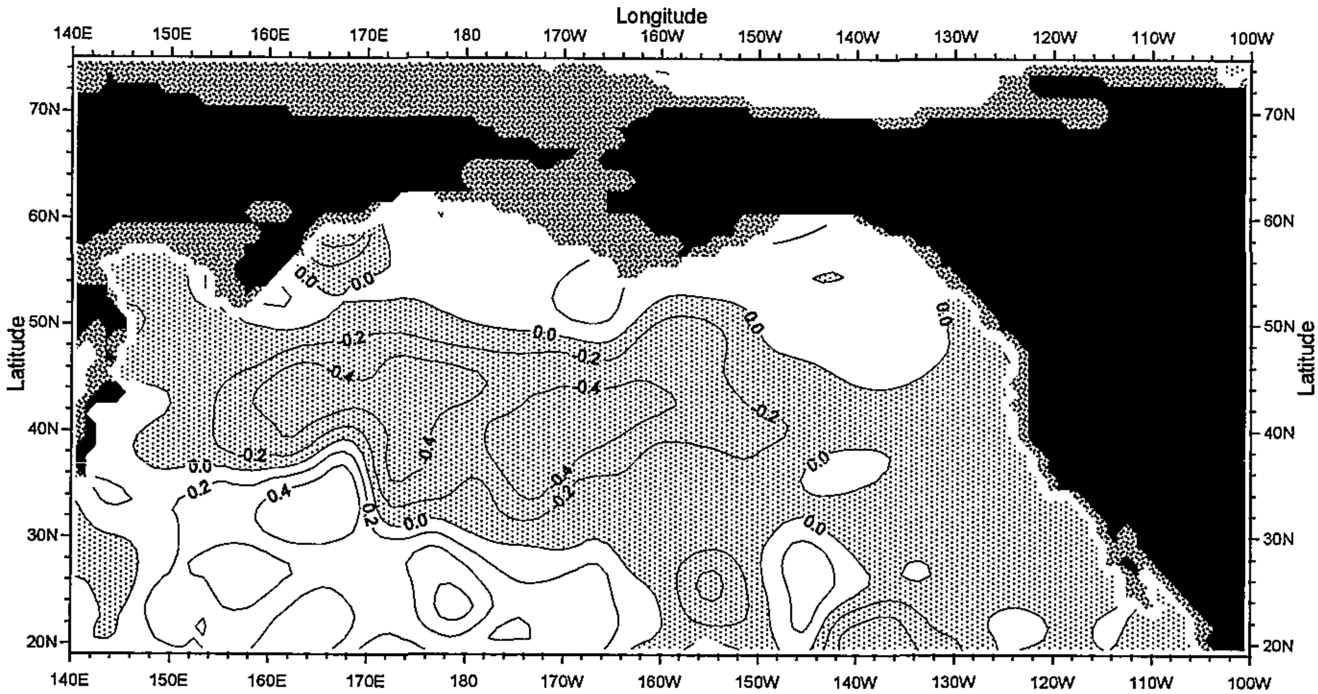


Fig.H24 Mean (1960-1962) temperature anomaly ( C) field at 250 m depth

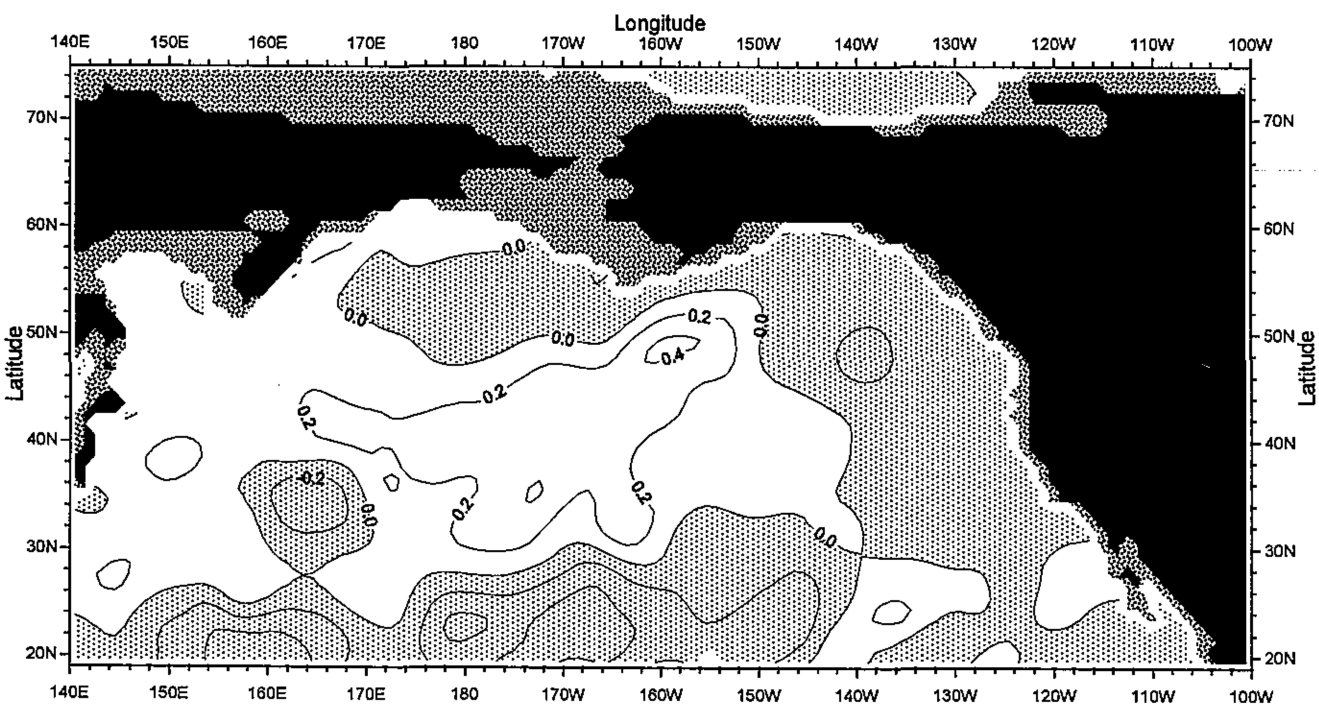


Fig.H25 Mean (1965-1969) temperature anomaly ( C) field at 250 m depth

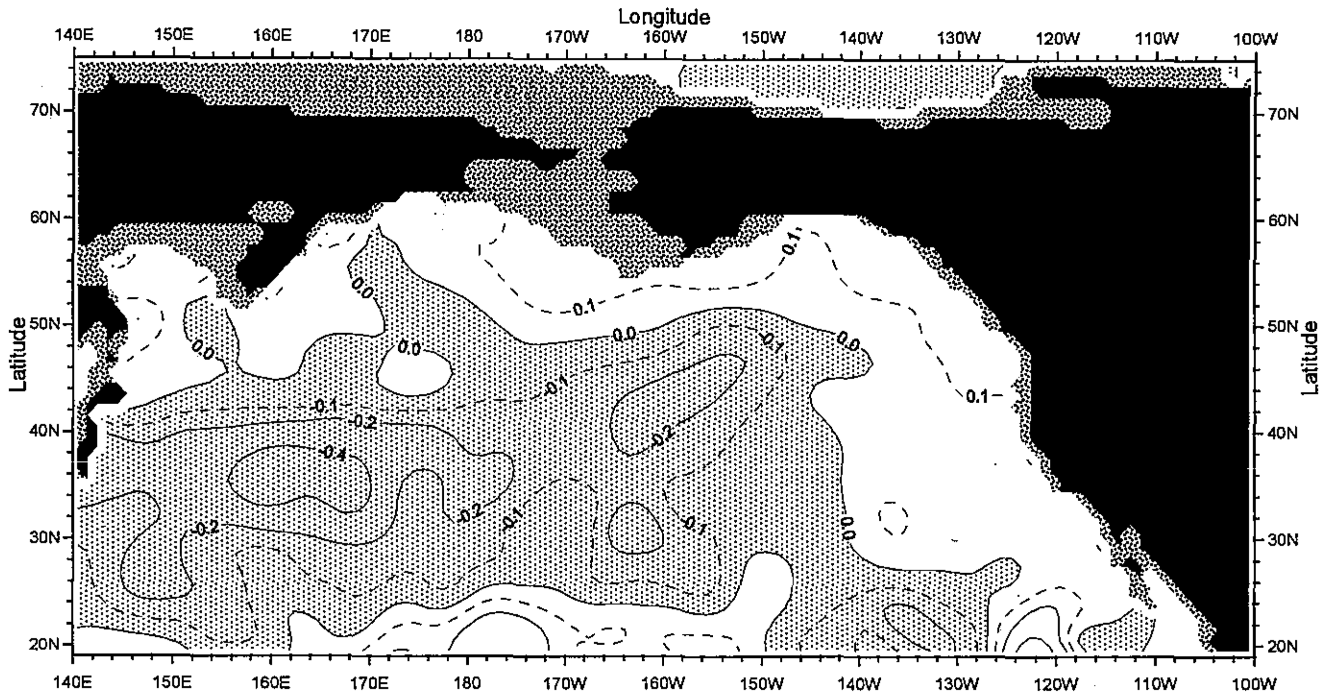


Fig.H26 Mean (1981-1985) temperature anomaly ( C) field at 250 m depth

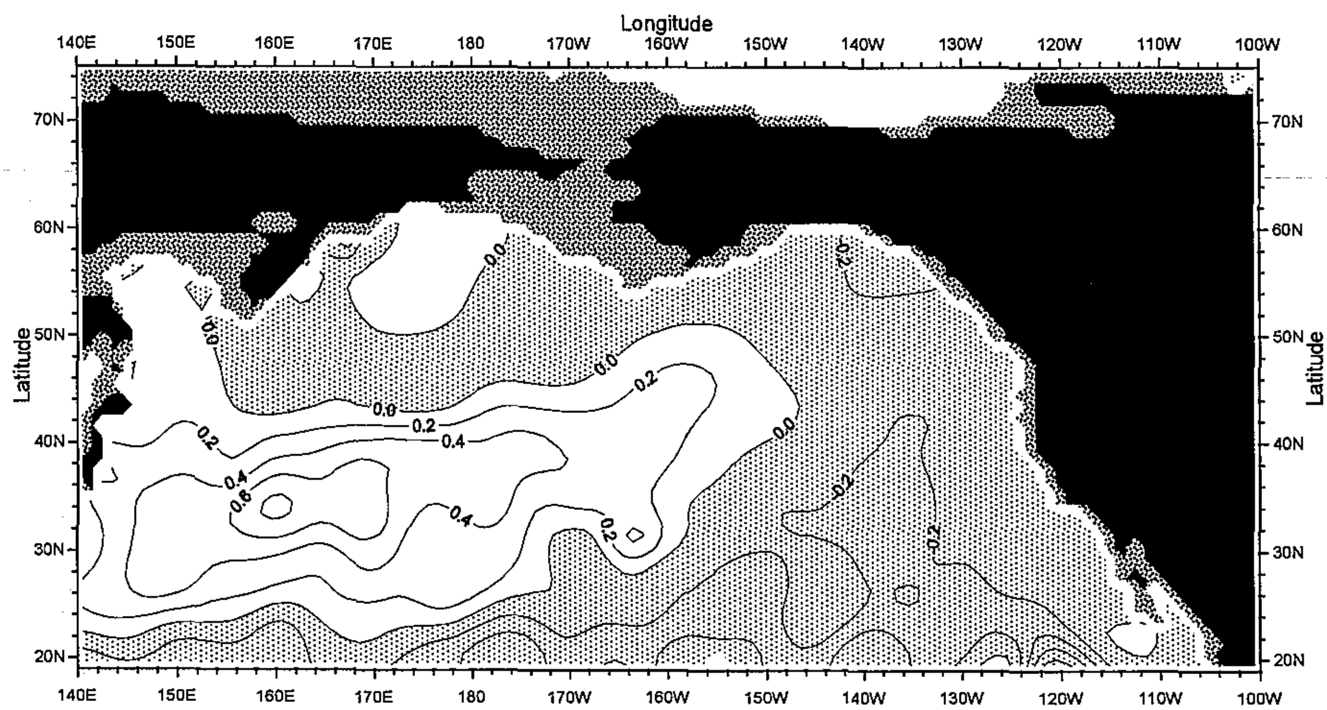


Fig.H27 Mean (1988-1990) temperature anomaly ( C) field at 250 m depth

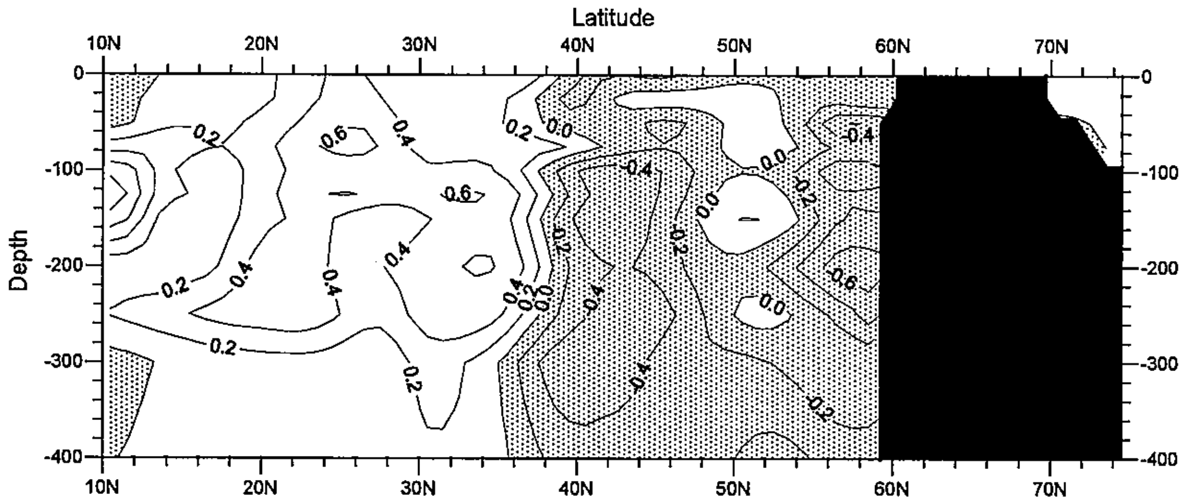


Fig.H28 Mean (1960-1962) temperature anomaly ( C) field at 164.5E

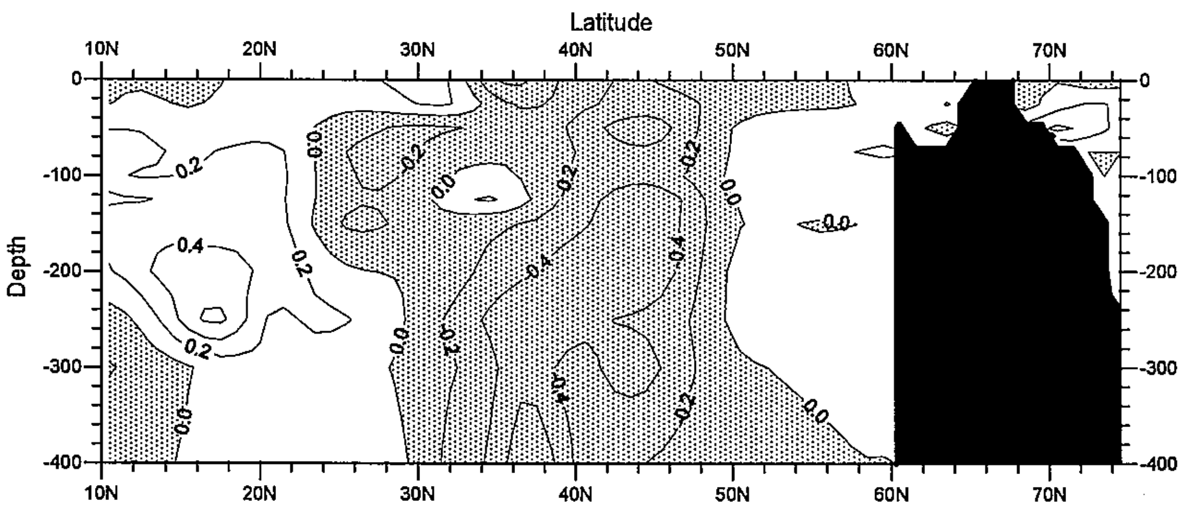


Fig.H29 Mean (1960-1962) temperature anomaly ( C) field at 174.5W

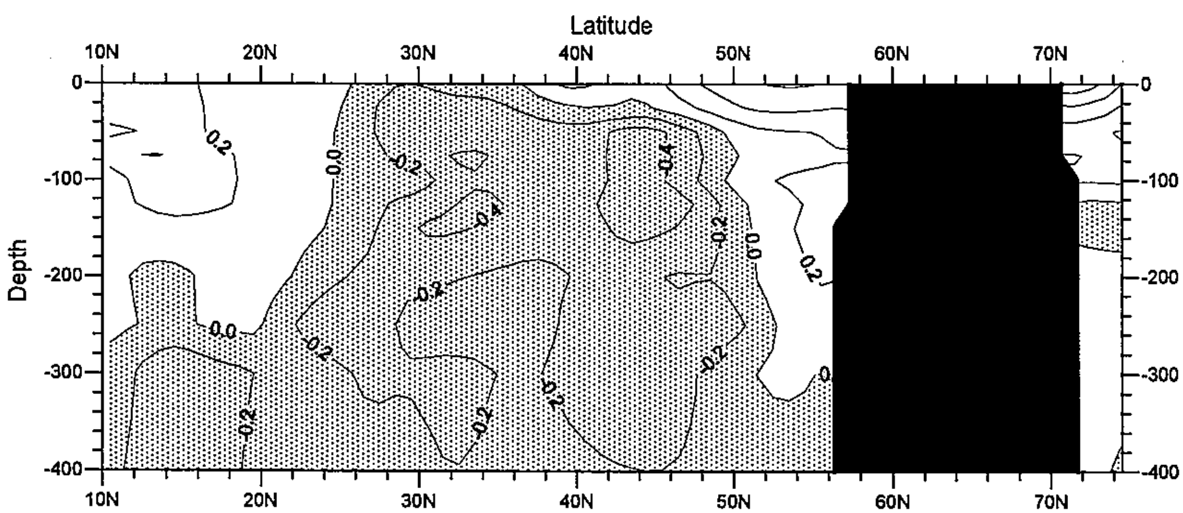


Fig.H30 Mean (1960-1962) temperature anomaly ( C) field at 156.5W

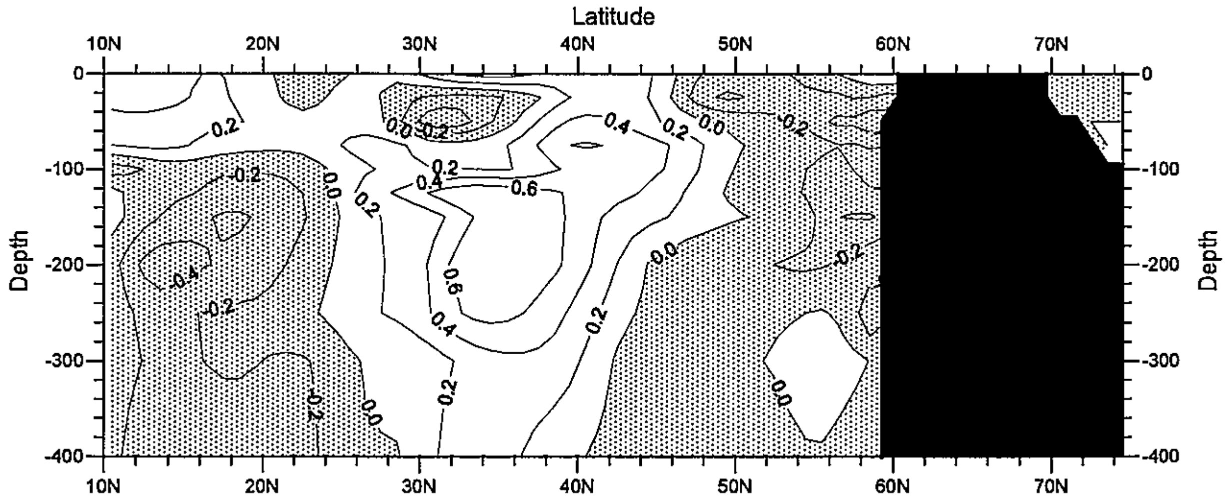


Fig.H31 Mean (1988-1990) temperature anomaly ( C) field at 164.5E

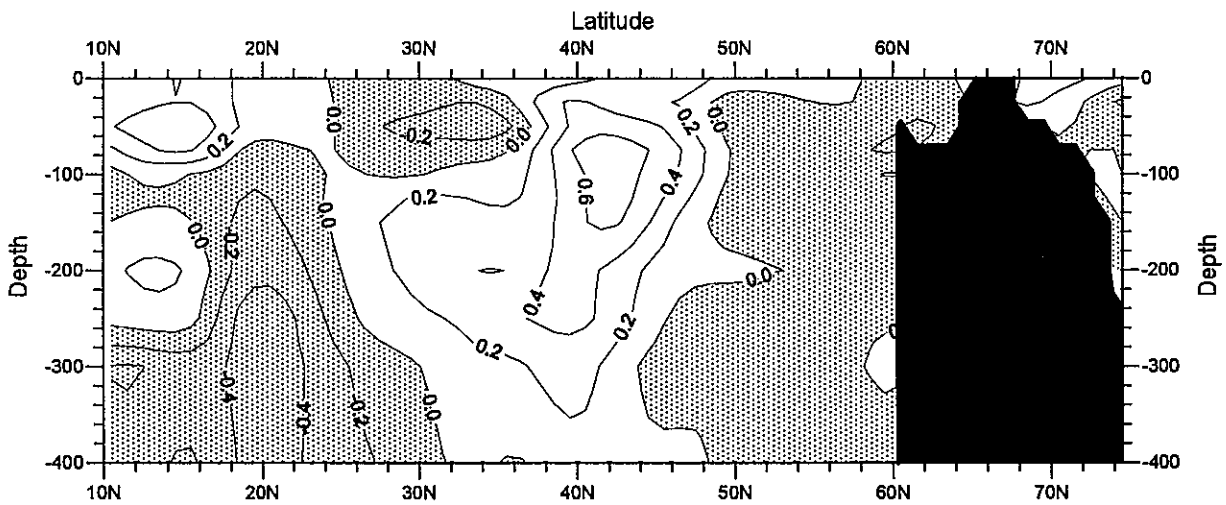


Fig.H32 Mean (1988-1990) temperature anomaly ( C) field at 174.5W

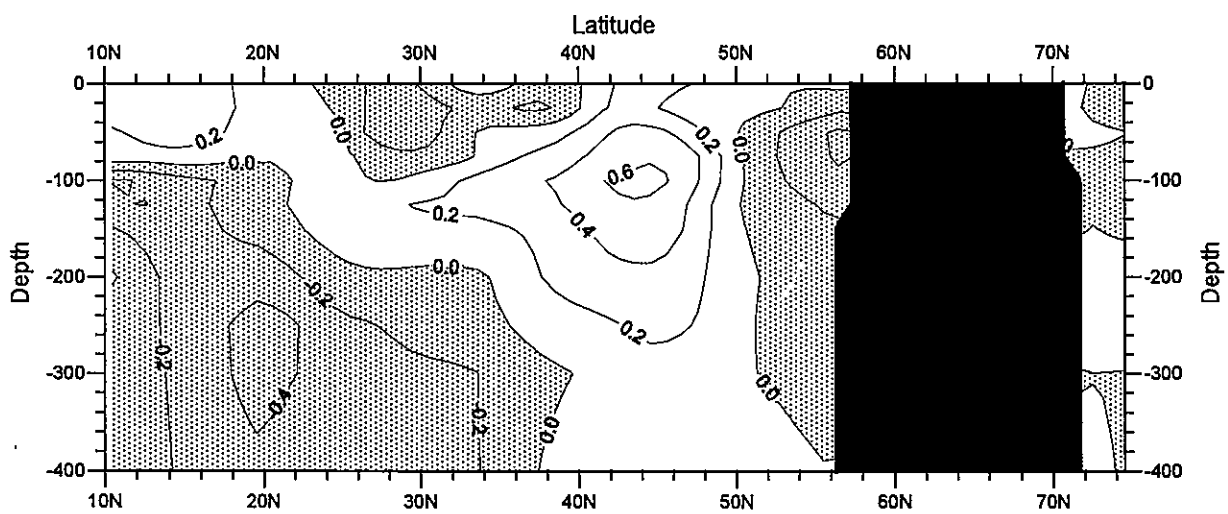


Fig.H33 Mean (1988-1990) temperature anomaly ( C) field at 156.5W

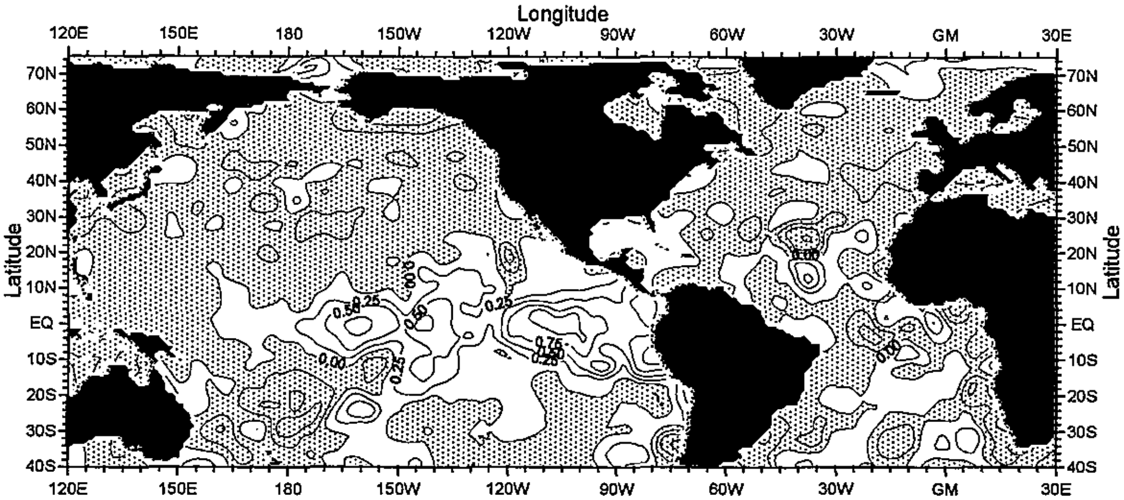


Fig.I1 El Nino composite temperature anomaly (C) fields (1969,72,76,82,86) at the surface

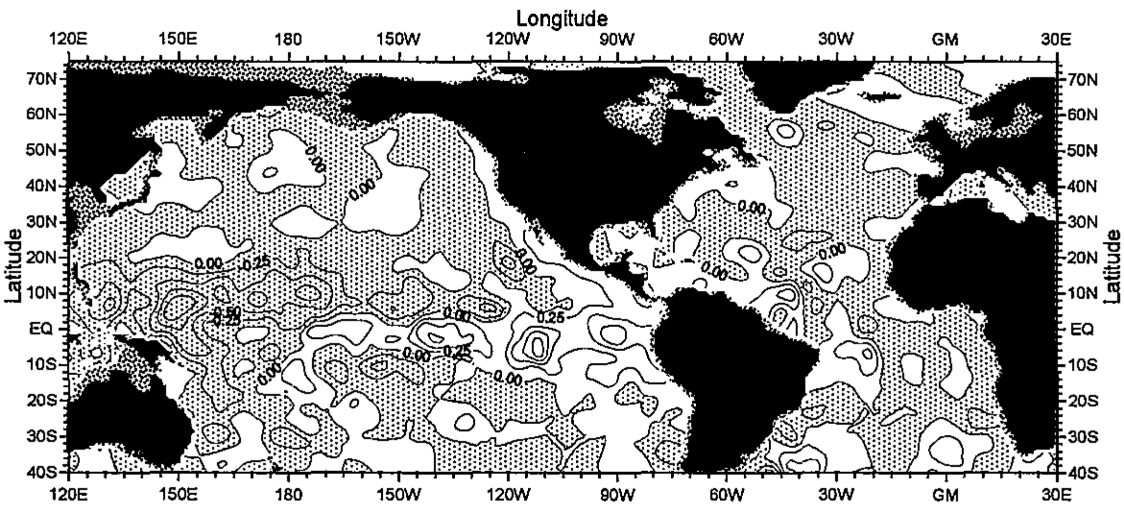


Fig.I2 El Nino composite temperature anomaly (C) fields (1969,72,76,82,86) at 125 m depth

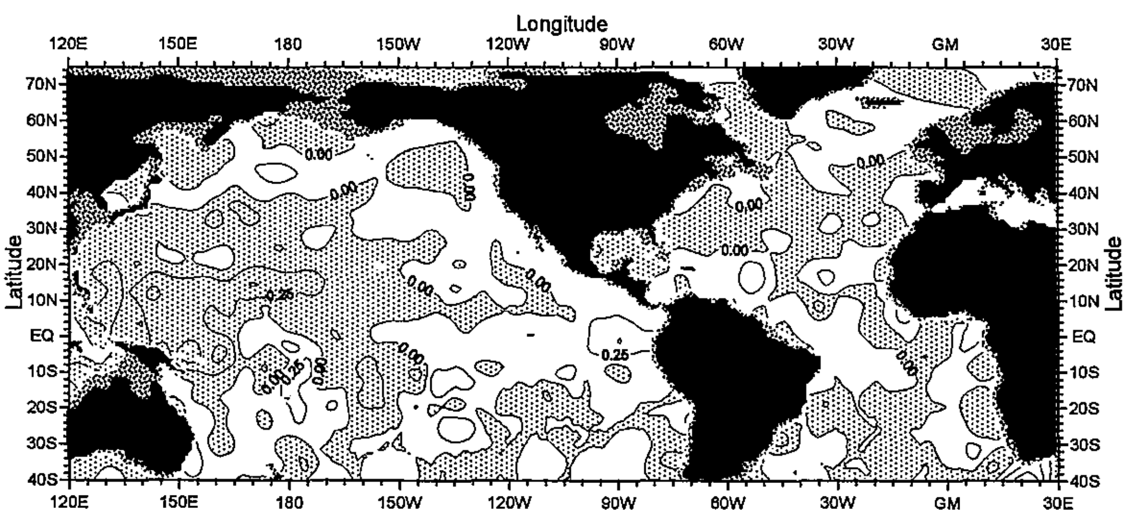


Fig.I3 El Nino composite temperature anomaly (C) fields (1969,72,76,82,86) at 250 m depth

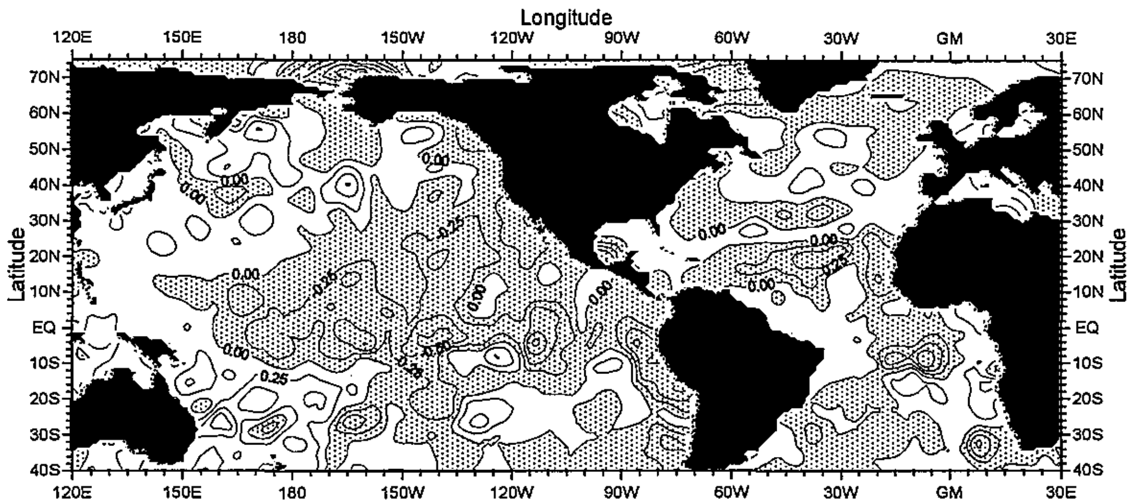


Fig.I4 La Nina composite temperature anomaly (C) fields (1964,70,73,75,88) at the surface

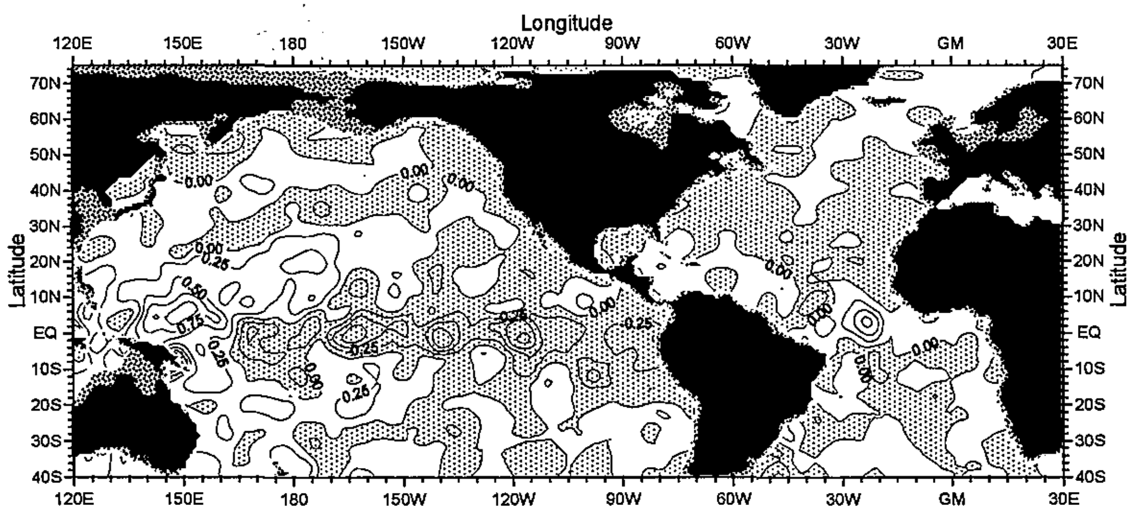


Fig.I5 La Nina composite temperature anomaly (C) fields (1964,70,73,75,88) at 125 m depth

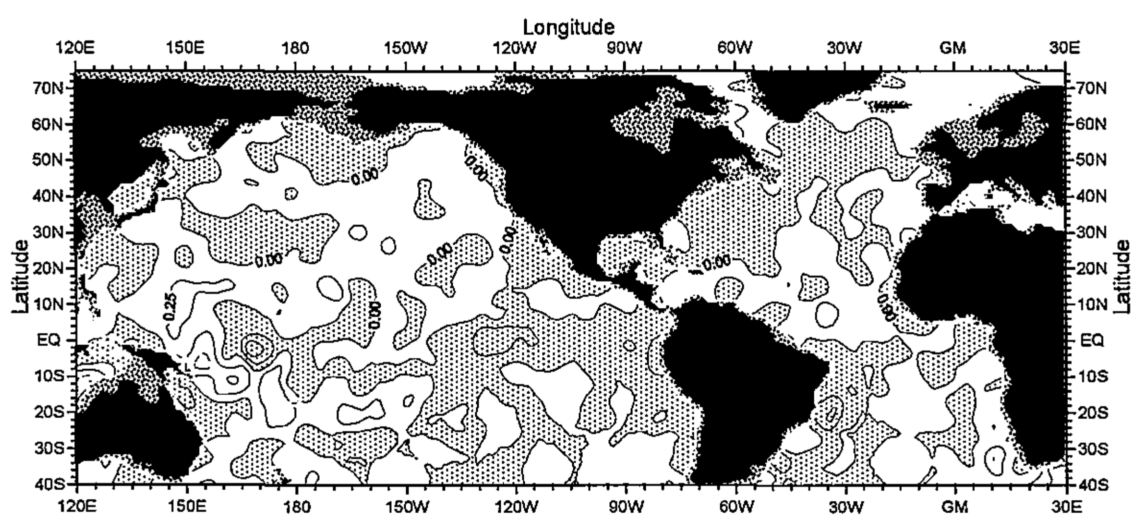


Fig.I6 La Nina composite temperature anomaly (C) fields (1964,70,73,75,88) at 250 m depth

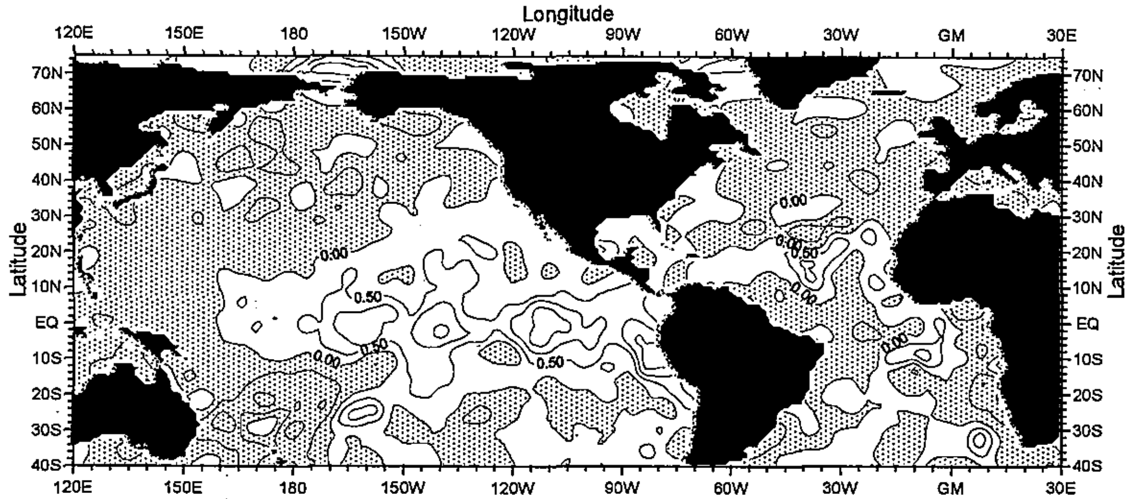


Fig.I7 Average of El Nino minus La Nina temperature anomaly (C) at the surface

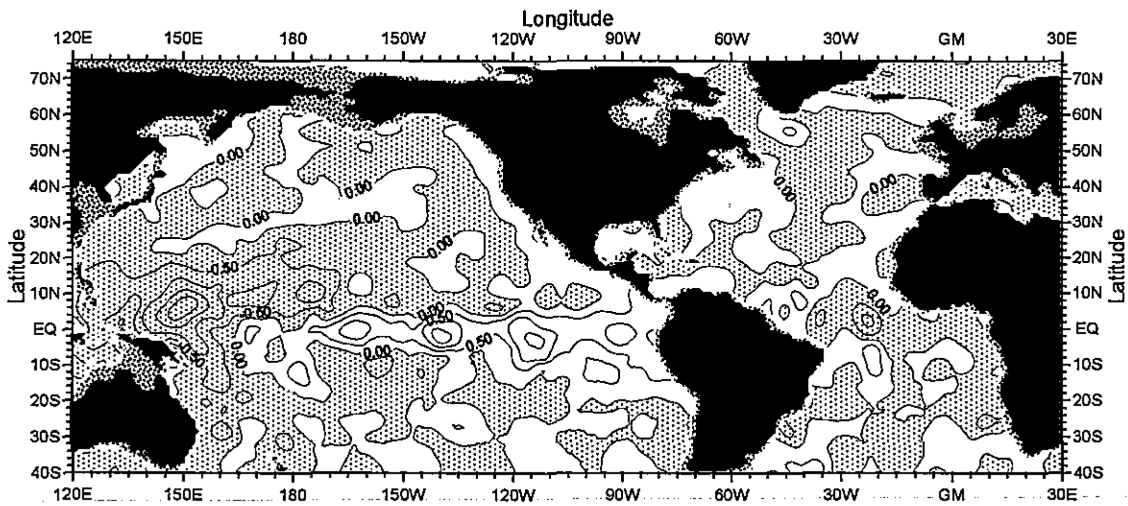


Fig.I8 Average of El Nino minus La Nina temperature anomaly (C) at 125 m depth

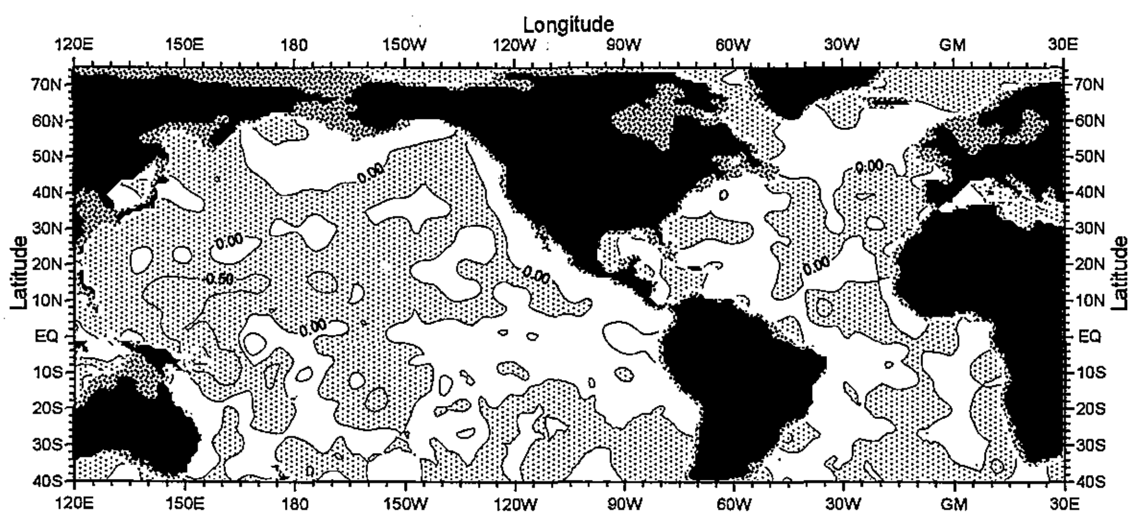


Fig.I9 Average of El Nino minus La Nina temperature anomaly (C) at 250 m depth

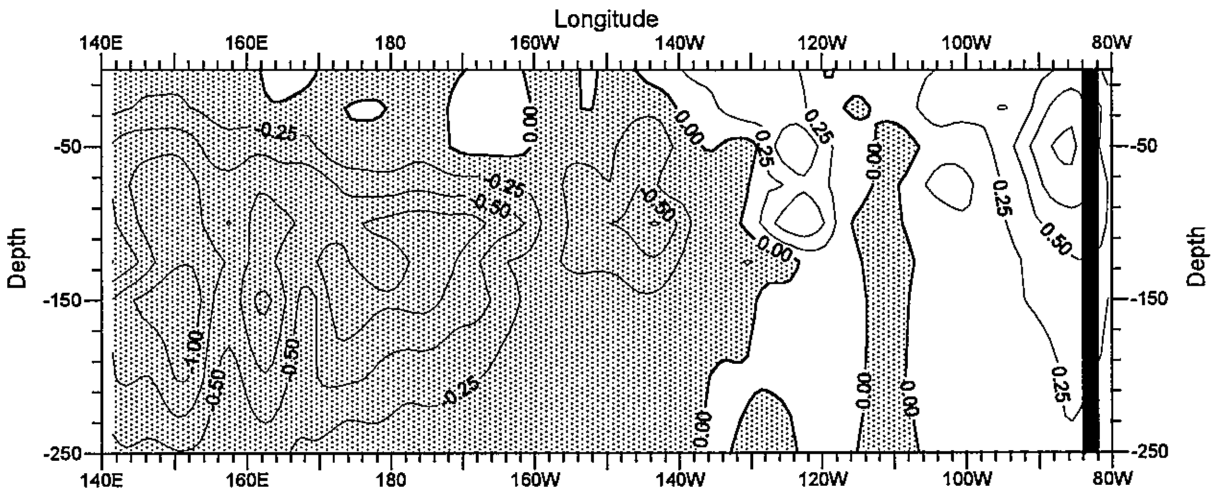


Fig.I10 Mean temperature anomaly (C) for El Nino composite along 9.5N

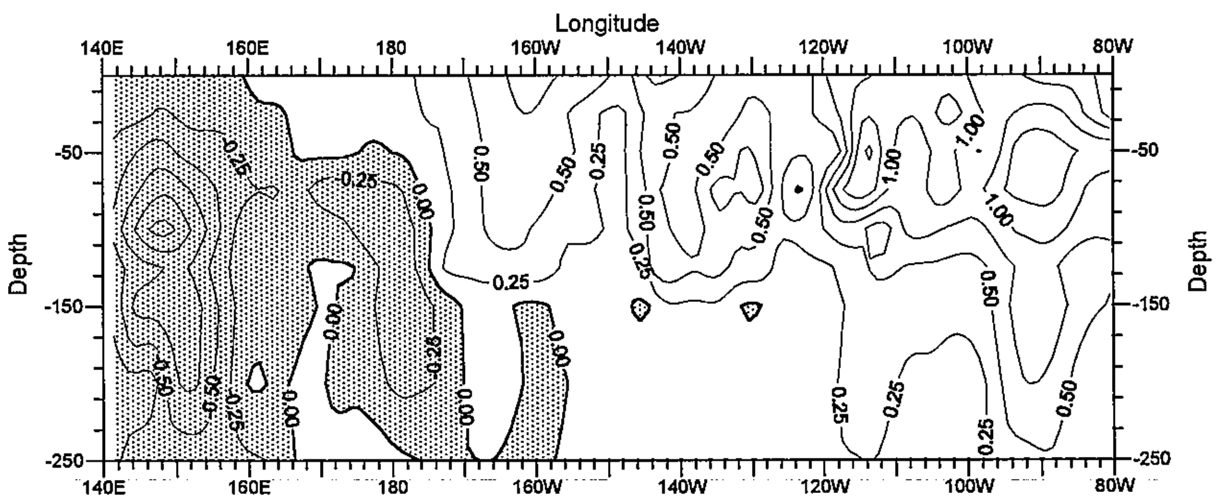


Fig.I11 Mean temperature anomaly (C) for El Nino composite along 0.5N

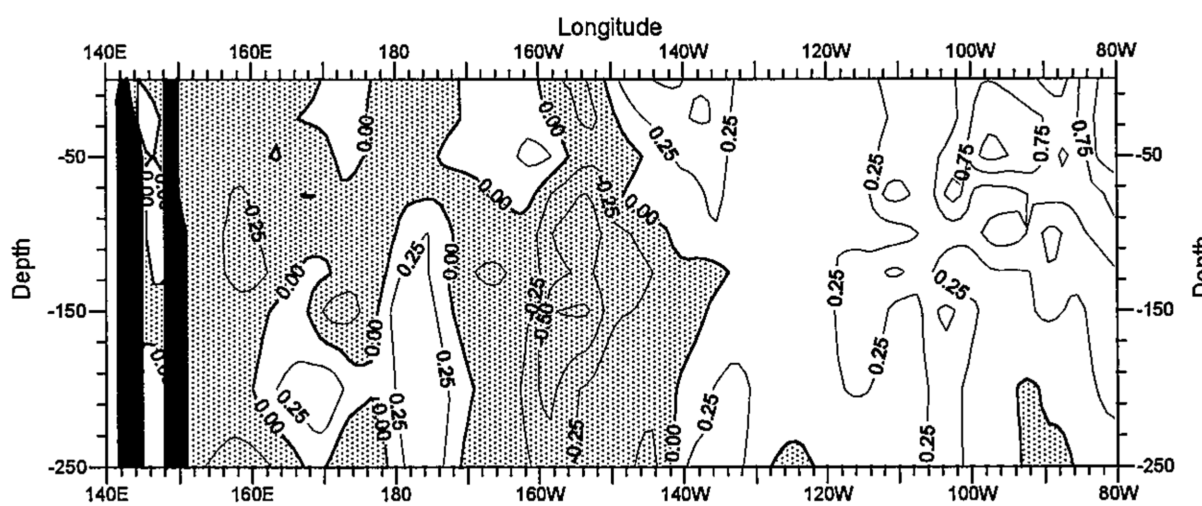


Fig.I12 Mean temperature anomaly (C) for El Nino composite along 9.5S

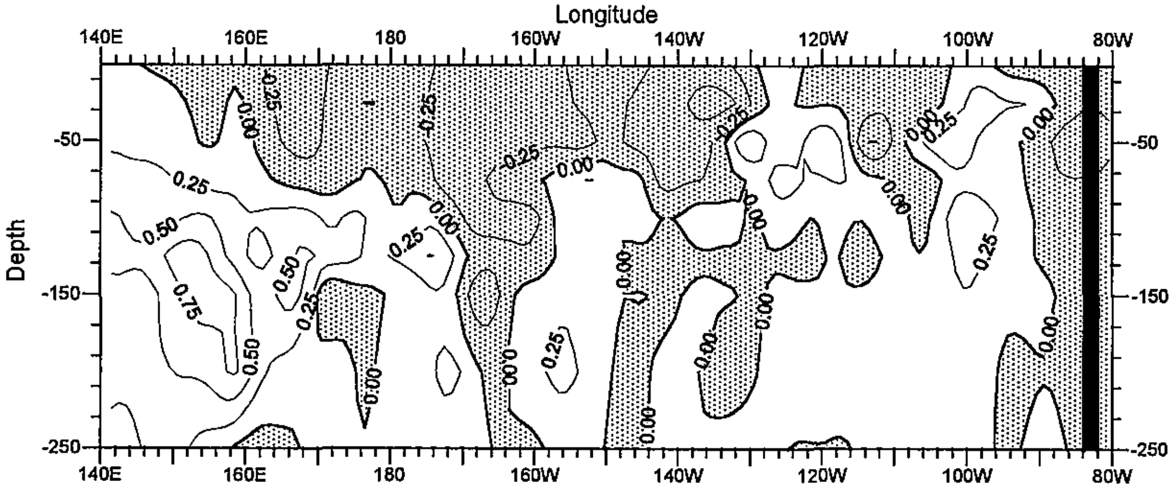


Fig.I13 Mean temperature anomaly (C) for La Nina composite along 9.5N

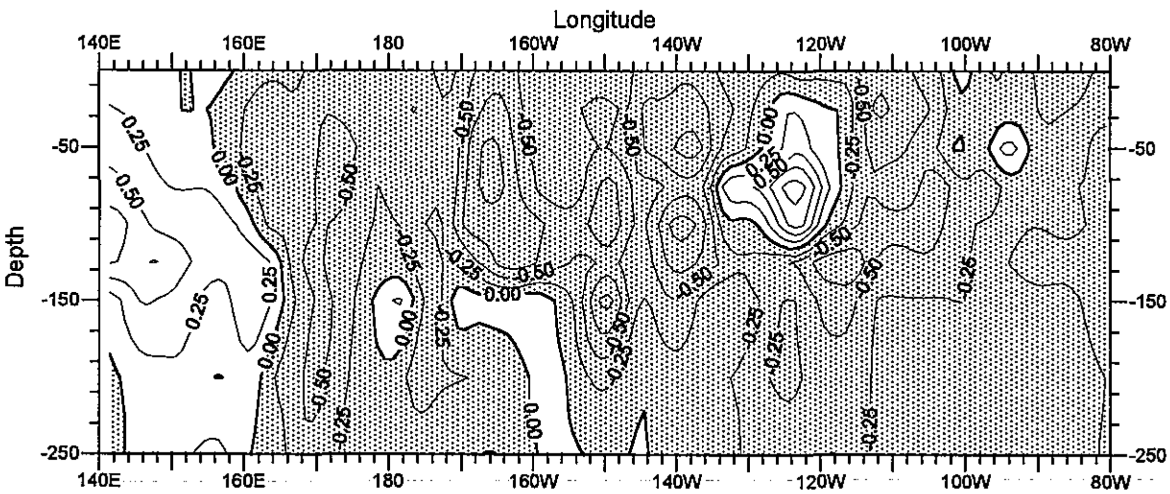


Fig.I14 Mean temperature anomaly (C) for La Nina composite along 0.5N

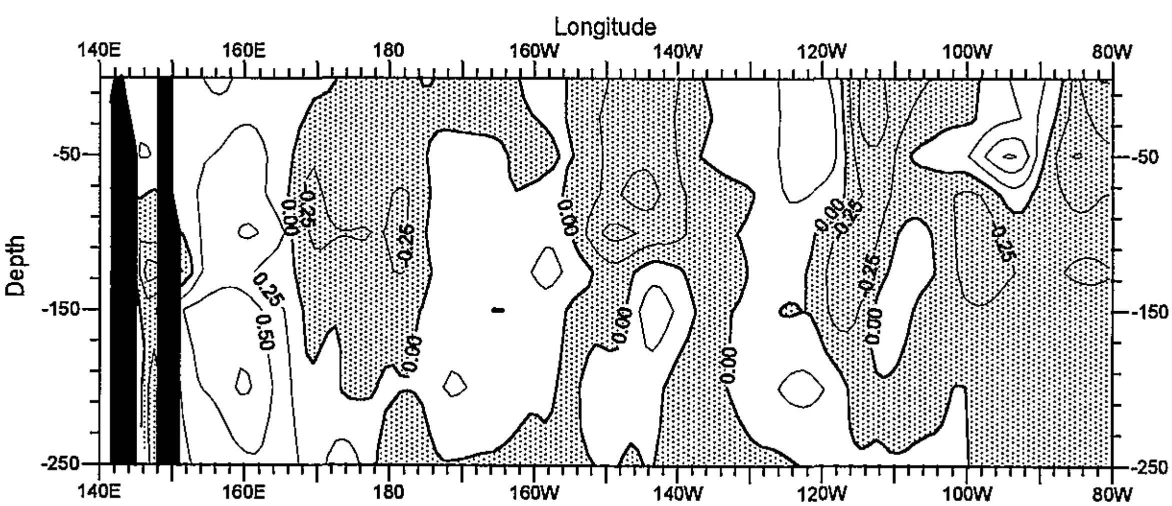


Fig.I15 Mean temperature anomaly (C) for La Nina composite along 9.5S

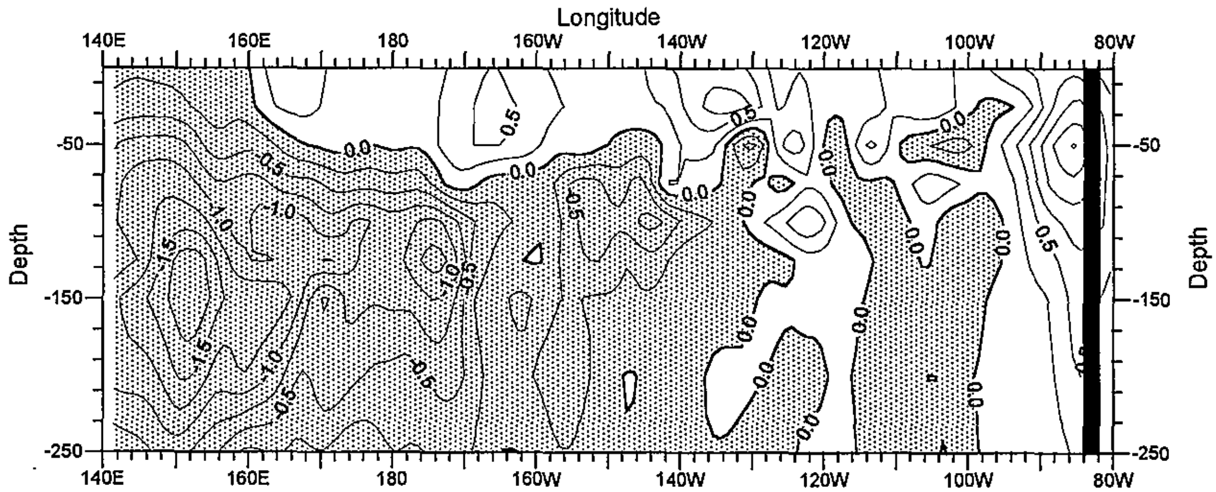


Fig.I16 Temperature difference (C) for El Nino composite minus La Nina composite along 9.5N

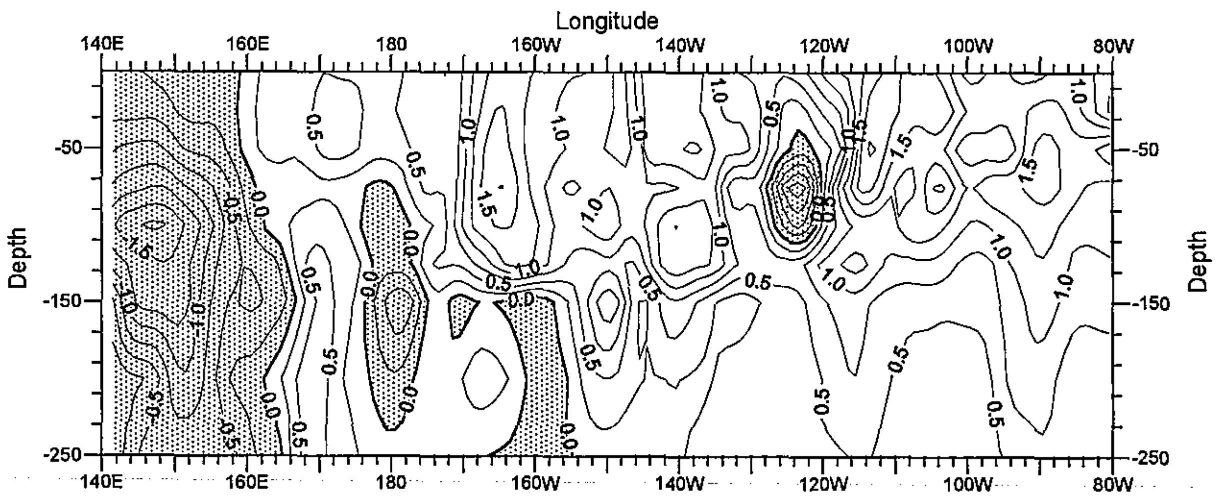


Fig.I17 Temperature difference (C) for El Nino composite minus La Nina composite along 0.5N

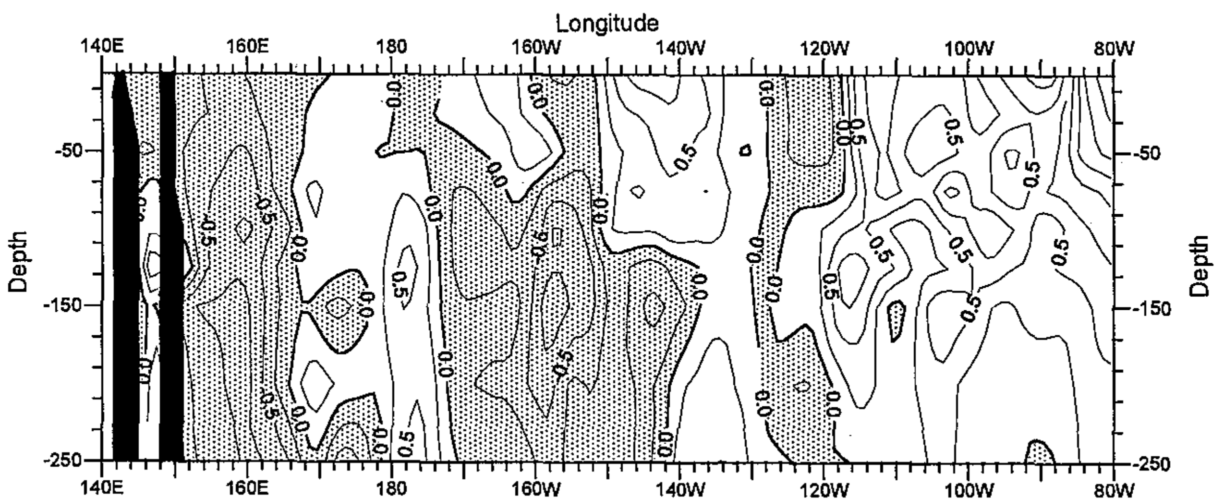


Fig.I18 Temperature difference (C) for El Nino composite minus La Nina composite along 9.5S